THE BELL SYSTEM
TECHNICAL JOURNAL

A New Carrier System for Rural Service

By R. C BOYD, J. D. HOWARD, JR, and L. PEDERSEN

A study of the problem of providing telephone service to rural customers indicated the need for a flexible carrier system that could be used economically on new and existing rural cable and open wire lines. The desire for low cost required new approaches to almost every phase of the carrier system design for rural service, which has been designated Type P1.

Use of transistors led to sweeping changes in the detailed circuitry and also created demand for other new components. Mounting and interconnecting the circuit components by means of printed wiring boards emphasized the necessity for close coordination between design and manufacturing objectives. The low power-drain requirements of transistor circuitry were supplied economically by the use of similar solid state devices, a new storage battery, and efficient packaging.

A fast, accurate and simple method has been evolved for applying the P1 carrier system to rural lines with a minimum of line treatment or rearrangement. Plug-in equipment, readily accessible test points, and a carrier test set provide the ease of maintenance needed in the use of telephone equipment at remote locations. Use of the P1 carrier system will extend the application of electronic equipment outside of the telephone central office and provide a carrier system whose performance will be consistent with requirements for high quality communication service at low cost.

1. INTRODUCTION

Although carrier has been used successfully to provide trunks in the Bell System for more than 35 years, it has not been economically feasible, up to the present time, to apply carrier telephone techniques extensively to the rural telephone plant. The technical and economic problems associated with providing telephone service to customers in rural areas has long been one of the most difficult problems facing the telephone industry. The widely scattered locations of customers in rural areas have led to a large number of rural telephone routes with only a few customer lines per route. This has precluded the use of large cables on any one route, which would be economically attractive in urban areas. The extensive use of carrier has not been feasible because the distances from the rural customers to the Central Office are in the 5- to 20-mile range in which carrier has not been generally economical in the past.

The two lines of attack which were taken on this problem were to reduce the cost of telephone plant through less expensive small cables and open-wire plant,[1] and to provide an economically attractive carrier system designed to meet the particular needs of rural telephone service.

This paper discusses the broad objectives for a rural customer carrier system, the major parameters of the P1 system which was developed to meet those objectives, and its circuit, equipment, and power arrangements. It also covers the engineering and maintenance methods to be used by the Bell System Operating Companies to install and operate the system.[2]

2. BROAD OBJECTIVES FOR P1 CARRIER SYSTEM

The broad objectives for the Type P1 carrier system resulted from the stringent economic limits imposed on the system to enable it to prove in over conventional rural plant of the latest and most economical design, from the requirements of rural telephone transmission and signaling, and from Bell System experience gained with earlier carrier systems for customer and trunk use. The low cost objective for this system also implied the need to achieve an appropriate balance among an economic first cost of equipment, low in-place cost due to simplified engineering and installation practices, and accompanying low annual costs due in part to simplified system maintenance.

To achieve an economic carrier system for rural telephone use, the dc power requirements of the terminals and repeaters had to be kept low.

---

[1] Lester Hochgraf and R. G. Watling, Telephone Lines for Rural Subscriber Service, A.I.E.E. Communication and Electronics, No. 18, p. 171, May, 1955.

[2] These aspects of the P1 system are covered in more detail in four papers on "The P1 Carrier System." A.I.E.E. Communication and Electronics, No. 24, pp. 188, 191, 195, 205, May, 1956.

This was especially important since previous Bell System experience indicated that where commercial power is used to supply the system, some form of reserve must be provided, and where commercial power is not available, the use of primary batteries places a premium on minimizing the power required.

From these considerations two additional major objectives were derived: low manufacturing costs for the components and assembled equipment, and the use of transistors to minimize power supply drains. In addition, flexibility was needed in the proposed carrier system because of the difficulty of accurately forecasting the demand for rural service.

These objectives have been met in the design of the Type P1 rural customer telephone system. It is a fully-transistorized system consisting of independent two-way carrier channels applicable in increments of one to four at a time in the frequency band above the regular voice frequency circuit. Each channel uses a terminal at the central office and at a remote point with intermediate repeaters as necessary. Between terminals, the system is equivalent to a rural voice frequency line with no changes required in the central office or rural customer equipment. Beyond the outlying terminal, distribution is by voice frequency wire on a single or multiparty basis. The system can be applied to existing and new lines utilizing combinations of fine gauge exchange cable and copper or steel open-wire. Systems can be used on each of several pairs on a given pole line, the number depending on the line characteristics.

3. MAJOR PARAMETERS OF P1 CARRIER SYSTEM

This section summarizes the important features incorporated in the P1 carrier system and the reasons governing their choice. The system has a number of features in common with Bell System toll carrier systems, but it also differs in several important aspects because of specific rural requirements. One aspect is the signaling, which requires different arrangements at the two ends of the circuit because of the widely different signals carried in the two directions. Another is that the remote terminals of the individual channels are usually distributed along the line rather than grouped at a common location.

3.1 *Transmission Plan*

It is difficult to divorce the considerations leading to the choice of carrier frequency range from those affecting the choice of modulation in the carrier system. Studies of growth on rural lines indicated that a system giving three or four channels (customer circuits) on one pair of wires, in addition to the physical circuit, should be sufficient if systems could be applied to each of several pairs on a given open-wire line.

The blocking out of the frequency range was controlled by a number of factors. Cost considerations required that the carrier frequencies be kept above the voice frequency range. If carrier extended into the voice range, the voice frequency circuit would be lost on a carrier pair. One of the carrier channels applied to that pair would have to be used to replace it. Thus, the addition of four carrier channels to a pair would yield a net gain of only three channels. This in turn would increase the net cost per gained channel. Filter costs determined how close to the voice frequency band the carrier frequency range could be placed and in conjunction with the number of channels required how closely the channels could be placed to each other.

Crosstalk considerations restricted the carrier frequency range to below about 100 kc in order to reduce the cost of line treatment and rearrangement of pairs on existing rural lines. By using this frequency range it appeared possible to apply more than one carrier system to crossarms on an open-wire route. The rapid rise in attenuation with frequency of steel wire used on rural lines dictated that the range of frequencies be kept low. As a result of these two sets of considerations, development work on the P1 carrier system was concentrated in the 8- to 100-kc range.

Amplitude modulation of the carrier frequencies was chosen over other forms of modulation because of the simpler terminal circuitry and equipment and because of the saving in bandwidth. Use of amplitude modulation and the use of compandors, discussed in a later section, were felt to compensate for possible transmission advantages that could
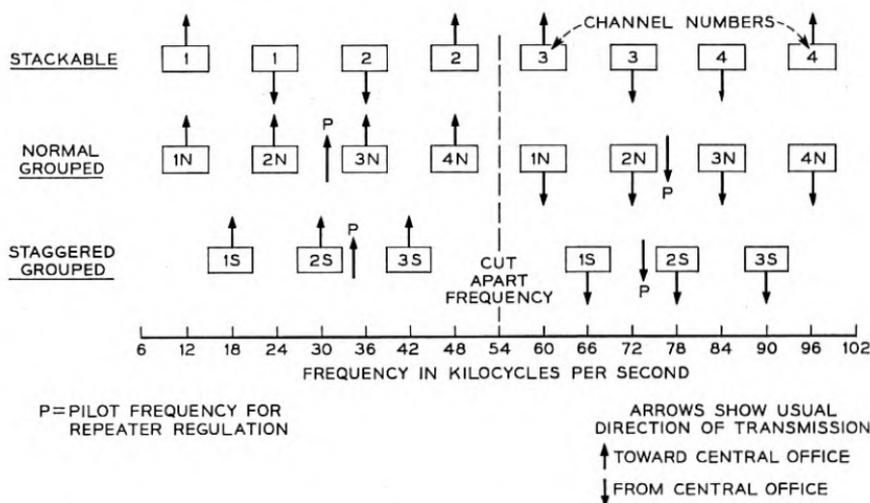

Fig. 1 — Type P1 Carrier Frequency Plan.

be obtained by using angular modulation (frequency or phase) with a large modulation coefficient.

Cost was again a major factor in the choice between double sideband and single sideband amplitude modulation. Past experience with other carrier systems has indicated that filters are a major part of the cost of a system and, when frequency space is available, double sideband filters are, in general, less expensive than those for single sideband. In addition, the cost of a single sideband system would be increased because of the problem of obtaining the necessary carrier supply at the terminal.

The frequency plan developed for the P1 carrier system is shown in Fig. 1. The unusually wide carrier spacing of 12 kc was adopted in order to minimize filter costs. Since the remote terminals are generally distributed along the line, it was not practical to use double modulation to accomplish filtering in the most efficient frequency range. Instead, filtering was done at line frequencies. Every effort was made to achieve channel filter designs with maximum efficiency of element utilization. Advantage was taken of the more leisurely rising characteristics of the double sideband filters permitted by the wide frequency spacing.

The stackable frequency arrangement was provided for non-repeatered operation, because when the lowest two carrier frequencies are used to provide a channel, it can be used over substantially longer distances than channels using higher frequencies. The grouped arrangements were provided for repeatered systems to reduce the cost and number of the repeater filters and amplifers needed to separate the two directions of transmission. The staggered grouped arrangement can be used with the normal grouped arrangement on a pole line having poor crosstalk coupling in order to increase the effective coupling loss between carrier channels on different pairs. The grouped and stackable arrangements cannot be used on the same pole line, because certain frequencies would be used for both directions of transmission. This would produce large differences between transmitted and received carrier power at terminals and repeaters which would lead to intolerable crosstalk.

A number of terminal arrangements were studied in order to implement the above frequency plan. The arrangement for a remote terminal shown in Fig. 2 was chosen as the simplest terminal meeting all of the system requirements. It is very similar to the channel terminal arrangement used in the Type N1 carrier system, another double sideband amplitude modulation system used for long distance trunks of the Bell System. The several shaded portions in the figure show the breakdown of the terminal functions into individual sub-units, which are the basis for the equipment arrangements discussed in Section 5 of this paper. A number of the other important features that make up the terminal arrangement are discussed in the following sections.
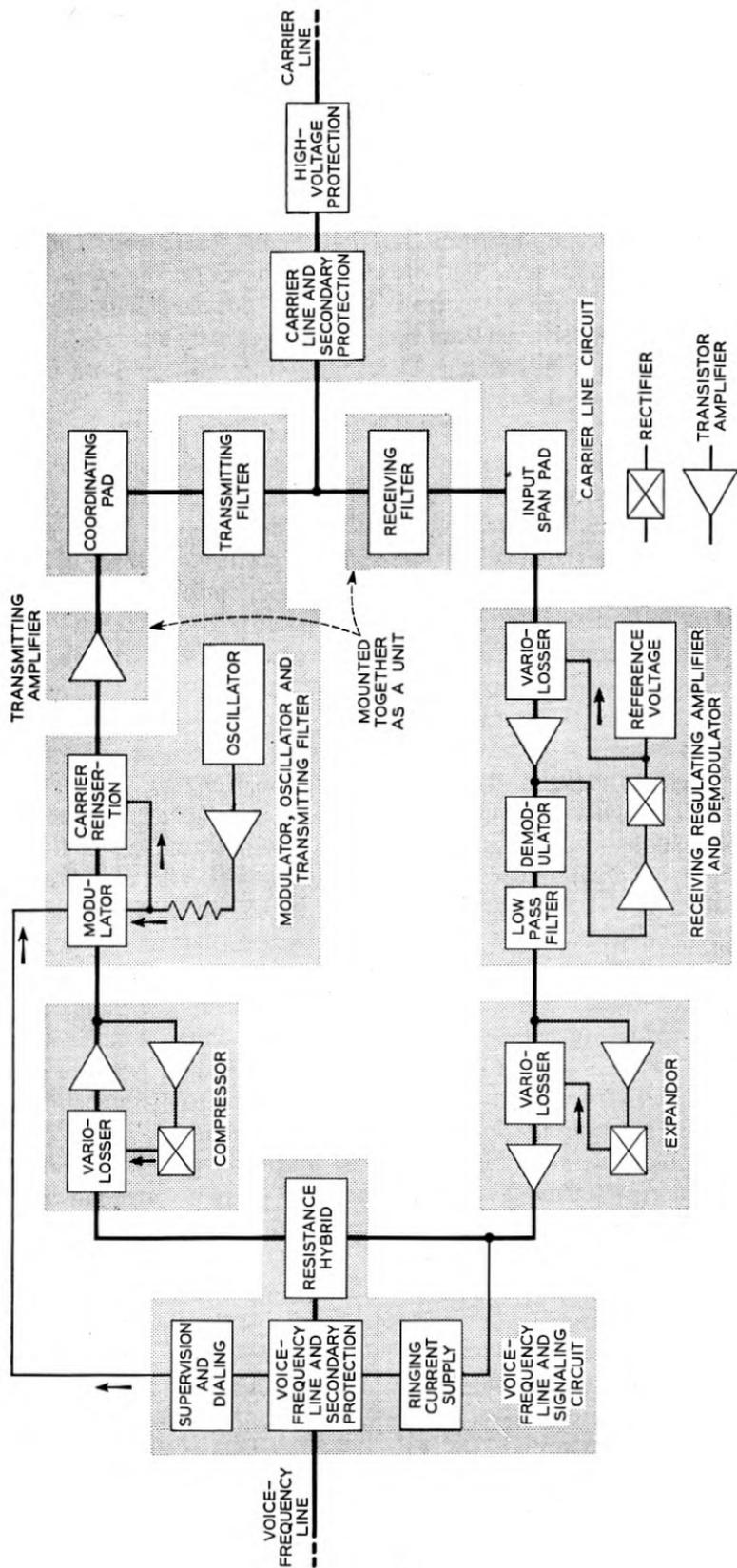
Fig. 2 — P1 Carrier remote terminal block diagram.

354

3.2 Use of Transistors

Transistors were chosen for use in the P1 system because they are low voltage, low power devices as compared to electron tubes suitable for transmission circuitry. Also, transistors are expected to be lower in cost and inherently longer life devices than electron tubes, thus contributing to reduced initial and operating costs.

The dc power requirements for the P1 system, using transistors, may be compared to those for a channel terminal in the Type N1 system as an indication of the dc power saving that has been achieved with the P1 system. A transistorized P1 terminal requires about 1.2 watts while it is in operation compared to 40 watts required for an N1 terminal,
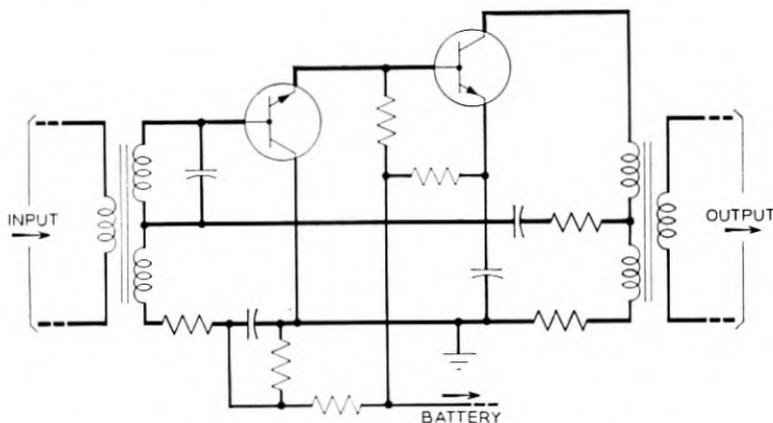

Fig. 3. — P1 transistor transmitting amplifier circuit.

which represents a substantial power reduction achieved by the use of transistors. Because part of the P1 terminal is turned off during idle periods, the average power required over a day is about 0.9 watt.

During the development of the P1 terminals it was found that a single design of a transistor amplifier could be used in several different places. These included the compressor and expandor amplifiers, the transmitting amplifier and the input portion of the receiving amplifier. The circuit for that amplifier is shown in Fig. 3.

The amplifier uses Western Electric NPN grown junction type transistors coded 4B for the voice frequency amplifiers and 4C transistors for the carrier amplifiers. The first transistor is connected as a common collector and the second as a common emitter. By using them in this manner it is possible to employ the same type of transistor in both stages. Feedback is obtained by using hybrid coils at both the input and output

of the circuit in much the same manner as for electron tube circuits. One significant difference is that in this transistor circuit only the second transistor introduces a 180-degree phase shift. This permits both input and output coils to return to a common ground as in a three-tube electron-tube circuit and thereby avoids the circuit complications of a two-tube circuit where one of the coils must float off ground. A simple resistance interstage is used and battery filtering completes the circuit.

3.3 *Low Voltage Protection*

Use of transistors gave rise to the need for supplementary protection from voltage surges on the line below those for which conventional carbon blocks afford protection. This additional protection was obtained by using the reverse voltage breakdown characteristics of newly developed silicon-aluminum junction diodes as shown in Fig. 4. Protection is provided in the 50- to 1,000-volt range by the diodes and above a nominal value of 750 volts by the carbon blocks. During the normally short period of operation the small diodes carry a current of up to 10 amperes.

3.4 *System Levels and Carrier Line Loss*

The carrier frequency output power of the transistorized transmitting amplifier in the terminals was set at +6 dbm. This level was limited primarily by the power handling capabilities of the transistors used. Because of the loss of the secondary protection circuitry, band filters, and the line transformer, this became +4 dbm at the carrier line terminals. This is equal to the highest carrier power transmitted by the Type N1 carrier system. With 50 per cent modulation of the carrier, the effective sideband level at the transmitting line terminals is only 2 db below that transmitted by the Type O carrier system, the most recent carrier system used for open-wire long distance trunks of the Bell System.
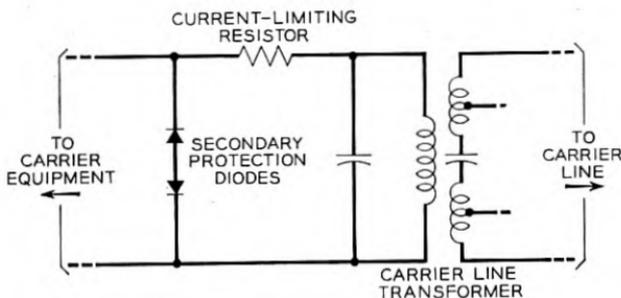

Fig. 4 — Secondary protection circuit in carrier portion of P1 carrier terminal.

The +4 dbm output level coupled with noise and crosstalk considerations indicated that 30-db bare carrier line loss between terminals would be possible. A survey of existing and planned Bell System rural telephone lines indicated that substantial amounts of entrance cable and open wire would be encountered in potential carrier layouts. Calculations of carrier frequency loss of those facilities showed that 30-db loss would not be sufficient to care for all of the necessary rural applications, which confirmed the need for carrier repeaters.

3.5 *Compandors*

Compandors were incorporated in the P1 system because their several advantages more than offset their added cost. The crosstalk and noise advantage provided by their use reduced the need for expensive line treatment to reduce crosstalk. In addition, the compandor noise advantage permitted lower received carrier levels to be used, thus increasing the permissible carrier line loss. Compandors also eased the requirements on terminal and repeater filters, thus reducing filter cost.

The compandor in the P1 system is a simplified version of the syllabic compandor used in Type N1 and O carrier systems, but its performance is comparable to those units. The new problem of matching the compressor and expandor characteristics in P1 terminals operating in different ambient temperatures has been simplified by the use of silicon-aluminum junction diodes in the compandor variolossers and control circuits.

3.6 *Channel Regulation*

Channel regulation was necessary to provide satisfactory transmission performance and keep maintenance adjustments to a minimum. The regulation was designed to compensate for daily and seasonal carrier circuit net loss variations caused by changes in line attenuation with temperature. It would be desirable to have the terminal regulation range equal to 30 db, the maximum line loss that can be spanned between the terminals, to ease engineering layout considerations. However, cost considerations led to a 15-db range, with span pads used where required by system layout to adjust the received carrier power to the center of the range of the regulator.

The regulation in the receiving amplifier is of the backward-acting type. A reference control signal, derived from the receiving amplifier output, is used to vary the loss of the balanced diode variolosser at the amplifier input. The regulator "stiffness" of 1.6-db change in channel voice frequency output for 15-db variation in carrier input is obtained

Fig. 5 — Plain-line block schematic.
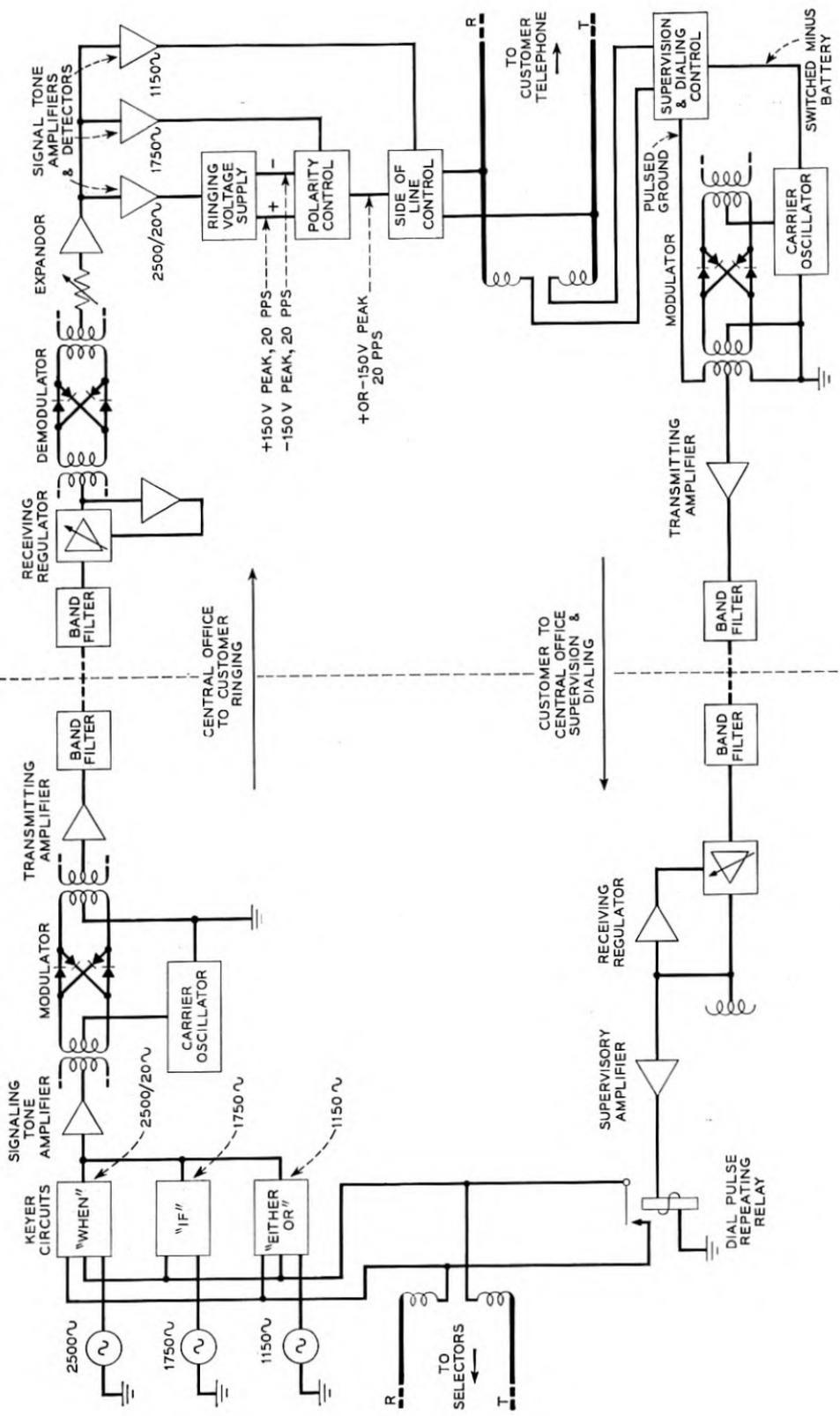
by the combination of the rectified control signal voltage exceeding the reference voltage of a silicon-aluminum junction diode and by the expansion characteristic of the variolosser. The variolosser uses a specially coded set of the silicon diodes which are matched for both ac and dc characteristics. Modulation products introduced by the variolosser have been kept below those produced in the associated receiving demodulator.

3.7 *Signaling*

The need to transmit customer signaling information over a carrier channel required the development of means of passing dialing and supervision signals toward the central office. It also required passing ringing information to the remote terminal for the types of multiparty ringing generally used in the Bell System, including four-party selective service, eight-party semi-selective service and divided code ringing.

These requirements were met in such a way that the carrier system can be inserted into a normal voice frequency circuit and function without requiring any change in the existing signaling equipment in the central office or in the customer's telephone. The central office terminal is activated by 20-cycle ringing signals which are reproduced at the remote terminal. The remote terminal is activated by switchhook signals and dial pulses which are reproduced at the central office terminals. Thus, the two directions of signaling require completely different circuits. A block schematic of the arrangement used is shown in Fig. 5.

3.7.1 *Ringing*

The customer signaling originating in Bell System central offices consists of 20 cycles superimposed on plus or minus battery and applied between either tip or ring and ground. These signals control the transmission over the P1 carrier system of three in-band frequency tones, the proper combination of two of them serving to select the party to be rung from the far end. The third tone (2,500 cycles), modulated at a 20-cycle rate, carries the information as to whether 20-cycle ringing is present or absent. In-band frequencies were chosen to encode ringing information for transmission over the carrier channel because of the substantially lower cost of in-band filters as compared to those required for out-of-band transmission.

The three signaling tones are generated by three transistor tone oscillators incorporated in a P1 central office terminal. One set of three oscillators can be arranged to supply four central office channel terminals.

The transmission of the tones is controlled by three diode-operated
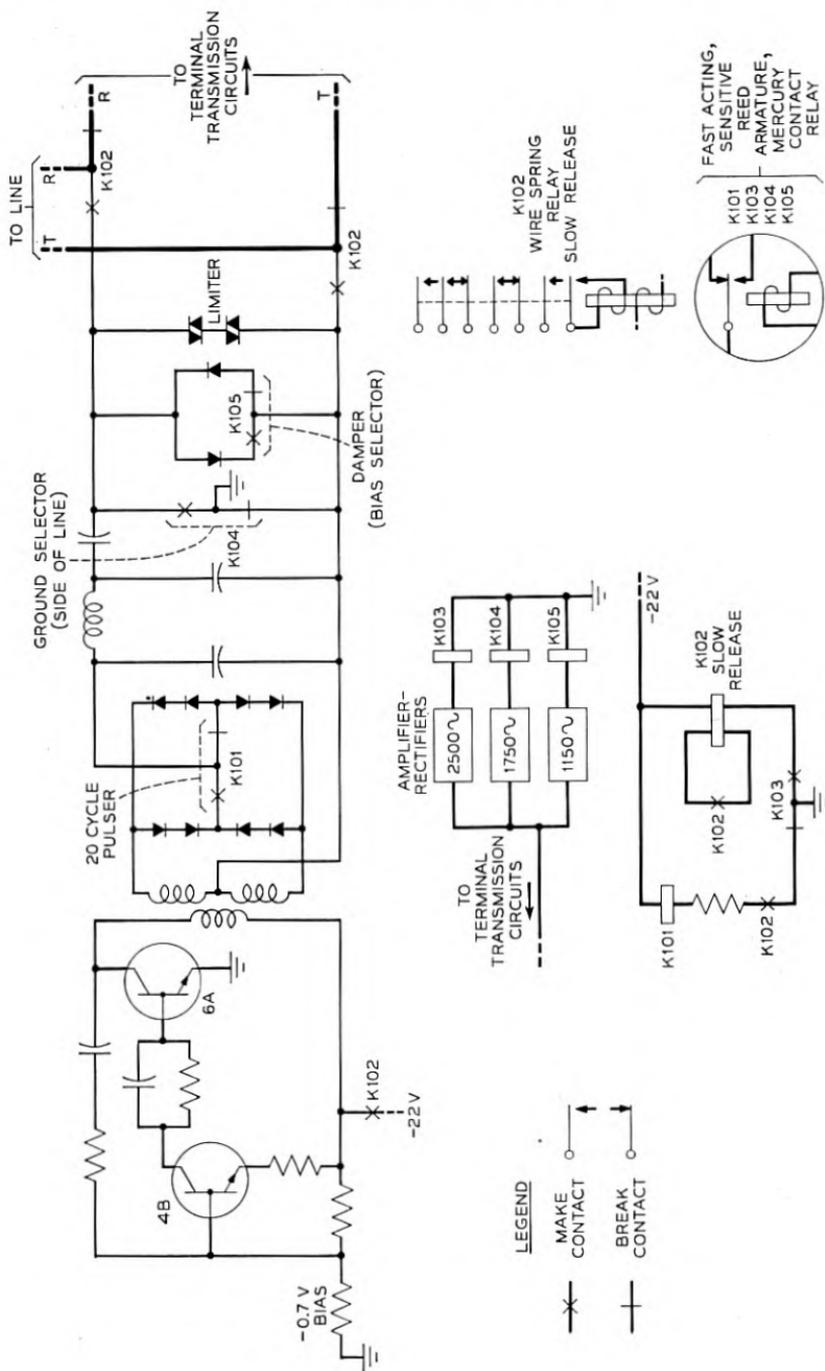
Fig. 6 — Remote terminal 20-cycle ringing generator.

keyers which function independently, depending on the nature of the ringing signal. The 2,500-cycle keyer responds to 20 cycles applied to either the tip or ring conductors. The gating diode is back biased about 3 volts to prevent random noise peaks from operating it. The 1,750-cycle keyer responds to any ringing signal applied to the tip circuit. A diode oppositely poled to the gating diode has a high breakdown so that any reverse voltage peaks leaking through to it will not open the gate. The 1,150-cycle keyer responds to 20-cycle ringing voltage superimposed with either plus bias voltage applied to the tip or with minus bias voltage applied to the ring conductor.

At the remote terminal the signaling tones are each selected at the output of the expandor by tuned circuits, amplified by a transistor and rectified to activate relays controlling the customer ringing. The 2,500-cycle tone interrupted at a 20-cycle rate controls the remote ringing generator, the 1,750-cycle tone determines whether ringing is to be on the tip or ring side of the line, and the 1,150-cycle tone whether the bias applied to the line is positive or negative.

The ringing power at the remote terminal is provided by a 3,000-cycle transistor oscillator which uses a 2-watt 6A transistor in the second of its two stages, as shown in Fig. 6. The rectified output of the oscillator is pulsed at a 20-cycle rate by a relay controlled by the 2,500-cycle inband tone and applied to the line through a low-pass filter to reduce the harmonic content of the ringing signal. Positive or negative bias is provided from one of two clamper diodes. In order to obtain sufficient power from the ringing generator, two electrolytic capacitors are used in a voltage doubler configuration. The ringing generator draws nearly 500 mils of battery current which, by P1 standards, is a heavy power drain. In order to keep this drain to a minimum, the ringing generator is activated only during the ringing period. Also the generator is connected to the customer's line only during the ringing period to remove its shunting effect on the talking circuit.

3.7.2 *Supervision and Dialing*

Carrier on-off signaling was chosen to transmit supervision and dialing signals from the customer to the central office. This method was used because of the ease of implementing it and because of savings in dc power drain at the remote terminal achieved by transmitting the carrier from that terminal to the central office only during the off-hook condition.

An off-hook signal on the voice frequency extension of the remote terminal, caused by the customer lifting his handset, is used at the remote terminal to activate the transmitting amplifier and to remove a short-

circuit from its input. This results in carrier being transmitted to the central office terminal, where it causes relays in the terminal to recreate the customer's line short across the line connecting the central office carrier terminal and the central office switching equipment.

Dialing at the customer's instrument alternately opens and shorts the voice frequency extension at each dial pulse. Opening of the line operates a relay in the remote terminal which short-circuits the transmitting amplifier input and causes the relays in the central office to follow the pulsing of the received carrier, recreate the dial pulses there, and operate the central office switching equipment.

3.8 *Repeater*

Repeaters are used in the P1 system whenever the line transmission loss exceeds the maximum that the terminals can accommodate. The repeaters use transistors for gain instead of electron tubes, but otherwise are schematically very much like previous repeaters as shown in Fig. 7. The two directions of transmission have similar functions differing only in the frequency band that is amplified and the options that are used in the gain regulating circuits.

Identical high-low pass directional filters at each end of the repeater separate the directions of transmission into the high and low frequency groups. Optional phase correction sections for these directional filters are used along a line to improve the phase characteristics in the cut-apart region. The directional filters are connected to the line through the same line matching coils and secondary protection circuits used in the terminals. Repeater input span pads are used to build out the line loss to its
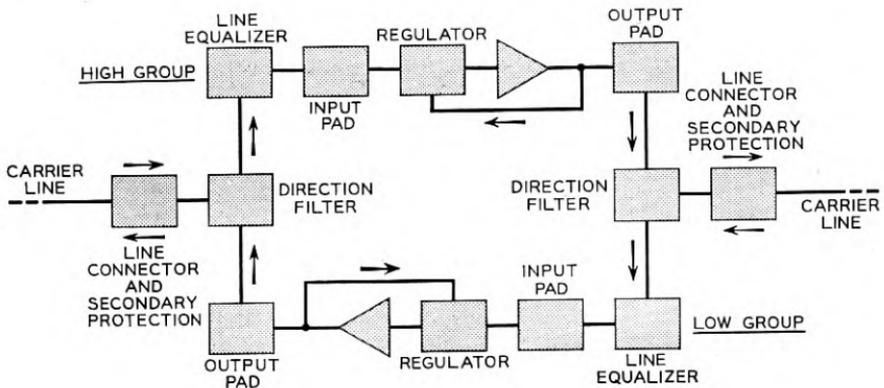

Fig. 7 — P1 repeater block schematic.
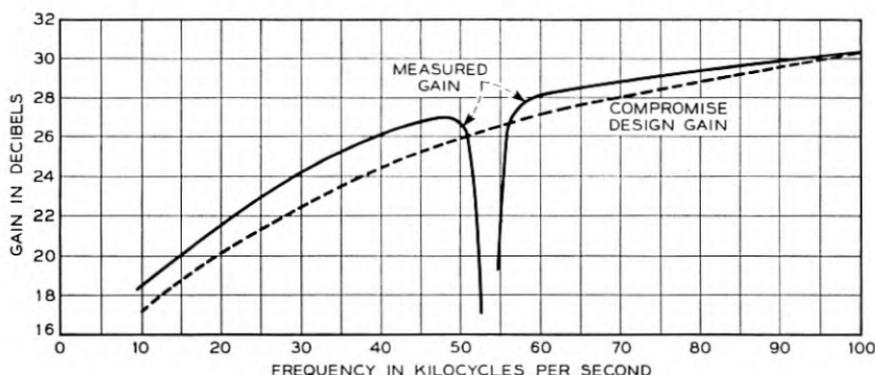
Fig. 8 — P1 repeater gain-frequency characteristic.

proper value for the nonregulated repeater and to adjust the power of the received carriers to the center of the regulator range for a regulated repeater. The output span pads are used where it is necessary to adjust the repeater output power in order to equalize levels between a P1 system and other P1 systems or other types of carrier systems operating on the same open wire line. These pads provide attenuation in 2 db steps up to 30 db.

The repeater amplifiers were designed to have a wide enough frequency band to cover both high and low groups of frequencies, so that each repeater contains two identical amplifiers. Each amplifier has three transistors with each stage connected as a common emitter. Western Electric Company PNP 7B and 6B transistors are used in the first and last stages, respectively, and a NPN type 4C transistor is used in the second stage. Local feedback is required around each transistor to reduce the gain spread and phase variations among units. Overall feedback is obtained around the three transistors with hybrid coils at input and output.

The repeater equalizer characteristic represents a compromise for several types of transmission facilities generally encountered in the rural plant. The equalizer design also covers both the high and low frequency groups so that identical equalizers are used for both the high group and low group sides of the repeater.

A preliminary characteristic for the overall repeater gain is shown in Fig. 8 plotted against the design objective. There is a significant departure in shape only at the cut-apart frequencies. This will be corrected sufficiently to permit as many as four repeaters to be used in tandem. As the design objective is a compromise of the loss of several types of lines that may be encountered in the use of this system, the departures
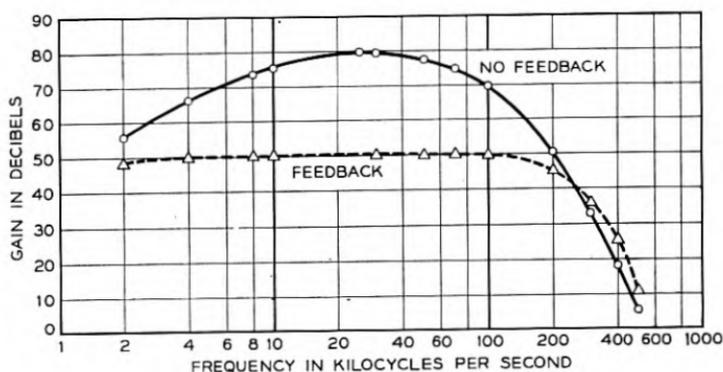
Fig. 9 — P1 Repeater amplifier gain-frequency characteristic.

in system performance may vary considerably from that shown. The repeater amplifier gain frequency characteristic, plotted in Fig. 9, shows a non-regenerative peak gain of the three-stage transistor amplifier of 80 db and a feedback gain characteristic of 50 db. This provides 20 db or more of feedback over the transmitted band to produce the necessary operating stability with temperature and power supply variations, and a working value of modulation suppression.

3.9 *Repeater Regulation*

Repeater regulation will be furnished as an option where variations in line loss exceed the terminal regulating range. It will usually be necessary on systems employing more than one repeater in order to control noise performance. Repeater regulation in the direction of transmission from central office to remote terminal is controlled by the total carrier power of the channels working on one system. In the opposite direction, the repeaters will regulate on a low level carrier frequency pilot because the channel carriers are not always present in that direction of transmission due to their signaling function. The pilot frequencies are shown in Fig. 1.

The repeater regulator, shown in schematic form in Fig. 10, functions in much the same manner as the terminal regulator. The principal differences between the two regulators arise from the requirement that interchannel modulation must be appreciably less than 1 per cent in the repeater. To limit the contribution of the repeater regulator to a small value, the variolosser operates into a lower impedance and at a higher control current than used in the channel regulator.

The input section to the control amplifier is either a flat bridging pad for the case where all carriers are always present on the line or a pilot pick-off filter and its associated single transistor amplifier where carriers are turned on and off for supervision. The latter extra amplifier is necessary because the pilot power is 20 db below the power in each normal carrier.

The regulator stiffness provided by the repeater regulator results in a variation of 1 db in output carrier power for a 10-db variation in received total carrier or pilot power.

4. COMPONENTS

Development of the passive components of the P1 carrier system, including the various filters and other networks, were influenced by three major considerations. The manufacturing cost had to be as low as possible consistent with the traditional standards of Bell System service life. The components had to lend themselves to maximum utilization of the printed wiring techniques to be used as the basic equipment method. And lastly, advantage wherever possible was to be taken of the fact that transistors are low power devices.

4.1 *Filters*

Component-wise, filters are the most important single assembly determining the first cost of a carrier system employing frequency division multiplexing and frequency separation for obtaining equivalent four-wire
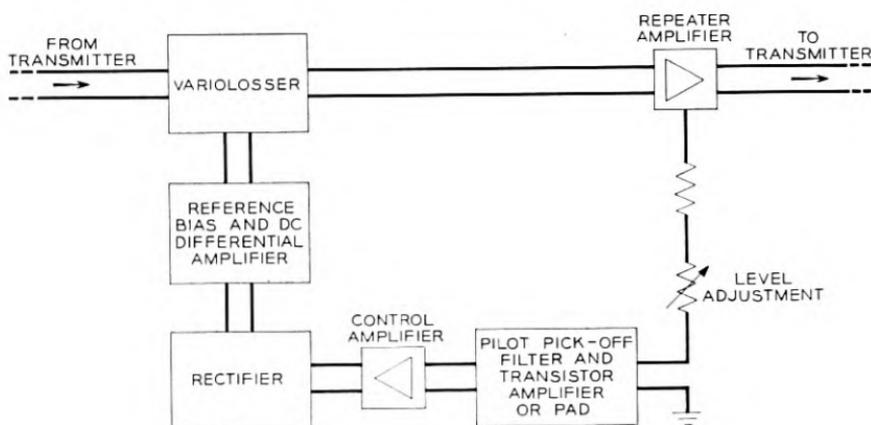

Fig. 10 — P1 Repeater regulator block schematic.
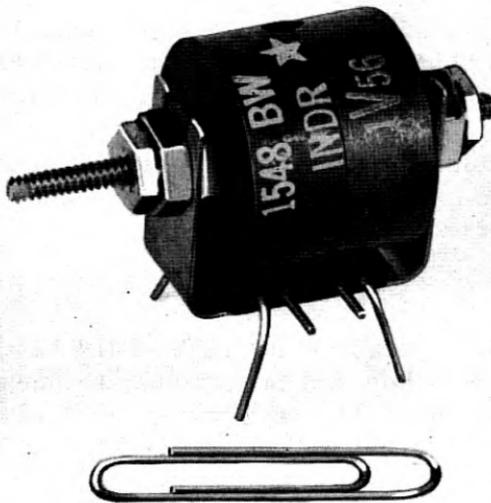
Fig. 11 — Miniaturized inductor for P1 carrier.

operation on the line. Past experience has shown that one-quarter or more of the first cost is often chargeable to the various filter. The decision to employ double sideband modulation was largely based on the knowledge that when frequency space is available the double sideband channel filters are generally the least expensive.

With this decision made, every effort was directed toward the achievement of channel filter designs of maximum efficiency in element utilization. Inexpensive wide-limit capacitors were used, and the desired performance achieved through the use of an adjustable ferrite inductor expressly developed for the P1 system. The filters are rapidly adjusted in the manufacturing process using visual display testing circuits.

4.2 *Inductors*

The inductor which makes this possible is shown in Fig. 11. It is designed for printed wiring use and provides a wide range of inductance while maintaining excellent "Q" performance in the carrier and voice range. This is accomplished in a single basic design by so selecting the winding for particular nominal inductances that the air-gap adjustment remains at or near its most efficient setting. Inductors of this type were

used not only in all the channel, demodulator, and signaling filters in the terminal and in the directional filters at the repeater, but also in the channel oscillators and other parts of the circuitry where an inexpensive, adjustable element offered manufacturing or service advantages.

4.3 *Capacitors*

Most of the wide-limit capacitors used in the filters are of the commercially available molded mica type. Where the capacitance values would require large and expensive mica units both in filters and other parts of the circuit, newly available foil-Mylar capacitors were used. These take the form of very small pigtail units in a range of physical sizes similar to those of the solid tantalum capacitors described below. The Mylar capacitors have low working voltages in these miniature sizes and can
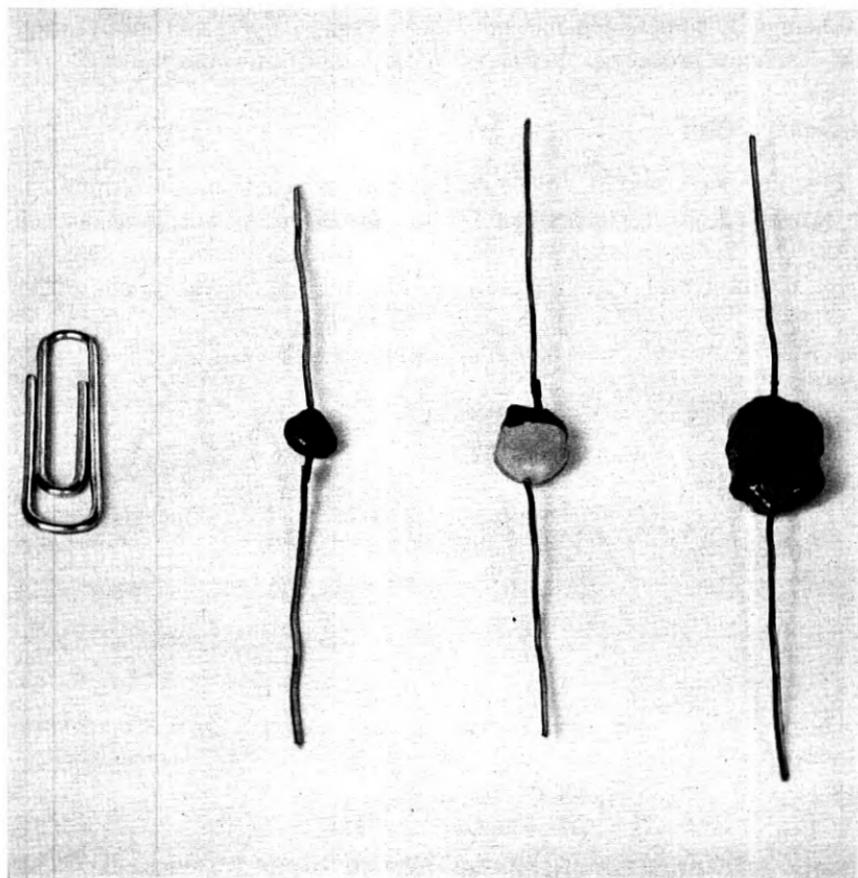

Fig. 12 — Prototype solid tantalum capacitors for P1 carrier.

be employed because of the low voltage protection provided for the transistorized circuits. Both cost and space savings are realized in these capacitors since no cans or potting are required due to the stability of the Mylar dielectric under moisture exposure.

Another new type of capacitor has found widespread use in the P1 system. This is a solid tantalum electrolytic capacitor used in place of the usual paste or liquid electrolytic capacitor. The solid electrolyte is manganese dioxide deposited upon the capacitor surfaces. The anode is made from tantalum metal and upon its surfaces is deposited the tantalum oxide which forms the dielectric. The cathode is an enveloping metal completing the capacitor structure. This new design of capacitor is now available in values up to 100 microfarads in a very small volume. It is expected to be less expensive than other electrolytic capacitors while at the same time providing a rugged structure which is relatively inert electrochemically and which has better stability in operation and storage. Fig. 12 shows prototype models of typical solid tantalum units.

4.4 *Transformers*

Transformer needs in the P1 system are met by two miniature structures which were made possible by the use of low power transistor circuits. The carrier frequency units employ a manganese zinc ferrite core, a spool winding and wire terminals which permit assembly on printed
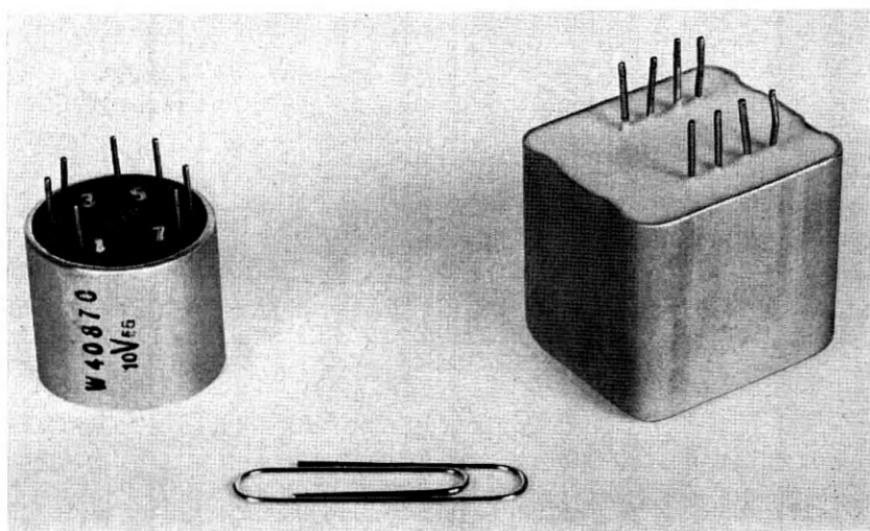

Fig. 13 — Carrier and voice frequency transformers for P1 carrier.
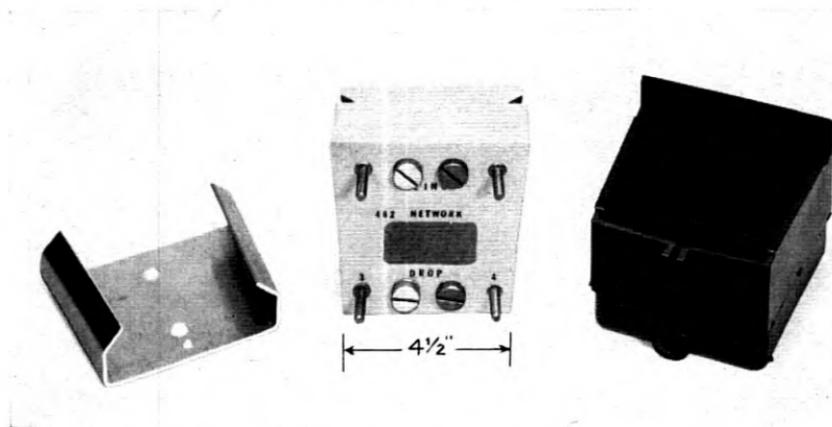
Fig. 14 — Example of P1 carrier line network.

wiring boards. They are potted with an asphalt compound in a cylindrical aluminum can. The voice frequency transformers are wound on laminated core structures of permalloy. The units are potted in an epoxy resin in rectangular aluminum cans. The terminal plate carrying the wire terminals for mounting is a cast unit of a styrene polyester. Both types of transformer are shown in Fig. 13.

4.5 *Line Networks and Filters*

Also deserving mention is a new series of line networks and filters (which do not form part of either the terminal or repeater equipment) with specific functions described in Section 7. All of the networks have been designed with the same type mounting arrangement shown in Fig. 14 with two sizes used depending on the number of components housed. The networks are cast in a styrene polyester. High voltage protection is self-contained and sturdy terminals are provided for bridle wire connection. By means of side slots in the casting the network is mounted on a wedge-shaped holder which is fastened to the crossarm or pole. A flexible rubber cover is snapped over the face of the network to protect against weather effects.

5. EQUIPMENT ARRANGEMENTS

The emphasis placed on economy in this development project made it necessary to consider a number of different approaches before deciding on the physical arrangement provided for both central office and pole mounted equipment. At both locations the terminals for each channel
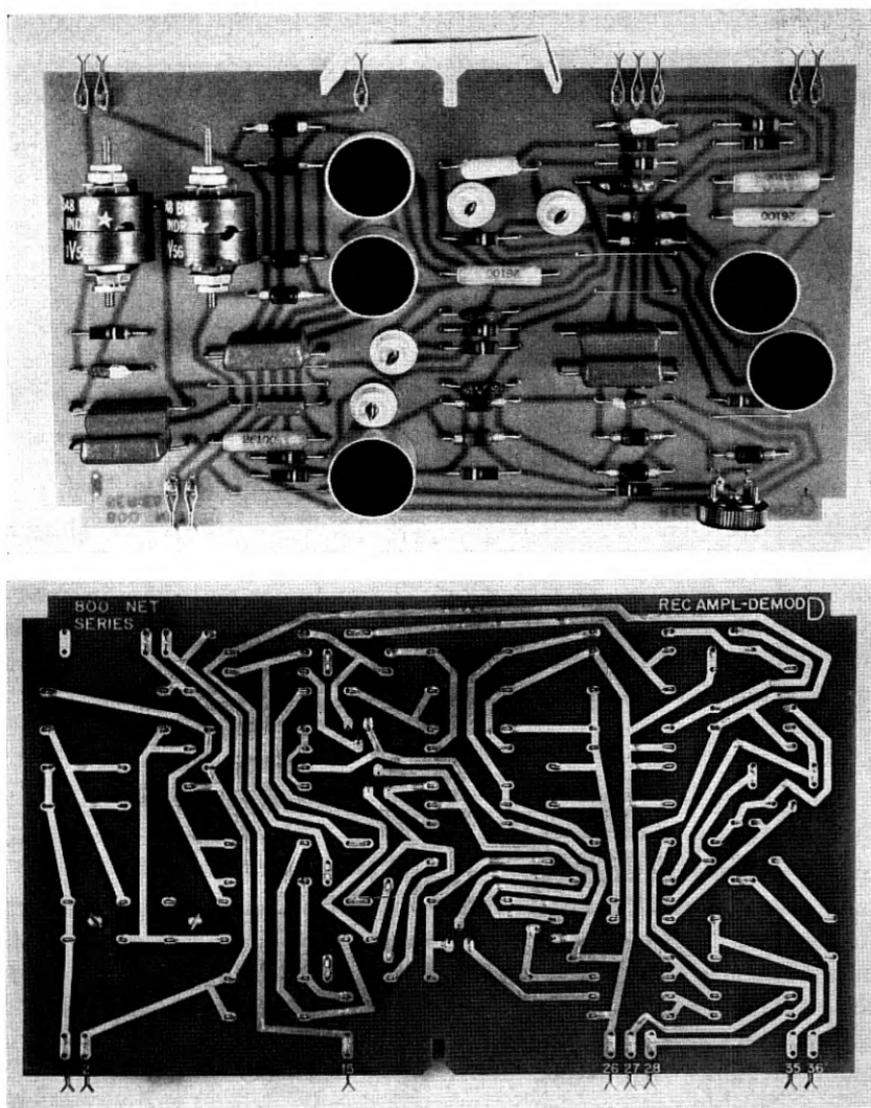
Fig. 15 — Front and back of typical printed wiring board.

were treated on an independent basis, thus providing maximum flexibility in application. While the use of transistors made it possible to take advantage of miniaturized components, the major emphasis in design has not been on miniaturization; instead it has been to achieve low manufacturing costs, simplicity of engineering and installation, and a minimum of maintenance effort. The recent trend toward automation in

manufacture of electronic equipment has also influenced the design to a great extent.

5.1 *Printed Wiring Boards*

To best meet these objectives, use has been made of plug-in units which have proved successful in other carrier systems, such as the N1 and O. The assembly technique used here, however, is an entirely new approach for carrier equipment in that the plug-in unit consists of a printed wiring board on which all components are mounted. Printed wiring, which is a comparatively new engineering technique, was selected because of its applicability to automatic assembly, including mass soldering of connections. In addition, the use of printed wiring greatly simplifies testing and inspection and assures a more uniform product. The two sides of a typical printed wiring board are shown in Fig. 15.

5.2 *Interconnection of Boards*

The interconnection of the various plug-in units or printed wiring boards, required to make up a complete P1 terminal or repeater, is accomplished by means of a wire connector specifically developed for this project. Basically, the connector consists of a number of accurately spaced bare wires running parallel to each other and imbedded in cross member strips of insulating plastic material. At fixed intervals the wires are exposed, and this is where contact is made to terminal connectors mounted on the printed wiring boards. These terminal connectors, shown in Fig. 16, are made of spring tempered phosphor bronze
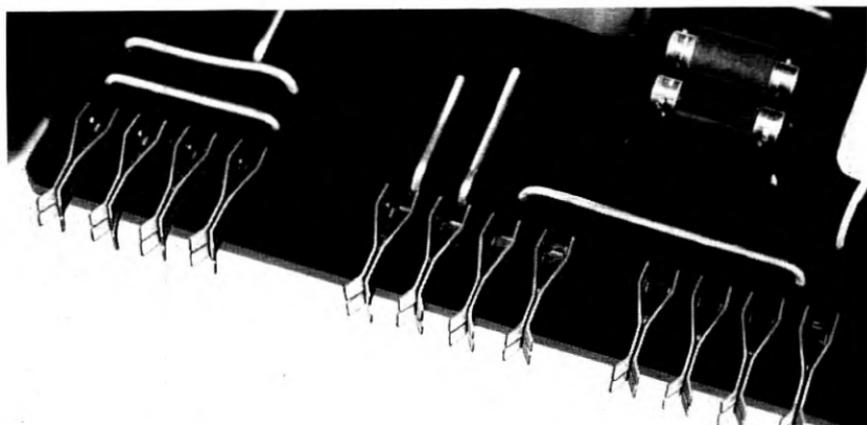
Fig. 16. — Closeup of terminal connectors.

and consist of bifurcated cantilever springs, providing a total of four contacts for each connection.

As can be seen in Fig. 17, the wire connector is actually a molded phenolic box into which are inserted all of the printed wiring boards that make up a complete terminal or repeater. The terminal connectors on the boards thus engage the wires that are imbedded in the back of the connector. To insure contact reliability, a finish of precious metal is provided on both the wires of the connector and the terminal connectors on the board. Additional flexibility in the interconnection of the boards is
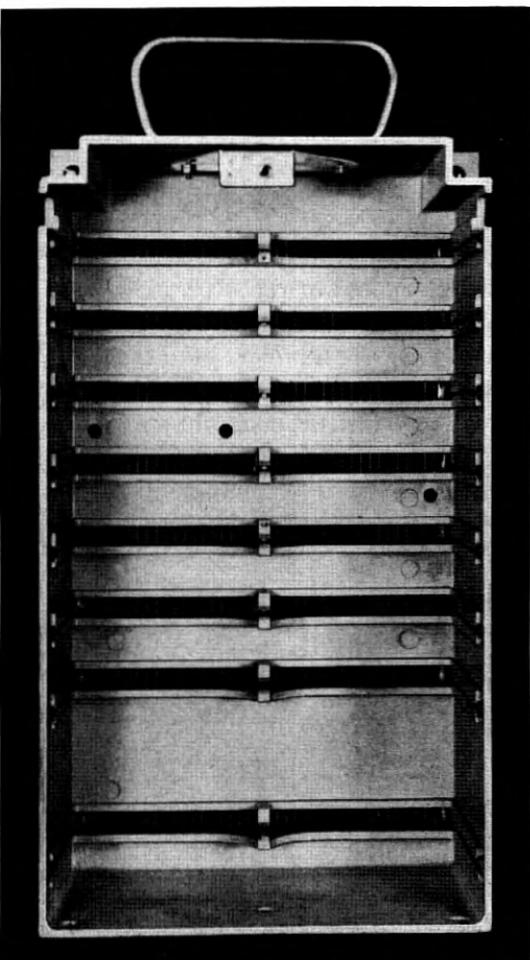
Fig. 17 — Prototype model of connector box unequipped showing grid wires.
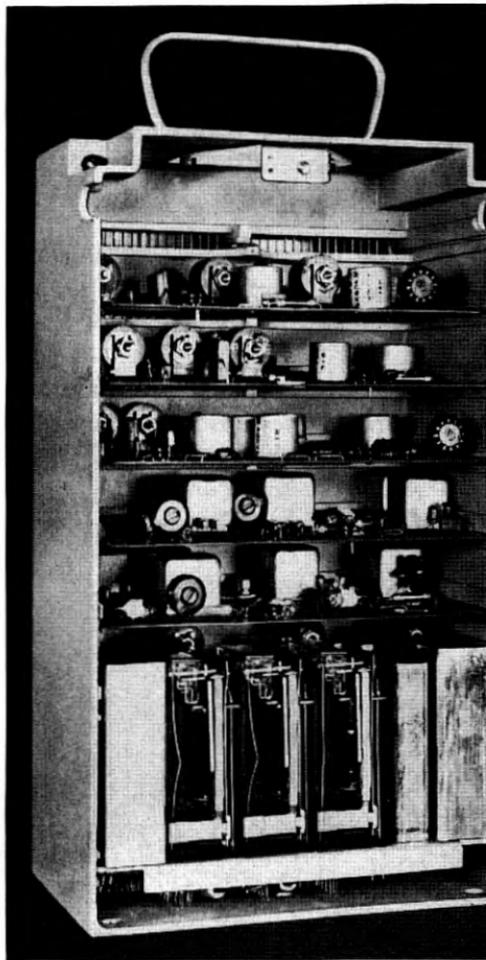
Fig. 18 — Typical terminal networ mounted in a prototype connector box

obtained by cutting the wires at various points by simply drilling holes in the phenol structure supporting the wire.

5.3 *Terminal and Repeater Mounting*

A complete terminal ready for installation at a remote location is shown in Fig. 18. The top position in the connector is shown vacant. This is where the connections to line and power supply are made by means of another plug-in printed wiring board with attached flexible wiring for the external connections.
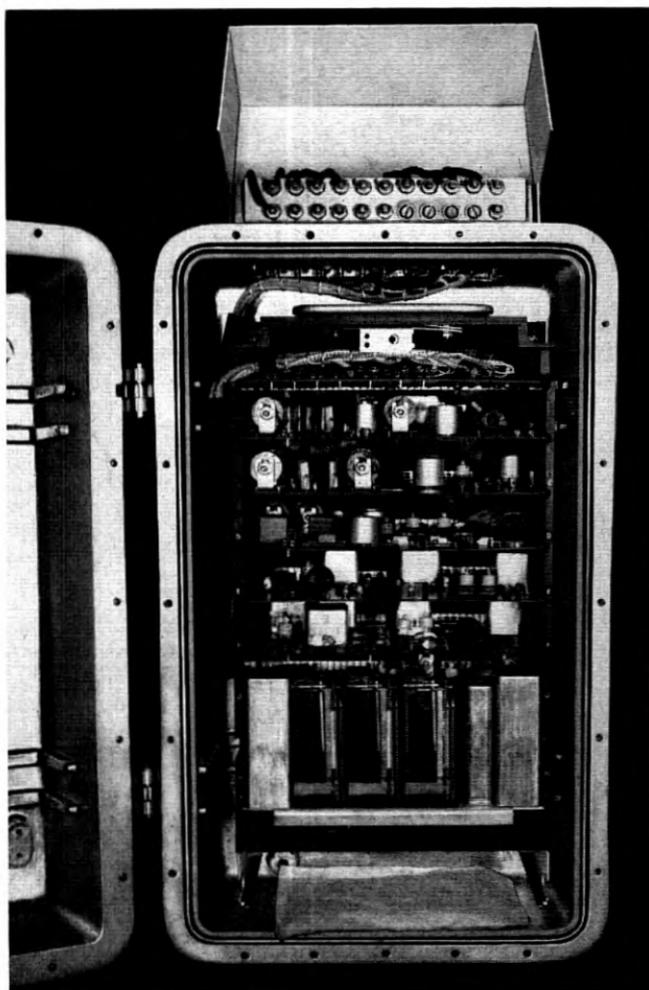
Fig. 19 — P1 carrier remote terminal in pole mounted cabinet.

The equipment described here is equally adaptable to central office mounting and pole mounting at remote locations. At the remote locations, however, it is necessary to provide the equipment with an outer housing which gives protection from all kinds of weather and even from moisture condensation. The opened housing is shown in Fig. 19. Fig. 20 shows a typical remote mounting of the housing on the left. In previous electron tube carrier systems the amount of heat generated by the equipment itself was sufficient to prevent moisture condensation. In the case

Fig. 20 — Example of remote mounting of P1 terminal and ac power supply.

of the P1 carrier, however, the heat dissipation during the idle period is less than 1 watt for the entire terminal. To prevent condensation, the housing or apparatus case is sealed by means of a neoprene gasket. To further reduce the moisture content of the trapped air, the use of a desiccant is specified. The apparatus case is made of die-cast aluminum with the outside walls finished in white enamel to keep heat absorption to a minimum. The system was designed to operate between temperature extremes of −40°F and +140°F. This limitation might necessitate the additional installation of sun shields in a few cases where extreme temperatures prevail.

The terminal equipment at the central office makes use of the same type of printed wiring boards plugged into a connector as used at the remote location. In the central office, however, the outer housing is dispensed with and the connector is mounted on mounting brackets on standard relay racks. The relay rack layouts can be arranged in a number of ways to suit the particular installation, since no shop wired bays are used. A typical 11′6″ relay rack layout will provide for 10 terminals. No line jacks or alarm features are provided and fusing may be obtained from existing fuse boards in the office. The equipment also lends itself to wall mounting in locations where relay rack space is not available.

5.4 *Testing and Maintenance Features*

One great advantage of the equipment design used in the P1 carrier system is the ease with which an entire terminal or repeater can be transported to, and installed at, a remote location. In case of trouble, the entire equipment unit, be it a terminal or a repeater, can be readily replaced. It is not expected that the maintenance man will attempt to replace an individual printed board at a remote location; however, this procedure is perfectly feasible in a central office. To facilitate the location of trouble in a unit, the various boards are provided with test points located at the outer end of the boards so as to be easily accessible to the maintenance man.

Certain precautions will have to be taken at central repair centers in replacing defective individual components in order not to damage the printed wiring. Too much heat applied by a large soldering iron will destroy the adhesive bond between the copper conductor and the phenolic board, but repair can be made under certain controlled conditions. A limited amount of wiring modifications can also be made to the printed wiring by inserting strap wires in place of components.

6. POWER SUPPLIES

The design of a carrier system with low power drain made possible the development of a low-cost, reliable dc power supply for the carrier equipment. Because the central office carrier terminal was designed to utilize standard central office voltages (24 or 48 volts), only the power supply for the remote equipment will be described here.

Early exploratory studies showed that conventional power supply designs would miss the first and annual cost objective by an uncomfortable margin. A number of unconventional approaches were studied:

(a) Storage batteries charged over the carrier line.

(b) Storage batteries placed in service with full charge and removed to a central point for recharging.

(c) Solar power plants.

(d) Wind power plants.

(e) Thermoelectric power plants.

(f) Dry cells.

In all of the above cases the power plant was either too costly, too large, or technically unfeasible, and none could prove in over the conventional conversion of ac to dc where commercial power is available. This was true despite need for a storage battery to operate the system during ac power failure intervals and to provide peak ringing power.

6.1 *AC Rectifier-Storage Battery Plant*

The basic elements of the power plant circuit, as shown in Fig. 21, are the conversion section represented by the step-down transformer T1 and
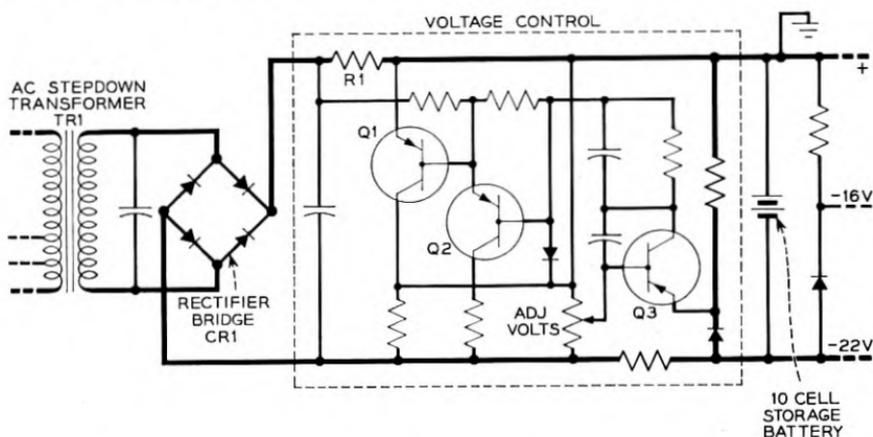

Fig. 21 — Schematic of ac rectifier-battery power supply.

the semiconductor rectifier bridge CR1, the voltage control circuit represented by that part of Fig. 21 enclosed in dashed lines, and the energy storage circuit represented by the battery.

Rectification is obtained with germanium rectifiers that are very efficient, have long life with negligible aging, and are very compact physically. The output of this rectifier is not constant, because the output voltage will vary with the ac input voltage and the dc load current drawn by the carrier terminal. Thus a regulating circuit must be provided.

The regulating network senses the voltage across the battery and compares this voltage to a reference obtained from a silicon junction diode biased in the reverse dirction.[3] Any error in the output voltage is converted to a current signal in the first amplifier stage and amplified by the second stage transistor Q2. The amplified error current is then used to control the impedance of transistor Q1 which acts as a current shunt around the battery.

The fundamentals of the operation of this regulating system are shown in Fig. 22. If the load voltage is too high, the network adjusts the resistance of transistor Q1 so that some of the rectifier output current is shunted around the load. The load voltage will then return very quickly to the regulated value. Because the rectifier circuit must not be overloaded by a discharged battery, some form of current limiting must be provided; this is automatically taken care of by resistor R1. The rectifier is capable of supplying indefinitely the current that would be drawn to charge a battery after a very long power failure.

The storage battery is shown in Fig. 23 near the bottom of the power plant housing. It is a new design with a high specific gravity sulphuric

[3] D. H. Smith, Silicon Alloy Junction Diode as a Reference Standard, A.I.E.E., Communication and Electronics, No. 16, pp. 645–651, Jan. 1955.
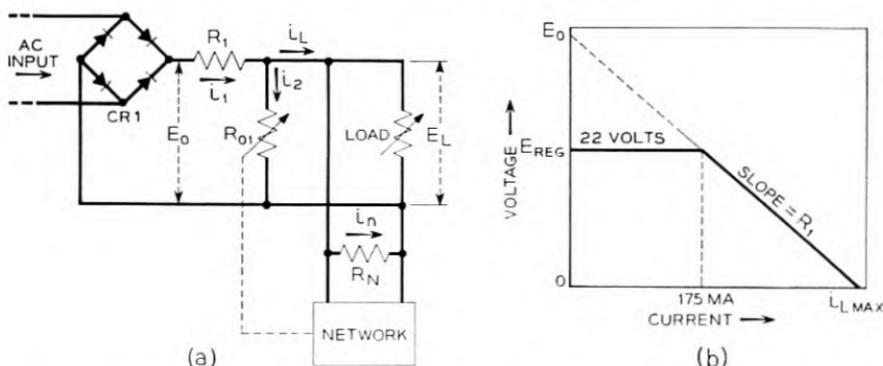
Fig. 22 — Simplified schematic and regulation characteristic of ac power supply.
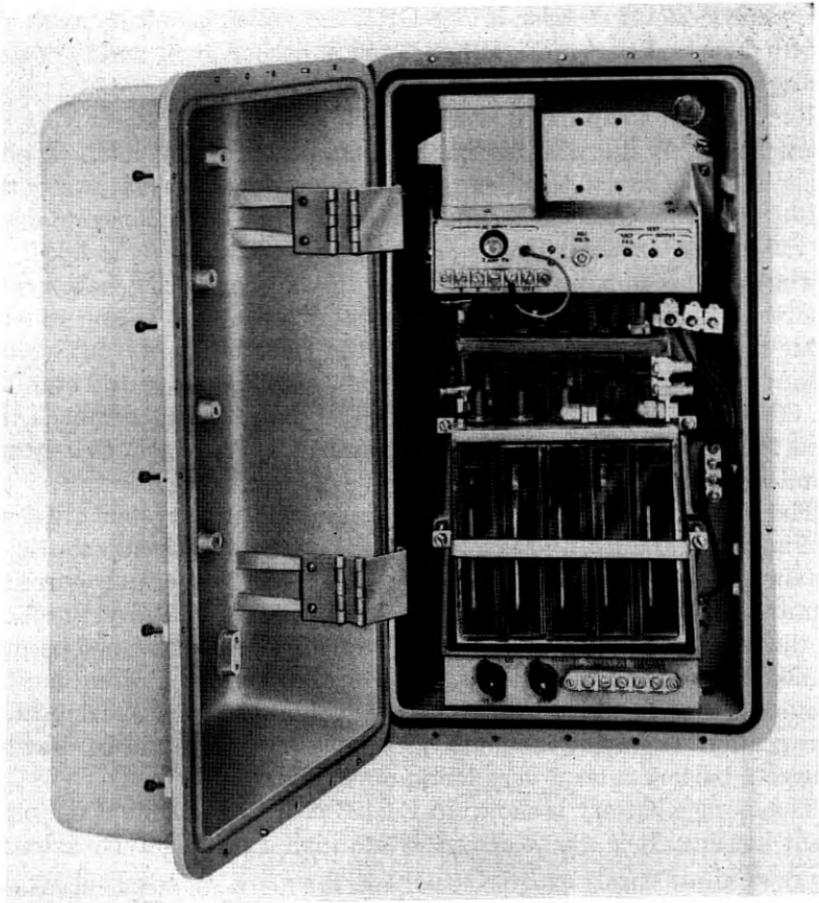
Fig. 23 — P1 carrier ac power plant in cabinet for pole mounting.

acid electrolyte for good low temperature operation and lead calcium alloy electrodes for long life. The battery has 10 cells housed in two jars of five cells each. It is operated at about 23.5 volts and weighs about ten pounds. It provides about six days' reserve for a remote terminal or about two days for a remote repeater. The battery should not freeze at temperatures as low as   40°F, but the storage capacity may be reduced 90 per cent at this extreme. The battery is mounted on steps so that the electrolyte level can be seen through the transparent plastic battery jars. Fig. 23 also shows the compact packaging of the entire power supply within the same type of aluminum housing as used for the carrier terminal. A typical pole mounted installation is shown in Fig. 20. Fig. 24 is a

close-up of the bottom of the rectifier chassis which shows the regulating network mounted on a printed wiring board.

6.2 *Air Cell Primary Battery Plant*

Because ac will not be readily available at all remote locations, an alternate power supply has been developed and this is shown in Fig. 25.
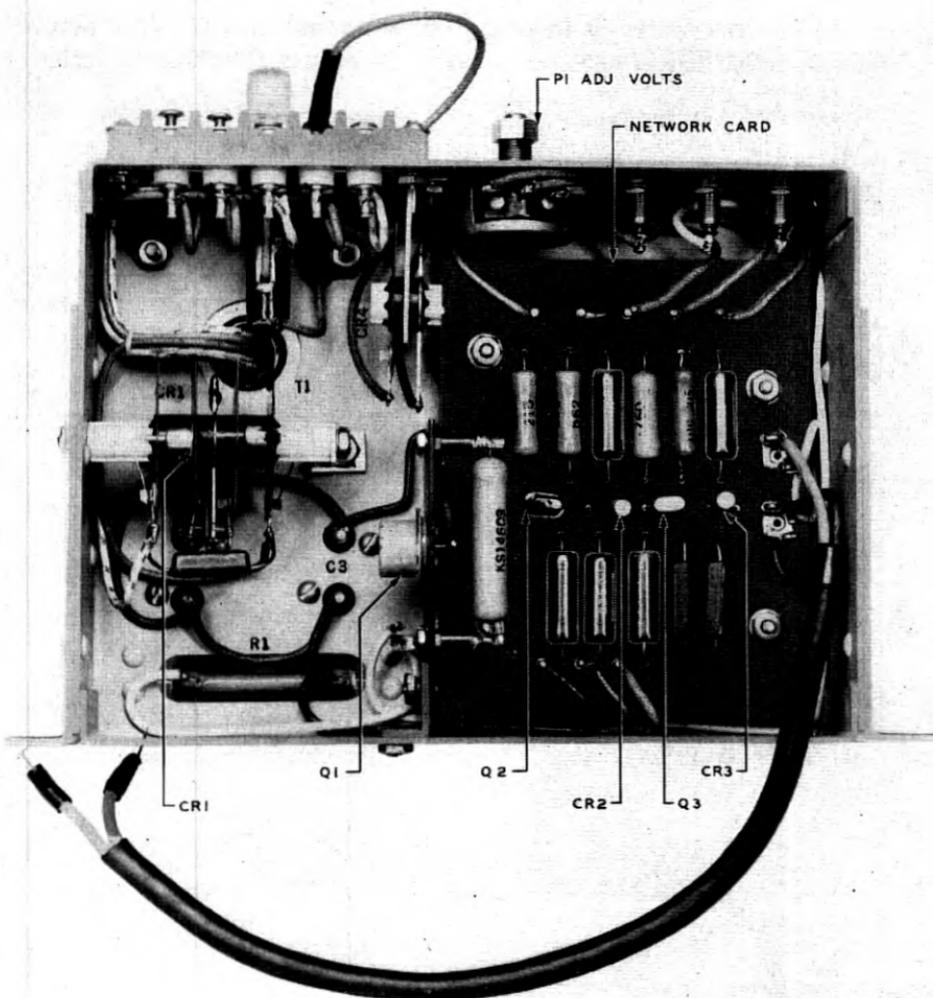
Fig. 24 — Close-up of bottom of rectifier chassis.

The alternative supply uses oxygen-depolarized primary cells having an alkaline electrolyte, and has been used for many years in railway signaling circuits and in the telephone plant. Sixteen battery cells are connected in series to provide enough power for three years of operation of a remote terminal or about one year for a remote repeater. The battery is discarded when fully discharged and is then replaced by a new battery.

7. APPLICATION OF P1 CARRIER TO RURAL TELEPHONE LINES

The P1 carrier system is to be applied to normal exchange loop plant facilities engineered in accordance with the present Resistance Design
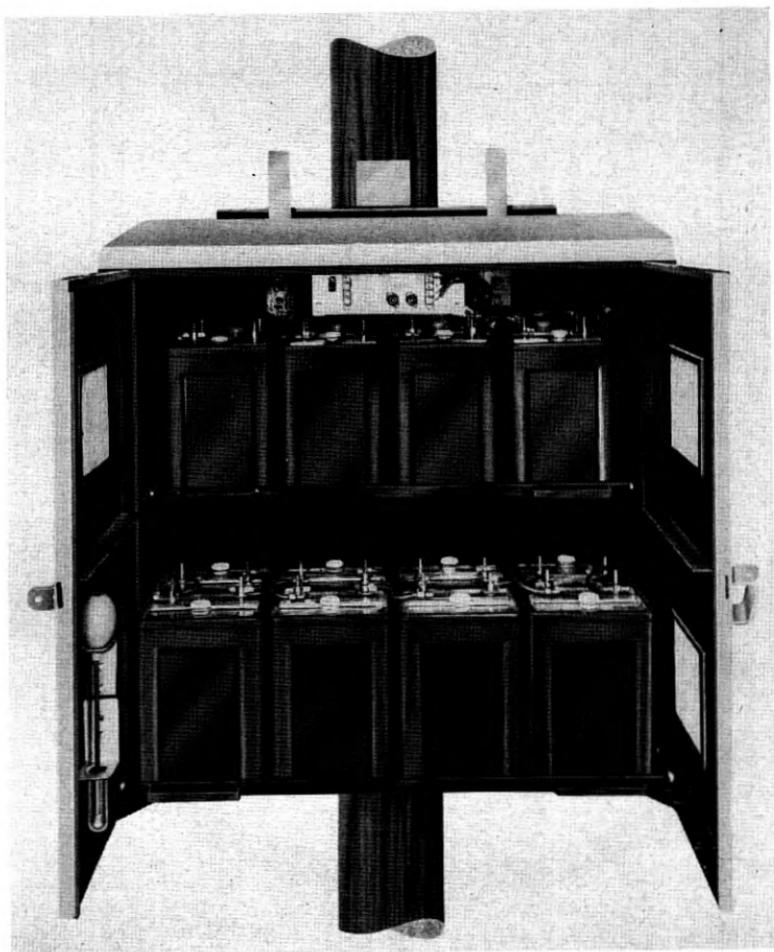
Fig. 25 — Primary battery power plant.

Methods used generally throughout the Bell System.[4] These facilities consist of mixed gauges of high capacitance cable extended at their outer ends by 109-mil steel, 104 mil-copper or copper steel open wire.

In engineering the carrier line design or carrier layout, the Plant Engineer will determine the carrier line layout necessary to meet the over-all requirements for a suitable carrier transmission path on the available physical facilities. To do so he need only be familiar with the general capabilities of the carrier system, its basic "building blocks," and the limitations that must be considered in applying the system to the physical line. The capabilities of the carrier system have been described in earlier sections. From those descriptions it can be seen that the basic "building blocks" for a P1 carrier system are:

1. Central office channel terminals
2. Remote channel terminals
3. Repeaters
4. Ac or dc remote terminal and repeater power supplies
5. Carrier line networks and filters

A carrier application of these "building blocks" is shown in schematic form in Fig. 26.

The low-pass filters or carrier blocking networks shown are placed at the junctions of the carrier line and side leads of customer drops served by physical or derived voice frequency circuits on the base carrier facility. These filters are required to reduce the bridging loss of the side leads at carrier frequencies and to keep carrier frequencies out of the customer drops to prevent annoyance to the customers. High-pass filters are provided to make the carrier line continuous at carrier frequencies, but divide it into isolated sections for voice frequency distribution.

In addition to these blocks, an autotransformer may be required at the junction of the open wire and cable. The autotransformer, either alone or in conjunction with a junction line filter, is required to eliminate reflection losses and reduce crosstalk at carrier frequencies due to impedance mismatch between the cable and open wire. The junction line filter is required to allow the carrier and physical voice frequency circuit to be used on different pairs in the cable and on the same open-wire pair beyond the cable-open-wire junction. This is necessary where the physical circuit is so long that load coils are required on the voice frequency cable pair and non-loaded cable pairs are required for carrier. A pair of junction line filters may also be used to provide a voice frequency by-pass around a repeater. As illustrated in Fig. 26, this may be necessary

---

[4] L. B. Bogan and K. D. Young, Simplified Transmission Engineering in Exchange Cable Plant Design, A.I.E.E. Communication and Electronics, No. 15 page 498, Nov. 1954.
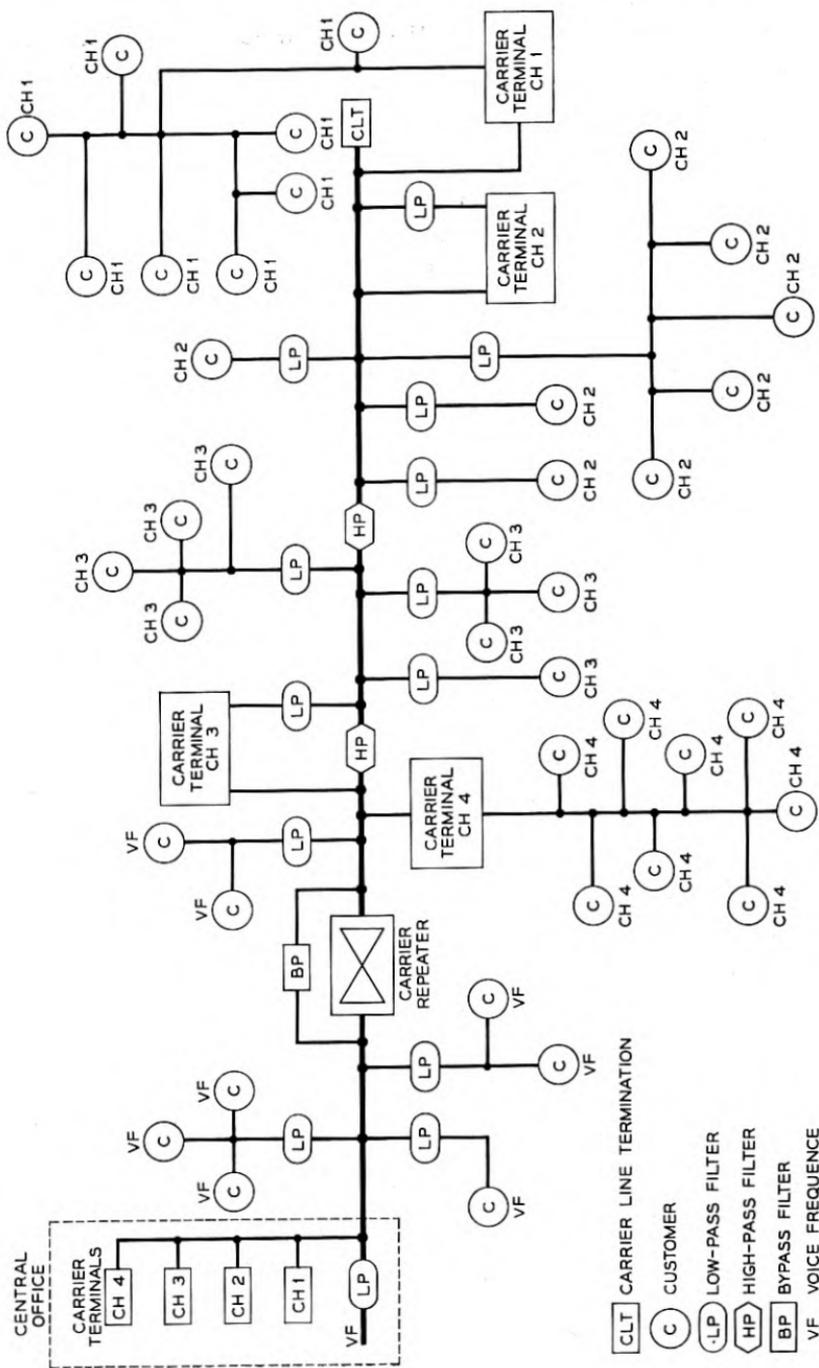
Fig. 26 — Typical P1 carrier application schematic.

CLT CARRIER LINE TERMINATION
C   CUSTOMER
LP LOW-PASS FILTER
HP HIGH-PASS FILTER
BP BYPASS FILTER
VF VOICE FREQUENCE

to serve customers beyond that point from physical voice frequency circuit.

A carrier line termination network is also provided to terminate the end of the carrier line at all frequencies and thus prevent reflections from interfering with the transmission at remote carrier terminals spaced along the line. This network and all of the other line networks are available in the pole or crossarm mounted arrangement shown in Figure 14 and described in Section 4.5.

Fig. 26 also gives examples of two types of subscriber distribution beyond the remote carrier terminals. One, wire distribution, is indicated by the voice frequency extensions of Channels 1 and 4 and the other, filter distribution, is shown for Channels 2 and 3. Filter distribution permits the carrier line to be used simultaneously for carrier transmission and voice frequency distribution of the derived voice frequency circuit, thus saving the pair of wires required if wire distribution were used.

7.1 Layout Procedure and Ground Rules

P1 carrier channel layouts for a given rural line will be based on the forecast of commercial requirements for that route. The Plant Engineer must determine the number and arrangements of channels which can be applied within the system limits to meet that forecast. The locations of remote terminals are then chosen based on customer locations, channel frequency arrangements, and the availability of commercial ac power. With the terminal locations fixed, the line losses are determined at appropriate frequencies and repeaters are specified as necessary along with any line networks and filters required for the layout.

The characteristics and limitations of the P1 system lead to certain simplified ground rules which may be used in laying out the carrier channels. Some of these rules are summarized in Fig. 27. The stackable frequency arrangement is used for non-repeatered operation, and the design of the carrier channels permits the bare line loss of each individual channel to be 30 db at the top frequency between the central office terminal and the remote terminal.

Another limit shown in the figure is that the dc loop resistance of the voice frequency extension beyond the remote terminal can not exceed 390 ohms (5 miles of 109-steel wire). The 390-ohm limit is determined by the talking battery supply requirements of the 500-type customer telephone sets when the battery is supplied from the remote P1 terminal power supply. The P1 carrier system has been designed to operate with the 500-type telephone set. The improved dialing, ringing and transmission features of that set will help to insure satisfactory performance of the

over-all carrier derived circuit. In keeping with the system objectives, the over-all transmission of a carrier channel and its voice frequency extension, using the 500-type telephone set, will be as good or better than that obtained on long rural lines using physical plant laid out by the Resistance Design Method mentioned earlier.

As shown in Fig. 27, the normal and staggered grouped frequency arrangements used for repeater operation allow 30-db bare line attenuation at the top frequency (96 kc) between the central office terminal and the first repeater or between repeaters, and about 30 db between the last repeater and each remote channel terminal at the top frequency used for that channel. Directional filter characteristics limit the repeater system can use a maximum of four repeaters for a total line loss of about 150 db at 96 kc. However, noise and crosstalk requirements will permit no more than two of the four repeaters to be used in the open-wire line, with the last cable repeater at least one mile back in the cable from the cable-open-wire junction, as shown in Fig. 27. Spacings must be limited to somewhat less than 30 db on certain line facilities such as B rural wire to insure proper terminal regulation.[5]
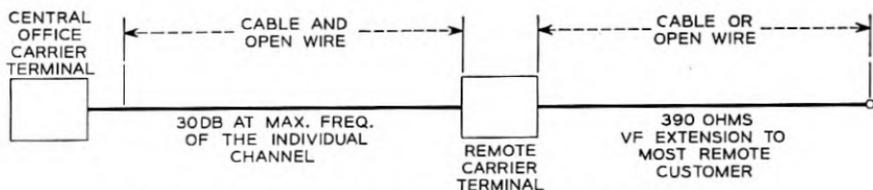
(a) STACKABLE FREQUENCY ARRANGEMENT: NON-REPEATED
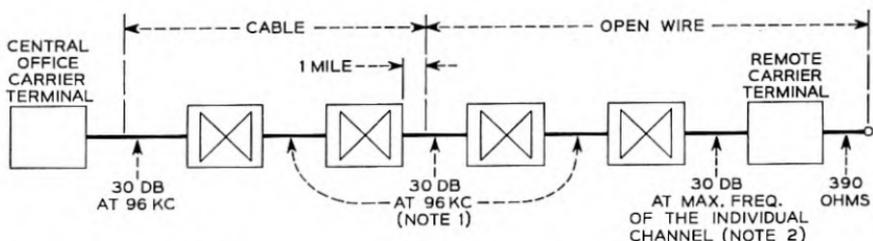
NOTE 1
CHECK MAXIMUM LOSS AT 30KC AND IF LESS THAN GAIN IN REMOTE TERMINAL TO CENTRAL OFFICE DIRECTION, PLACE INPUT PAD EQUAL TO DIFFERENCE AT INPUT OF REPEATER.

NOTE 2
CHECK MINIMUM LOSS AT MINIMUM FREQUENCY OF EACH CHANNEL FOR THE LAST REPEATER TO REMOTE TERMINAL SECTION AND IF THIS IS LESS THAN THE REPEATER GAIN AT THAT FREQUENCY, PLACE PAD IN OUTPUT OF TERMINAL TO BUILD SECTION OUT TO REPEATER GAIN VALUE.

(b) GROUPED FREQUENCY ARRANGEMENTS: REPEATED

Fig. 27 — P1 carrier application ground rules.

[5] C. C. Lawson, Rural Distribution Wire, Bell Lab. Record, pp. 167–170, May, 1954.

In addition to bare line loss, the ground rules make allowance for approximately 3 db of miscellaneous losses in any normal channel layout, including bridging losses of carrier blocking networks and other terminals on the carrier line, insertion losses of high-pass filters, and losses in the autotransformer and junction line filters used at the cable-open-wire junction. Since these losses do not all add directly, it is simpler to use an average loss factor to cover most conditions rather than make computations to determine a definite loss for each set of conditions that might exist. Thus for channels using a stackable frequency arrangement, a maximum of about 33 db loss, including the bare line loss and miscellaneous losses, may be expected between the points where the terminals connect to the line.

A further loss is experienced because the remote terminals are bridged onto the carrier line. As a result the carrier power transmitted toward the central office terminal is only +0.5 dbm due to a bridging loss of about 3.5 db at that point. Therefore, in the remote-to-central office direction, the minimum power will be −32.5 dbm (0.5 dbm − 33 dbm) at the line terminals of the central office terminal. The minimum carrier power in the central office to remote direction will be −29 dbm (+4 dbm − 33 dbm) at the bridging point of the remote terminal.

7.2 *Terminal and Repeater Location*

In laying out the carrier line design, it is first necessary to determine the possible locations for the remote terminals based on distances to the customers to be served and the availability of commercial ac power, since this is the most economical power source. (When commercial ac power can not readily be made available, the primary air cell batteries can be used.) Having determined the ideal location of the terminals from a physical standpoint, the makeup of the physical circuits back to the central office must be determined and computations made of the carrier frequency attenuation of the facilities. These loss computations are used to determine the number of repeaters required, if any, and their locations, once again modified by availability of commercial power. The Plant Engineer must also check for the necessity of input and output pads at the terminals and repeaters.

The need for loss computations led to the development of length-loss charts so that a carrier line design could be made in a manner very similar to the loop cable design using the Resistance Design Methods as mentioned earlier.[4] Fig. 28 shows one of the 96-kc length-loss charts used to lay out repeater spacings and Channel 4 over-all circuit design. Fig. 29 shows the 48-kc length-loss charts as an example of the charts that are provided at each carrier frequency other than 96 kc for terminal-to-
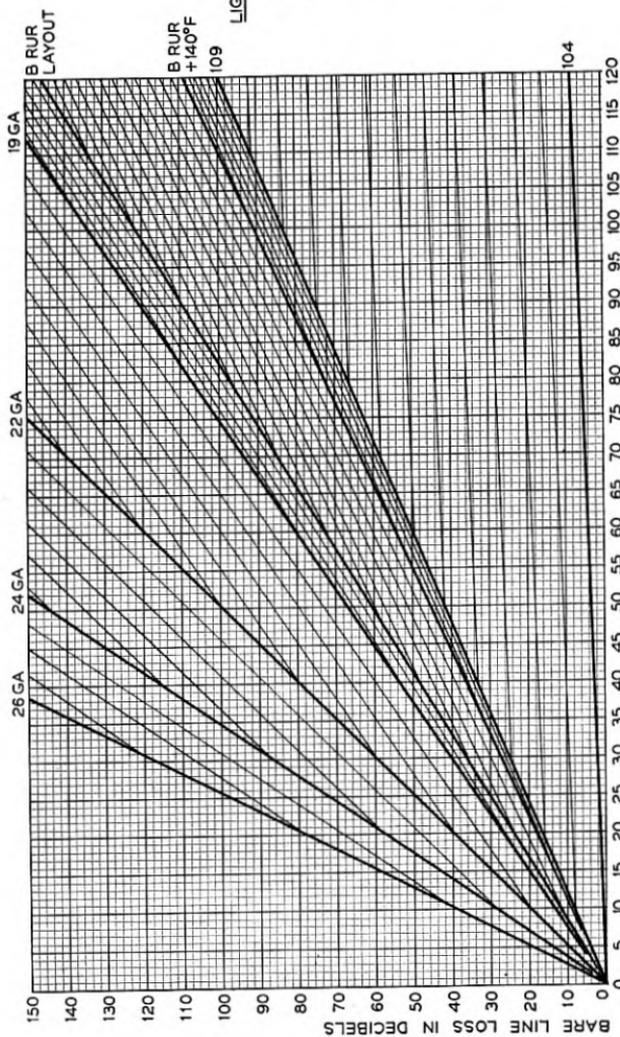
Fig. 23 — 96 kc bare-line charts.

LIGHT STORM LOADING AREA

MAXIMUM BARE LINE LOSS:
+140°F*

FOR DETERMINING:
CARRIER LINE LAYOUT
PAD VALUES
LINE-UP DATA

*B RURAL AS SHOWN

LIGHT, MEDIUM OR HEAVY STORM
LOADING AREA

MINIMUM BARE LINE LOSS:
-40°F

FOR DETERMINING:
CARRIER LINE LAYOUT
PAD VALUES
LINE-UP DATA
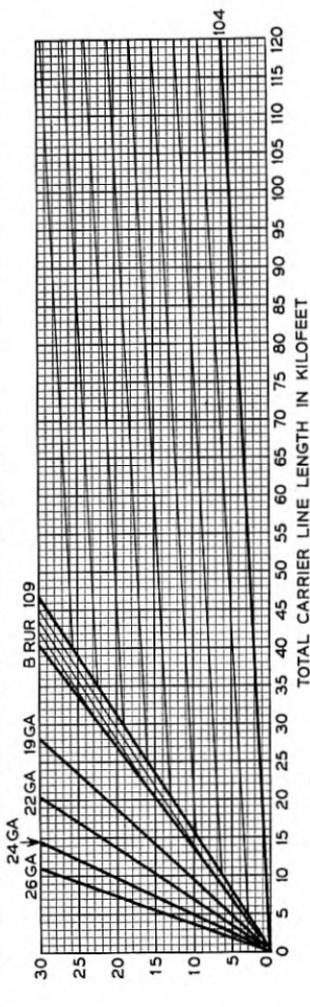
LENGTH – DB LOSS CHARTS, 96KC		
TYPE OF SYSTEM	CHAN NO.	CARRIER
STACKABLE	4	UPPER
NORMAL	4	UPPER

BARE LINE LOSS IN DECIBELS

TOTAL CARRIER LINE LENGTH IN KILOFEET

MEDIUM OR HEAVY STORM LOADING AREA

MAXIMUM BARE LINE LOSS:
CABLE +30°F WIRE—SLEET

FOR DETERMINING:
CARRIER LINE LAYOUT
PAD VALUES
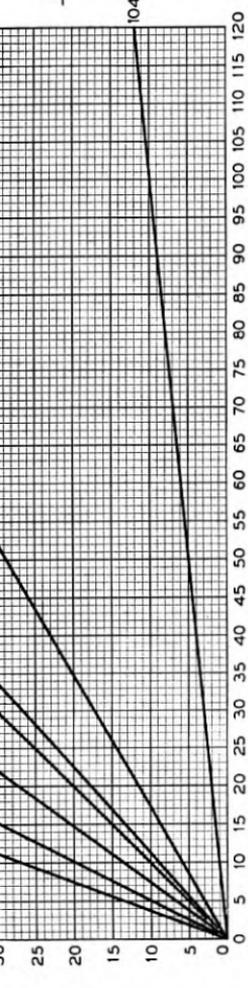
LIGHT STORM LOADING AREA

MAXIMUM BARE LINE LOSS:
+140°F*

FOR DETERMINING:
CARRIER LINE LAYOUT
PAD VALUES
LINE-UP DATA

*B RURAL AS SHOWN
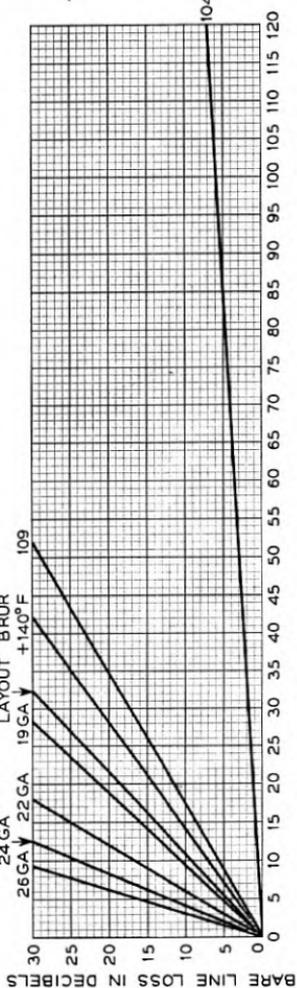
LIGHT, MEDIUM OR HEAVY STORM
LOADING AREA

MINIMUM BARE LINE LOSS:
-40°F

FOR DETERMINING:
CARRIER LINE LAYOUT
PAD VALUES
LINE-UP DATA
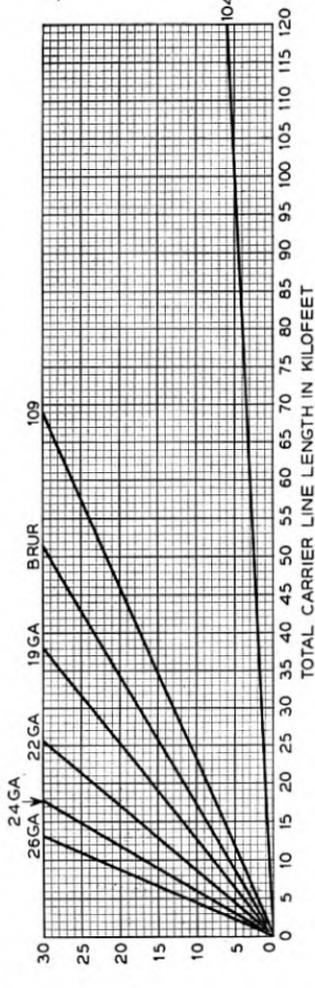
LENGTH-DB LOSS CHARTS, 48KC	CHAN NO.	CARRIER
TYPE OF SYSTEM		
		UPPER
		LOWER
STACKABLE	2	UPPER
NORMAL	4	LOWER

104

BRUR
LAYOUT BRUR
+140°F

109
19GA
24 GA 22GA
26GA

BRUR

109
19 GA
22 GA
24GA
26GA

BARE LINE LOSS IN DECIBELS

TOTAL CARRIER LINE LENGTH IN KILOFEET

Fig. 29 — 48-kc length-loss charts.

terminal section layouts of all channels using the stackable frequency arrangement or repeater-to-terminal section layouts for channels using grouped normal or staggered frequency arrangements.

7.3 *Pad Selection*

The Plant Engineer is given general ground rules for determining the values of input and output pads used in the terminals and repeaters. Charts are provided for use in determining the input and output pads, and they are so arranged that the engineer can take values directly from the length-loss charts and enter them into the appropriate slots to calculate the proper pad values.

7.4 *Crosstalk Limitations*

The Plant Engineer must be given information showing how many carrier channels can be applied to each circuit of open wire, cable or B-rural wire on a rural route. Crosstalk studies and tests have indicated that the stackable frequency arrangement or the grouped frequency arrangements used singly or in combination can be used on cable or B rural wire with a full system complement of channels applied to each pair. However, in the case of open wire, the frequency arrangement and number of channels which can be applied is very dependent on the type of transposition system used. The R1 design is the most commonly used transposition design on rural lines of the Bell System, and Fig. 30 gives
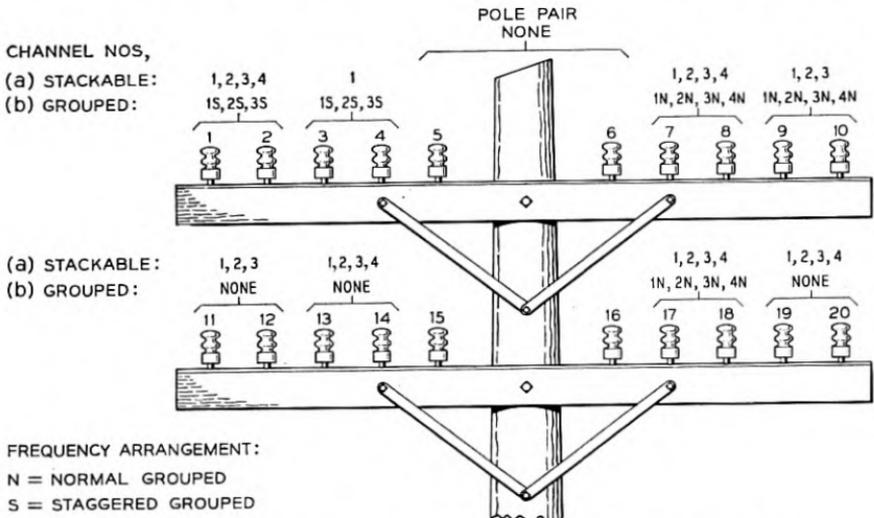
Fig. 30 — Number of P1 carrier channels on an R1 transposed line.

the carrier assignments for the various frequency arrangements on a one and two-crossarm route using the R1 transposition design. Use of a transposition system giving better carrier frequency crosstalk performance than the R1 design is expected to permit the application of a number of additional channels over those shown in Fig. 2.

It will be noted that the grouped arrangement provides four channels less on a two-crossarm basis than the stackable arrangement. From a transmission standpoint, equal numbers of channels would be possible by assigning one or two channels to a pair, but these arrangements will usually be uneconomical for grouped systems because of the high cost per channel of repeaters.

7.5 *Line Networks*

The location of the line networks and filters, which are a permanent part of the carrier layout, will be designated by the Plant Engineer, and the location and type of the remaining networks, which will vary with changes in subscriber service, will be selected by the plant forces. The low-pass filters or carrier blocking networks used on the carrier lines are simple resonant circuits designed to match given ranges of capacitance that will be presented by the drop wire or open-wire side leads. Since this capacitance varies considerably with various lengths of facility, a method will be provided by which the total capacitance of the drop can be determined and the proper network chosen. The other line networks are applied to the line as necessary to achieve their particular functions.

8. INSTALLATION AND MAINTENANCE

A portable field test set has been developed which will simplify the installation and maintenance of the P1 carrier system. The new set, known as the 7F test set, will provide the carrier and audio frequencies and a means of measuring them required to align and troubleshoot units of the system. The set, which is battery operated, contains a carrier oscillator to supply test frequencies from 10 to 100 kc, an audio frequency oscillator having six selected frequencies in the range of 250 to 2,500 cycles, a modulator to modulate the carrier frequency signal with the audio signal, a demodulator for calibrating the modulated signals, and a wide-band amplifier-detector for making level and transmission measurements. The model of the set shown in Fig 31 included a precision dial for signaling testing which was subsequently found unnecessary and eliminated. An ac operated set providing the same desired facilities is now under development.

The carrier channel installation and lineup procedure is set up on the basis of using the test set and a generally available volt-ohmmeter to make a series of measurements in a specified order. This will permit potentiometers to be adjusted as necessary until the specified meter readings are obtained at built-in test points. Lineup of the terminals and repeaters done first in the central office to insure proper operation and then at the in-plant locations to check system performance.

Maintenance will be handled on a complete terminal replacement basis and will consist of making a series of checks with the test set to determine whether the terminal is functioning satisfactorily. If it is not and it cannot be adjusted to restore satisfactory operation, a replacement terminal will be used to restore service. All repairs and isolation of trouble within the terminal unit or on the individual boards will be handled at a centralized testing or repair point so as to require a minimum of personnel with electronic experience. The test set has been designed to handle all tests for a P1 carrier system, when used with the volt-ohmmeter, and when used by trained personnel will permit trouble to be isolated to a given printed wiring board in the P1 carrier equipment.
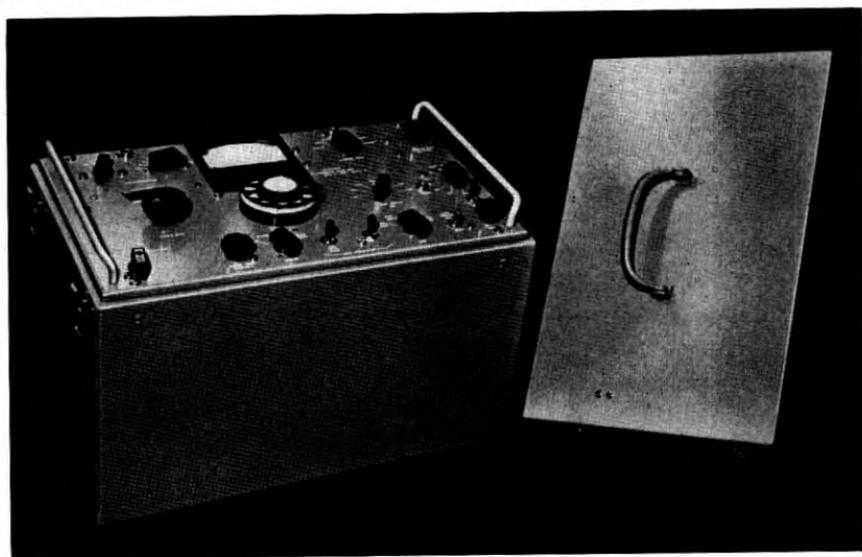
Fig. 31 — P1 carrier 7F test set.

An Experimental Dual Polarization Antenna Feed for Three Radio Relay Bands

By R. W. DAWSON

(Manuscript received April 26, 1956)

The fundamental problems associated with coupled-wave transducers which operate over a 3-to-1 frequency band have been explored and usable solutions found. The experimental models described are directed toward the broad objectives of feeding the horn-reflector antenna with two polarizations of waves in the 4-, 6- and 11-kmc radio relay bands.

INTRODUCTION

There are at least two communications problems which require frequency selective filters that operate in waveguides over an approximately 3-to-1 frequency interval: (1) channel-separation filters for a circular-electric waveguide system in which it is desirable to use the medium from perhaps 35 to 75 kmc,[1] and (2) band-separation networks needed for the horn reflector antenna that permits simultaneous transmission or reception in the 4, 6 and 11 kmc bands with both polarizations.[2, 3] The research reported in this paper was directed at determining the capabilities of coupled-wave transducers for solving such problems. Experimental work was directed toward the second problem (above) because it is more immediate.

Fig. 1, which is a schematic representation of the feed array, comprised of three sets of directional couplers, shows that the 4-kmc bands are
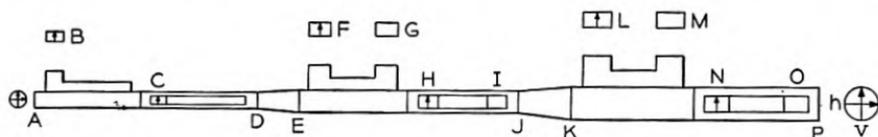
Fig. 1 — Schematic of dual-polarization feed for three microwave bands.

separated one at a time at the antenna end of the array. The 6-kmc bands are separated next and the 11-kmc bands are added or removed at the far end of the array.

GENERAL OBJECTIVES

Negligible loss of power should result when coupling $TE_{10}^{\square}$ waves to $TE_{11}^{\bigcirc}$ waves for the six bands concerned.* The 6- and 11-kmc waves of both polarizations must pass through the round guide of the 4-kmc transducers without significant attenuation. Waves in the 11-kmc band must also pass through the circular guide of the 6-kmc transducers without appreciable loss. A good impedance match is desired at all ports. No cross coupling is desired between the orthogonally polarized waves in the round guide.

FUNDAMENTAL PROBLEMS ENCOUNTERED

The frequency-selectivity required to separate various bands in the same polarization can be achieved in a coupled-wave device by either varying the coupling coefficient and/or varying the phase constant, as illustrated by the expression for the amplitude of the selected wave:[4]

$$|E| = \frac{1}{\sqrt{1 + \left(\dfrac{\beta_1 - \beta_2}{2c}\right)^2}} \sin\left\{\sqrt{1 + \left(\dfrac{\beta_1 - \beta_2}{2c}\right)^2}\right\} cx \qquad (1)$$

where c = coupling coefficient

x = length of coupling array

β = phase constant

In the present designs some of the frequency selectivity is in the coupling holes. The greater part of the selectivity is in the design of the phase constants; they are made equal in the band to be selected ($\beta_1 - \beta_2 = 0$) and very unequal

$$\left(\frac{\beta_1 - \beta_2}{2c} \gg 2c\right)$$

in the frequency bands to be passed.

The size of the coupling hole must be controlled to avoid coupling hole resonance in any of the three bands that may be present. This problem is especially bothersome in the 4 kmc coupler where signals are present

---

* As used in this article, superscripts $\bigcirc$ and $\square$ refer to round and rectangular waveguides, respectively.

in all three bands. To keep the coupler length within a reasonable size, the individual hole dimensions must be on the order of $\lambda_0/4$ (at 4 kmc), which *will* permit coupling hole resonance within the 3-to-1 frequency band. A further consideration is the selection of the hole shape to avoid perturbing the $TE_{11}{}^{\circ}$ wave that is orthogonal to the strongly coupled $TE_{11}{}^{\circ}$ wave.

Spacing of the coupling holes must *not* be $\lambda_g/2$ to avoid: (1) large reflections in the driven waveguide, and (2) large backward-travelling waves in the adjacent coupled waveguide. This requirement is easily met in the 11-kmc coupler where only one band is present; however, the presence of signals in two or three bands makes the non $\lambda_g/2$ spacing more difficult in the 6- and 4-kmc couplers.

Another phenomena of importance exists in coupled waveguides operating over an extended frequency range. A coupling aperture in the side wall (see Fig. 1) may interact with a high-order mode at the latter's cutoff frequency, resulting in a significant perturbation of the desired coupling. For example, at the frequency where $TE_{21}{}^{\circ}$ passes through cut off, the coupling between $TE_{11}{}^{\circ}$ and $TE_{10}{}^{\square}$ will be perturbed *if* the coupling hole is of sufficient size. Small coupling holes do not allow this perturbation to manifest itself. Coupling holes in a realistic design do become large enough to allow this effect to appear. Since dominant mode guides in the 4- and 6-kmc bands can support other modes in the higher frequency bands, considerable caution must be exercised in selecting the round guide sizes on this account alone. (The size of the round guide is determined also by the phase velocity in the rectangular guide).

SELECTION OF COUPLING APERTURES

A series of holes in either the narrow or broad side of the rectangular guide can, in principle, be used to achieve complete power transfer from $TE_{10}{}^{\square}$ waves to $TE_{11}{}^{\circ}$ waves. The specific consequences of coupling through holes located along the center line of the broad side will be considered first. (Off center holes are not of interest because they couple $TE_{10}{}^{\square}$ waves to both polarizations of $TE_{11}{}^{\circ}$ waves in a frequency-sensitive way.) The transverse magnetic field H_{φ} and the electric field E_{ρ} of the $TE_{11}{}^{\circ}$ waves can couple to $TE_{10}{}^{\square}$ waves. When two fields couple, the backward wave in the undriven guide can be greater than the forward wave in the same guide. To avoid this possibility, transverse slots can be used to prevent electric field coupling. The coupling of a transverse slot increases as the frequency is increased which suggests that 11 kmc signals be introduced at the position nearest to the antenna because the largest tolerable apertures for an 11-kmc coupler would not perturb 6- or 4-kmc

waves. Unfortunately, coupling to slots in this orientation is small, requiring several hundred for complete power transfer. Such a large number would make the coupler too long.

Coupling through holes in the center of the narrow wall of the rectangular waveguide as shown in Fig. 2 allows only the longitudinal magnetic field H_z to couple when the electric field of the TE_{11}^O wave is parallel to the hole containing wall. No coupling exists between the $TE_{10}^{\square}$ waves and the TE_{11}^O wave having an electric field perpendicular to the plane of the hole. The use of longitudinal slots where practicable minimizes perturbation of this wave. Since the desired $TE_{10}^{\square} - TE_{11}^O$ coupling decreases by 15 db from the 4 kmc to the 11 kmc bands (for 1.872 × 0.872″ and 2.2″ diam. guide), the layout of Fig. 1 suggests itself since some coupling discrimination is present for the higher frequency waves that pass through the lower frequency couplers.

DESIGN OF 11-KMC COUPLER

The objective of this design is to transfer all of the power from a dominant mode rectangular guide into one polarization of the TE_{11}^O forward traveling wave in an adjacent circular guide. Fundamental coupled-wave theory[4] shows that phase velocities must be matched in the two guides to achieve complete power transfer.

A standard rectangular guide size is selected and the round guide size that has the same phase constant is calculated for the center of the 1,000-mc wide band. An approximate total length is selected for the series of coupling holes that permits the holes to be spaced approximately $\lambda_g/4$ apart. The hole spacing is not critical although the non-directional properties of $\lambda_g/2$ spacing must be avoided. The required magnitude of multiple discrete couplings is shown in equation (40) of Reference 4 to be:

$$\alpha = \sin\left(\frac{\pi/2}{n}\right) \tag{2}$$

where n is the number of coupling holes and α is the amplitude of the wave transferred at a single coupling hole for unit incident amplitude.

Equation (3) expresses the power coupled from TE_{11}^O waves to $TE_{10}^{\square}$ waves through a circular hole in a common wall of zero thickness where P_2 is the power propagating away from the coupling point in either direction in the undriven guide, and P_1 is in the driven guide. This derivation is based on the work of H. A. Bethe[5] and some unpublished notes of S. P. Morgan.

$$\frac{P_2}{P_1} = \frac{0.6805\lambda_0^2 r^6}{ba^3R^4\sqrt{1 - \left(\frac{\lambda_0}{2a}\right)^2}\sqrt{1 - \left(\frac{\lambda_0}{3.413R}\right)^2}} \tag{3}$$

The quantities a and b are the large and small dimensions of the rectangular waveguide and R is the round guide radius. The wavelength in air is designated by λ_0, and the radius of the coupling hole by r. A correction for the finite thickness of the wall is made by considering the circular coupling hole to be a round waveguide beyond cutoff.[6] The additional loss is

$$\Delta = \frac{16t}{r}\sqrt{1 - \left(\frac{3.413r}{\lambda_0}\right)^2} \text{ (decibels)} \tag{4}$$

where t is the wall thickness. Total coupling loss per hole is defined by

$$20 \log_{10} \alpha = 10 \log \frac{P_2}{P_1} - \Delta \tag{5}$$

The number of coupling holes n is found from the approximate coupling length and hole spacing. Equation (2) is used to find α and then the hole radius r is calculated from (3).

Waveguide dimensions must be corrected to allow for the perturbation of the phase constants due to the coupling holes. The perturbed phase constant* for the round guide is

$$\beta_p^{\circ} = \beta^{\circ} + \frac{\sqrt{p^{\circ}}}{d} \tag{6}$$

where d is the hole spacing and p° is the coupling between a pair of round guides

$$p^{\circ} = \frac{0.1056r^6\lambda_0^2}{R^8\left[1 - \left(\frac{\lambda_0}{3.413R}\right)^2\right]} \tag{7}$$

The perturbed phase constant for the rectangular guide is

$$\beta_p^{\square} = \beta^{\square} + \frac{\sqrt{p^{\square}}}{d} \tag{8}$$

$$p^{\square} = \frac{4\pi^2 r^6\lambda_0^2}{9a^6b^2\left[1 - \left(\frac{\lambda_0}{2a}\right)^2\right]} \tag{9}$$

---

* This correction is due to S. A. Schelkunoff as noted on page 708 in Reference 4.
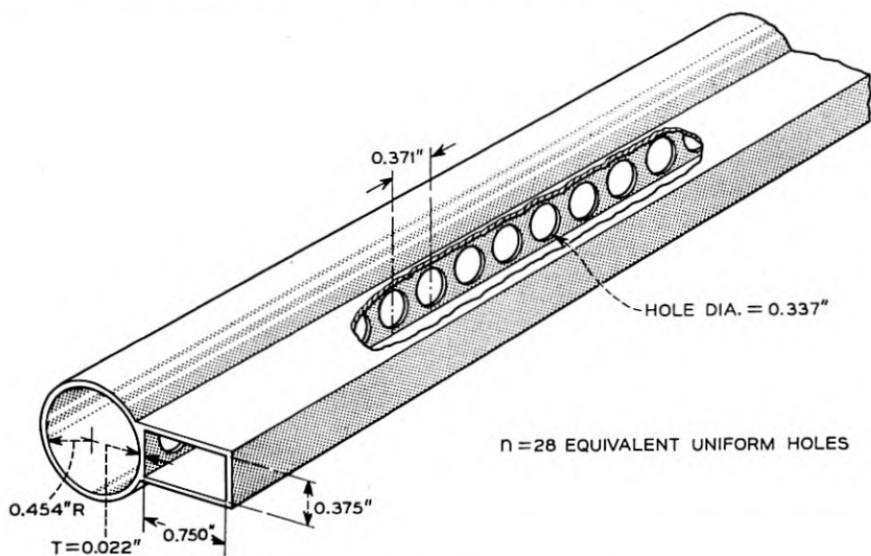
Fig. 2 — 11-kmc coupler sketch.
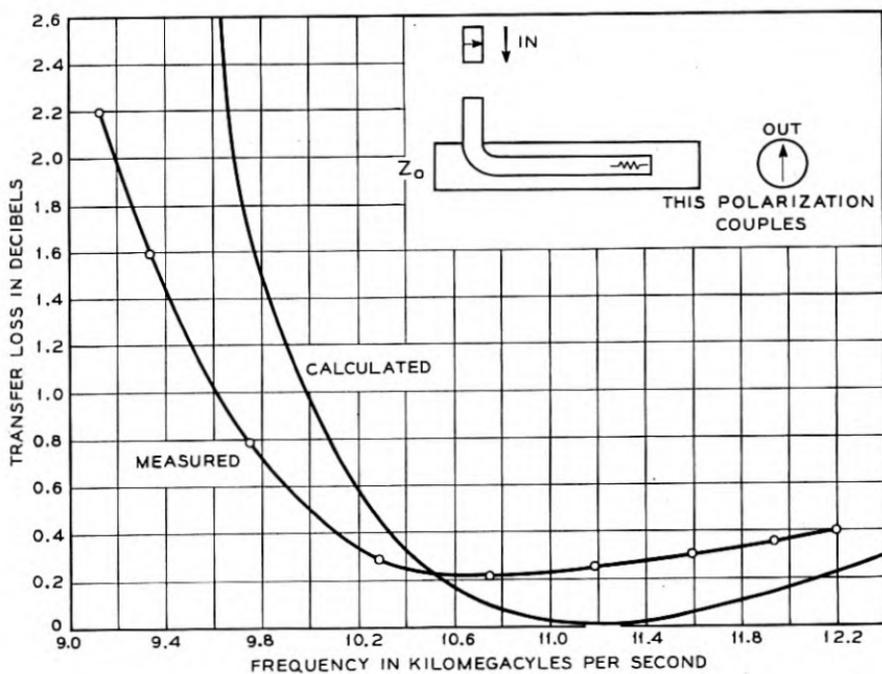
Fig. 3 — 11-kmc coupler transfer loss.

The perturbed phase constants are made equal through a suitable choice of R and a, this choice being somewhat influenced by the coupling-hole radius r.

Three coupling apertures of successively reduced size are used at the ends of the array of identical holes to produce four reflections having the relative amplitudes of 1, 2.7, 2.7, 1. The modified binomial distribution was chosen because impedance matching can be secured over a broader
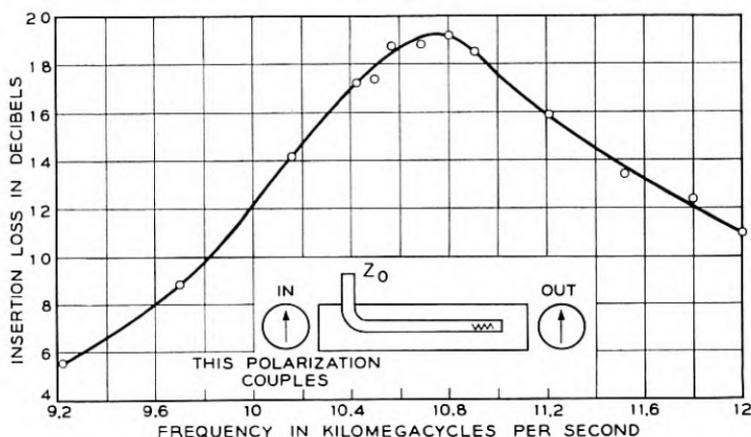
Fig. 4 — 11-kmc coupler insertion loss.

band (with minor degradation of the center-frequency match) when compared to a standard binomial distribution. Amplitude reflections* from the start of the coupling array are

$$A_r = \frac{\lambda_g Q}{4\pi d} \tag{10}$$

where Q is the reflection from a single coupling hole.

Fig. 2 is a sketch of the coupler with the final design dimensions. Fig. 3 shows the measured and theoretical transfer loss of an 11 kmc coupler. Fig. 4 indicates the measured insertion loss for the same coupler.

DESIGN OF 6-KMC COUPLER

The 6-kmc coupler as shown in Fig. 5 utilizes a partially dielectric-filled rectangular guide coupled to the circular guide. The use of dielectric loading makes it possible for the phase velocities to be equal in the two guides in the center of the 500-mc wide 6-kmc band, and unequal in

---

* Information given to S. E. Miller by S. A. Schelkunoff in an informal communication.

0.060"

n = 30 EQUIVALENT UNIFORM HOLES
  FOR ONE ROW
HOLE SIZE = 0.030" x 0.627"
SPACING = 0.660"

1.688"D
T = 0.030"

1.310"
0.211"
0.622"
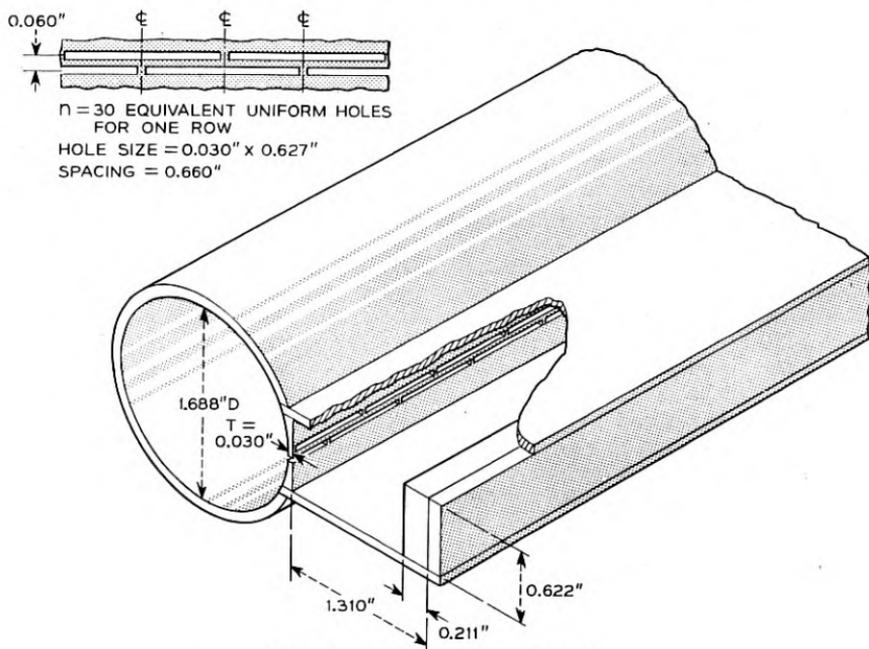
Fig. 5 — 6-kmc coupler sketch.

IN   OUT
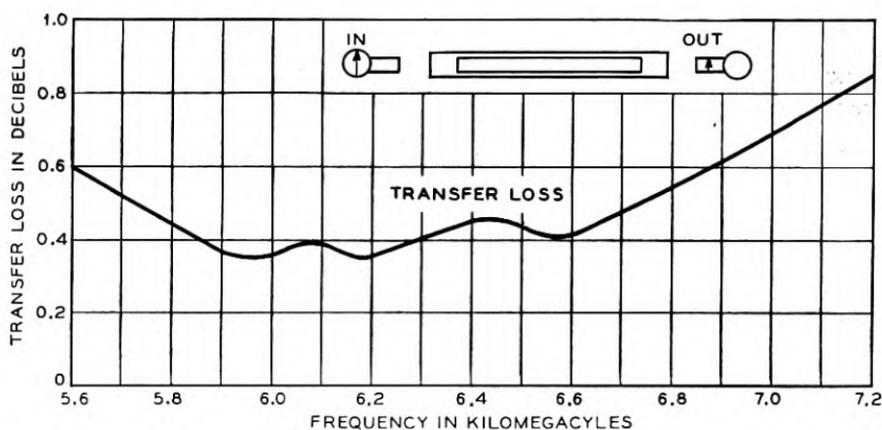
TRANSFER LOSS

Fig. 6 — Transfer loss of 6-kmc coupler.

the 11-kmc band; thereby low transfer loss is obtained in the 6-kmc band and a high transfer loss in the 11-kmc band. Measurements have shown that when the cut-off frequencies of higher modes occur in the band of interest an uncontrolled increase of coupling may result. Special precautions are required in selecting the round guide size to avoid this condition. The design process is shown in Appendix I. Figs. 6 and 7 show the transfer and insertion losses in the 6-kmc band.
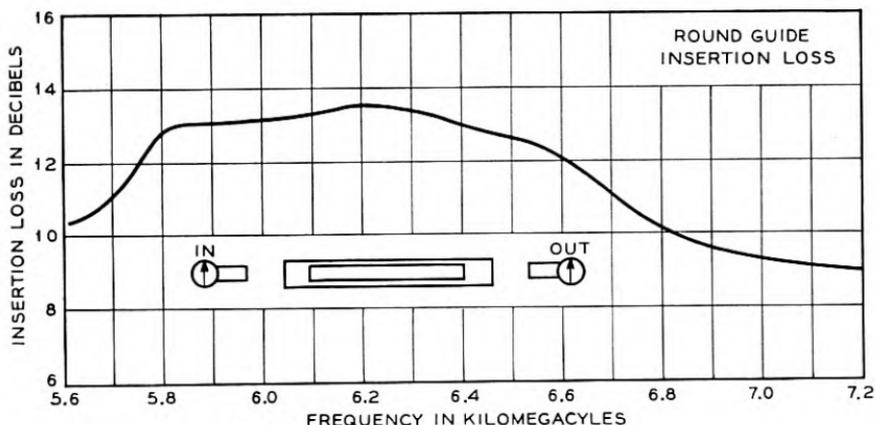
Fig. 7 — Insertion loss of 6-kmc coupler.

SLOT SIZE = 0.740″ x 0.0786″
SPACING = 0.780″
POST DIA = 0.300″
GUIDE SIZE = 1.724″ x 0.872″

2.070″

0.050″

COUPLING ARRAY CONSISTS
OF 38 FULL SIZE SLOTS &
6 REDUCED SIZE SLOTS
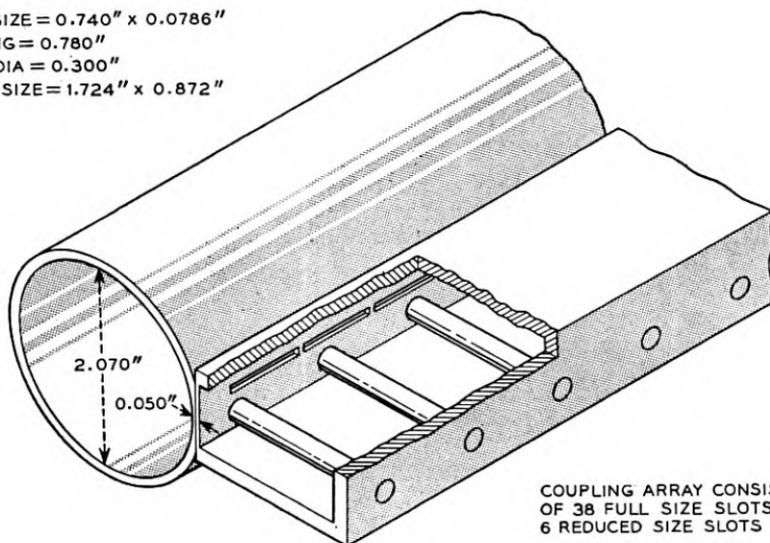
Fig. 8 — 4-kmc coupler sketch.
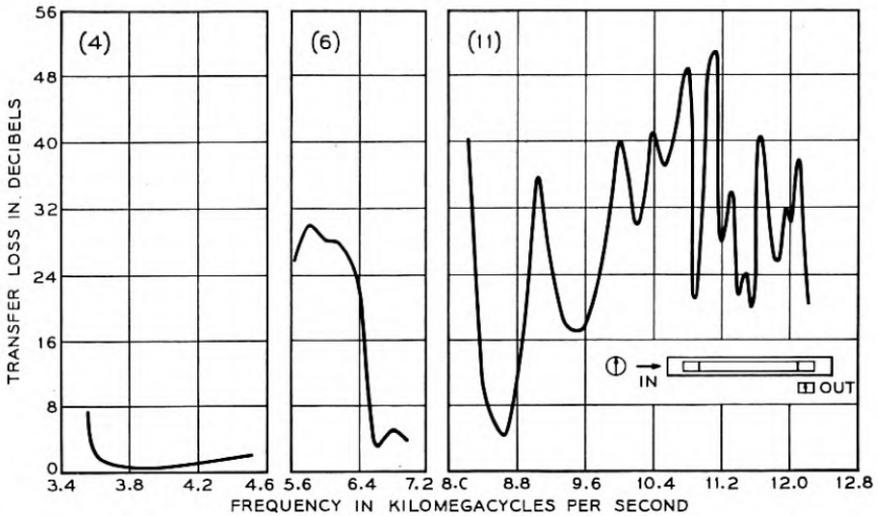
Fig. 9 — Transfer loss of 4-kmc coupler in 4-, 6- and 11-kmc bands.
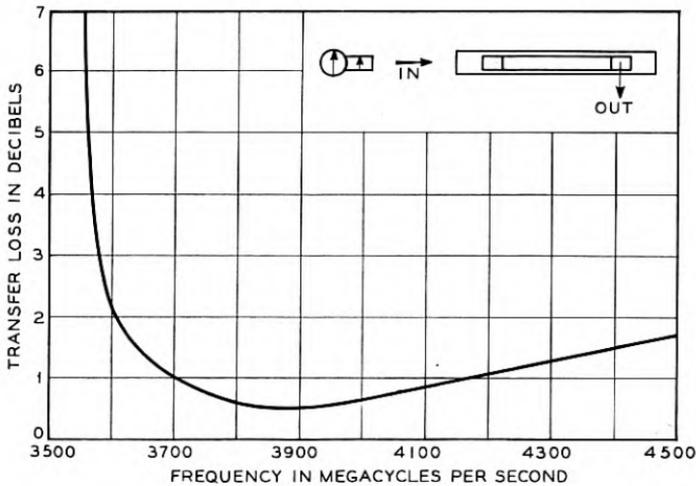
Fig. 10 — Transfer loss of 4-kmc coupler in 4-kmc band.

4-KMC DESIGN

The use of periodic loading in the rectangular guide is not suitable for use in a 4-kmc coupler design. When the phase constants are made equal in the 4-kmc band, the resulting difference of phase constants in the 6-kmc band is too small to create a sufficiently high transfer loss in that band. Periodic loading can produce the desired result.

Capacitive rods form a periodic structure in the rectangular guide, as shown in Fig. 8, that creates a rejection band in the 6-kmc region. Fig. 9 illustrates how effectively the rejection band increases the transfer loss in the 6-kmc region. Phase velocities are made equal in the rectangular and round guides at the center of the 500-mc wide 4-kmc band to secure a low transfer loss. Due to the rejection bands and the difference of phase constants, high transfer losses result in the 6- and 11-kmc bands. To prevent uncontrolled coupling the round guide size is chosen so that no modes cut off in the three bands. Details of the design are covered in Appendix II. Figs. 10 and 11 show the measured transfer and insertion losses in the 4-kmc band.

MEASURED CHARACTERISTICS OF ARRAY

The three pairs of couplers were assembled in a tandem array with linear taper sections between them. In the discussions that follow the port designations of Fig. 1 will be used. Transfer loss measurements indicate
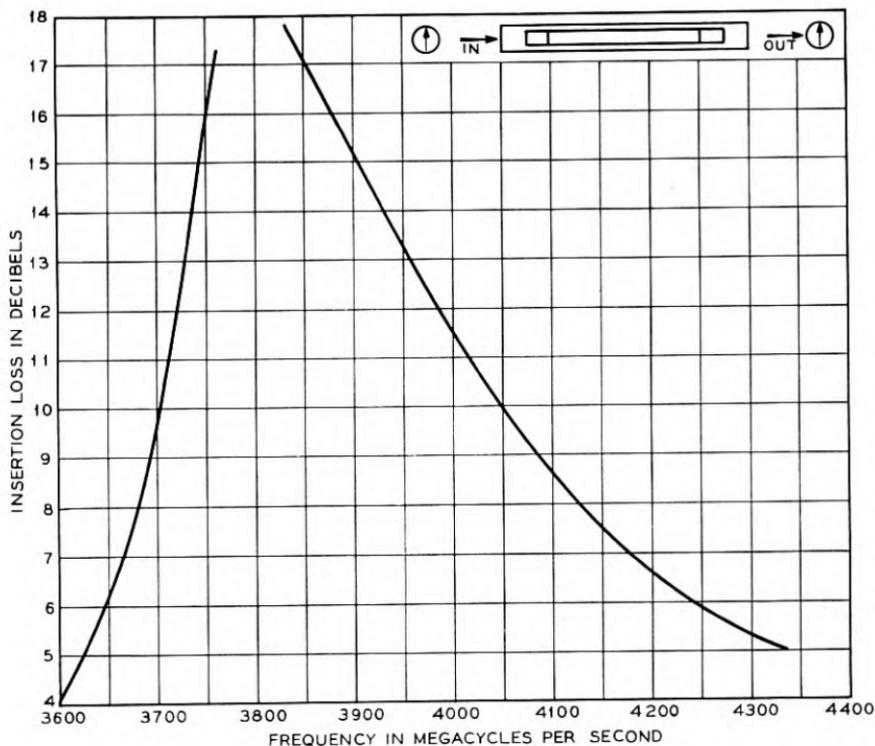
Fig. 11 — Insertion loss of 4-kmc coupler in 4-kmc band.

how much power in a forward traveling $TE_{11}{}^{\bigcirc}$ wave is transferred to a forward traveling $TE_{10}{}^{\square}$ wave. Figure 12 shows that the coupling polarization transfer loss remains under 1.1 db in the three bands except for a small region in the 11-kmc band, while the transfer loss for the non-coupling polarization exceeds 20 db in the three regions as shown in Fig. 13. The return loss at Port P exceeded 23 db over the 4-kmc band. This result included the total reflection of 4-kmc signals from Taper J-K after attenuation by twice the coupler insertion loss, and also included the reflections from the rectangular guide port N or L which
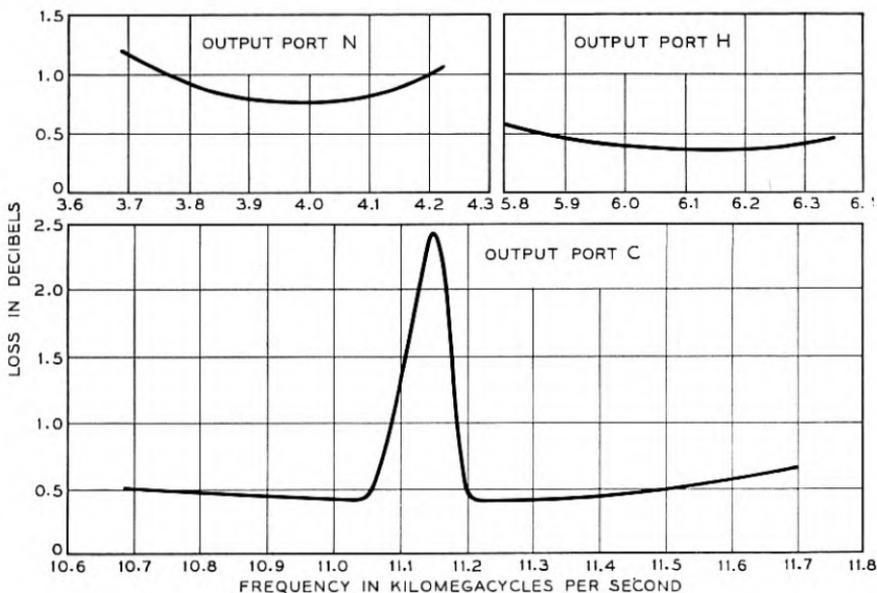
Fig. 12 — Transfer losses in the array for coupling polarization.

are separated from P by only the small transfer loss. Return loss for the 6- and 11-kmc bands exceeded 23 db at Port P. Cross polarization is the ratio of the energy in the coupling polarization waves to the orthogonal non-coupling polarization waves emerging at Port P. Cross polarization figures are no lower than 20, 32 and 22 db in the 4,-6- and 11-kmc bands.

CONSTRUCTION OF COUPLERS

The coupler design requires that the coupling aperture exist in a narrow wall of the rectangular guide that is common to the round guide. The 4-kmc coupler consists of machined rectangular and round sections. A two-piece rectangular guide was milled from brass and
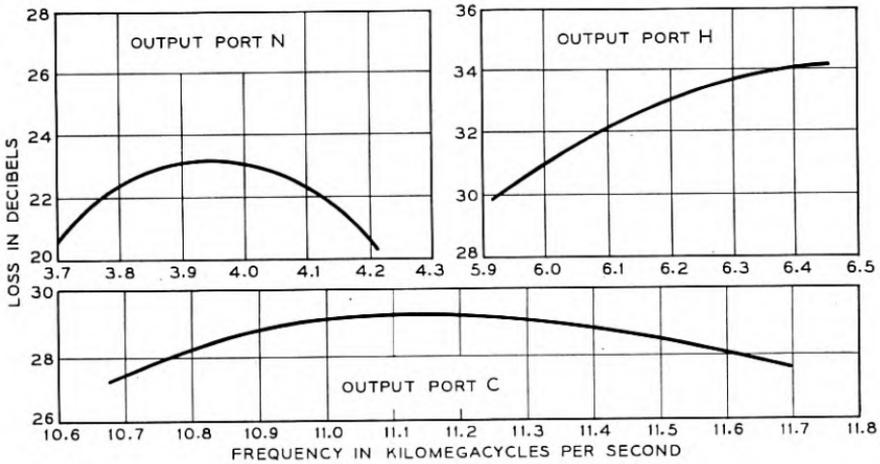
Fig. 13 — Transfer losses in the array for non-coupling polarization.

soldered to the round guide. The coupling slots were then cut through the common wall. An electroforming technique was used to fabricate the 6- and 11-kmc couplers. A rectangular guide with precut coupling holes was clamped to a round mandrel and the entire structure was electroformed. The mandrel was later removed by dissolving it in a hot concentrated solution of sodium hydroxide. A typical mandrel and rectangular guide is shown in Fig. 14. An illustration of the entire ensemble appears as Fig. 15.

DESIGN REFINEMENTS

Return loss at the round Port P might be improved in a revised design by broad-banding the $TE_{10}^{\square}$-TE_{11}° transfer loss, with an associated increase in the TE_{11}° insertion loss. This might be done without introducing mode troubles, by using ridged waveguide. In Fig. 12 the abrupt peak of transfer loss for coupling polarization waves in the 11
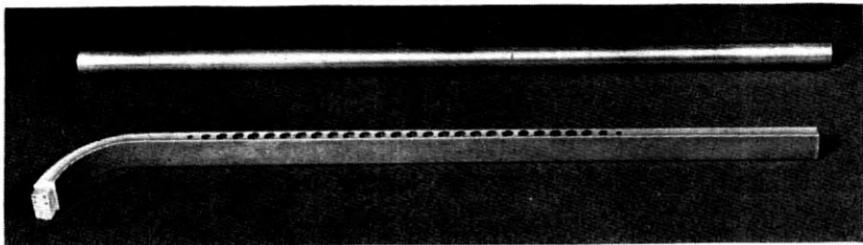
Fig. 14 — Mandrel and rectangular guide.
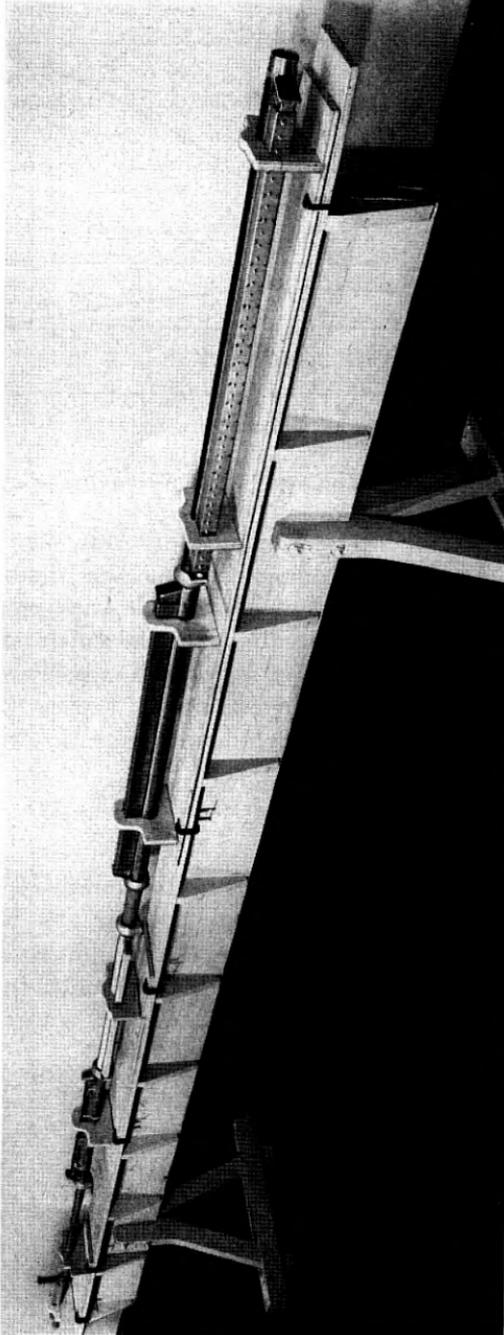
Fig. 15 — The array.

kmc band is due to an appreciable coupling of $TE_{11}{}^\bigcirc$ waves to $TE_{30}{}^\square$ waves in the 4 kmc couplers in the vicinity of the $TE_{30}{}^\square$ cutoff. The $TE_{30}{}^\square$ cutoff might be moved above the 11-kmc band by using ridged rectangular guide.

SUMMARY

A combination of three pairs of coupled-wave transducers has successfully permitted six distinct bands to be fed from individual $TE_{10}{}^\square$ rectangular waveguides into the two orthogonal polarizations of $TE_{11}{}^\bigcirc$ waves in a multi-mode round waveguide. The resulting structure enabled low transfer loss values to be obtained simultaneously over two 500-mc wide bands and one band 1000-mc wide distributed over a 3-to-1 frequency interval.

ACKNOWLEDGMENT

APPENDIX I

DESIGN OF 6-KMC COUPLER

A rectangular guide size is chosen and a reasonable value selected for the phase constant such as $\beta^\square = 1.5\pi/\lambda_0$. The resulting round guide size must prevent modes from cutting-off within the 6-kmc band and preferably the cut-off frequency should be above the 6-kmc band. The thickness of the dielectric (polystyrene) strip is determined[7] from (11), (12), and (13) where K_1 and K_2 are transverse wave numbers of the air-filled and of the dielectric sections of the guide.

$$K_1 = \sqrt{\left(\frac{2\pi}{\lambda_0}\right)^2 - \beta_\square{}^2} \tag{11}$$

$$K_2 = \sqrt{\varepsilon_r \left(\frac{2\pi}{\lambda_0}\right)^2 - \beta_\square{}^2} \tag{12}$$

$$\text{Cot } K_2 d = -\frac{K_1}{K_2} \cot K_1(a - d) \tag{13}$$

In the above equations ε_r is the relative dielectric constant and d is the slab thickness. After solving for d the equations are resolved for K_1 and K_2 values at the 6-kmc band edges and also at the lower end of the 11-kmc band. Resulting rectangular-guide phase constants should cause a very

low and a high value of transfer loss as indicated by (14) which represents the forward traveling coupled wave amplitude where cx is the total coupling strength.[4]

$$E_2 = \frac{1}{\sqrt{\dfrac{(\beta_\Box - \beta_\bigcirc)^2}{4c^2} + 1}} \, i \sin\left[\sqrt{\frac{(\beta_\Box - \beta_\bigcirc)^2}{4c^2} + 1}\right] cx \qquad (14)$$

At midband $cx = \pi/2$ and experience has shown $x \cong 10\,\lambda_0$; therefore $c \cong \pi/20\lambda_0$ at midband. The coupling hole radius is found from (3). Because longitudinal slots are used instead of round holes the equivalent hole radius r is found from $\frac{4}{3}r^3 = P\ell^3$, where P is the magnetic polarizability[8] and ℓ is the length of the chosen slot. To avoid slot resonance in either band, the length was chosen to be approximately $\lambda_0/4$ in the 6-kmc band and $\frac{5}{8}\lambda_0$ in the 11-kmc band. The power expression of (3) must be corrected by the wall thickness effect (4) and also multiplied by the factor F due to the presence of the dielectric slab[7] (15).

$$F = \frac{2a^3 K_1{}^4}{\pi\beta_\Box\lambda_\Box[K_1(\theta_1 - \frac{1}{2}\sin 2\theta_1) + A^2 K_2(\theta_2 - \frac{1}{2}\sin 2\theta_2)]}$$

$$\theta_1 = K_1(a - d) \qquad \theta_2 = k_2 d \qquad A = \left(\frac{K_1}{K_2}\right)^2 \frac{\cos\theta_1}{\cos\theta_2} \qquad (15)$$

Theoretical coupling loss per hole is defined by

$$20 \log_{10} \alpha = 10 \log \frac{P_2}{P_1} - (\Delta + 10 \log_{10} F) \qquad (16)$$

An additional correction which reduces the coupling loss is due to the long length of the slot. Although the slot resonates near 9 kmc, an increase of 3 db in a single slot coupling results at 6 kmc. This effect was found experimentally from a sample test line with several slots. To avoid excessive length two rows of coupling slots were employed. They were staggered to improve the continuity of coupling from discrete points. An approximate design is on hand at this point. The final dimensions for the guides and coupling holes are found after the perturbations of the phase constants are considered by the same process as noted in the discussion of the 11-kmc design. Impedance matching for the dielectric strip and the coupling slot array was patterned after the technique shown for the coupling hole array in the 11 kmc design.

Appendix II

DESIGN OF 4-KMC COUPLER

A round guide size is selected so that no modes are cut-off in the three bands. Coupling power varies with wavelength as shown in (17) for TE_{10} to $TE_{11}^{\bigcirc}$ coupling.

$$Y = \frac{\lambda_0^2}{\left[1 - \left(\frac{\lambda_0}{3.413R}\right)^2\right]} \qquad (17)$$

To maintain the minimum variation across the band, the following requirements must be met which were deduced from the coupled wave theory[4] and (17).

$$\sin (cx)_1 = \sin (cx)_2 \qquad (18)$$

$$\frac{(cx)_1}{(cx)_2} = \frac{\lambda_0}{\sqrt{1 - \left(\frac{\lambda_0}{3.413R}\right)^2}} \qquad (19)$$

$$(cx)_1 + (cx)_2 = \pi \qquad (20)$$

The equations are solved for $\sin cx$ (the minimum band edge transfer loss) which for a diameter of 2.10″ is 0.5 db. A value of 30 db is chosen for α, (2), as the first approximation. Because the band edge transfer loss is 0.5 db due to frequency variation of coupling, an additional loss of only 0.2 db is allowed for the phase constant difference $(\beta_L^{\square} - \beta^{\bigcirc})$. It is now necessary to make $\beta^{\bigcirc} = \beta_L^{\square}$, where $\beta_L^{\square}$ is the phase constant of the loaded rectangular guide. Equation (21) gives a theoretical periodic loading formula where L is the spacing between loading elements.[9]

$$\cos \beta_L^{\square} L = A \cos (\beta^{\square} L + \Phi)$$

$$\Phi = \arctan \frac{b_0}{2} \quad A = \sqrt{1 + \left(\frac{b_0}{2}\right)^2} \qquad (21)$$

Assume initially that $L = \pi/\beta^{\bigcirc}$. The required susceptance b_0 of the capacitive rods can be found experimentally from a loaded test line by varying b_0 until the first rejection band covers the 6 kmc band. An iterated process is used to find L because it is dependent on $\beta^{\square}$ which is the parameter being sought. Measurements indicated that (21) does not predict $\beta^{\square}$ very accurately and for that reason an experimental adjustment of $(\beta_L^{\square} - \beta^{\bigcirc})$ is desirable.

The guide dimensions are now known; however, they must be corrected for the perturbations of the phase velocities as outlined in the 11-

kmc coupler design. A single row of longitudinal coupling slots which are not resonant in the 6- or 11-kmc bands is used. The radius of a round hole equivalent to the slot is obtained as in Appendix I, by setting $\frac{4}{3}r^3 = P\ell^3$.

Impedance matching of the coupling array and of the loading elements is accomplished by tapering the amplitude of the end elements as indicated by a discrimination function of the coupled wave theory.[4] For a 5 element series $1 - n_1 - n_2 - n_1 - 1$

$$D = \frac{2(n_1 + 1) + n_2}{2\left(n_1 \cos \dfrac{4\pi Z}{\lambda_g} + \cos \dfrac{8\pi Z}{\lambda_g}\right) + n_2} \tag{22}$$

where Z is the spacing between elements.

The discrimination D is set equal to infinity which permits the denominator to be set equal to zero and solved simultaneously for n_1 and n_2 by using both band edge wave-lengths. Round hole sizes are readily obtained since the coupling coefficient is directly proportional to the cube of the hole radius from which the necessary equivalent longitudinal slot can be calculated. Susceptance values of the capacitive posts are found from the absolute value of the reflection coefficient which equals

$$\frac{b_0}{\sqrt{b_0{}^2 + 4}}$$

REFERENCES

1. S. E. Miller, Waveguide as a Communication Medium, B.S.T.J., Nov., 1954.
2. A. T. Corbin and A. S. May, Broadband Horn Reflector Antenna, Bell Laboratories Record, **33**, p. 401, Nov., 1955.
3. A. P. King, Dominant Wave Transmission Characteristics of a Multimode Round Waveguide, Proc. I.R.E., **40**, Aug., 1952.
4. S. E. Miller, Coupled Wave Theory and Waveguide Applications, B.S.T.J., May, 1954. (See page 681.)
5. H. A. Bethe, Physical Review, **66**, p. 63, 1944. Also Report 43–22, Lumped Constants for Small Irises, Mar. 24, 1943; Report 43–26, Formal Theory of Wave Guides of Arbitrary Cross Section, Mar. 16, 1943; and Report 43–27, Theory of Side Windows in Wave Guides, Apr. 4, 1943; from M.I.T. Radiation Lab.
6. N. Marcuvitz, Waveguide Handbook, p. 408, McGraw Hill.
7. H. Seidel, private communication re: Slab Width Determination and Effects on Coupling Parameters in Partial Dielectric Loading.
8. S. B. Cohn, Determination of Aperture Parameters by Electrolytic Tank Measurements, Proc. I.R.E., Nov., 1951.
9. J. C. Slater, Microwave Electronics, p. 183, Van Nostrand.

The Character of Waveguide Modes in Gyromagnetic Media

By H. SEIDEL

A magnetized gyromagnetic medium is birefringent. The effect of bire-fringence is studied in rectangular and circular waveguides with special attention paid to propagation characteristics in guides of arbitrarily small cross-section. Propagating, small-size structures are found in certain ranges of magnetization for both types of guide.

I. INTRODUCTION

A gyromagnetic medium, isotropic in the absence of a magnetizing field, becomes axially symmetric with respect to that field when magnetized. A tensor susceptibility[1] is thus produced which reflects the resulting anisotropy. Two essentially different types of rays appear in the medium in much the same manner in which the ordinary and extra-ordinary optical rays form in a calcite crystal. These rays may combine to produce results in a ferrite loaded waveguide quite alien in character to those of a conventional isotropic guide. Since the ferrite is, to first order, characteristic of general gyromagnetic media we shall discuss all gyromagnetic phenomena in terms of ferrites alone.

One very startling phenomenon observed in ferrite loaded waveguides is the occurrence of propagation in a waveguide of arbitrarily small transverse dimensions.[2] We shall show that this type of wave guide behavior is a consequence of the particular form of the birefringent character of the medium.

In order to understand the nature of the ferrite loaded case let us first consider the conventional isotropic small wave guide. Fig. 1 shows, schematically, the field distribution encountered in a small rectangular waveguide operating in a (1,1) mode. The x axis is shown along the wide transverse dimension and z is along the narrow height dimension. The y axis is chosen to coincide with the guide axis.

The field solutions of such a waveguide may be obtained as a super-
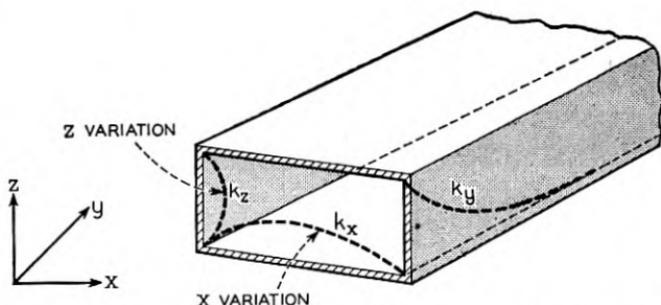
Fig. 1 — Rectangular waveguide mode in isotropic medium for cutoff guide.

position of plane waves of dependence $\varepsilon^{-i\mathbf{k}\cdot\mathbf{R}}$. If we represent $\mathbf{k}$ in a cartesian frame, the wave equation is satisfied for the condition

$$k^2 = k_x{}^2 + k_y{}^2 + k_z{}^2 = \omega^2\mu\varepsilon$$

where μ and ε are the permeability and permittivity respectively of the medium. Satisfaction of wall boundary condition requires that k_x and k_z be real and that each be of the order of the reciprocal of the transverse guide dimensions. Small transverse dimensions thus cause $k_y{}^2$ to be negative, driving the waveguide into a cutoff condition.

We shall now find that birefringence permits another class of modes in the small size ferrite loaded waveguide. Letting the magnetic axis be in the z direction, it will be shown in the text that corresponding to any mode of the guide k_y and k_z are unique. Birefringence generally requires that two different magnitudes of $\mathbf{k}$ occur simultaneously, causing two different values of k_x to appear. In particular, let us postulate that both these values of k_x are imaginary. Given two exponentials, it is possible now to satisfy the requirements of electric field nulls at either side wall, as shown in Fig. 2. At the other side wall we shall show that the exponentials decay so fast as to effectively cause the field to vanish there. Since $k_{z1,\,2}^2$ are now negative quantities, there is no contradiction in presuming that $k_y{}^2$ may now be positive, thus permitting propagation in an arbitrarily small size waveguide.

The effect of birefringence may then be that of transforming a class of longitudinally cutoff modes into another class that propagates longitudinally but cuts off transversely. The condition of this occurrence will be shown to be that for which the diagonal term of the Polder tensor, μ, is positive and is less in magnitude than the magnitude of the off diagonal term κ. In the case of a small rectangular guide, propagation occurs anomalously for negative values of μ, as well but in a manner not as

substantially dependent on the birefringent character of the medium for large width to height aspect ratios of the waveguide. We shall find, further, that propagation occurs with entirely real values of k_x and k_z.

It will be shown that the proper wave equation for one of the two birefringent rays is satisfied in the small waveguide limit by the relationship

$$k_x^2 + k_y^2 + k_z^2/\mu = 0.$$

In the region of $\mu > 0$, and k_z real, we confirm somewhat more rigorously the requirement stated earlier that either k_x or k_y be imaginary. However, k_x and k_y may both be real over a range of negative values of μ, permitting boundary conditions to be satisfied, approximately, in waveguides having aspect ratios of the type discussed earlier, by just one class of rays in the small size waveguide.

Propagation in small size circular guide employing the essential character of birefringence, occurs over the entire range of $|\mu| < |\kappa|$. This range is divided into that of $\mu > 0$ and that of $\mu < 0$. Transmission occurs in one sense of circular polarization in each of these regions and for both senses for $\mu < 0$. Thompson[3] has suggested that propagation in a small circular waveguide might be attributed to the negative permeability of one preferred polarization; it appears, however, that propagation is possible over a considerably wider range of conditions and for somewhat different reasons.

In the case shown in Fig. 2, higher propagating modes occur in a rectangular waveguide when one half or more sinusoids of field variation occurs in the z direction. These simply produce the result of stronger
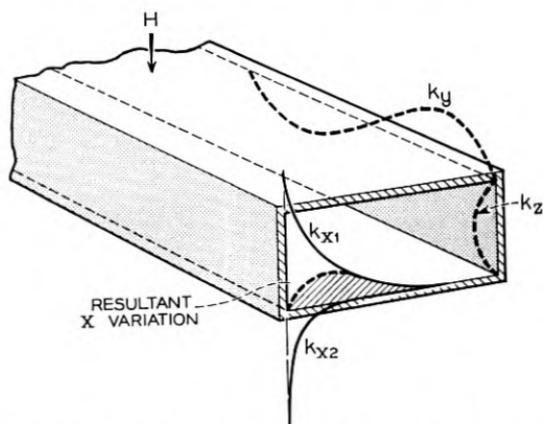
Fig. 2 — Mode in ferrite filled rectangular guide.

transverse cutoff. Therefore, by demonstrating the existence of the lowest order mode we show that an infinite number of these anomalous modes may propagate simultaneously. These modes are, however, bound very tightly as surface waves to the side walls of the guide because of their strong transverse cutoff. The medium is therefore used in a very inefficient manner and high loss results, the loss increasing with mode number.

The higher propagating rectangular waveguide modes have an analogue in the higher propagating modes in a ferrite filled circular waveguide. This analogue occurs in terms of the integral number of peripheral variations. We find, similarly, an infinite number of such propagating modes each one corresponding to a given polarization sense and having a given number of peripheral variations. The reservations on practical transmission still hold in the same manner as in the rectangular case.

In the course of preparing this publication it was brought to the author's attention that Mikaelyan[4] employed an analysis similar, in part, to that developed here. It is felt, in the present analysis, that the physical results are made more readily evident by a consideration of the limiting case of small guides, with large ratios of width to height in the case of rectangular waveguides. The choice of such large ratios is made to simplify analyses involving imaginary values of k_{x1} and k_{x2}, wherein the wave is considered to be bound to one wall of the guide and reflections from the opposite wall are of negligible amplitudes.

II. ANALYSIS OF TRANSVERSELY MAGNETIZED FERRITE IN RECTANGULAR GUIDE

The character of the ferrite medium is introduced through the Polder permeability tensor:

$$T = \begin{pmatrix} \mu & i\kappa & 0 \\ -i\kappa & \mu & 0 \\ 0 & 0 & 1 \end{pmatrix} \tag{1}$$

The quantities μ and κ relate to the self and inductive permeabilities transverse to the z axis. The relative permeability along the z axis is given as unity. These permeabilities may be expressed as follows in gaussian units.[1]

$$\mu = 1 + \frac{4\pi M_s \gamma \omega_0}{\omega_0^2 - \omega^2} \tag{2a}$$

$$\kappa = \frac{4\pi M_s \gamma \omega}{\omega_0^2 - \omega^2} \tag{2b}$$

$$\gamma = 2.80 \text{ Mc/sec/oersted}$$

$$\omega_0 = \gamma H_0$$

$$H_0 = \text{Internal dc magnetic field}$$

$$4\pi M_s = \text{Saturation magnetization}$$

Maxwell's equations are given as:

$$\text{Curl } \boldsymbol{H} = i\omega\varepsilon\boldsymbol{E} \tag{3a}$$

$$\text{Curl } \boldsymbol{E} = -i\omega\mu_0 T \cdot \boldsymbol{H} \tag{3b}$$

Assuming a plane wave of dependence $\varepsilon^{i(\omega t - \boldsymbol{k}\cdot\boldsymbol{R})}$, and appropriately combining (3a) and (3b), we have,

$$[\boldsymbol{kk} - k^2 I + \omega^2\varepsilon\mu_0 T]\cdot\boldsymbol{H} = 0 \tag{4}$$

The operator in square brackets is a dyadic which may be represented in matrix form. The quantity I is the idemfactor, having a unit diagonal representation. If we are to require that a non-trivial field $\boldsymbol{H}$ exist, the determinant of the operator in (4) must vanish. Since all rays traveling perpendicularly to the magnetizing axis are equivalent the medium is degenerate in the transverse plane, and some simplification is achieved in causing $\boldsymbol{k}$ to lie in the yz plane and letting $k_x = 0$. Some further simplification is achieved in normalizing the Polder tensor such that

$$T = \frac{1}{\omega^2\varepsilon\mu_0}\begin{pmatrix} f & ig & 0 \\ -ig & f & 0 \\ 0 & 0 & h \end{pmatrix} \tag{5}$$

The following secular equation is then formed.

$$\begin{vmatrix} -k^2 + f & ig & 0 \\ -ig & -k_z^2 + f & k_y k_z \\ 0 & k_y k_z & -k_y^2 + h \end{vmatrix} = 0 \tag{6}$$

Introducing the substitution $p \equiv k_z^2/k^2$, and recognizing that

$$k_y^2 = k_z^2\left(\frac{1-p}{p}\right)$$

we have upon expanding (6),

$$p^2[(f^2 - g^2)h + k_z^2(f^2 - fh - g^2)] \\ + p[(h-f)k_z^4 - k_z^2(f^2 + fh - g^2)] + k_z^4 f = 0. \tag{7}$$

We note, in general, two solutions in p corresponding to each value of k_z, indicating birefringence of the medium. In particular k_z must be non-vanishing for birefringence to occur or, stated alternatively, rf field gradients must exist parallel to the applied magnetic field to obtain birefringence.

The characteristic vector solutions of (4) may be expressed for each solution of (7); they are the magnetic fields,

$$H = H_x \begin{pmatrix} 1 \\ \dfrac{i}{g}\left(f - \dfrac{k_z^2}{p}\right) \\ \mp \dfrac{i}{g} k_z^2 \left(\dfrac{1-p}{p}\right)^{\frac{1}{2}} \dfrac{\left(f - \dfrac{k_z^2}{p}\right)}{\left(h - k_z^2\left(\dfrac{1-p}{p}\right)\right)} \end{pmatrix} \varepsilon^{-i(k_y y + k_z z)} \quad (8)$$

and the corresponding E fields,

$$E = \frac{k_z}{\omega\varepsilon} H_x \begin{pmatrix} i\,\dfrac{h}{g}\,\dfrac{\left(f - \dfrac{k_z^2}{p}\right)}{h - k_z^2\left(\dfrac{1-p}{p}\right)} \\ -1 \\ \pm \left(\dfrac{1-p}{p}\right)^{\frac{1}{2}} \end{pmatrix} \varepsilon^{-i(k_y y + k_z z)} \quad (9)$$

The sign indeterminacy above is defined with respect to the ratio k_y/k_z, the upper sign being given by the positive value of this ratio.

We shall analyze the rectangular waveguide by first seeking parallel plane solutions and then utilizing these solutions to form those of the rectangular guide. We choose as parallel planes those perpendicular to the applied magnetic field, or z direction and having a separation b. Because of the absolute uniformity of this type of structure, the field configurations as a function of the coordinates transverse to the magnetic field, x and y, may change only by a uniform phase factor. Again, the choice of transverse axes is made such that these phase variations occur only along y.

From (7) we would find that a specification of k_y leads to a quadratic equation in p, with an appropriate consequent multiplicity in k_z^2. Let us define as a partial wave any standing wave in the z direction corre-

sponding to some linear combination of the positive and negative values of k_z for one of the values of $k_z{}^2$. Examination of (9) reveals that the ratio of E_y to E_x, the field components tangent to the bounding walls, to be independent of the sign of k_z. Hence, each partial wave has an individual value of this ratio irrespective of its standing wave distribution in the z direction. It is thus impossible, in general, to provide a mutual cancellation of two or more partial waves at the electric walls by combinations of such partial waves, with the consequence that each partial wave must individually satisfy the boundary requirement. We find, then, that each partial wave takes on the familiar condition $k_z = m\pi/b$.

The parallel plane waves now will be appropriately oriented and superposed to satisfy the side wall boundary conditions in the rectangular guide. Since, as shown in Fig. 2, mutual cancellation is required on the side walls of the rectangular guide, the rate of vertical variation must be identical for all the component parallel plane waves; thus m is a constant of the waveguide mode and k_z is uniquely specified.

Two essential characteristics thus define a rectangular waveguide mode in a transversely magnetized, ferrite filled, medium.

1. The modes are ordered by integral values of m in the relationship $k_z = m\pi/b$.

2. The propagation constant k_y is uniquely specified.

Standing waves may now be formed in the z direction satisfying electric boundary conditions at the parallel planes. Each partial wave of the electric field may then be expressed as follows corresponding to its appropriate value of p:

$$E = \frac{m\pi}{b\omega\varepsilon} H_x \begin{vmatrix} \dfrac{h}{g} \dfrac{\left(f - \dfrac{1}{p}\left(\dfrac{m\pi}{b}\right)^2\right)\sin\dfrac{m\pi}{b}z}{h - \left(\dfrac{m\pi}{b}\right)^2\left(\dfrac{1-p}{p}\right)} \\[2em] i\sin\dfrac{m\pi z}{b} \\[1em] \left(\dfrac{1-p}{p}\right)^{\frac{1}{2}}\cos\dfrac{m\pi}{b}z \end{vmatrix} \varepsilon^{-i(m\pi/b)(1-p/p)^{\frac{1}{2}}y} \quad (10)$$

Let us now specialize our analysis to the small guide case. The requirement of birefringence to produce small guide propagation demands that k_z be non-vanishing and that m take on an integral value of unity or greater. We have, from (7), the two limiting values of p corresponding

to a small value of b,

$$p_1 = \frac{f}{f - h} = \frac{\mu}{\mu - 1} \tag{11a}$$

$$p_2 = k_z^2 \frac{f - h}{f^2 - fh - g^2} = \frac{k_z^2}{\omega^2 \mu_0 \varepsilon} \frac{\mu - 1}{\mu^2 - \mu - \kappa^2} \tag{11b}$$

Discarding the z dependence in equation (10) and dropping a constant multiplier, the two characteristic electric field solutions become:

$$E^{(1)} = \begin{vmatrix} \dfrac{1 - \mu}{\kappa} \\ i \\ i\mu^{-\frac{1}{2}} \end{vmatrix} \varepsilon^{(m\pi/b)\mu^{-\frac{1}{2}}y} \tag{12}$$

$$E^{(2)} = \begin{pmatrix} 0 \\ i \\ i \end{pmatrix} \varepsilon^{(m\pi/b)y} \tag{13}$$

Equations (12) and (13) are parallel plane solutions obtained for some arbitrary direction, y, transverse to the magnetic field. This direction need not be intrinsically real; mathematically, it simply satisfies Maxwell's equations. We may transform to a desired waveguide frame of reference by rotations φ_1 and φ_2, corresponding to p_1 and p_2, about the z axis, where these rotations may possibly be made through complex angles. We then have for the electric fields in the new space:

$$E^{(1)} \to \begin{vmatrix} \dfrac{1 - \mu}{\kappa} \cos \varphi_1 + i \sin \varphi_1 \\ -\left(\dfrac{1 - \mu}{\kappa}\right) \sin \varphi_1 + i \cos \varphi_1 \\ i\mu^{-\frac{1}{2}} \end{vmatrix} \varepsilon^{(m\pi/b)\mu^{-\frac{1}{2}}(y\cos\varphi_1 + x\sin\varphi_1)} \tag{14}$$

$$E^{(2)} \to \begin{vmatrix} i \sin \varphi_2 \\ i \cos \varphi_2 \\ i \end{vmatrix} \varepsilon^{(m\pi/b)(y\cos\varphi_2 + x\sin\varphi_2)} \tag{15}$$

The new y axis of the transformed coordinates is now considered the longitudinal axis of the waveguide.

The partial wave fields of (14) and (15) may be joined to form a single

mode by equating the propagation constant. Therefore,

$$\cos \varphi_2 = \mu^{-\frac{1}{2}} \cos \varphi_1 \tag{16}$$

where $\cos \varphi_2$ is imaginary for propagation. Propagation may therefore occur for $\mu > 0$ and $\cos \varphi_1$ imaginary and/or, $\mu < 0$ and $\cos \varphi_1$ real.

Boundary conditions require E_y and E_z to vanish at both guide side walls. Four equations result which may be satisfied, in turn, by a superposition of four transverse waves involving k_{x_1}, $-k_{x_1}$, k_{x_2}, and $-k_{x_2}$ corresponding to values $\pm\varphi_{1,2}$. For $\mu > 0$ both of the birefringent rays have transverse decay. Since the magnitudes of $k_{x_{1,2}}$ are large in small size guide (see Introduction) boundary conditions need be satisfied for practical purposes at only a single wall. We are then left with the simplification of only two equations in two unknowns.

Setting $x = 0$ in (14) and (15) and taking equation (16) into account, we have the boundary conditions

$$A\left[- \frac{(1 - \mu)}{\kappa} \sin \varphi_1 + i \cos \varphi_1\right] + B[i\mu^{-\frac{1}{2}} \cos \varphi_1] = 0 \tag{17}$$

$$A[\mu^{-\frac{1}{2}}] + B = 0 \tag{18}$$

With the result that

$$\cot \varphi_1 = -i \frac{\mu}{\kappa} = \left(\frac{k_y}{k_{x_1}}\right) \tag{19}$$

Choosing k_y positive real, k_{x_1} is positive imaginary for κ positive and negative imaginary for κ negative. The rf field therefore hugs the right wall for $\kappa > 0$ and the left for $\kappa < 0$, or, alternatively, switches sides in the change from a forward to backward direction of propagation.

Equation (19) may be written equivalently as

$$\cos^2 \varphi_1 = \frac{\mu^2}{\mu^2 - \kappa^2} \tag{20}$$

Propagation, occurring for imaginary values of $\cos \varphi$ and $\mu > 0$, is obtained for $|\mu| < |\kappa|$.

Let us now analyze, the possibility of small guide propagation for $\mu < 0$. We find, from (16), that $\cos \varphi_1$ is real for this case. Two cases arise; the first for which $|\cos \varphi_1| < 1$ and the second for the reverse situation.

Let us first consider the case of $|\cos \varphi_1| < 1$. From (14), k_{x_1} is real whereas from (15) k_{x_2} is imaginary. Let us associate wave amplitudes

with x dependences as follows:

$$A\varepsilon^{-ik_{x1}x}$$

$$B\varepsilon^{ik_{x1}x}$$

$$C\varepsilon^{-ik_{x2}x}$$

$$D\varepsilon^{ik_{x2}(x-a)}$$

where a is the guide width. Let us assume that k_{x_2} is a sufficiently large imaginary quantity of such sign that

$$\varepsilon^{-ik_{x2}a} \ll 1$$

This assumption will be seen to be consistent with the solution. [(26b) for small size guide.]

Setting up the boundary conditions for E_y and E_z at $x = 0$, we have from (14), (15), and (16),

$$(A - B)\left(\frac{\mu - 1}{\kappa}\right)\sin\varphi_1 + i(A + B)\cos\varphi_1 + iC\mu^{-\frac{1}{2}}\cos\varphi_1 = 0 \quad (21a)$$

$$(A + B)\mu^{-\frac{1}{2}} + C = 0 \quad (21b)$$

let $r = B/A$. Combining these last two equations we have

$$\frac{1 - r}{1 + r} = \frac{\kappa}{\mu}\cot\varphi_1 \quad (22)$$

Satisfying the boundary conditions at $x = a$ produces an equation similar to (22) with the substitution

$$r \to r\varepsilon^{-i2k_{x1}a} = r\varepsilon^{-i2\lambda}$$

Thus

$$\frac{1 - r}{1 + r} = \frac{1 - r\varepsilon^{-i2\lambda}}{1 + r\varepsilon^{i2\lambda}} \quad (23)$$

Equation (23) is satisfied by the condition $\lambda = n\pi$. Since $k_{x_1} = i(m\pi/b)\mu^{-\frac{1}{2}}\sin\varphi_1$, we have

$$\sin\varphi_1 = i\mu^{\frac{1}{2}}\frac{n}{m}\frac{b}{a} \quad (24)$$

The assumption that $\cos\varphi_1$ is real and less, in magnitude, than unity is realized by the condition

$$(-\mu)^{\frac{1}{2}}\frac{n}{m}\frac{b}{a} < 1 \quad (25)$$

Only in the limiting condition of a infinitely greater than b do all modes (m, n) propagate in the negative region of μ. In this particular case, $\sin \varphi_1 = 0$ and we find from (21a) and (21b) that $C = D = 0$. Thus we find a situation in which the guide boundary conditions are satisfied by but a single class rays of the two classes available.

This result is entirely comprehensible if we observe the wave number relationship obeyed by $\boldsymbol{k}_1$ and $\boldsymbol{k}_2$. Employing the definition of p which states that $k^2 = k_z^2/p$, and using (11a) and (11b), we have

$$k_{x_1}^2 + k_{y_1}^2 + k_z^2/\mu = 0 \qquad (26a)$$

$$k_{x_2}^2 + k_{y_2}^2 + k_z^2 = 0 \qquad (26b)$$

As stated in the Introduction, it is an entirely consistent procedure to satisfy boundary requirements with real wave numbers over the negative range of μ using the class of rays indicated for (26a) above.

More generally, (25) shows a complex relationship of the ordering of propagation modes by n and m, for finite a, for a given negative value of μ. In contrast to the $\mu > 0$ case, propagation may possibly not occur for a range of lower order integral values of m. As μ becomes increasingly large in magnitude, m must likewise take on increasingly higher values for transmission to occur.

The case of $\cos \varphi_1$ real and greater, in magnitude, than unity, leads to trivial result. Both partial waves have imaginary values of k_x, for this case, and the far wall receives essentially no coupling. Analysis simply repeats the result of (20) and we find that $|\mu| > |\kappa|$ and $\mu < 0$. If the Polder tensor components given in (2a) and (2b) are plotted (see Fig. 5). We find that this last set of inequalities form an impossible combination.

Summarizing we find that a rectangular waveguide of any dimension (and, in particular a guide of arbitrarily small dimensions), filled with a lossless transversely magnetized ferrite medium, will support an infinite number of freely propagating modes at any frequency for which $|\mu| < |\kappa|$. The character of these modes differs considerably in the two regions of $\mu < 0$ and $\mu > 0$ and somewhat different viewpoints of propagation must be taken. We shall find similar results relating to the longitudinally magnetized ferrite filled circular waveguide in the following section.

III. ANALYSIS OF LONGITUDINALLY MAGNETIZED FERRITE IN CIRCULAR GUIDE

We now proceed to a second structural geometry in which an anomalous behavior occurs attributable to the birefringence of the medium.

This is the circular guide which has been the subject of considerable analysis by Suhl and Walker. It is instructive, however, to repeat the analysis of this case, in the small guide limit, showing more pointedly its behavior from the viewpoint of combinations of the two types of waves in the medium.

The character of transmission in undersized circular waveguide is very similar to that of the undersized rectangular case. We may demonstrate the physical significance of this statement by the following argument. The excitation in a rectangular waveguide, for $|\mu| < |\kappa|$ and $\mu > 0$, is essentially that of a surface wave bound very tightly to a single wall. Considering this wall alone, which may now be extended to arbitrary dimensions but with k_z kept large, it may be wrapped upon itself either about the magnetic field as an axis or containing the magnetic field peripherally. In either event, the wrapped guide must start and terminate at the same phase, requiring a multiplicity of 2π around the circumference, and the wave must thus continue to have a large k_z value. Considering the large value of k_z and the state of excitation of the ferrite, the small circular guide may propagate.

Analysis will demonstrate that propagation also takes place in the region $\mu < 0$. The quantity k_{x_1} is real and k_{x_2} imaginary, see (26), leading to a case essentially similar to that of the rectangular waveguide. The analogy is appropriate to the case of b/a of finite value for which the rectangular guide requires the appearance of both refractions. We now proceed to obtain the field solutions for the circular guide.

Referring to (9) for the plane wave solution of the electric field, let us define to within a constant multiplier.

$$E = \begin{pmatrix} iE_x \\ E_y \\ E_z \end{pmatrix} \varepsilon^{-i(k_y y + k_z z)} \tag{27}$$

where, for the case of large k_z (9, 12, 13)

$$E_x^{(1)} = \frac{1-\mu}{\kappa} \qquad E^{(2)} = 0$$

$$E_y^{(1)} = E_2^{(2)} = -1$$

$$E_z^{(1)} = i\mu^{-\frac{1}{2}} \qquad E_z^{(2)} = i$$

$$\frac{k_{y_1}}{k_z} = i\mu^{-\frac{1}{2}} \qquad \frac{k_{y_2}}{k_z} = i$$

We shall consider here, of the two possible wrapped-wall structures, that case in which the magnetic field is applied axially as shown in Fig. 3. Referring to Fig. 4, the cylindrical drical electric wave satisfying Max-
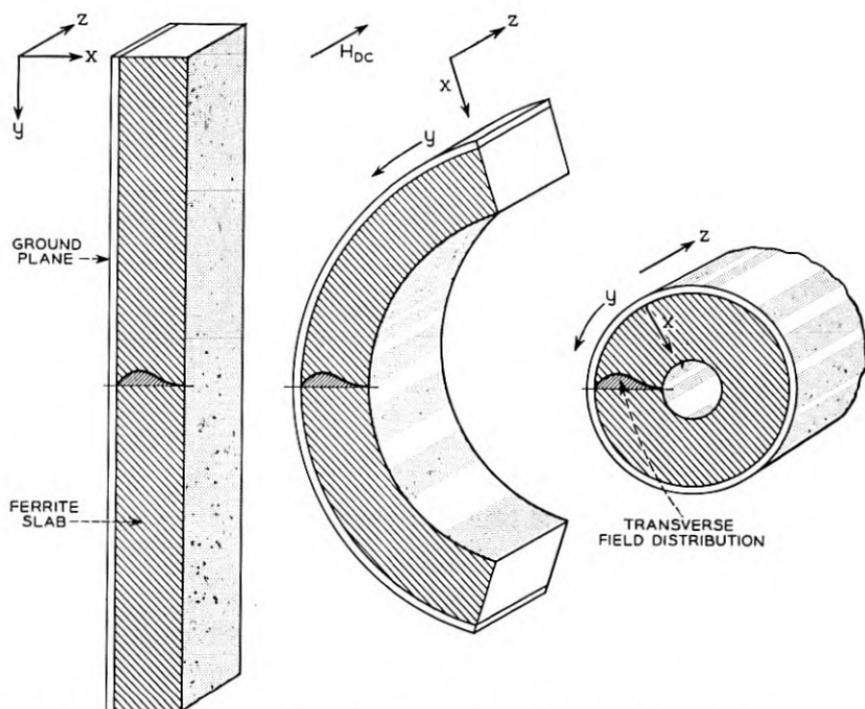
Fig. 3 — Axially magnetized filled circular guide formed by wrapping wall.
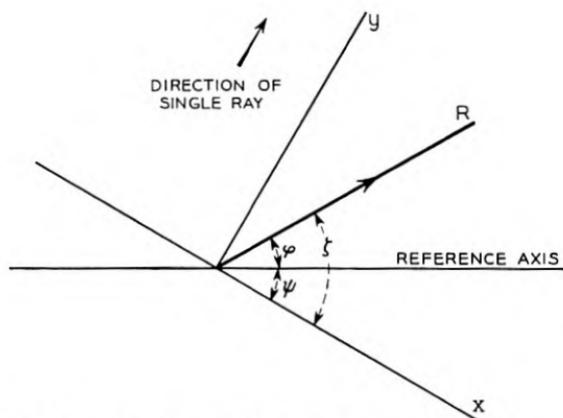
Fig. 4 — Transformation to polar coordinate frame.

well's equations and the boundary conditions for this structure is obtained by integrating plane waves of the form of (27) traveling at all possible angles ψ, the integration being subject to a weighting factor $G(\psi)$ to obtain the most general field. The coordinates (r, φ) refer to the physical system and the coordinate ψ identifies a plane wave traveling along a particular y axis. We have thus in an (r, φ, z) coordinate frame:

$$\underline{E} = \frac{1}{2\pi} \int_0^{2\pi} G(\psi) \begin{pmatrix} \cos \zeta & \sin \zeta & 0 \\ -\sin \zeta & \cos \zeta & 0 \\ 0 & 0 & 1 \end{pmatrix} \begin{pmatrix} iE_x \\ E_y \\ E_z \end{pmatrix} \varepsilon^{-i(k_y y + k_z z)} \, d\psi \tag{28}$$

Recognizing that

$$d\psi = d\zeta$$

$$y = r \sin \zeta$$

and

$$G(\psi) = G(\zeta - \varphi)$$

an integration results over the variable ζ. Because of the uniqueness of the field as a function of φ, the only term containing φ, $G(\zeta - \varphi)$, must be a periodic function in its argument. A typical mode is formed by choosing one of the terms of the Fourier series of $G(\zeta - \varphi)$, namely $\varepsilon^{in(\zeta - \varphi)}$.

We find from (28) that

$$\boldsymbol{E}_n = \begin{pmatrix} i \left[E_x \dfrac{n}{\rho} J_n(\rho) + E_y J_n{'}(\rho) \right] \\ E_x J_n{'}(\rho) + E_y \dfrac{n}{\rho} J_n(\rho) \\ E_z J_n(\rho) \end{pmatrix} \varepsilon^{-i(k_z z + n\varphi)} \tag{29}$$

where $\boldsymbol{E}_n$ is that partial expansion of the total field $\boldsymbol{E}$, corresponding to the number of angular variation n, and $\rho = k_y r$. There are two values of ρ corresponding to the two values of k_y, and each leads to a partial wave. Let A and B be the respective partial wave amplitude; satisfying the boundary conditions on E_φ and E_z, we have from (29):

$$A \left(\frac{1 - \mu}{\kappa} \right) J_n{'}(\rho_1) - \frac{nA}{\rho_1} J_n(\rho_1) - J_n(\rho_2) = 0 \tag{30a}$$

$$A \mu^{-\frac{1}{2}} J_n(\rho_1) + B J_n(\rho_2) = 0 \tag{30b}$$

where ρ_1 and ρ_2 are defined for $r = R$, the radius of the cylinder. Recog-

nizing that $\rho_1 = \mu^{-\frac{1}{2}}\rho_2$, we have from (30)

$$\frac{\mu}{\kappa}J_n'(\rho_1) + n\frac{J_n(\rho_1)}{\rho_1} = 0 *$$ (31)

where $\rho_1 = ik_z\mu^{-\frac{1}{2}}R$.

Equation (21) may be modified by a recurrence relationship to become

$$\frac{\kappa}{\mu} + 1 = \frac{\rho_1}{n}\frac{J_{n+1}(\rho)}{J_n(\rho_1)}$$ (32)

For $\mu > 0$ the quantity ρ_1 is a pure imaginary for large real values of k_z. Since the nth order Bessel function is monotonic in imaginary arguments and possesses the multiplier $(i)^n$, the right-hand side is negative for n positive. For $n > 0$, propagation occurs for

$$|\kappa| > |\mu|$$

$$\operatorname{sgn}\kappa = -\operatorname{sgn}\mu$$

Inspection of (31) reveals that a reversal of the sign of n is equivalent to reversing the sign of κ. This conforms to the physical situation in which reversal of the sense of circular polarization is equivalent to the reversal of magnetic field. Thus for $n < 0$ and $\mu > 0$,

$$|\kappa| > |\mu|$$

$$\operatorname{sgn}\kappa = \operatorname{sgn}\mu$$

We find, from the above arguments, that just one sense of circular polarization propagates in an undersized circular guide for $\mu > 0$ and for a given direction of the magnetic field. It will be demonstrated shortly that propagation occurs for $\mu < 0$, but with an entirely different structure of modes. The right-hand side of (32) is monotonic as a function of ρ for $\mu > 0$, leading to only one solution for each value of n. This will not be the case for $\mu < 0$.

It is of interest first, however, to observe the limiting approach to $\mu = 0$ in the region of $\mu > 0$. The right-hand side of (32) is finite for finite imaginary values of ρ_1, so that the only solution as μ approaches zero is that for which the magnitude of ρ_1 becomes infinitely great. The Bessel function is asymptotically expansible as a cosine divided by a square root of its argument. Thus

$$J_n(\rho_1) = \frac{1}{2}\sqrt{\frac{2\pi}{\rho_1}}\left(\varepsilon^{i(\rho_1+[2n+1](\pi/4))} + \varepsilon^{-i(\rho_1+[2n+1](\pi/4))}\right)$$ (33)

---

* Equation (31) may likewise be obtained from the small radius limit in (34) of Reference 2.

Considering ρ_1 to be positive imaginary, as $\rho_1 \to i\infty$, (32) becomes

$$\frac{\kappa}{\mu} = \frac{-i\rho_1}{n} \tag{34}$$

Substituting for ρ_1, we have

$$k_z = \frac{n\kappa}{\mu^{\frac{1}{2}}R} \tag{35}$$

Thus, as μ approaches zero from values greater than zero, the propagation constant tends to become singular. Physically, however, μ does not vanish but approaches a small imaginary value caused by ferrite losses. The propagation constant k_z becomes complex and takes on a large imaginary component, signifying large guide attenuation. Since these losses occur in the limited neighborhood of $\mu = 0$, we may construe this waveguide behavior as corresponding to a system resonance.

In the region $\mu < 0$, ρ_1 becomes real while ρ_2 remains imaginary. The right-hand side of (32) is now composed of only real arguments. Since the zeros of different order Bessel functions alternate, the right side of (32) contains a succession of poles and zeros, leading to an infinite number of branches with each containing a solution ρ_1 to the equation. Thus there are an infinite number of propagating modes corresponding to each value
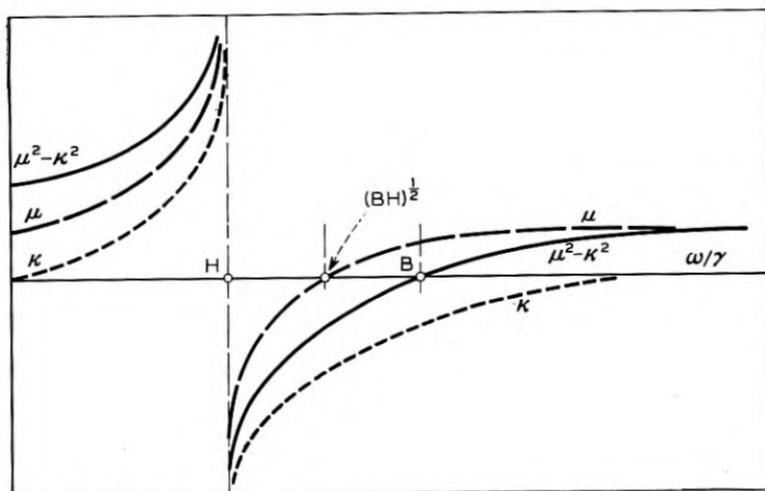
Fig. 5 — Frequency characteristics of Polder tensor components.

of n, in marked contrast to the case of $\mu > 0$. The solutions remain identical, as before, if both κ and n are simultaneously reversed in sign, but differ if only one of the two quantities is reversed.

Since $\mu = 0$ is a branch point, the limiting condition as μ approaches zero for values $\mu < 0$ differs from that for the reverse case. Equation (32) is now satisfied in the limit of small μ by the real zeros of $J_n(\rho_1)$. Since these roots are finite, k_z, equal to $-(-\mu)^{\frac{1}{2}}\rho_1/R$, tends towards zero for all modes. Since the formulae developed in this paper always presume large wave numbers, we may infer a vanishing value of k_z to simply represent a value which is small relative to the reciprocal of the wave-guide radius. In any event, k_z is no longer singular at $\mu = 0$, and there is no resonance in the approach from negative values of μ.

In sum, the features of the circular guide strongly resemble those of the rectangular guide in the region of $\mu > 0$. This was to be anticipated by the "wrapped wall" construction where the wave is tightly bound to the wall. The wrapped equivalences do not hold in the region $\mu < 0$ since, with harmonic transverse dependence, the wave is no longer bound to the wall. This lack of equivalence is manifested in the matter of ordering modes. For a rectangular waveguide of finite aspect ratio, we find from (25) that there are but a finite number of modes corresponding to each value of m for $\mu < 0$. The circular guide differs in providing an infinite number of modes corresponding to each value of n. Further, whereas the circular guide covers the entire range of $|\mu| < |\kappa|$, (25) indicates that the various modes of the rectangular guide covers a more restricted range determined by the guide aspect ratio.

IV. CONCLUSIONS

The waveguide behavior analyzed in this paper has been experimentally observed[5] and good correlation has been obtained. From the viewpoint expressed of forming a guide cross-section by wrapping a wall to which a surface wave is bound, we may anticipate that the unusual behavior observed in the two types of guides examined is probably characteristic of many other structures.

It is not clear, at this time, if the complete set of modes of either the rectangular or circular guides have been exhausted. We already observe that an infinite number of modes propagate simultaneously so that scattering problems become considerably more complex than in the usual cases. It is felt by the author that the field of waveguide analysis calls for new methods and techniques of modal synthesis when ferrite loaded structures are considered.

ACKNOWLEDGMENT

I feel particularly indebted to R. C. Fletcher and H. Boyet for their many valuable comments and suggestions.

REFERENCES

1. D. Polder, Phil. Mag., **40,** p. 99, Jan., 1949.
2. H. Suhl and L. R. Walker, B.S.T.J., **33,** 3, May, 1954. See Fig. 9g, p. 615, and Table I, p. 642.
3. G. H. B. Thompson, Nature, **175,** p. 1135, June 25, 1955.
4. A. L. Mikaelyan, Doklady, A. N. USSR, **98,** 6, pp. 941–944, 1954.
5. H. Seidel, Proc. I.R.E., **44,** p. 1410, Oct., 1956.

Measurement of Dielectric and Magnetic Properties of Ferromagnetic Materials at Microwave Frequencies

By WILHELM VON AULOCK and JOHN H. ROWEN

Some experimental techniques are discussed which permit measurement of the magnetic and dielectric properties of ferrite materials in the microwave region by observing the perturbation in a cylindrical cavity due to insertion of a small ferrite sample. A comparison of the properties of thin disc samples with those of small spheres shows that discs yield more accurate results in the region below ferromagnetic resonance whereas spheres are preferable for the study of ferrite properties near resonance. A short description of instrumentation for cavity measurements at 9,200 mc is given and experimental results of disc measurements are reported for a low-loss BTL ferrite and several disc diameters. A comparison of experimental results with Polder's theory indicates that the loss of polycrystalline ferrites below resonance is considerably lower than that predicted from an evaluation of the width of the resonance absorption line.

1. INTRODUCTION

The dielectric and magnetic properties of semi-conducting ferromagnetic materials such as ferrites have been the subject of intense study in recent years. Analytical expressions for the components μ and κ of the permeability tensor of a loss-free single-crystal ferrite were derived by Polder.[1] These expressions were later modified to include a loss factor α.[2,3] Yager and others[4] measured the resonance absorption of single crystals of nickel ferrite and found very good agreement with theory provided the loss factor α was determined from the width of the measured resonance absorption line. However, when Artman and Tannenwald[5] measured the real and imaginary parts of μ and κ for polycrystalline ferrites they found that agreement with theory was somewhat less than perfect if α was also determined from the measured line width. Discrepancies were observed for both real and imaginary parts of $\mu +$

κ in the region below resonance because the effects of polycrystalline structure and anisotropy forces were neglected in Polder's and Hogan's[2] analysis. Furthermore, it was assumed in the derivation of the permeability tensor that the ferrite is saturated with a biasing dc magnetic field which is large compared to the microwave magnetic field.

There exists a great need for experimental data for all those conditions where some of the above assumptions do not hold. In particular, the region of biasing magnetization between zero and ferromagnetic resonance is of interest because it is the operating region for many ferrite devices such as phase shifters, modulators, and field displacement isolators. Techniques for the measurement of ferrite parameters below resonance were investigated and it was found that the measurement of the perturbation of a degenerate cylindrical cavity by a thin ferrite disc yielded accurate results, whereas observation of the cavity perturbation caused by a small sphere produced less accurate data.

It is the purpose of this paper to describe and discuss the thin disc method and to compare it with other techniques described in the literature.[5, 7] After defining the ferrite parameters as constants in Maxwell's equations it is shown how these parameters can be obtained from various measuring techniques. Instrumentation for the thin disc technique is described and a few remarks are made pertaining to experimental difficulties. Finally, some measurements of low-loss ferrites are reported and compared with values predicted by Polder's relations.

2. DESCRIPTION OF FERRITE PARAMETERS

It is customary[8] to define the electric and magnetic polarization vectors $\vec{P}$ and $\vec{M}$ in terms of the field vectors $\vec{E}$ (electric field intensity), $\vec{D}$ (electric displacement), $\vec{H}$ (magnetic field intensity), and $\vec{B}$ (magnetic induction). In the M.K.S. system we have:

$$\vec{P} = \vec{D} - \varepsilon_0 \vec{E}$$

$$\vec{M} = \vec{B}/\mu_0 - \vec{H}$$

$\varepsilon_0 = 8.854 \times 10^{-12}$ farad/meter, permittivity of free space

$\mu_0 = 4\pi \times 10^{-7}$ henry/meter, permeability of free space

Then, the intrinsic parameters of a ferrite medium are defined as those quantities which relate $\vec{P}$ and $\vec{M}$ to the electric and magnetic fields in the medium respectively.

$$\vec{P} = \varepsilon_0 \chi_e \vec{E}$$

$$\vec{M} = \overleftrightarrow{\chi_m} \vec{H}$$

Whereas the electric susceptibility χ_e is a scalar quantity in ferrites the

magnetic susceptibility $\overleftrightarrow{\chi_m}$ is known to have tensor properties. Assuming that the static magnetic field H_z is in the z-direction we have

$$\overleftrightarrow{\chi_m} = \begin{vmatrix} \chi_m & -j\kappa & 0 \\ j\kappa & \chi_m & 0 \\ 0 & 0 & 0 \end{vmatrix} \qquad (1)$$

If we restrict ourselves to sinusoidal time variation of the RF fields we may describe electric and magnetic losses in the ferrite by regarding χ_e, χ_m, and κ as complex quantities:

$$\chi_e = \chi_e' - j\chi_e''$$
$$\chi_m = \chi_m' - j\chi_m''$$
$$\kappa = \kappa' - j\kappa''$$

Thus, it is seen that the RF properties of a ferrite medium regardless of geometry are completely described by six "intrinsic" parameters, χ_e', χ_e'', χ_m', χ_m'', κ', and κ''. The dielectric constant ϵ and permeability $\overleftrightarrow{\mu}$ of the material are obtained from

$$\varepsilon = \chi_e + 1$$
$$\overleftrightarrow{\mu} = \overleftrightarrow{\chi_m} + 1$$

where 1 is the unit matrix.

It is the objective of the measurement to obtain each of the above parameters as a function of one or more variables of interest such as frequency, saturation magnetization, static magnetic field, temperature, applied power and others. Measurements may be made on single ferrite crystals — mostly for research purposes — or on polycrystalline material for many purposes in connection with the development of ferrite materials and devices. These measurements are generally compared to the behavior of χ_m and κ as predicted by Polder's equations. One obtains from the equation of motion of magnetization[1]

$$\chi_m = \mu - 1 = \frac{\gamma^2 M_z H_z}{\gamma^2 H_z^2 - \omega^2}$$

$$\kappa = -\frac{\omega |\gamma| M_z}{\gamma^2 H_z^2 - \omega^2}$$

Using Suhl and Walker's[3] notation this may be written as

$$\chi_m = \frac{p\sigma}{\sigma^2 - 1}$$

$$\kappa = -\frac{p}{\sigma^2 - 1}$$

where $p = |\gamma| M_z/\omega$ normalized saturation magnetization

$\sigma = |\gamma| H_z/\omega$ normalized static magnetic field in the ferrite

$|\gamma| = 2.8$ mc per oersted, gyromagnetic ratio

ω = operating frequency

It appears that some cavity techniques measure the eigenvalues of (1), $\chi_m + \kappa$ and $\chi_m - \kappa$, directly, which are seen to be

$$\chi_m \pm \kappa = \frac{p}{\sigma \pm 1} \tag{2}$$

Suhl and Walker show that a loss term may be introduced by replacing σ by $\sigma + j\alpha(\text{sgn } p)$ in (2).* Separating real and imaginary parts we get

$$\chi_m' \pm \kappa' = \frac{p(\sigma \pm 1)}{(\sigma \pm 1)^2 + \alpha^2} \tag{3}$$

$$\chi_m'' \pm \kappa'' = \frac{\alpha p(\text{sgn } p)}{(\sigma \pm 1)^2 + \alpha^2} \tag{4}$$

For the determination of α from measurements it is convenient to define a loss tangent

$$\delta_\pm \equiv \frac{\chi_m'' \pm \kappa''}{\chi_m' \pm \kappa'} = \frac{\alpha(\text{sgn } p)}{\sigma \pm 1} \tag{5}$$

Typical curves for $\chi_m \pm \kappa$ and $\delta_\pm$ assuming $p = 0.5$ and $\alpha = 5 \times 10^{-2}$ are shown on Figure 1.† For the purpose of describing and comparing experimental results, it may be convenient to distinguish among various regions of H_z as indicated on the graph because a different measurement technique may be required for accurate measurements in each region.

3. METHODS FOR MEASURING MAGNETIC PROPERTIES

Three measurement methods have been reported in the literature all of which employ the detuning and change in $1/Q$ of a resonant cavity by a small ferrite sample. Van Trier[7] used very thin long cylindrical samples in a coaxial cavity. Artman and Tannenwald[5] employed small spheres, and we used thin discs[9] both placed close to the endwall of a cylindrical degenerate cavity excited by a TE_{111} mode (Figs. 2 and 3). Recently, Berk and Lengyel[6] suggested the use of a cylindrical post at the center

---

* By definition sgn $p = +1$ for $p > 0$ and sgn $p = -1$ for $p < 0$.

† Since it is customary to use $\chi_m + \kappa$ for the designation of the resonance line this notation has been used here. Consequently, p and σ should be assumed negative.
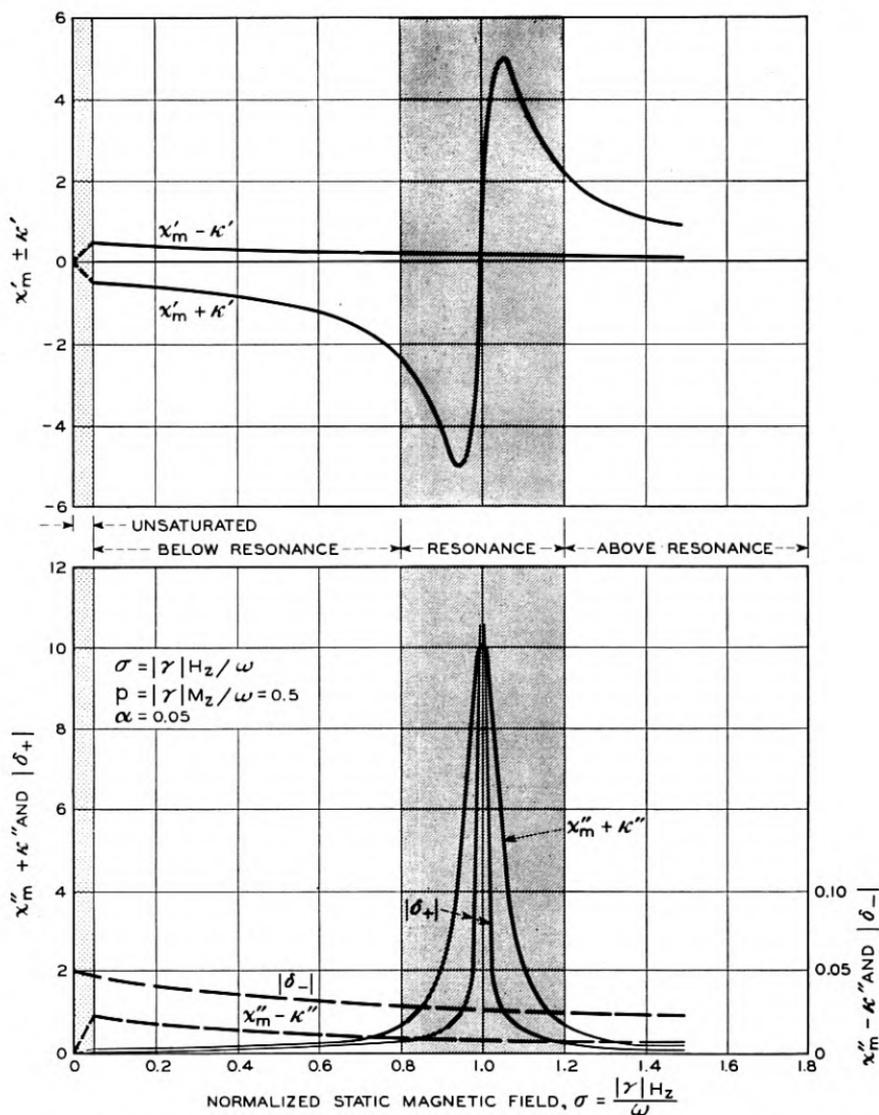
Fig. 1 — Theoretical values of $\chi_m \pm \kappa$ and loss tangent $\delta_\pm$ *versus* normalized static field σ.

of a degenerate rectangular cavity.* In principle, all these methods permit the determination of the six parameters χ_e', χ_e'', χ_m', χ_m'', κ', and κ''. However, in practical applications there are significant differences, e.g.,

* As this paper was being written another variation of the thin cylinder technique using the TM_{110} mode in a circular cavity was reported by Spencer and LeCraw at the I.R.E. Convention, New York, Mar. 21, 1956.

between the use of a spherical sample and a thin disc, such as the perturbing effect on the cavity field, the accuracy of small loss measurement, the occurrence of resonance at a static field where the intrinsic parameters are not at resonance,[10] and the possibility of making accurate measurements of the electric susceptibility. Therefore, the sphere method and the disc method will be reviewed briefly and an attempt will be made to compare their capabilities. It is hoped that this comparison will also be helpful for the evaluation of other measuring techniques not covered in this paper.

3.1 The Small Sphere Method

In order to appreciate the significance of the quantities measured with the small sphere method it is expedient to define an effective susceptibility tensor $\overleftrightarrow{\chi}_{ms}$ by relating the magnetization vector* to the applied
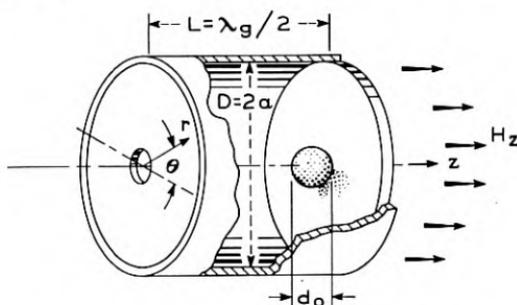
Fig. 2 — Degenerate TE$_{111}$ cylindrical cavity with ferrite sphere.
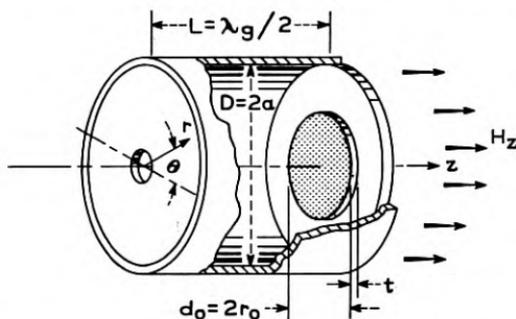
Fig. 3 — Degenerate TE$_{111}$ cylindrical cavity with ferrite disc.

* R. A. Waldron (Institute of Electrical Engineers, Convention Oct. 29 to Nov. 2, on Ferrites, London, 1956) related the magnetic induction vector $\vec{B}$ in a

field $\vec{H}^0$

$$\vec{M} = \overleftrightarrow{\chi}_{ms}\vec{H}^0$$

and observing that the RF components of $\vec{M}$ and $\vec{H}^0$ (denoted by lower case letters) are related in a cylindrical coordinate system by

$$m_r = \chi_{ms}h_r{}^0 - j\kappa_s h_\theta{}^0$$
$$m_\theta = j\kappa_s h_r{}^0 + \chi_{ms}h_\theta{}^0 \tag{6}$$

Placing the small ferrite sphere close to the endwall of the cavity (Fig. 2) and observing the splitting of the resonance into two frequencies $\omega_\pm$ (related to the positive and negative circularly polarized modes) and the two changes in $1/Q$ of the cavity after application of a static magnetic field in the axial direction leads to two measurable quantities

$\Delta\omega_\pm = \omega_0 - \omega_\pm$ frequency shift

$\Delta(1/Q)_\pm = 1/Q_\pm - 1/Q_0$ change in internal Q of the cavity

where ω_0 and Q_0 are resonance frequency and Q of the empty cavity. It can be shown that real and imaginary part of χ_{ms} and κ_s can be obtained from†

$$\frac{2\Delta\omega_\pm}{\omega_0} = 0.6982\,\frac{\lambda_0{}^2}{D^2}\cdot\frac{d_0{}^3}{L^3}\,(\chi_{ms}{}' \pm \kappa_s{}') \tag{7}$$

$$\Delta(1/Q)_\pm = 0.6982\,\frac{\lambda_0{}^2}{D^2}\cdot\frac{d_0{}^3}{L^3}\,(\chi_{ms}{}'' \pm \kappa_s{}'') \tag{8}$$

The quantities d_0, D, and L are the sphere diameter, cavity diameter and length respectively, λ_0 is the wavelength in free space associated with ω_0. In order to obtain the intrinsic parameters χ_m and κ from (7) and (8) one may use the relationships[6]

$$\vec{H}^0 = \vec{H} + \vec{M}/3 \tag{9}$$

$$\chi_{ms} \pm \kappa_s = \frac{3(\chi_m \pm \kappa)}{\chi_m \pm \kappa + 3} \tag{10}$$

---

sphere to the applied field by writing $\frac{1}{\mu_0}\vec{B} = \overleftrightarrow{\mu}_s\vec{H}^0$ where $\overleftrightarrow{\mu}_s$ may be designated the external relative permeability tensor. It can be readily shown that Waldron's results are in agreement with ours if one notes that $(2/3)\overleftrightarrow{\chi}_{ms} = \overleftrightarrow{\mu}_s - 1$. We found that the use of the effective susceptibility tensor $\overleftrightarrow{\chi}_{ms}$ is much to be preferred over $\overleftrightarrow{\mu}_s$ because it simplifies notation and interpretation of experimental results in terms of the intrinsic quantities χ_m and κ.

† Equations (7) and (8) are identical to Artman and Tannenwald's[5] expressions, if $4\pi^2 D^2/(13.56 + \pi^2 D^2/L^2)$ is substituted for $\lambda_0{}^2$.

Equation (10) has a pole at $\chi_m \pm \kappa = -3$ which simply indicates the resonance condition for a sphere as derived by Kittel.[10] This can be verified from (2):

$$\chi_m \pm \kappa = \frac{p}{\sigma \pm 1} \tag{11}$$

Note that p and σ are either both positive or both negative, hence, only one of the two quantities $(\chi_m + \kappa)$ or $(\chi_m - \kappa)$ goes through resonance at $|\sigma| = 1$. A similar situation exists for $\chi_{ms} \pm \kappa_s$ expressed in terms of (11)

$$\chi_{ms} \pm \kappa_s = \frac{3p}{p + 3(\sigma \pm 1)} \tag{12}$$

One of the two quantities $(\chi_{ms} \pm \kappa_s)$ goes through resonance at

$$|\sigma|_s = 1 - |p|/3 \tag{13}$$

Observing that the field in the sphere is given by (9) this may be written as

$$\frac{\omega_r}{|\gamma|} = H_z + M_z/3 = H_z^0 \tag{14}$$

(Kittel's resonance frequency of a ferrite sphere)

It is easily seen that this resonance of the spherical sample makes the evaluation of χ_m and κ from (10) rather unattractive because one would expect inaccurate results for χ_m and κ in the vicinity of the sphere resonance σ_s. Furthermore, for all numerical computations (10) must be separated into real and imaginary parts

$$\chi_{ms}' \pm \kappa_s' = 3 \frac{(\chi_m' \pm \kappa' + 3)(\chi_m' \pm \kappa') + (\chi_m'' + \kappa'')^2}{(\chi_m' \pm \kappa' + 3)^2 + (\chi_m'' \pm \kappa'')^2} \tag{15}$$

$$\chi_{ms}'' \pm \kappa_s'' = 9 \frac{\chi_m'' \pm \kappa''}{(\chi_m' \pm \kappa' + 3)^2 + (\chi_m'' \pm \kappa'')^2} \tag{16}$$

In general higher order terms of χ_m'' and κ'' may be neglected, but in the vicinity of sphere resonance these terms predominate as the term $\chi_m' \pm \kappa' + 3$ vanishes. It can be seen from the preceding discussion that the determination of χ_m', χ_m'', κ', and κ'' from χ_{ms} and κ_s has its difficulties. Fortunately, there is an easier way to the interpretation of χ_{ms} and κ_s in terms of the intrinsic parameters χ_m and κ. We use (9) to define a new quantity σ' in terms of the applied magnetic field.

$$\sigma' = \sigma + p/3 = |\gamma| H_z^0/\omega \tag{17}$$

Now (12) may be written in terms of the normalized applied static field as

$$\chi_{ms} \pm \kappa_s = \frac{p}{\sigma' \pm 1} \tag{18}$$

Comparison with (11) shows that the functional dependency of the effective parameters χ_{ms} and κ_s on the applied field H^0_z is identical to Polder's relations for $\chi_m \pm \kappa$. This permits plotting $\chi_{ms} \pm \kappa_s$ versus H^0_z and relabeling the coordinates $\chi_m \pm \kappa$ and H_z, provided that Polder's equations hold exactly. It would appear however that one of the reasons for measuring ferrite parameters is the fact that Polder's equations are known to be approximations which do not always hold and which are subject to many restrictions as pointed out earlier in this paper. Summing up, one may say that measurements of the parameters of a small ferrite sphere lead to excellent results in terms of effective quantities χ_{ms} and κ_s as a function of the applied static field, but may only be approximations when interpreted in terms of the intrinsic parameters χ_m and κ.

3.2 *The Thin Disc Method*

The use of a thin disc rather than a small sphere as a cavity perturbation eliminates most of the difficulties enumerated in the previous section because the intrinsic parameters $\chi_m \pm \kappa$ are measured directly. Placing a thin disc against the endwall of a cylindrical TE$_{111}$ mode cavity (Fig. 3) and observing the splitting of the resonance frequency and change in $1/Q$ as before one obtains the following relationships (see Appendix for derivation)

$$\frac{\Delta\omega_\pm}{\omega_0} = \frac{1}{4} \frac{\lambda_0^2 t}{L^3} (\chi_m' R_1 \pm \kappa' R_2) \tag{19}$$

$$\Delta\left(\frac{1}{Q}\right)_\pm = \frac{1}{2} \frac{\lambda_0^2 t}{L^3} (\chi_m'' R_1 \pm \kappa'' R_2) \tag{20}$$

The quantity t denotes the thickness of the disc, and R_1 and R_2 are functions of the geometry which take into account that the RF magnetic field is not constant over the face of the disc. A plot of R_1 and R_2 versus the ratio of disc diameter to cavity diameter (Fig. 4) shows that the functions are closely equal for disc diameters less than $\frac{1}{2}D$. This implies circular polarization of the magnetic field in this region whereas the field becomes elliptically polarized as one approaches the outer diameter of the cavity. It might be argued that the disc should be small enough
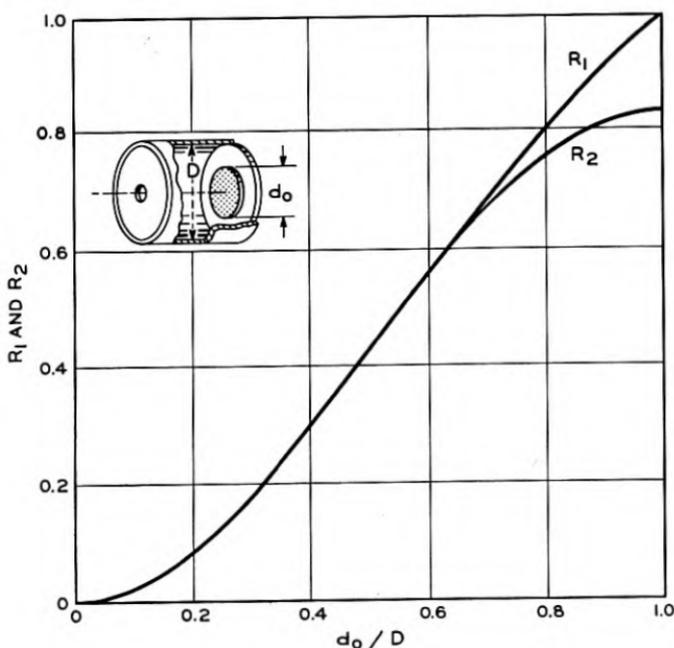
Fig. 4 — The functions R_1 and R_2 *versus* the ratio of disc diameter d_0 to cavity diameter D.

to be entirely within the circularly polarized region. However, this requirement appears to assume that there is some interaction, such as spinwave coupling, between adjacent regions in the disc. It is possible that such interaction exists in single crystals and leads to multiple resonance effects. However in polycrystalline material it is safe to assume that each crystallite reacts independently with the RF magnetic field, enabling us to sum these effects by simple integration.

This integration has been performed in the derivation of (19) and (20) under the assumption that the disc is thin enough to introduce only a first order perturbation into the cavity field. It will be shown presently that these assumptions are consistent with experimental results.

The measured effects $\Delta\omega_\pm$ and $\Delta(1/Q)_\pm$ depend on the volume of the perturbing body, hence one would expect that these effects are at least an order of magnitude larger for thin discs than for small spheres. This permits very accurate measurement of ferrite parameters in the region below saturation and below and above resonance. In particular, the loss parameters $\chi_m'' \pm \kappa''$ of modern low-loss ferrites can be determined accurately in these regions. However, in the resonance region, the measured effects become so large that measurement becomes difficult. Hence,

we do not recommend this method for measurement of resonance line-width. The greatest advantage of the thin disc method lies in its ability to explore the region below resonance where many ferrite devices operate. It will be noted that this region is wider for the disc than for a small sphere or for a thin cylinder magnetized normal to its axis. Using Kittel's relations we find the field in the ferrite at which resonance occurs for a given saturation magnetization and operating frequency

$$H_{res} = \frac{\omega}{|\gamma|} \qquad H_{res} = \frac{\omega}{|\gamma|} - \frac{M_z}{3} \qquad H_{res} = \frac{\omega}{|\gamma|} - \frac{M_z}{2} \qquad (21)$$
Thin Disc   Small Sphere   Thin Cylinder

It is seen that for some materials a small sphere or a thin cylinder may be at resonance even before it is saturated.

4. METHODS FOR MEASURING THE DIELECTRIC PROPERTIES

In principle the electric susceptibility χ_e may be measured with any of the three sample shapes discussed above provided the sample is placed into a region of maximum electric and vanishing magnetic field, e.g., the center of a TE_{111} mode cylindrical cavity. A simple computation shows that a small sphere located at the center of the cavity produces a frequency shift and change in $1/Q$ as follows:

$$\frac{\Delta\omega}{\omega_0} = 4.189 \frac{\chi_e{}'}{\chi_e{}' + 3} \cdot \frac{d_0{}^3}{D^2 L} \qquad (22)$$

$$\Delta(1/Q) = 25.136 \frac{\chi_e{}''}{(\chi_e{}' + 3)^2} \cdot \frac{d_0{}^3}{D^2 L} \qquad (23)$$

In actual measurements it is found that the dielectric constant is not entirely independent of the diameter of the sphere, and that the measurement of the loss factor $\chi_e{}''$ is difficult because the change in $1/Q$ is very small. An additional inherent difficulty of this method is the fact that (22) is rather insensitive to large values of χ_e as are frequently encountered with ferrites. Again the thin disc method permits greater ease of measurement, larger effects, and a simpler relationship between the observed quantities and χ_e. We find (see Appendix A)

$$\frac{\Delta\omega}{\omega_0} = \chi_e{}' \frac{t}{L} R_1 \qquad (24)$$

$$\Delta(1/Q) = 2\chi_e{}'' \frac{t}{L} R_1 \qquad (25)$$
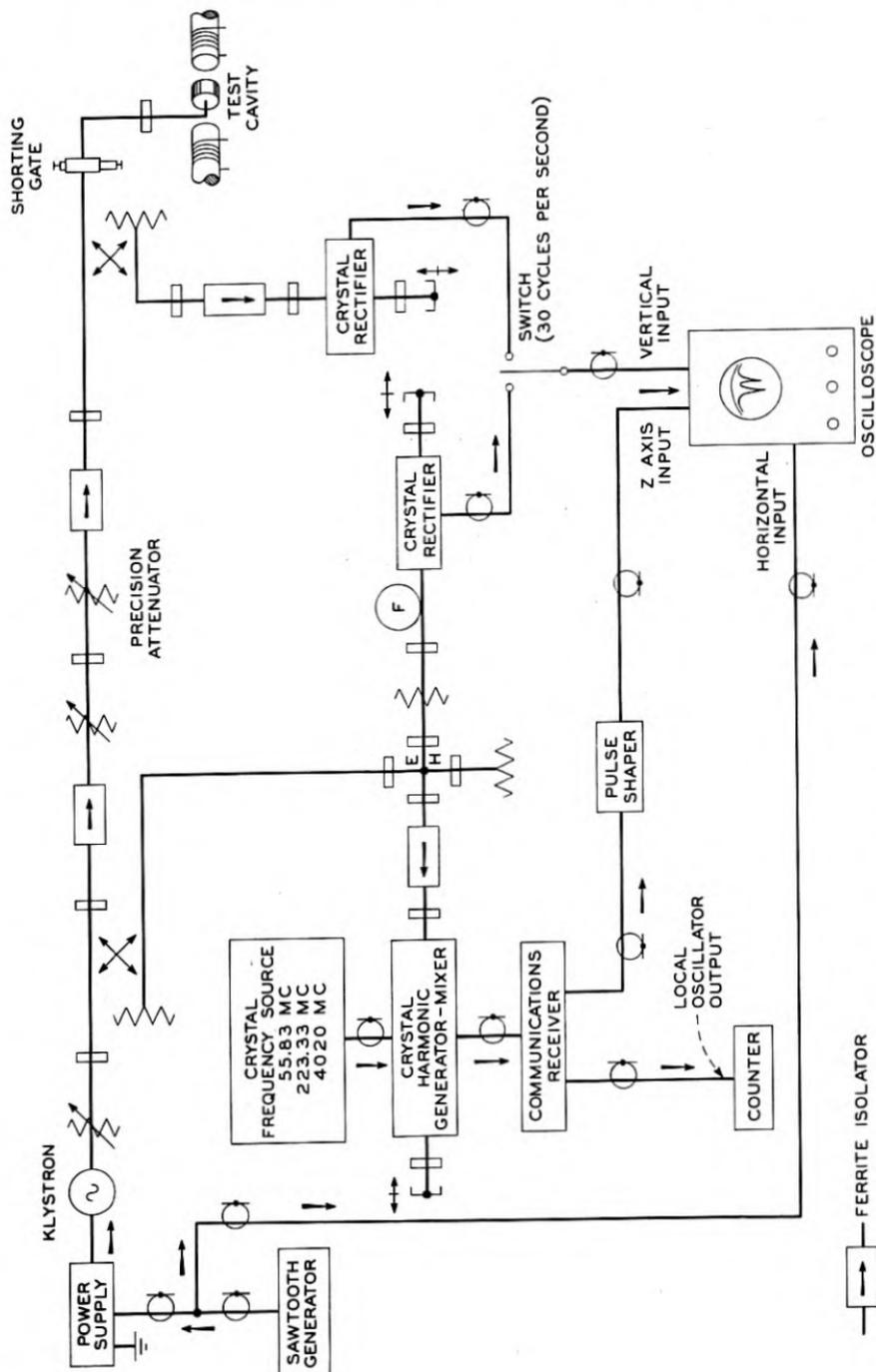
Fig. 5 — Microwave circuit for measuring ferrite parameters.

5. INSTRUMENTATION

Our measurement technique has been influenced by a number of practical considerations including the need for determining accurately and quickly a figure of merit for a large number of different ferrite materials. In particular, a variety of low loss materials has become available in experimental quantities requiring a precise technique for measuring small loss factors below resonance as a guide for further ferrite development. Therefore we were faced with the problem to develop an instrumentation capable of measuring these small loss factors but simple enough to be operated without detailed knowledge of microwave techniques. Fortunately the use of thin discs permits us to introduce a fairly large volume of ferrite into the cavity without violating the basic assumption of a small perturbation. As a consequence frequency shifts of the order of 10 mc are obtained at static magnetic fields just sufficient to saturate the material. Thus the quantities χ_m' and κ' may be measured without difficulty in the regions below and above resonance.

The thickness of the disc should be chosen to attain an aspect ratio (diameter/thickness) of 50 or larger. Discs of 0.005 to 0.007-inch thickness were employed in actual measurements at 9200 mc. For a typical measurement of a 0.005-inch disc at 9200 mc, a change of $1/Q$ of about 2 per cent corresponds to a loss term $\chi_m'' + \kappa'' = 2 \times 10^{-3}$. Measurement of Q with a reproducibility of 1 per cent has been accomplished initially by careful work, and it has been our objective to maintain this accuracy in routine measurements by semiskilled operators. This required the use of rather elaborate circuitry for the precise measurement of the changes in $1/Q$ of the cavity. Although most of these techniques have been used before in the field of microwave spectroscopy we hope that the description of this instrumentation will be of interest.

Fig. 5 shows a block diagram of the circuit. A klystron Type V58 (Varian Associates) is swept through a frequency band of about 80 mc at X-band. The resulting signal with a center frequency of 9,200 mc is used to excite a TE_{111} mode cylindrical cavity. Incident and reflected signals are separated by means of directional couplers and displayed on an oscilloscope. Both signals can be aligned with the aid of a shorting gate and a precision attenuator in front of the cavity. The reflected signal shows clearly the cavity resonance which splits into two if a ferrite disc is placed against the endwall of the cavity and magnetized along the cavity axis.

One of the major problems of the measurement is the accurate determination of these new cavity resonance frequencies and of the line width of the displayed resonance curves between half-power points. In the

solution of this problem, more than ordinary emphasis was placed on ease of operation and elimination of ambiguities in the frequency determination. The resulting instrumentation uses as a stable reference frequency a crystal-controlled oscillator and a frequency multiplier which yields three reference frequencies; 55.8, 223.3 and 4,020 mc. These are mixed in a crystal harmonic generator and mixer leading to a line spectrum of numerous reference frequencies with a constant spacing of 55.8 mc. The same crystal mixer produces a beat frequency signal between the incident signal from the klystron and each of these reference frequencies. A communication receiver with modified IF stage permits selection of a frequency marker out of these beat frequency signals. This marker appears as a blank spot on the traces of incident and reflected signal, and can be moved to any desired point by simply changing the frequency setting of the receiver. Since the receiver dial cannot be read with great accuracy on the high frequency ranges, a frequency counter connected with the local oscillator of the receiver permits a reading of the oscillator frequency to an accuracy of 1 kcps. Noting that the local oscillator is 0.455 mc removed from the difference signal, one obtains the frequency of the difference signal with more than sufficient accuracy.

6. *Results of Measurements*

Transmission- and reflection-type cylindrical cavities have been employed for measurements with linearly and circularly polarized excitation in the 6,000- and 9,000-mc frequency bands. Circular polarization is preferable in the region below saturation where frequency shifts are small.

It is not necessary to choose ferrite discs of relatively small diameter for the purpose of staying within the region of circular polarization close to the cavity axis. The derivation of $\chi_m \pm \kappa$ is not restricted to circularly polarized fields, and the result takes into account that the field becomes more and more elliptically polarized as one approaches the edge of the cavity. This can be seen by rewriting (19) and (20) as follows:

$$\chi_m' \pm \kappa' = \frac{1}{\omega_0 F R_1 R_2} [\Delta\omega_\pm (R_1 + R_2) - \Delta\omega_\mp (R_1 - R_2)]$$

$$\chi_m'' \pm \kappa'' = \frac{1}{2 F R_1 R_2} [\Delta(1/Q)_\pm (R_1 + R_2) - \Delta(1/Q)_\mp (R_1 - R_2)] \quad (26)$$

where $F = t\lambda_0^2/(2L^3)$.

The factor $(R_1 - R_2)$, which is zero for circular polarization, corrects the values for $\chi_m \pm \kappa$ if the disc extends into the region of elliptical

polarization. For relatively small discs ($R_1 = R_2$), one obtains

$$\chi_m' \pm \kappa' = \frac{2}{\omega_0 F R_1} \Delta\omega_\pm$$

$$\chi_m'' \pm \kappa'' = \frac{1}{F R_1}\Delta(1/Q)_\pm$$

(27)

A large number of measurements was made with a half-wave, reflection-type cavity and linearly polarized excitation. Some typical results will be discussed below to demonstrate the applicability of the disc technique. The frequency shift measurements and $\chi_m' \pm \kappa'$ for a ferrite material of 1,300 oersted saturation magnetization are shown on Fig. 6. The ferrite disc has a thickness of 0.0063 inch and completely covers the endwall of the cavity. If the field in the cavity were circularly polarized throughout, then the frequency shift would vary as $\chi_m' \pm \kappa'$. However, elliptical polarization causes a deviation of the measured curves for $\Delta\omega_\pm$ from $\chi_m' \pm \kappa'$. Agreement between theoretical and experimental values of $\chi_m' \pm \kappa'$ is good in the regions below and above resonance. Measurements in the resonance region are not possible with a disc of this size because frequency shift and change in Q are so large that the assumption of a small perturbation is violated. In order to establish further that measurements of $\chi_m' \pm \kappa'$ are independent of disc diameter three discs of the same material (saturation magnetization 1300 oersted) with diameters of 0.249, 0.400, and 1.050 inches were measured in the above-mentioned cavity. Plots of χ_m' and κ' (Fig. 7) indicate good agreement for κ' and some scattering of values for χ_m'. This can be explained by noting that the resonance frequency of the empty cavity enters into the computation of χ_m', but cancels out for κ' (equation 19). Consequently, a very small change in the length of the cavity, as might be expected from opening and reassembling the device, will produce a noticeable error in the low-field region. A change in cavity length of 10^{-4} inch will produce a frequency shift of 1 mc at an operating frequency of 10,000 mc and introduce an error of the order of 0.02 into the measurement of χ_m'. This error may be minimized by using a relatively large disc.

Discs with a diameter of 0.4 inch yielded good measurements of the imaginary quantities $\chi_m'' \pm \kappa''$ in the low-field region. A typical result for a low-loss ferrite (Fig. 8) shows the measured quantities $\Delta(1/Q)_\pm$ and the corresponding $\chi_m'' \pm \kappa''$ as a function of the applied magnetic field. (The internal field in the ferrite is obtained by subtracting the magnetization from the applied field). It is noted that only $\Delta(1/Q)_-$ can be observed in the resonance region, whereas $\Delta(1/Q)_+$ becomes too
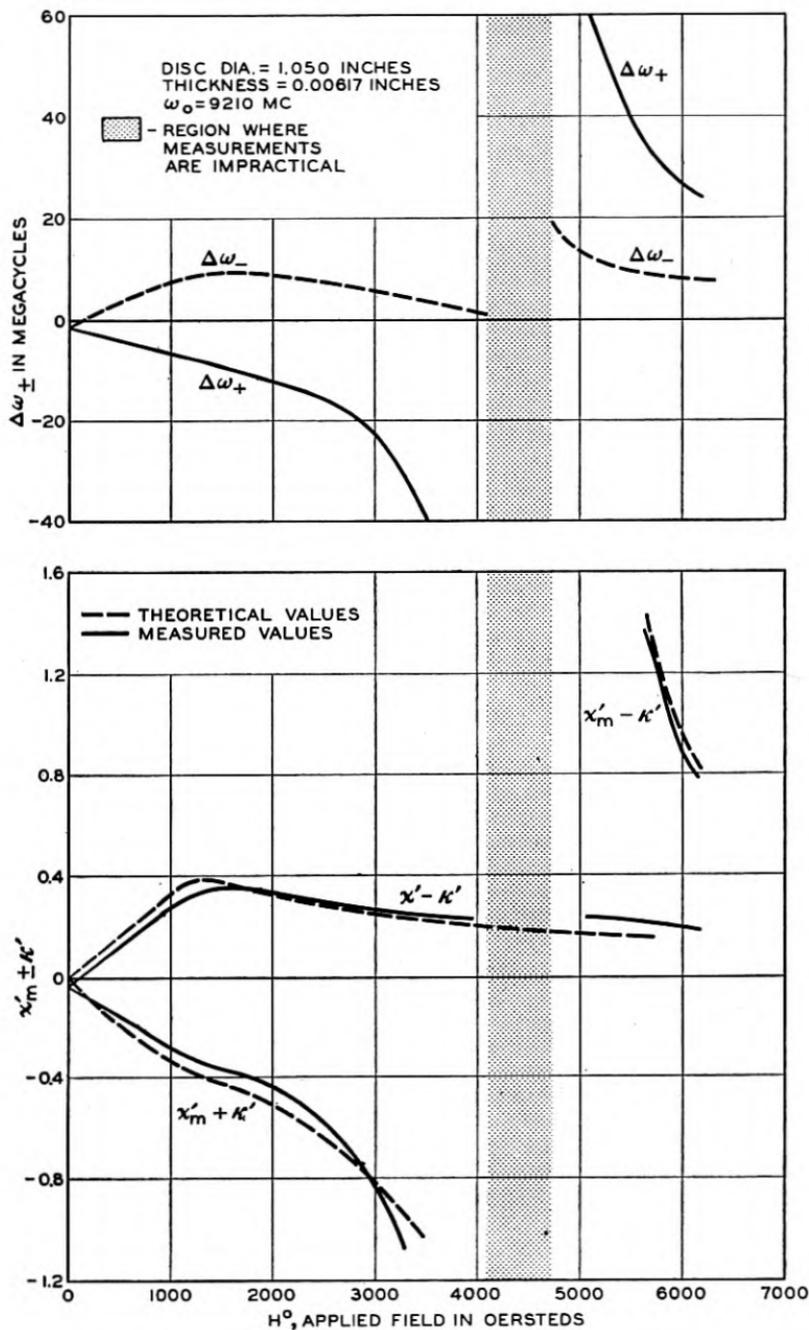
FIG. 6 — Evaluation of $\chi'_m \pm \kappa'$ from measurements of frequency shift $\Delta\omega_\pm$ and comparison with Polder's theory. Low-loss BTL ferrite, saturation magnetization 1300 oersted.
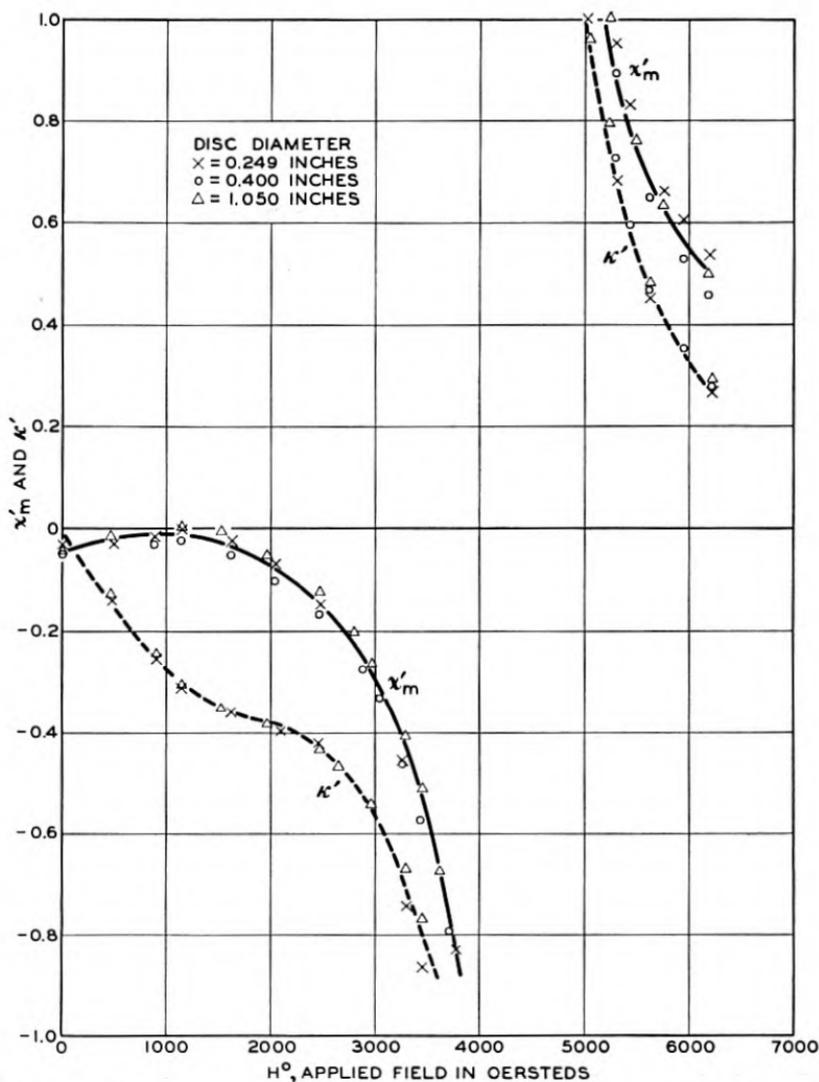
FIG. 7 — Measurement of χ_m' and κ' versus applied static field for three different discs, cut from the same ferrite block.

large to be measured. Knowledge of $\Delta(1/Q)_-$ is not sufficient to determine $\chi_m'' - \kappa''$ in the resonance region because here the correction term $\Delta(1/Q)_+(R_1 - R_2)$ (cf. equation 26) becomes comparable to the term $\Delta(1/Q)_-(R_1 + R_2)$ and is needed to compensate for the anomalous peak of the $\Delta(1/Q)_-$ curve. The loss parameters $\chi_m'' \pm \kappa''$ assume values of the order of 10^{-2} below and above resonance. The estimated error of the measurement is 3×10^{-3}.
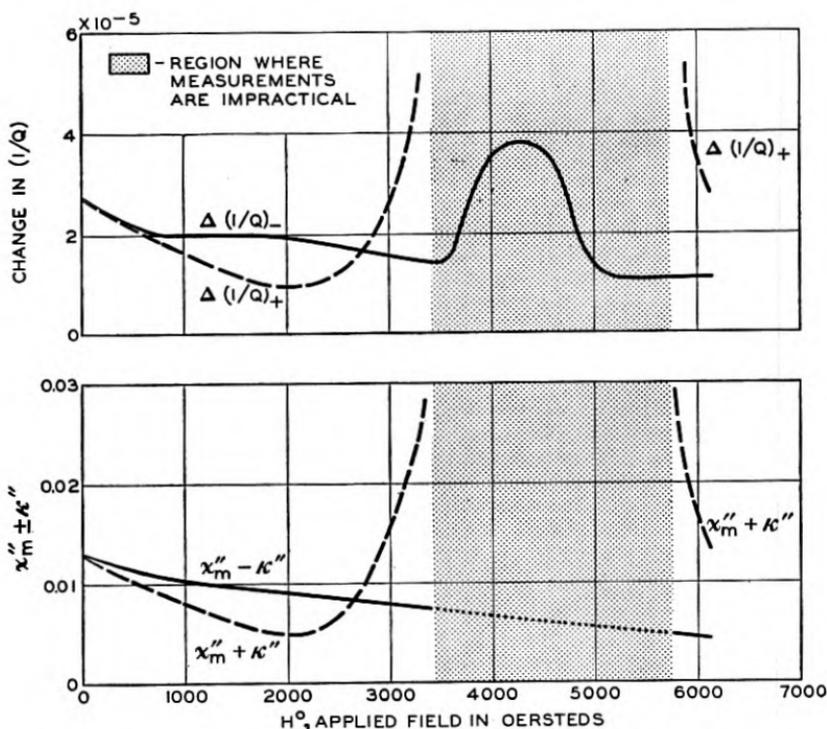
FIG. 8 — Evaluation of $\chi_m'' \pm \kappa''$ from measurements of $\Delta(1/Q)_\pm$ for low-loss BTL ferrite, saturation magnetization 1300 oersted.

Whereas it is possible to obtain good agreement between measured and theoretical curves of $\chi_m' \pm \kappa'$ from Polder's relations (3), such an agreement cannot be obtained for $\chi_m'' \pm \kappa''$ from a comparison with (4). This discrepancy is assumed to be caused by the fact that Polder's theory was developed for single ferrite crystals and did not take into account the random orientation of crystal axes in polycrystalline materials, such as the ferrites used in these measurements. It is reasonable to expect a broadening of the resonance line and a departure from the Lorentzian shape in polycrystalline ferrites; hence, the expression for the absorption line (4) no longer holds.

Measurement of the electric susceptibility of ferrites did not present any major difficulties, provided some care was used in the suspension of the discs at the cavity center.

Summing up these results it may be said that the disc method has yielded satisfactory measurements of the intrinsic parameters of polycrystalline ferrites below and above resonance as well as in the un-

saturated region. Measurements of single crystals and of resonance curves with this method have not yet been made.

It is anticipated that in both cases smaller and thinner discs would be needed than have been available so far. However, it can be hoped that these difficulties will be overcome in the near future and that the disc method will be useful also for the study of ferromagnetic resonance phenomena.

Appendix

PERTURBATION OF A DEGENERATE CYLINDRICAL CAVITY DUE TO A THIN DISC

The general perturbation equation for a lossless cavity can be derived from energy considerations or directly from Maxwell's equations. We obtain for the shift of resonance frequency due to a small perturbation:

$$2\frac{\omega_0 - \omega_1}{\omega_0} = \frac{\frac{\mu_0}{2}\int_{v_1} \vec{m}\cdot\vec{h}^{0*}\,dv + \frac{1}{2}\int_{v_1} \vec{P}\cdot\vec{E}^{0*}\,dv}{\frac{\mu_0}{2}\int_{v_2} \vec{h}^0\cdot\vec{h}^{0*}\,dv} = \frac{W_m^{(s)} + W_e^{(s)}}{W^{(c)}} \quad (A1)$$

ω_0 resonance frequency of the empty cavity

ω_1 resonance frequency of the cavity after insertion of the perturbing sample

$\vec{h}^0$ magnetic field intensity vector in the empty cavity

$\vec{E}^0$ electric field intensity vector in the empty cavity

v_1 volume of sample

v_2 volume of cavity

*   indicates the conjugate value

The denominator in (A1) indicates the total energy $W^{(c)}$ stored in the empty cavity at resonance, whereas the numerator is equal to the additional magnetic energy $W_m^{(s)}$ and electric energy $W_e^{(s)}$ stored in the perturbing sample.

Equation (A1) is valid if the frequency shift is small,

$$\frac{\Delta\omega}{\omega_0} = \left| \frac{\omega_1 - \omega_0}{\omega_0} \right| \ll 1 \quad (A2)$$

and if the field in the cavity remains essentially unchanged after insertion of the sample. In order to apply (A1) to the determination of the tensor components χ_m and κ we should attempt to satisfy three conditions: the electric field should vanish at the sample, the magnetic field should be normal to the static magnetic field, and the relationship between RF

magnetization $\vec{m}$ and RF magnetic field $\vec{h^0}$ in the cavity should be simple. All three conditions can be satisfied if a thin ferrite disc is placed against the endwall of the cavity (Fig. 3). Noting that the tangential component of the magnetic field intensity is continuous at the plane face of the disc we have:

$$
\begin{aligned}
m_r &= \chi_m h_r^0 - j\kappa h_\theta^0 \\
m_\theta &= j\kappa h_r^0 + \chi_m h_\theta^0
\end{aligned}
\tag{A3}
$$

Inserting (A3) into (A1) we find the additional magnetic energy stored in the disc

$$
W_m^{(s)} = \frac{\mu_0}{2} \int_{v_1} [\chi_m(h_r^0 h_r^{0*} + h_\theta^0 h_\theta^{0*}) + j\kappa(h_r^0 h_\theta^{0*} - h_\theta^0 h_r^{0*})] \, dv \tag{A4}
$$

In order to evaluate (A4) we use the fact that the TE_{111}-mode can be expressed as the sum of two circularly polarized modes rotating in opposite directions

$$
\begin{aligned}
\vec{h^0} &= \vec{h_1^0} + \vec{h_2^0} \\
\vec{E^0} &= \vec{E_1^0} + \vec{E_2^0}
\end{aligned}
\tag{A5}
$$

Thus, we have

$$
h_{r1,2}^0 = B \frac{\beta}{k_c} J_1{}'(k_c r) e^{\pm j\theta} \cos \beta z
$$

$$
h_{\theta 1,2}^0 = \pm j B \frac{\beta}{k_c^2 r} J_1(k_c r) e^{\pm j\theta} \cos \beta z \tag{A6}
$$

$$
h_{z1,2}^0 = B J_1(k_c r) e^{\pm j\theta} \sin \beta z
$$

$$
E_{r1,2} = \pm B \frac{\omega \mu_0}{k_c^2 r} J_1(k_c r) e^{\pm j\theta} \sin \beta z
$$
$$
\tag{A7}
$$
$$
E_{\theta 1,2} = j B \frac{\omega \mu_0}{k_c} J_1{}'(k_c r) e^{\pm j\theta} \sin \beta z
$$

B	amplitude factor
J_1	Bessel function of the first kind
$\beta = (\beta_0{}^2 - k_c{}^2)^{\frac{1}{2}}$	propagation constant in the z-direction
$k_c = p_1'/a$	propagation constant in the r-direction
$\beta_0 = 2\pi/\lambda_0$	propagation constant in free space
L	length of cavity
λ_0	wavelength in free space
a	radius of cavity
$\lambda_g = 2L$	wavelength in the cavity
$p_1' = 1.841$	first zero of the derivative of J_1

Integration of the electric or magnetic field over the volume of the cavity yields the stored energy in the empty cavity at resonance for one of the two circularly polarized modes

$$W^{(c)} = 0.2387 \frac{\pi\mu_0}{4} \cdot \frac{\beta_0^2}{k_c^2} B^2 a^2 L \tag{A8}$$

The magnetic energy $W_m^{(s)}$ in the disc is found by integrating (A4) over the volume of the disc and assuming that the field is constant over the thickness t of the disc. We obtain:

$$W_m^{(s)} = 0.2387 \frac{\pi\mu_0}{2} \frac{\beta^2}{k_c^2} B^2 a^2 t (\chi_m R_1 \pm \kappa R_2) \tag{A9}$$

The two functions R_1 and R_2 depend on the ratio of disc radius to cavity radius

$$R_1 = 4.1893 \frac{r_0^2}{a^2} \left[(J_0(k_c r_0))^2 + \left(1 - \frac{2}{(k_c r_0)^2} \right) (J_1(k_c r_0))^2 \right] \tag{A10}$$

$$R_2 = 2.4720 (J_1(k_c r_0))^2 \tag{A11}$$

It is interesting to note that these two functions are approximately equal (Fig. 4) if the disc radius is less than half the cavity radius. In this region the field in the cavity is essentially circularly polarized, whereas elliptical polarization exists near the wall of the cavity. Inserting (A8) and (A9) into (A1) we find the desired relationship between the two frequency shifts associated with positive and negative circular polarization and the tensor components χ_m and κ.

$$2 \frac{\Delta\omega_\pm}{\omega_0} = \frac{1}{2} \frac{\lambda_0^2 t}{L^3} (\chi_m R_1 \pm \kappa R_2) \tag{A12}$$

Equations (A1) and (A12) hold for complex χ_m and κ if a complex frequency shift is introduced as follows:

$$d\bar\omega = \omega - \omega_0 + j(\alpha - \alpha_0) \tag{A13}$$

The attenuation constant α may be defined in terms of the internal Q of the cavity, $\alpha = \frac{1}{2}\omega/Q$ and the internal Q is defined as

$$Q = \frac{\omega(\text{energy stored in circuit})}{\text{average power loss}}$$

Thus, the imaginary part of the frequency shift may be expressed as the difference between $(1/Q)$ of the perturbed cavity at the new resonance frequency ω and $(1/Q_0)$ referring to the empty cavity at ω_0.

$$\Delta(1/Q) = \frac{1}{Q} - \frac{1}{Q_0} = 2 \frac{(\alpha - \alpha_0)}{\omega_0} \tag{A14}$$

We note that the imaginary part of the right hand side of (A1) does indeed represent the power dissipation in the perturbing sample over the stored energy times ω. Hence, taking the imaginary part of (A12)

we have a relationship between the change in $(1/Q)$ and the loss terms χ_m'' and κ''

$$\Delta(1/Q)_\pm = \frac{1}{2} \frac{\lambda_0^2 t}{L^3} (\chi_m'' R_1 \pm \kappa'' R_2) \tag{A15}$$

Clearly, (A15) holds only if the initial Q of the empty cavity is very high and the change in Q is quite small.

The electric susceptibility of the ferrite disc can be obtained in a similar way, provided we place the disc at the cavity center where the electric field has a maximum. Then, the additional electric energy stored in the disc is found to be

$$W_e^{(s)} = 0.2387 \frac{\pi}{2} \mu_0 \chi_e \frac{\beta_0^2}{k_c^2} B^2 a^2 t R_1 \tag{A16}$$

It should be noted that there is an important difference between location of a thin disc at the endwalls and at the center of a cylindrical cavity. Whereas the electric field at the endwall may be neglected entirely, the magnetic field at the cavity center has a component parallel to the cavity axis. The effect of this component on the stored energy in the disc may be minimized by magnetizing the disc beyond saturation in the z-direction.

With the assumption that the effects of the magnetic RF field may be neglected we obtain relationships for the electric susceptibility and electric loss factor:

$$2(\Delta\omega/\omega_0) - j\Delta(1/Q) = (\chi_e' - j\chi_e'') \frac{2t}{L} R_1 \tag{A17}$$

Since χ_e is a scalar quantity there is no splitting of the cavity resonance.

REFERENCES

1. D. Polder, Phil. Mag., **40**, p. 99, 1949.
2. C. L. Hogan, Rev. Mod. Phys., **25**, p. 253, 1953.
3. H. Suhl and L. R. Walker, B.S.T.J., **33**, p. 579, 1954.
4. W. A. Yager, J. K. Galt, F. R. Merritt, and E. A. Wood, Phys. Rev., **80**, p. 744, 1950.
5. J. O. Artman and P. E. Tannenwald, J. Appl. Phys. **26**, p. 1124, 1955.
6. A. D. Berk and B. A. Lengyel, Proc. I.R.E., **43**, p. 1587, 1955.
7. A. A. Th. M. Van Trier, Appl. Sci. Res., **3**, p. 305, 1953.
8. J. Stratton, Electromagnetic Theory, Chapter 1, McGraw-Hill Book Co., New York, 1941.
9. J. H. Rowen and W. von Aulock, Phys. Rev., **96**, p. 1151, 1954.
10. C. Kittel, Phys. Rev., **73**, p. 155, 1948.

Sensitivity Considerations in Microwave Paramagnetic Resonance Absorption Techniques

By G. FEHER

(Manuscript received February 9, 1956)

This paper discusses some factors which limit the sensitivity of microwave paramagnetic resonance equipments. Several specific systems are analyzed and the results verified by measuring the signal-to-noise ratio with known amounts of a free radical. The two most promising systems, especially at low powers, employ either superheterodyne detection or barretter homodyne detection. A detailed description of a superhetrodyne spectrometer is given.

TABLE OF CONTENTS

I. INTRODUCTION

Within the past few years the field of paramagnetic resonance absorption has become an important tool in physical and chemical research. In many ways its usefulness is limited by the sensitivity of the experimental set up. A typical example is the study of semiconductors in which case one would like to investigate as small a number of impurities as possible. It is the purpose of this paper to analyze the sensitivity limits of several experimental set ups under different operating conditions. This was done in the hope that an understanding of these limitations would put one in a better position to design a high sensitivity electron spin resonance equipment. In the last section the performance of the different experimental arrangements is tested. The agreement obtained with the predicted performance proves the essential validity of the analysis. This paper is primarily for experimental physicists confronted with the problem of setting up a high sensitivity spectrometer.

II. GENERAL BACKGROUND

We will not consider here the detailed theory[1] of the resonance phenomenon but consider this part of the problem only from a phenomenological point of view. When a paramagnetic sample is placed into an RF field of amplitude H_1 of a frequency ω at right angles to which there is a dc magnetic field H_0, magnetic dipole transitions will be induced in the neighborhood of the resonance condition

$$h\omega = g\beta H_0 \qquad (1)$$

where g is the spectroscopic splitting factor, h is Planck's constant and β is the Bohr magneton. As a result of these transitions power will be absorbed from the microwave field H_1. This power absorption is associated with the imaginary part of the RF susceptibility χ''. The transmitted (or reflected) H_1 will also experience a phase shift which is associated with the real part of the RF susceptibility χ'. The sensitivity of the setup is then determined by how small a power absorption (or phase shift) one is able to detect when going through a resonance

III. Q CHANGES ASSOCIATED WITH THE ABSORPTION

The average power absorbed per unit volume of a paramagnetic sample is

$$P = \tfrac{1}{2}\omega H_1^2 \chi'' \qquad (2)$$

For low enough powers χ'' is not a function of H_1 (and even for very high powers never drops off faster than $1/H_1^2$), so that for a large power absorption one would like a large RF magnetic field. This suggests a resonant cavity which indeed is used in all experimental setups. The Q of a cavity into which a paramagnetic sample is placed is given by

$$Q = \omega \frac{\text{Energy Stored}}{\text{Average Power Dissipated}} = \omega \frac{\frac{1}{8\pi} \int_{V_c} H_1^2 \, dV_c}{P_1 + \frac{1}{2} \omega \int_{V_s} H_1^2 \chi'' \, dV_s} \qquad (3)$$

where P_1 = power dissipated in the cavity in the absence of any paramagnetic losses, V_s is the sample volume and V_c the cavity volume.

Assuming that the paramagnetic losses are small in comparison with P_1 we get

$$Q = Q_0 \left(1 - 4\pi \frac{\int_{V_s} H_1^2 \chi'' \, dV_s}{\int_{V_c} H_1^2 \, dV_c} Q_0 \right) = Q_0 (1 - 4\pi \chi'' \eta Q_0) \qquad (4)$$

$$\therefore \Delta Q = Q_0^2 4\pi \chi'' \eta$$

where Q_0 is the cavity Q in the absence of paramagnetic losses and η is the filling factor and depends on the field distribution in the cavity and the sample. For example, in a rectangular cavity excited in the TE_{101} mode

$$\eta = \frac{V_s}{V_c} \frac{4}{1 + \left(\frac{d}{a}\right)^2} \qquad (5)$$

where d is the length of the cavity and a the width along which the E field varies. In the above example it was assumed that the sample is small in comparison to a wavelength and is placed in the max. H_1 field.

IV. COUPLING TO RESONANT CAVITIES FOR MAXIMUM OUTPUT

Having established the Q changes associated with the resonance absorption, we will next determine the proper coupling to the resonant cavity in order that the Q changes result in a maximum change in transmitted or reflected power (or voltage). The derivation will be based on the assumption that we have a fixed amount of power available from our source and that the Q change is not a function of the RF power (no saturation effects).

A. Reflection Cavity

Fig. 1 shows a magic (hybrid) T which serves to observe the reflected power from the cavity. Arm 3 has a slide screw tuner which serves to balance out some of the power coming from arm 2. This does not affect the present analysis and will be considered later in connection with detector noise. It should be mentioned, however, that a certain amplitude or phase unbalance has to be left. This insures that the signal in arm 4 will be a function of either χ' or χ''.[1] In the case that the magic T is completely balanced out the signal in arm 4 will be a function of both χ' and χ'' and the experimental results become difficult to analyze.

Fig. 2 shows the equivalent circuit for a reflection cavity.[2] The $\sqrt{2}$ in the source voltage arises from the fact that half the power is lost in arm 3. From this equivalent circuit we can define the following relations:

$$\text{Unloaded } Q = Q_0 = \frac{\omega L}{r} \text{ (Losses due to cavity alone)} \tag{6}$$

$$\text{External } Q = Q_x = \frac{\omega L}{R_0 n^2} \begin{array}{l}\text{(Losses arising from power} \\ \text{leaking out of the cavity)}\end{array} \tag{7}$$

$$\text{Loaded } Q = Q_L = \frac{\omega L}{R_0 n^2 + r} \begin{array}{l}\text{(Losses due to both cavity} \\ \text{and leakage out)}\end{array} \tag{8}$$
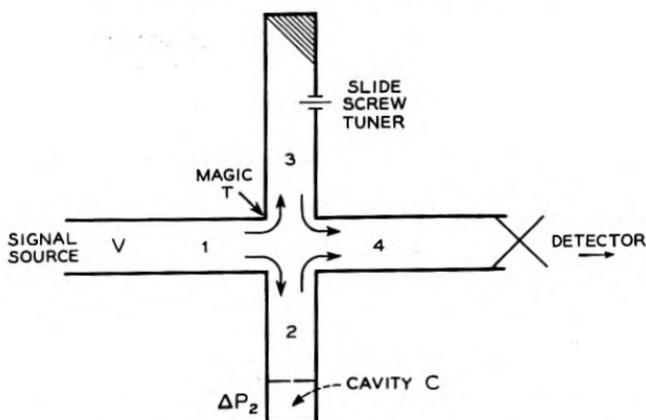
Fig. 1 — A simple arrangement to observe the reflected power from cavity C.
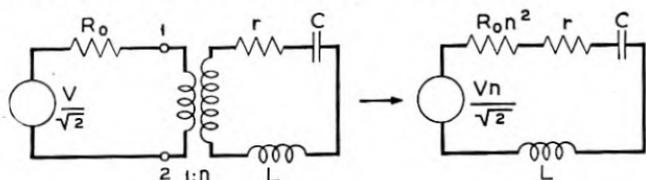
Fig. 2 — Equivalent circuit for a reflection cavity.

We define the coupling coefficient $\beta = Q_x/Q_0$ such that:

Critically coupled cavity $\beta = \dfrac{Q_0}{Q_x} = \dfrac{R_0 n^2}{r} = 1$ \hfill (9)

Overcoupled cavity $\dfrac{Q_0}{Q_x} > 1$ \qquad VSWR $= \beta = \dfrac{R_0 n^2}{r}$ \hfill (10)

Undercoupled cavity $\dfrac{Q_0}{Q_x} < 1$ \qquad VSWR $= \dfrac{1}{\beta} = \dfrac{r}{R_0 n^2}$ \hfill (11)

We will see that the coupling coefficient for maximum output depends on the characteristics of the detecting element. Two cases will be treated: the power (square law) detector and the voltage (linear) detector.

1. Detector Output Proportional to Incident Power

Power into the cavity at resonance

$$P_c = \left(\frac{Vn}{\sqrt{2}}\right)^2 \frac{r}{(R_0 n^2 + r)^2}$$

Max. power available from source (in arm 1)

$$P_0 = \frac{(Vn)^2}{4R_0 n^2} \quad \therefore \quad P_c = P_0 \frac{2R_0 n^2 r}{(R_0 n^2 + r)^2}$$

The change in reflected power ΔP_R equals the change in the power inside the cavity ΔP_c (since the incident power stays the same).

$$\Delta P_c = \frac{\partial P_c}{\partial r} \Delta r = 2R_0 n^2 P_0 \frac{R_0 n^2 - r}{(R_0 n^2 + r)^3} \Delta r \tag{12}$$

We want to optimize ΔP_c with respect to the coupling parameter n^2 (or $R_0 n^2$), i.e.,

$$\frac{\partial(\Delta P_c)}{\partial(R_0 n^2)} = (R_0 n^2)^2 - 4(R_0 n^2)r + r^2 = 0$$

$$\therefore \frac{R_0 n^2}{r} = 2 \pm \sqrt{3} \tag{13}$$

the positive sign being associated with the overcoupled, the negative with the undercoupled case. The experimentally measured quantity is the voltage standing wave ratio VSWR $= 2 + \sqrt{3} = 3.74$ corresponding to a reflection coefficient of 0.58. Putting this value into (12) we get for the maximum signal

$$\frac{\Delta P_c}{P_0} = \pm 0.193 \frac{\Delta r}{r} = \mp 0.193 \frac{\Delta Q_0}{Q_0} = \mp (0.193)(4\pi)\chi'' \eta Q_0 \tag{14}$$

the last step being obtained with the aid of (4). Equation (12) is plotted in Fig. 4. From the symmetry of the graph it is obvious that for a given VSWR, the signal will be the same for the overcoupled and undercoupled case. However, as we will see later from the standpoint of noise the 2 cases are not necessarily identical.

2. Detector Output Proportional to Input Voltage

Let Γ be the reflection coefficient, then V_{REFL} from the cavity is

$$V_{\text{REFL}} = \frac{V}{\sqrt{2}}\,\Gamma = \frac{V}{\sqrt{2}}\left(\frac{\text{VSWR} - 1}{\text{VSWR} + 1}\right) = -\frac{V}{\sqrt{2}}\left[1 - \frac{2\text{VSWR}}{\text{VSWR} + 1}\right]$$

With the aid of (10) and (11) this gives for the undercoupled case:

$$V_{\text{REFL}} = -\frac{V}{\sqrt{2}}\left(1 - \frac{2r}{R_0 n^2 + r}\right)$$

and the overcoupled case

$$V_{\text{REFL}} = -\frac{V}{\sqrt{2}}\left(1 - \frac{2R_0 n^2}{R_0 n^2 + r}\right)$$

We are interested only in the change of output voltage which is:

$$\Delta V_{\text{REFL}} = \frac{\partial V_{\text{REFL}}}{\partial r}\Delta r = \pm \sqrt{2}\, V\Delta r \frac{R_0 n^2}{(R_0 n^2 + r)^2} \qquad (15)$$

The two signs corresponding to the undercoupled or overcoupled case, respectively. In order to find the optimum coupling

$$\frac{\partial(\Delta V)}{\partial(R_0 n^2)} = R_0 n^2 - r = 0$$

$$\therefore \frac{R_0 n^2}{r} = 1$$

Putting this value into (15) we get the max. value

$$\frac{\Delta V_{\text{REFL}}}{V} = \pm \frac{\sqrt{2}}{4}\frac{\Delta r}{r} = \mp \frac{\sqrt{2}}{4}\frac{\Delta Q_0}{Q_0} = \mp \frac{\sqrt{2}}{4}4\pi\chi''\eta Q_0 \qquad (16)$$

(15) is again plotted in Fig. 4. From this graph we see that for maximum sensitivity we want to work near match. However, one should not work so close to match that the absorption signal will carry the cavity through the matching condition while sweeping through a resonance line. This would result (due to the sign reversal of the signal at match) in a distorted line. Incidentally, the sign of the signal may be conveniently used
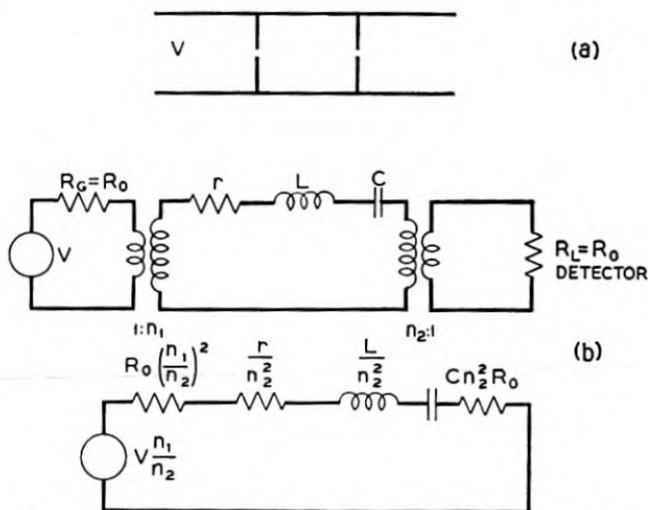
Fig. 3 — Equivalent circuit for a transmission cavity.

to determine whether the cavity is overcoupled or undercoupled. This information may be necessary in Q_0 determinations.[12]

B. *Transmission Cavity*

Fig. 3 shows the equivalent circuit for a transmission cavity,[2] the generator and the detector being matched to the waveguide, i.e.,

$$R_G = R_L = R_0$$

Analogous to the reflection cavity we define again two coupling coefficients

$$\beta_1 = \frac{R_0 n_1^2}{r} \qquad \beta_2 = \frac{R_0 n_2^2}{r} \qquad (18)$$

the relation between the unloaded and loaded Q being

$$Q_0 = Q_L(1 + \beta_1 + \beta_2) \qquad (19)$$

1. *Detector Output Proportional to Input Power*

$$\text{Power into load } P_L = \frac{V^2 n_1^2 n_2^2 R_0}{(R_0 n_1^2 + r + R_0 n_2^2)^2}$$

$$\text{Max. power generator can deliver } P_0 = \frac{(V n_1)^2}{4(n_1^2 R_0)}$$

$$\Delta P_L = \frac{\partial P_L}{\partial r} \Delta r = \frac{2V^2 n_1^2 n_1^2 R_0}{(R_0 n_1^2 + r + R_0 n_2^2)^3} \Delta r$$

(19)

In the case of the transmission cavity we have two coupling coefficients whose optimum value we have to determine.

$$\frac{\partial(\Delta P_L)}{\partial(n_1{}^2R_0)} = \frac{\partial(\Delta P_L)}{\partial(n_2{}^2R_0)} = 0$$

$$\therefore n_1{}^2R_0 = n_2{}^2R_0 = r \tag{20}$$

which means that the input and output coupling should be identical. Relation 20 looks superficially like a matching condition. However, it should be noted that the input impedance to the cavity contains besides the cavity impedance the load impedance. Hence, the VSWR is

$$\frac{R_0n^2 + r}{R_0n^2}$$

which represents an undercoupled case. One never can overcouple a transmission cavity with equal input and output couplings. Putting condition (20) into (19) we get:

$$\frac{\Delta P_L}{P_0} = -\frac{8}{27}\frac{\Delta r}{r} = -\frac{8}{27}\frac{\Delta Q_0}{Q_0} = -\left(\frac{8}{27}\right)4\pi\chi''\eta Q_0 \tag{21}$$

2. Detector Output Proportional to Input Voltage

The voltage across the load

$$V_L = \frac{Vn_1n_2R_0}{R_0n_1{}^2 + r + R_0n_2{}^2}$$

Again for max. sensitivity both couplings should be the same

$$\Delta V_L = \frac{\partial V_L}{\partial r}\Delta r = -V\left[\frac{n_2{}^2R_0}{(r + 2R_0n_2{}^2)^2}\right]\Delta r \tag{22}$$

$$\frac{\partial V_L}{\partial(n_2{}^2R_0)} = 0 \qquad \therefore R_0n^2 = \frac{r}{2} \tag{23}$$

$$\therefore \frac{\Delta V_L}{V} = -\frac{1}{8}\frac{\Delta r}{r} = -\frac{1}{8}\frac{\Delta Q_0}{Q_0} = -\frac{1}{8}4\pi\chi''\eta Q_0 \tag{24}$$

Fig. 4 is a plot of (12), (15), (19), and (22). It should be noted that the sensitivities of the reflection cavity are normalized to the input of the magic T (in Fig. 1) and not to the input of the cavity as in the transmission cases. This results in a 3-db decrease in output and causes the power sensitivity of the transmission cavity to look relatively higher. However this is somewhat arbitrary since a balanced transmission type scheme would also require a magic T with an accompanying reduction in usable power.

All the previous sensitivity expressions are proportional to χ''. For an unsaturated condition it may be replaced by χ' whenever the output is sensitive to phase changes in the cavity.[1]

It should be noted that we maximized the output from the detector. This will result in a maximum signal to noise ratio if the noise is a constant independent of the microwave power. This, however, is in general not the case and in the next section we will investigate the signal to noise ratio taking into account its dependence on the RF power.

V. MINIMUM DETECTABLE SIGNAL UNDER IDEAL CONDITIONS

The minimum signal is ultimately determined by the random thermal agitation. Due to this cause the power fluctuates by an amount $kT\Delta\nu$, where k is Boltzmann's constant, T the absolute temperature and $\Delta\nu$ the bandwidth. The minimum detectable microwave power will be then of the order of $kT\Delta\nu$. This is the problem one faces when designing sensitive microwave receivers. However, our problem is of a different nature. We want to detect a small change in the power level of a relatively large
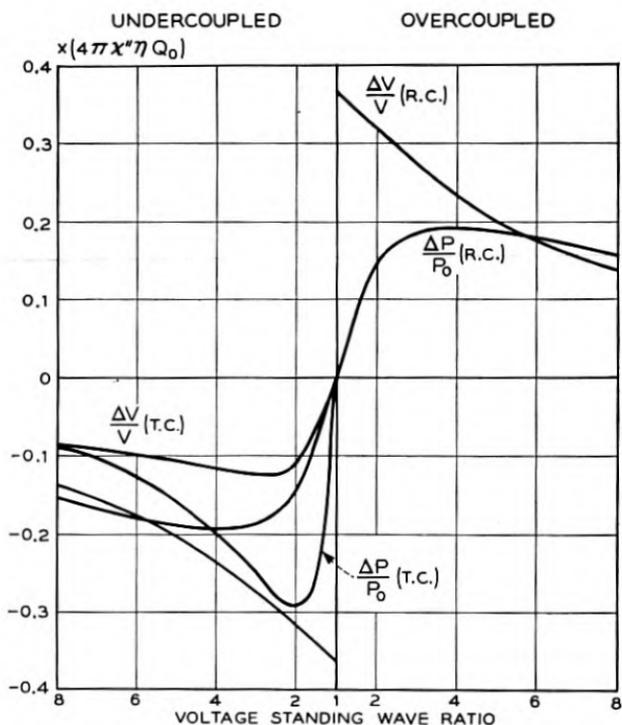
Fig. 4 — Output versus V.S.W.R. for reflection and transmission cavity.

microwave signal. This change in power level will have to be considerably larger than $kT\Delta\nu$ before it can be detected.[3] The physical reason for this is that the fluctuating fields associated with the noise power combine with the microwave fields to produce power fluctuations much larger than $kT\Delta\nu$. It is more straightforward to compare noise voltages rather than powers, especially since the power changes are not necessarily a constant of the system. In Fig. 1 for instance, the power change in arm 4 is

$$\Delta P_4 = \frac{(\Delta V)(V_4)}{R_0}$$

whereas the power change in arm 2 (for the same voltage change) is

$$\Delta P_2 = \frac{(\Delta V)(V_2)}{R_0}$$

It also shows that one wants to maximize the change in output voltage as was done in Section IV.

The open terminal RMS noise voltage of a system with an internal impedance R_0 is given by

$$V_{\text{RMS}} = \sqrt{4R_0 kT\Delta\nu}$$

If we terminate this system with a noiseless resistor R_0, the voltage across it will be $\sqrt{R_0 kT\Delta\nu}$. However, the terminating resistor is also at temperature T, so that the total RMS voltage across it will be $\sqrt{2}\,\sqrt{R_0 kT\Delta\nu}$.

Comparing this RMS noise voltage with the signal voltage obtained in (16), we get for the reflection cavity*

$$\Delta V = V\,\sqrt{2}\pi\chi''\eta Q_0 = \sqrt{2}\,\sqrt{R_0 kT\Delta\nu} \tag{25}$$

$$\therefore \chi_{\text{MIN}}'' = \frac{1}{Q_0\eta\pi}\left(\frac{kT\Delta\nu}{2P_0}\right)^{\frac{1}{2}} \tag{26}$$

As an example let us consider the following typical value for a 3-cm setup. $Q_0 = 5 \times 10^3$, $\Delta\nu = 0.1$ cps, $P_0 = 10^{-2}$ Watts

$$\eta = \frac{V_s}{V_c}\frac{4}{1+\left(\dfrac{d}{a}\right)^2} \simeq \frac{4V_s}{10\text{ cm}^3}.$$

For this case

$$(\chi_{\text{min}}'')(V_s) = \simeq 2 \times 10^{-14}$$

---

* In most cases the behaviour of the transmission and reflection cavity is similar, so that they will not be treated separately.

This corresponds for an unsaturated Lorentz line[1] to a static suscepti-bility $\chi_0 = \sqrt{3}\chi''(\Delta\omega/\omega)$, where $\Delta\omega$ is the line width between inflection points. For the free radical diphenyl picryl hydrazyl having a 2 oersted line width this expression at room temperature gives for the min. number of spins 10^{10}. A plot of the minimum RF susceptibility and minimum number of electrons versus microwave power is shown in Fig. 5.

VI. SIGNAL-TO-NOISE IN PRACTICAL SYSTEMS

A. General Considerations

1. Why Field Modulation?

From a design point of view it is instructive to consider the mini-mum fractional voltage change corresponding to the above $\chi_{min}''V_s$ of 2×10^{-14}. This turns out to be, see (16),

$$\frac{\Delta V_{min}}{V} \simeq 2 \times 10^{-10}.$$

From this figure one may safely conclude that it is not feasible to use any system in which the microwave carrier level reflected from the cavity has to be kept constant to this accuracy. Such systems would include straight detection, the dc being bucked out and amplified or systems employing amplitude modulation of the carrier. (Although
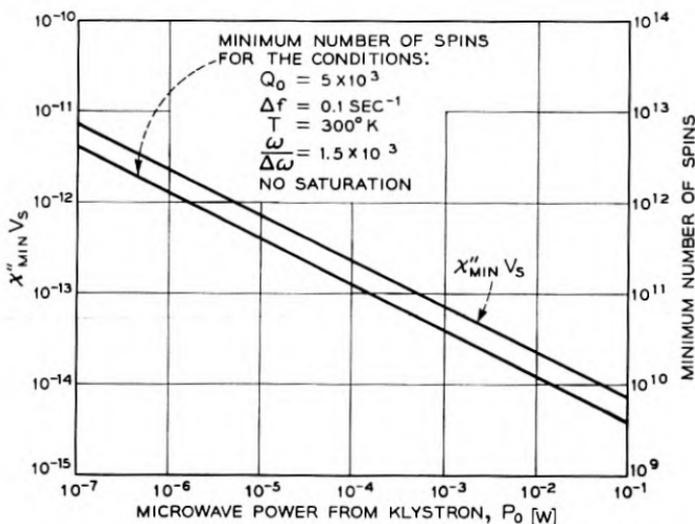
Fig. 5 — Minimum RF susceptibility and number of electrons which should be observable under thermal noise limitations. The conditions for the minimum number of spins correspond closely to those under which the experimental set-ups were tested.

the latter system may be improved by microwave bucking, it still remains very much inferior to the field modulation system to be described presently.) A system commonly used in which the requirements on the constancy of the microwave level is less stringent, makes use of a small external magnetic field modulation of angular frequency ω_M superimposed on the slowly varying dc magnetic field. Thus in the absence of a resonance line the output is zero except for some small Fourier components of the random fluctuations at the frequency ω_M. If the amplitude of the field modulation ΔH_M is small in comparison to the line width ΔH this method will sweep out the derivative of the line, i.e., the signal will not be proportional to χ'' as previously assumed but to $d\chi''/dH\ (\Delta H_M)$. In order to preserve the line shape one should sweep only over a fraction of the line width. The sensitivity will thereby be reduced by roughly the same fraction. It should be noted, however, that even if one overmodulates the line (in order to increase the sensitivity) the resonance condition (i.e., place of zero signal, corresponding to new slope in the absorption) will not shift for a symmetrical line and the correct g-value may be obtained. Also from the knowledge of the amplitude of the modulating field the increase in line width may be corrected for. For those reasons we will not be concerned with the reduction in sensitivity due to this field modulation scheme.

2. Choice of Frequency

Referring to (26)

$$\chi_{\min} \propto \left(\frac{V_c}{V_s}\right) \frac{1}{Q_0} \frac{1}{\sqrt{P_0}}$$

and the minimum total number of electrons $N_{\min}$.

$$N_{\min} \propto \chi_0 V_s \propto \left(\frac{V_c}{Q_0}\right)\left(\frac{\Delta\omega}{\omega}\right) \frac{1}{\sqrt{P_0}} \tag{27}$$

Assuming that we are dealing with the same type of cavity mode at different frequencies, the same power, and that the line width $\Delta\omega$ is constant, we have $V_c \propto \dfrac{1}{\omega^3}$, $Q_0 \propto \dfrac{1}{\omega^{\frac{1}{2}}}$

$$\therefore N_{\min} \propto \frac{1}{\omega^{7/2}} \tag{28}$$

Equation 28 shows that in order to see the smallest number of spins we want to go to as high as frequency as possible. The upper limit is given by the availability of components in the millimeter region, by the difficulty of handling them and by the maximum available power. The most commonly used setups operate at a wavelength of 1 cm and 3 cm.

The latter was used in the experimental part of this paper. From (28) we see that with a 1 cm setup the number of observable electrons should be approximately 40 times less than with a 3-cm setup. However, in most practical cases one is not limited by the amount of available sample, since one usually can increase the sample size at longer wavelengths. Therefore a better criterion is the minimum number of electrons per unit volume

$$\frac{N_{\min}}{V_s} \propto \left(\frac{V_c}{V_s}\right) \frac{1}{Q_0} \left(\frac{\Delta\omega}{\omega}\right) \qquad (29)$$

Keeping now the filling factor V_c/V_s constant we see that the sensitivity of a 3 cm setup as defined in (29) is only $\sqrt{3}$ worse than of a 1 cm setup. In addition the power outputs of 3-cm klystrons are usually sufficiently higher than those of 1-cm klystron to overcome even the $\sqrt{3}$ advantage. If RF saturation comes in, the power argument is not valid, but one has to consider the RF magnetic field H_1 inside the cavity which for a given power and Q_0 is prop. to ω. Thus at the higher frequencies (1 cm) saturation effects become more pronounced reducing again the advantage of a 1-cm over a 3-cm setup. In deciding the choice of the frequency in special cases (e.g., when $\Delta\omega$ is a function of the magnetic field, or the sample is larger than a skin depth) (29) should be used.

There are, of course, considerations, other than those of max. sensitivity, which have to be taken into account. For example one would always like to satisfy the condition $\Delta\omega/\omega \ll 1$ which favors higher frequencies. On the other hand, for very narrow lines (say less than 0.1 oersteds) fractional field instabilities and inhomogeneities will favor low magnetic fields, i.e., lower frequencies. One also might encounter samples which exhibit an excessive loss in a given frequency band which therefore has to be avoided.

3. Optimum Amount of Sample to be Used

The output voltage ΔV is proportional to the sample volume and the unloaded Q_0 of the cavity, see (26). If the sample is lossy an increase in its size will reduce the Q and therefore reduce the signal. We may roughly distinguish two limiting cases. In one case the losses are proportional to E^2 (e.g., high resistivity samples having dielectric losses), in the other case they are proportional to H_1^2 (e.g., low resistivity samples in which the losses are due to surface currents).

a. Losses Proportional to E^2

The paramagnetic sample is placed in the region of max. RF magnetic field for instance at the end plate of a rectangular cavity resonating in

the TE_{10} mode. The sample extends a distance x into the cavity, x being assumed to be small in comparison to the wavelength so that H_1 does not vary appreciably over the sample. The additional losses due to the sample will then be proportional to

$$A \int_0^x E_0^2 \sin^2\left(\frac{2\pi x}{\lambda}\right) dx \sim Cx^3$$

whereas the volume of the sample is proportional to x. The observed voltage change ΔV is then given by

$$\Delta V \propto Q_0' V_s \propto \left(\frac{1}{\frac{1}{Q_0} + Cx^3}\right)(x)$$

where Q_0 is the Q of the cavity without sample, and Q_0' the total Q of both cavity and sample. Maximizing the voltage change ΔV we get

$$\frac{\partial(\Delta V)}{\partial x} = 0 \qquad \therefore Cx^3 = \frac{1}{2Q_0} \tag{30}$$

$$\therefore Q_0' = \tfrac{2}{3}Q_0$$

Equation (30) tells us that we should load the cavity with the sample until the Q_0 is reduced to $\frac{2}{3}$ of its original value. It should be pointed out that we optimized the signal and not the more important quantity, the signal-to-noise ratio. Therefore the analysis is only valid as long as the noise is not a function of Q_0, (see Section VIB) and that we do not saturate the sample (see Section VIII). If either condition does not hold the amount of sample to be put in should exceed the above calculated value.

b. Losses Proportional to H_1^2

The losses do not vary along the sample so that we may write

$$\Delta V \propto Q_0' V_s \propto \left(\frac{1}{\frac{1}{Q_0} + Cx}\right)(x)$$

which clearly has no maximum for x. One should therefore put as big a sample into the cavity as possible (compatible with the assumption that if it be small in comparison to a wavelength), the same result as if one had no losses at all.

B. Noise Due to Frequency Instabilities

Before considering the signal-to-noise ratio for specific systems we will investigate a noise source which is common to all of them. It arises

from the random frequency variations of the microwave source or from the random variations of the resonant frequency of the cavity (e.g., rising helium bubbles at $4°K$ or just any microphonics).

From the equivalent circuit of a reflection cavity (see Fig. 2) we can write for the voltage standing wave ratio

$$\text{VSWR} = \frac{Z_{in}}{R_0 n^2} = \frac{r}{R_0 n^2} + \frac{j}{R_0 n^2}\left(\omega L - \frac{1}{\omega C}\right)$$

$$= \frac{r}{R_0 n^2}\left[1 + jQ_0\left(\frac{2\Delta\omega}{\omega}\right)\right] = \frac{r}{R_0 n^2}[1 + j\delta]$$

where $\delta = Q_0(2\Delta\omega/\omega)$ and $\Delta\omega$ is the frequency deviation from the resonant frequency of the cavity. The reflection coefficient Γ is then given by:

$$\Gamma = \frac{\dfrac{r}{R_0 n^2}(1 + j\delta) - 1}{\dfrac{r}{R_0 n^2}(1 + j\delta) + 1} = \Gamma_0 + 2\frac{\dfrac{R_0 n^2}{r}\delta^2}{\left(\dfrac{R_0 n^2}{r} + 1\right)^3} + 2j\frac{\dfrac{R_0 n^2}{r}\delta}{\left(\dfrac{R_0 n^2}{r} + 1\right)^2}$$

where Γ_0 is the reflection coefficient at the resonant frequency of the cavity. The other two terms giving the changes in Γ for a given frequency deviation $\Delta\omega$. The changes of $\Delta\omega$ (or $\Delta\Gamma$) having ac components near the modulation frequency will thus represent noise terms which will pass together with the signal through the detection system. The slide screw tuner (see Fig. 1) which is used to buck out part of the microwave power will introduce an additional reflection coefficient $\Gamma_R + j\Gamma_R'$. Thus the total reflection coefficient will be given by

$$\Gamma = \Gamma_0 - \Gamma_R + 2\frac{\dfrac{R_0 n^2}{r}\delta^2}{\left(\dfrac{R_0 n^2}{r} + 1\right)^3} - j\Gamma_R' + j2\frac{\dfrac{R_0 n^2}{r}\delta}{\left(\dfrac{R_0 n^2}{r} + 1\right)^2} \quad (31)$$

We are interested only in the magnitude of V (i.e., $|\Gamma|$) reaching the detector. Tuning to the dispersion mode (χ') the slide screw tuner is adjusted such that $\Gamma_R' \gg \Gamma_0 - \Gamma_R$. Under these conditions the output noise voltage will be given by

$$\left(\frac{\Delta V_N}{V}\right)_{\chi'} \simeq 2\frac{\dfrac{R_0 n^2}{r}\delta}{\left(\dfrac{R_0 n^2}{r} + 1\right)^2} \quad (32)$$

Tuning to the absorption (χ''), the condition $\Gamma_0 - \Gamma_R \gg \Gamma_R$ will be

satisfied and (31) becomes

$$\left(\frac{\Delta V_N}{V}\right)_{\chi''} \simeq 2\,\frac{\left(\dfrac{R_0 n^2}{r}\right)\delta^2}{\left(\dfrac{R_0 n^2}{r}+1\right)^3} + 2\,\frac{\left(\dfrac{R_0 n^2}{r}\right)^2\delta^2}{\left(\dfrac{R_0 n^2}{r}+1\right)^4(\Gamma_0 - \Gamma_R)} \tag{33}$$

An inspection of (31), (32), and (33) shows that the noise voltage, enters as a first order effect in δ when tuned to χ'. This is not too surprising since a frequency effect is expected to affect predominantly the dispersion mode. When tuned to χ'' the effect becomes second order as long as $|\Gamma_0 - \Gamma_R|$ is large. Under those conditions the 2 terms in (33) are of comparable magnitude. We can easily see the origin of the second term. It arises from the first order out-of-phase component of the noise voltage. Being, however, sensitive only to in-phase components it will be reduced to a second order effect—as long as $|\Gamma_0 - \Gamma_R|$ is large, i.e., as long as we have a carrier which makes us insensitive to out-of-phase components.* When $\Gamma_0 - \Gamma_R$ goes to zero (33) ceases to hold and the noise voltage will be given by (32).

There are two important conclusions to be drawn from (33).

We want to keep $\Gamma_0 - \Gamma_R$ as large as possible. Therefore in schemes (like the superheterodyne see section VI E) where this is not feasible, special care has to be taken to eliminate this noise source.

From (15) we find that the desired signal is proportional to

$$\frac{R_0 n^2}{r}\bigg/\left(\frac{R_0 n^2}{r}+1\right)^2$$

Comparing this expression with (33) we see that the signal-to-noise ratio may be improved by increasing $R_0 n^2/r$, i.e., overcoupling the cavity until this noise source does not contribute any more. A comparison of (15) with (32) shows that overcoupling will not improve the signal-to-noise ratio when tuned to χ'. In this connection it should be pointed out that only those frequency stabilization schemes can alleviate the problem of frequency instabilities whose response time is at least of the order to the inverse modulation frequency since the troublesome noise components are at this frequency. Some stabilization schemes make use of the cavity into which the sample is placed as the stabilizing element. Although this system may be excellent for the observation of χ'' (it is the only one which can compensate for cavity microphonic), it fails in the case of χ'. The reason is that χ' makes itself observable essentially by a frequency shift which in this scheme would be compensated for.

---

* For a similar reason one cannot avoid an admixture of dispersion to an absorption signal, when investigating a saturated sample in which $\chi'_{max} \gg \chi''_{max}$.

C. Noise Due to Cavity Vibrations

A noise source which can be very troublesome at high modulation fields arises from the currents induced in the walls of the cavity from the modulating field. The interaction of these currents with the dc magnetic field causes mechanical vibrations of the cavity walls. This produces a signal when tuned to the dispersion, but to first order should give no signal when one is tuned to the cavity and sensitive to the absorption. However, any detuning will result in a signal, which, having the right frequency will pass through the narrow band amplifier and lock-in detector. Since this signal is proportional to the magnetic field, it will result in a background signal whose amplitude will vary as the magnetic field is being swept and thus causing a continuous shift in the base line. In a rectangular cavity this effect can be greatly reduced by a proper orientation of the cavity with respect to the dc magnetic field. This is due to the fact that by squeezing the broad face of a rectangular cavity (TE_{10} mode) the frequency decreases, whereas by squeezing the narrow walls of the cavity the frequency increases. Thus in a proper orientation the two effects cancel each other out. We found another way of greatly reducing the effect by using a glass cavity having a silver coating* thick in comparison to a microwave skin depth but small in comparison to the modulation frequency skin depth, thereby decreasing the eddy currents without impairing the mechanical strength of the cavity.

D. Klystron Noise

There is very little data available on presently used klystrons. The data quoted by Hamilton, et al[4] are on a 723A klystron. With an IF of 30 mc, bandwidth of 2.5-mc microwave output of 50 mw they obtained a noise power of 5×10^{-12} watts. Expressing their results in terms of a noise figure N_k such that the noise power output in the two side bands P_k is given by

$$P_k = 2N_k(kT\Delta\nu) \qquad \therefore \ N_k = \frac{1}{2}\left(\frac{P_k}{P_0}\right)\frac{P_0}{kT\Delta\nu} = sP_0 \qquad (34)$$

Substituting their numerical values one obtains for $s = 5000$ Watt^{-1}. The values for s that we obtained with a 60 mc IF are:

Higher mode of V-153 klystron	$s \simeq 1,000$ Watt^{-1}
Lower mode of V-153 klystron	$s \simeq 3,000$ Watt^{-1}
Higher mode of X-13 klystron	$s \simeq 200$ Watt^{-1}
Lower mode of X-13 klystron	$s \simeq 400$ Watt^{-1}

---

* We are indebted to A. V. Hollenberg and V. J. DeLucca for the making of the glass cavities and to A. W. Treptow for the excellent silver coatings.

The method used to determine the above noise figures is similar to the one described in Reference 4. The figures are expected to be several times larger when a 30 mc IF is used. (A factor of 2 is quoted by Hamilton, et al.[4]) It is also worth noting that the relative noise power decreases on going to higher modes.

E. Signal-to-Noise Ratio for Specific Systems

In this section we will analyze specific systems under varying conditions. The reason why we do not present the analysis of one "The Best" system is that sometimes a compromise between complexity and sensitivity has to be reached and also because some systems may be superior at high power whereas others at low powers.

The expression for the noise power P_N at the output of the microwave detector (X-tal or bolometer) is[5]

$$P_N = (GN_K + F_{\text{AMPL}} + t - 1)(kT\Delta\nu) \tag{35}$$

where:

G = conversion gain of the detector (generally smaller than one. A quantity often used instead of G is the conversion loss $L = 1/G$).

N_K = noise figure at the input of the detector. Usually due to random amplitude or frequency fluctuations of the microwave source or the microwave components (see Section VID).

F_{AMPL} = noise figure of the amplifier

t = noise temperature of the detector

Comparing the equivalent voltage fluctuations of this noise power with the signal voltage as derived in (26), we get for the minimum detectable χ''

$$\chi_{\min}'' = \frac{1}{Q_0\eta\pi} \left[\frac{(GN_k + F_{\text{AMP}} + t - 1)kT\Delta\nu}{2GP_0} \right]^{\frac{1}{2}} \tag{36}$$

The above relation should apply to all systems. The problem then reduces to the determination of G, N_k, F_{AMP}, and t for the particular detection scheme. A difficulty arises from the fact that not only are those quantities a function of the RF power and modulation frequency but in the case of detectors vary from unit to unit. It is probably for this reason that the values quoted in the literature are sparse and are not in agreement with each other. The values used in this analysis for the X-band barretters (821) and crystals (1N23C) were obtained by us. Values for K-band crystals can be found in References 6 and 7. It should also be borne in mind that the values are time dependent and

will have to be modified as the "art" of detector manufacturing improves. Also new systems might come into prominence in the near future. An example would be the use of low noise travelling wave tubes preceding the detector or even low noise solid state masers.

1. Barretter (bolometer) detection.

The resistance of a barretter is given by the relation[2]

$$R = R_0 + kP^n \tag{37}$$

For practical purposes n may be taken as unity. The instantaneous power input to the barretter for a modulated microwave is given by

$$P = \frac{1}{R}\left[V_0 \sin \Omega t \left(1 + \frac{\Delta V}{V_0} \sin \omega t \right) + V_{dc} \right]^2 \tag{38}$$

where V_0 is the amplitude of the microwaves, ΔV the change of the amplitude due to the absorption given by (16), Ω the microwave frequency, ω the field modulation frequency, and V_{dc} the bias on the barretter. Expanding (38) and assuming that $\Delta V/V_0 \ll 1$ we get, after throwing out the high frequency terms,

$$R = R_0 + k\left(P_{RF} + P_{dc} + \frac{V_0 \Delta V}{R} \sin \omega t \right) \tag{39}$$

where P_{RF} is the power in the unmodulated carrier reaching the barretter. It is of course smaller than P_0 the microwave power from the klystron because of the power splitting in the magic T and the reflection from the cavity. Taking a reflection coefficient $\Gamma \simeq 0.5$ (see Section IVA), $P_{RF}/P_0 \simeq 0.1$. The desired voltage fluctuation associated with the resistance change is: $\delta V = I_0 \Delta R$, where

$$\Delta R = \frac{dR}{dP}\Delta P = \frac{dR}{dP}(\Delta P_{RF} + I_0^2 \Delta R), = \frac{dR}{dP}\left[\frac{1}{1 - I_0^2 \frac{dR}{dP}} \right]\Delta P_{RF} \tag{40}$$

$$\therefore \delta V \simeq I_0 k \frac{V_0 \Delta V}{(1 - I_0^2 k)} \sin \omega t$$

I_0 is the current bias on the barretter which we want to keep constant for a maximum voltage change δV.

The power gain of this device G is given by

$$G = \frac{\text{Signal Power from Barretter}}{\text{Power in the Sidebands}} = \frac{\delta V^2}{2R} \Big/ \frac{\Delta V^2}{4R} = 4\frac{I_0^2 k^2 P_{RF}}{R(1 - I_0^2 k)}$$

$$= 4k^2 \frac{P_{dc} P_{RF}}{R^2(1 - I_0^2 k)} \tag{41}$$

The noise figure of the audio amplifier following the detector is given in general by:

$$F_{\text{AMP}} = \frac{R_{\text{equ}} + R_G}{R_G} \qquad (42)$$

where R_G is the generator input resistance in this case the barretter resistance and R_{equ} is an equivalent noise resistor in series with the generators. The best input tube that we found was the General Electric GL 6072 triode* for which we measured an R_{equ} at 100 c.p.s. of $\sim 10^5$ Ω. (This is due to flicker noise of the tube and has a $1/f$ dependence.) If we were to connect the barretter, having a resistance of ~ 200 Ω straight to the grid of the input tube we would get a noise figure of ~ 500. However, by using a step-up transformer with a turns ratio $n > \dfrac{R_{\text{equ}}}{R_B}$ the noise figure of the amplifier can be reduced to nearly unity. We will assume in the following analysis that this has been done.

The noise temperature of the barretter t_B was thought to be approximately 2 since it is merely a platinum wire operating at an elevated temperature. To our surprise the measured value turned out to vary for different units between 4 and 40.† The noise figure was measured on about 20 different units obtained from 4 different manufacturers (P.R.D.; F.X.R. Narda, Sperry). The reason for this noise is not entirely clear at present. A possible explanation is the non-uniform heating of the wire which could set up air currents. They in turn can cool the wire in a random fashion giving rise to an additional noise component. An improvement of the noise figure was noted upon evacuating the barretter. The noise figure of a unit which was initially 10, dropped to the expected value of 2 after evacuation. However, it should be pointed out that this cannot be taken as a definite proof for the "air current theory" since the characteristics of the barretter changed markedly after evacuation. The sensitivity of the evacuated barretter went up from $5\Omega/mW$ to $200\Omega/mW$ which necessitated a reduction of the dc current from 8 to 1.5 mA. Also the response time went up by a factor of 20, so that the effectiveness of any noise mechanism with a $1/f$ spectrum would be greatly reduced. This approach however looks definitely promising in trying to design more sensitive and less noisy barretters. In the present work commercial unevacuated barretters were used, their noise temperature being taken as 4 in the following analysis. Under

---

* We are indebted to R. G. Shulman for bringing this tube to our attention.

† One unit which exhibited an extremely large noise figure of 1,000 was eliminated entirely. The solder point of the platinum wire was apparently defective.

those assumptions (36) becomes:

$$\chi''_{\text{MIN}} = \frac{1}{Q_0 \eta \pi} \left(\frac{kT\Delta\nu}{P_0} \right)^{\frac{1}{2}} \left(\frac{4 + N_k G}{G} \right)^{\frac{1}{2}} \tag{43}$$

a. Straight detection

A block diagram of the microwave part of a simple barretter system is shown in Fig. 6. The attenuator serves the purpose of preventing power saturation of the sample or burn out of the bolometer at high powers. By means of the slide screw tuner and magic T arrangement one makes the system sensitive to either the real or imaginary part of the suscepti-bility.

The characteristics of a typical barretter (like the Sperry No. 821) are: $R = 250\ \Omega$; $k = 4.5\ \Omega/mW$; $P_{\text{MAX}} = 32\ mW$. We take the worst generator noise figure reported, i.e., $N_k = 5{,}000\ P_{\text{RF}}$ (see Section VID).

The ratio of the minimum susceptibility $\chi''_{\text{MIN-OBS}}$ that can be de-tected with this system to the minimum theoretical value if one were limited by thermal noise only becomes with the aid of (41) and (43)

$$\frac{\chi''_{\text{MIN-OBS}}}{\chi''_{\text{MIN-TH}}} = \left(\frac{4 + N_K G}{G} \right)^{\frac{1}{2}} = \left(\frac{1 + 5 \times 10^3 P_{RF} k^2 \dfrac{P_{RF} P_{\text{de}}}{R^2 (1 - I_0^2 k)}}{k^2 \dfrac{P_{RF} P_{\text{de}}}{R^2 (1 - I_0^2 k)}} \right)^{\frac{1}{2}} \tag{44}$$
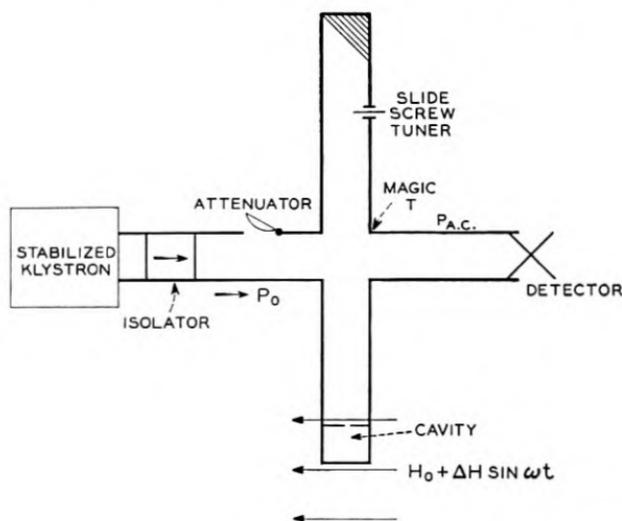
Fig. 6 — Essential microwave parts of a simple barretter or crystal set-up.
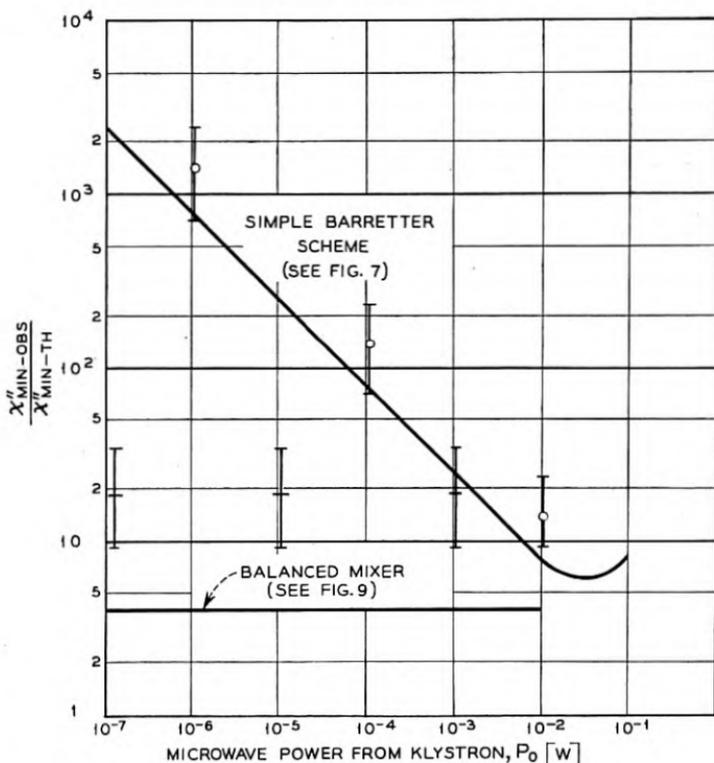
Fig. 7 — The ratio of the minimum detectable susceptibility to the minimum theoretical value versus microwave power for 2 different barretter schemes. Full lines correspond to the predicted sensitivity and dots indicate experimental values.

Equation (44) is plotted in Fig. 7. From this plot we see that the system is extremely poor at low powers (which is due to the low conversion gain of barretters) and also starts getting worse at high powers (due to the signal generator noise). The latter point is not of great importance since one can always buck down the microwave power by means of the slide screw tuner to the desired level. By using the evacuated barretter as mentioned earlier, the curve in Fig. 7 would be shifted to the left corresponding to the increased conversion gain.

b. Balanced mixer detection

An improved barretter scheme is shown in Fig. 8. It eliminates the poor conversion gain at low powers by employing a balanced mixer into which a large amount of microwave power P_2 can be fed from the same signal generator. Since the barretter noise should not be power

dependent (unlike in crystals) this procedure improves the conversion gain without increasing the noise. Since a balanced mixer is used the noise from the signal generator is also cancelled. A necessary precaution in this set-up is to include extra isolation between the second magic T and the mixer in order to prevent any microwave power from leaking through the balanced mixer into the cavity.

For this arrangement (44) becomes:

$$\frac{\chi''_{\text{MIN-OBS}}}{\chi''_{\text{MIN-TH}}} \sqrt{2} \sqrt{\frac{4}{G}} \tag{45}$$

The factor of $\sqrt{2}$ arises from the fact that we had to split the power P_0 in the first magic T. Since in this scheme we are at liberty to vary the input power to the barretter we want to maximize G with respect to P_2. For a fixed total power to the barretter given by its burn-out ratings (i.e., $P_2 + P_{\text{dc}} = $ constant) (41) is a maximum for $P_2 \simeq P_{\text{dc}} \simeq \frac{P_{\text{MAX}}}{2}$. Taking again the data for the No. 821 barretter we get for $G_{\text{MAX}} \simeq 0.5$ and for

$$\frac{\chi''_{\text{MIN-OBS}}}{\chi''_{\text{MIN-TH}}} \simeq 4 \tag{46}$$

Since the value of P_2 can be held constant irrespective of the power in the cavity, this ratio will be a constant (see Fig. 7).

It should be pointed out that in this system a wrong phasing of arm P_2 will result not only in a reduction of the signal, but also in an admixture of χ' and χ''. Therefore after changing the power by means of a
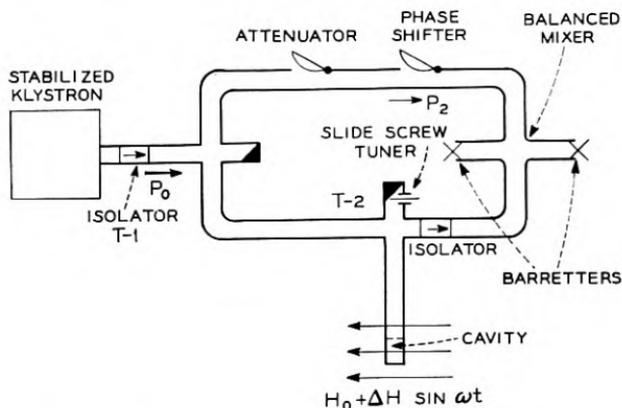
Fig. 8 — Barretter system with balanced mixer.

variable flap* attenuator (which also introduces a phase shift) or after changing the slide screw tuner the system has to be rephased again. This makes saturation measurements less convenient than in the superheterodyne system to be discussed in the next section. The obvious advantage of the homodyne detection scheme is that it requires only one microwave oscillator.

2. Crystal detection

A simple set-up is shown in Fig. 6. Although its microwave components are identical to the ones used in the barretter scheme, the analysis of this set-up is more complicated. The reason is that not only do crystal characteristics vary greatly from unit to unit but they cannot be described by one simple relation over the entire range of incident microwave power. One can roughly divide their characteristics into a square law region where the rectified current I is proportional to P_0 (holds for $P_0 < 10^{-5}$ Watts) and the linear region where I is proportional to $\sqrt{P_0}$. (holds for $P_0 > 10^{-4}$ Watts). The output noise of a crystal can be represented in general by the relation.[5, 8, 9]

$$P_N = \left(\frac{\alpha I_0^2}{f} + 1 \right) kT\Delta\nu \ \dagger \tag{47}$$

where f is the frequency around which the bandwith $\Delta\nu$ is centered. This relation reduces for the square law region to:

$$P_N = \left(\frac{\beta P_{RF}^2}{f} + 1 \right) kT\Delta\delta \tag{48}$$

and for the linear region to

$$P_N = \left(\frac{\gamma P_{RF}}{f} + 1 \right) kT\Delta\nu \tag{49}$$

The average values of β we determined experimentally are:

$$\beta \simeq 5 \times 10^{14} \text{ Watt}^{-2} \text{ sec}^{-1} \qquad \text{and}$$

$$\gamma \simeq 10^{11} \text{ Watt}^{-1} \text{ sec}^{-1}$$

The conversion gain G of the crystal can be represented by

$$G = SP_{\mathbf{RF}} \tag{50}$$

in the square law region and by

$$G = \text{constant} = C \tag{51}$$

---

* The phase shift associated with the Hewlett-Packard X-382-A attenuator is quite small.

† Values of α for K-band crystals are quoted in References 6 and 7. They differ however from each other by approximately 3 orders of magnitude.

in the linear region. Values of S and C for the 1N23C were found to be $S \simeq 500$ Watt^{-1} and $C \simeq 0.3$.

a. Simple straight detection

If one does not make use of the bucking possibilities of the magic T (i.e., eliminate the slide screw turner in Fig. 6) one has the simplest possible set-up sensitive to χ''. Under those conditions the microwave power reaching the crystal will be identical to the reflected power from the cavity. Equation (36) becomes:

$$\frac{\chi''_{\text{MIN-OBS}}}{\chi''_{\text{MIN-TH}}} = \left(\frac{GN_k + F_{\text{AMP}} + t - 1}{G} \right)^{\frac{1}{2}} \tag{52}$$

With the aid of (48), (49), (50), and (51), this relation reduces for the 1N23C in the square law region to:

$$\frac{\chi''_{\text{MIN-OBS}}}{\chi''_{\text{MIN-TH}}} = \left(\frac{1 + 5 \times 10^9 P_0^2}{50 P_0} \right)^{\frac{1}{2}} \tag{53}$$

and for the linear region to:

$$\frac{\chi''_{\text{MIN-OBS}}}{\chi''_{\text{MIN-TH}}} = (3 \times 10^7 P_0)^{\frac{1}{2}} \tag{54}$$

A plot of (53) and (54) is shown in Fig. 9. As before the assumption was made that $P_{\text{RF}}/P_0 \simeq 0.1$ (see barretter case). The noise figure of the amplifier F_{AMP} was taken as unity which again can be closely approached by means of a step-up transformer. The field modulation frequency was assumed to be 1,000 c.p.sec., although (47) shows that from a point of view of noise one would like to go to as high a frequency as possible. However practical consideration such as power requirements for getting a given modulation field, pick-up problems, skin depth losses in the cavity wall usually set an upper limit. The modulation frequency may be also dictated at times by the relaxation times of the investigated sample.[10]

b. Straight detection with optimum microwave bucking

From Fig. 9, we see that the straight crystal detection scheme suffers at low powers because of the poor conversion gain of the crystal and at high powers because of excess crystal noise. This situation can be greatly improved by adding some microwave power to the crystal when the reflected power from the cavity is low (to be referred to as positive bucking) or subtracting some of the power in the other case (negative bucking). In this section we will find the improvement over the unbucked system and the amount of bucking required to effect it,
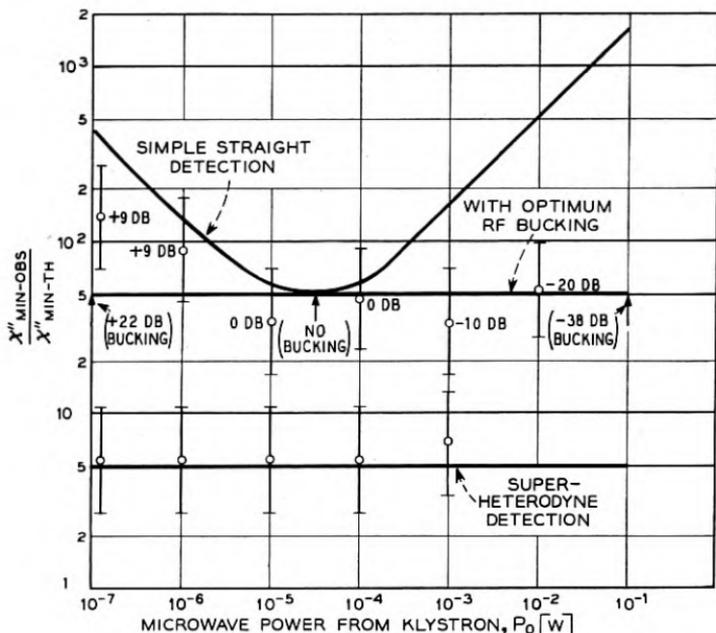
Fig. 9 — The ratio of the minimum observable susceptibility to the minimum theoretical value versus microwave power for different crystal detection schemes. Full lines correspond to the predicted sensitivity and dots indicate experimental values.

We define the bucking parameter B by the relation

$$P_x = BP_{RF} \qquad (55)$$

Where P_{RF} is the microwave power at the crystal before and P_x after the bucking is applied. We further assume that after the bucking is applied the crystals will operate in the square low region. Combining (49), (50), and (52) and neglecting the term GN_k which is small in comparison to the other term we get for the bucking scheme:

$$\frac{\chi''_{\text{MIN-OBS}}}{\chi''_{\text{MIN-TH}}} = \left(\frac{F_{\text{AMP}} + \dfrac{\beta B^2 P_{RF}^2}{f}}{SBP_{RF}} \right)^{\frac{1}{2}} \qquad (56)$$

In order to find the optimum bucking parameter, we set

$$\frac{d}{dB}\left(\frac{\chi''_{\text{MIN-OBS}}}{\chi''_{\text{MIN-TH}}}\right) = 0 \text{ which results in}$$

$$\left(B = \frac{F_{\text{AMP}}f}{\beta P_{RF}^2} \right)^{\frac{1}{2}} \qquad (57)$$

Putting in the numerical values for the 1N23C as quoted previously we get that $B = 1.4 \times 10^{-6}/P_{RF}$. Equation (56) becomes with the optimum bucking parameter

$$\frac{\chi''_{\text{MIN-OBS}}}{\chi''_{\text{MIN-TH}}} = \left[\frac{2F_{\text{AMP}}}{S \left(\dfrac{F_{\text{AMP}}f}{\beta} \right)^{\frac{1}{2}}} \right] \tag{58}$$

For the case under discussion this ratio turns out to be $\simeq 50$ independent of P_0. Fig. 9 shows a plot of (58). The values in parenthesis indicate the degree of bucking necessary to accomplish this ratio as determined from (57). It should be noted that the negative bucking can be easily accomplished by means of the slide screw tuner in the magic T arm (see Fig. 6) whereas for large positive buckings a scheme like in Fig. 8 has to be used. (Some positive bucking can of course be also accomplished by means of the slide screw tuner).

c. The superheterodyne scheme

The RF bucking system just described bears a certain resemblance to the balanced mixer barretter scheme. In both cases additional microwave power was added to the detector in order to increase the conversion gain. However in the crystal scheme this resulted in an increase in noise power whereas this should not be the case with barretters. The question arises whether a decent conversion gain in crystals has to be always accompanied by a large noise power. An inspection of (49) shows that around frequencies of tens of megacycles* or higher the noise output of the crystal becomes negligible. As pointed out earlier such high magnetic field modulation frequencies are not feasible. However in a superheterodyne system the crystal outputs will be at an intermediate frequency of 30 or 60 mc. This will make the flicker noise components negligible even at high powers where the conversion gain is good. The conventional way to obtain the intermediate frequency is to beat the reflected signal from the cavity with a local oscillator (see Fig. 10) which is removed from the signal generator by the I.F. frequency. In order to eliminate the noise from the local oscillator a balanced mixer should be employed. The ratio

$$\left(\frac{\chi''_{\text{MIN-OBS}}}{\chi''_{\text{MIN-TH}}} \right) \text{ becomes then from equ. } 52 \left(\frac{F_{IF} + t - 1}{G} \right)^{\frac{1}{2}} \tag{59}$$

The expression in the brackets is called in radar work[11] the overall

_____

* It was shown by G. R. Nicoll[9] that this equation holds up to this frequency range.

noise figure of the receiver F. We found that a noise figure of about 11–14 db is easily attainable with commercial I.F. amplifiers and balanced mixer. This would give us a ratio of

$$\frac{\chi''_{\text{MIN-OBS}}}{\chi''_{\text{MIN-TH}}} \simeq 5$$

which is plotted together with the other crystal schemes in Fig. 9. Although this system does necessitate 2 stable microwave sources, it is not difficult to operate once they are set-up. This was not considered as a major disadvantage at least not at X-band. The phasing problem discussed in connection with the mixer barretter scheme of comparable sensitivity is eliminated. An additional small advantage is the ruggedness of crystals in comparison to barretters and the availability of good commercial balanced crystal mixers. There are other double frequency schemes which do not need 2 separate microwave signal generators. The other frequency may be obtained by amplitude or phase modulating one signal generator by an IF frequency. The side bands which are produced in this way are displaced by just the IF frequency and may be utilized instead of the second signal generator. Schemes of this sort look particularly promising for frequencies well above X-band in which case it might prove difficult to maintain the difference frequency of two separate microwave generators within the band width of the IF.

F. Experimental Determination of Sensitivity Limits

1. Preparation of samples

In order to get an experimental check on the previous analysis, samples with a known number of spins had to be prepared. Two sets of samples were made. One consisted of single $CuSO_4 \cdot 5H_2O$ crystals of varying sizes hermetically sealed between 2 sheets of polyethylene. The other set consisted of different amounts of diphenyl picryl hydrazyl* which were similarly sealed up. D.P.H. samples having less than 10^{17} spins were prepared by dissolving known amounts of the free radical in benzene and putting a drop of this solution on the polyethylene. After the benzene had evaporated, it was sealed up with another sheet of polyethylene. The g-values of $CuSO_4 \cdot 5H_2O$ and D.P.H. differ enough so that both samples can be conveniently run simultaneously. This was done in order to check the self consistency of the two sets of samples. The measured integrated susceptibility of all the D.P.H. samples

---

* We are indebted to A. N. Holden for supplying us with this material.

with more than 10^{16} spins agreed within a few percent with the calculated value. The calculated value being based on the known amount of D.P.H. and the measured value being referred to the known amount of $CuSO_4 \cdot 5H_2O$. D.P.H. samples with less than 10^{16} spins had all a smaller number of effective spins than calculated. The discrepancy was more pronounced the smaller the sample. There was also evidence that the smaller D.P.H. samples deteriorated with time. As a typical example we quote a sample which started out as 10^{15} effective spins and was reduced after 4 weeks to 4×10^{14} effective spins and another one which initially had 10^{14} spins, deteriorated in the same time interval to 10^{13} spins. Since only the smaller samples were noticeably affected, this deterioration seems to be associated with a surface reaction. It was also observed that the line width between inflection points of the D.P.H. samples with less than 10^{15} spins increased from 1.8 oersteds to 2.7 oersteds. This broadening probably arises from a reduction in the exchange narrowing mechanism due to the spreading out of the sample.

2. Comparison of experimental results with theory

In checking the sensitivity of the equipment D.P.H. samples were used and the signal to noise was estimated from the recorded output. The experimental points thus obtained are shown in Fig. 7 and Fig. 9. We believe that the results are significant to within a factor of 2, the main error arising from the estimate of the RMS noise. The band width of the lock-in detector was $\Delta\nu = 0.03$ sec^{-1}, $Q_0 = 4,000$, and the field modulation used was 3 oersteds p.t.p., 100 c.p.sec. for the barretter schemes and 1,000 c.p.sec. for the crystal schemes. This large modulation field somewhat distorts the line, but, as mentioned earlier was done in order to get the full signal. The D.P.H. samples were calibrated against $CuSO_4 \cdot 5H_2O$ before each run. Even so it was not felt safe to use samples which had less than 10^{13} spins.

Referring to Fig. 8 we see that for the straight barretter detector the experimental points agree fairly well with the predicted value, but in the balanced mixer scheme fall short by about a factor of 4. A possible explanation of this discrepancy is that the barretters were not completely matched in which case the noise from the local oscillator would not be compensated for.

Fig. 9 shows the experimental points for the crystal schemes. For powers between 10^{-7} W and 10^{-5} W the system used fell between the simple straight detection scheme and the one utilizing optimum RF bucking. The reason is that it was very easy to obtain a certain amount of positive bucking ($+9$ db) by merely adjusting one arm of the magic T.
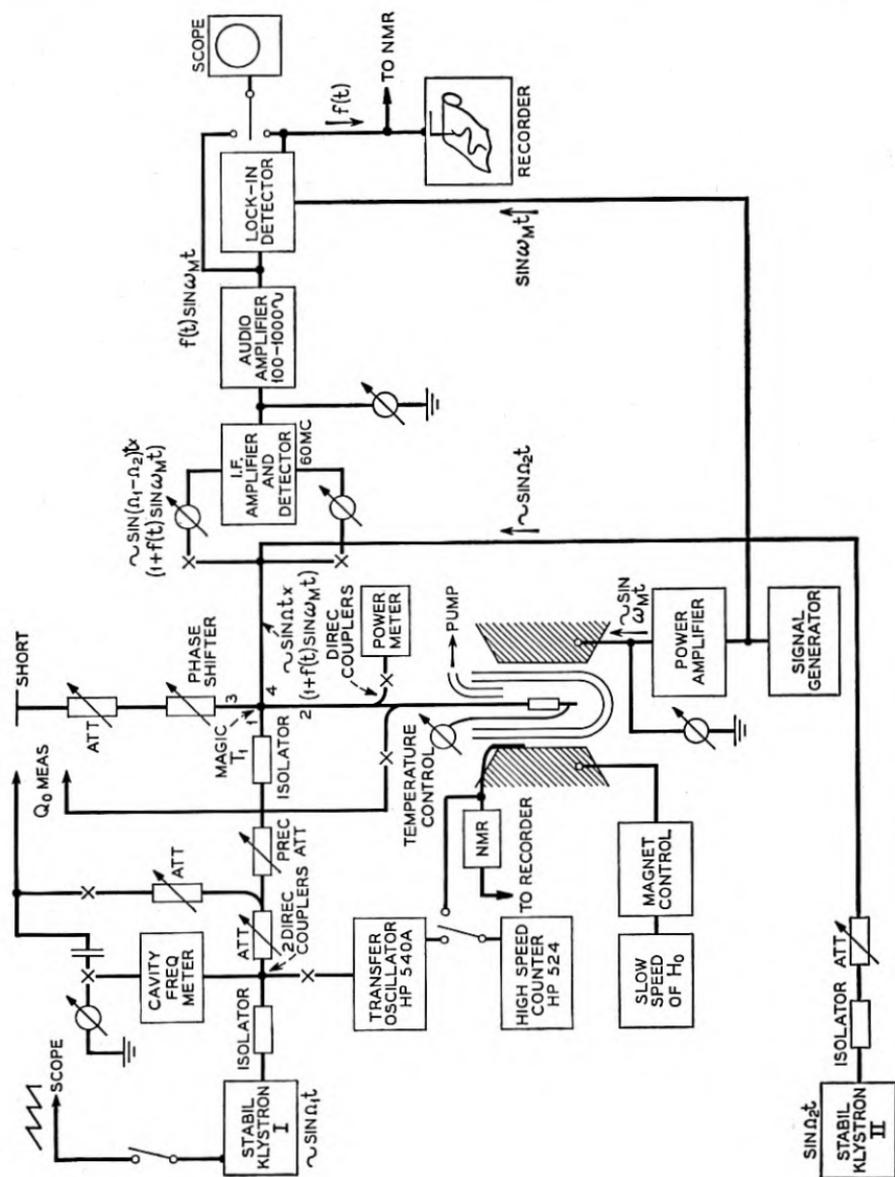
Fig. 10 — Block diagram of a superheterodyne paramagnetic resonance spectrometer.

It would however have been a great deal more difficult to obtain the entire bucking of $+22$ db at 10^{-7} W since a set-up like in Fig. 8 would have to be used. Thus for the sake of simplicity the extra factor in signal to noise of 2 or 3 was abandoned. The amount of negative bucking at the higher powers will be limited by the stability of the bridge. A practical limit of (40–50) db was characteristic of our set-up. We see from Fig. 9 that the agreement between the experimentally determined sensitivity and the theoretically predicted sensitivity is satisfactory.

The experimental results on the superheterodyne scheme agrees again very well with the predicted values up to a power level of 10^{-3} W. (This corresponds to less than 10^{12} spins in D.P.H.) Above this level T_1 (see fig. 10) has to be balanced to better than 40 db to keep the IF carrier amplitude within the required value. Instabilities in the bridge due to mechanical vibrations and thermal drifts start to contribute to the noise. Thus at high power levels the superhet scheme starts to loose some of its advantages unless special precautions are being taken to eliminate the above mentioned noise factors. A great deal in this direction could probably be accomplished by shock-mounting the microwave components and better temperature stability for slow drifts. Since we were mainly interested in powers below 1 mW, our efforts were limited to controlling the temperature of the room to $\pm1°C$.

Since the superhet scheme was found to be the most sensitive one, it might be worthwhile to discuss it in more detail. A block diagram of the set up is shown in Fig. 10.

The signal generator feeds into the magic T, where its power is split between arm 2 and 3. Arm 2 has the reflection cavity with the sample, the reflected voltage being bucked out with the aid of arm 3. For this purpose arm 3 has a phase shifter and attenuator, an arrangement which was found to be more satisfactory than a slide screw tuner as far as stability and ease of operation goes. The desired signal appears then in arm 4. It is fed into a balanced mixer which receives the local oscillator power from the stabilized klystron II. The output of the balanced mixer is then fed through the IF amplifier, detector, audio amplifier and lock-in detector. The circuits of each of those components is fairly standard and will not be dwelled upon further. The microwave power is measured in arm 2 of the magic T. The power reflected from the cavity is also monitored in arm 2. This is of great help in finding the cavity when klystron I is swept in frequency by means of a sawtooth voltage on its reflector. Since the klystron mode itself might have some dips in it, (which might be mistaken for the cavity), it proved helpful to display on the scope the klystron mode simultaneously with the reflected power

from the cavity. This also provides a convenient way to measure the Q_0 of the cavity.[12] The frequency is measured roughly by means of a cavity frequency meter and more precisely by means of a transfer oscillator and high speed counter. The magnetic field is measured by means of a nuclear magnetic resonance set-up, its frequency being measured on the same counter as the microwave frequency. The nuclear resonance signal is recorded on the same trace as the electron resonance signal. Thus if the magnetic field is homogeneous enough, the nuclear sample will see the same field as the electronic sample and g-values can be conveniently determined to the accuracy of the nuclear moment (this also assumes that the signal is large enough, so that no additional error is introduced in determining the exact location of the resonance.) The field modulation coils are mounted on the pole faces and are energized by a 50-watt power amplifier. A field of 50 oersteds p.t.p. is available at 1,000 cps and a slightly higher field at 100 cps.

The magnet is a Verian 12″ modified so that it can rotate around an axis perpendicular to H_0. This was done mainly in order to make anistropy measurements more convenient. This enables one to make quick saturation measurements in isotropic materials without having to change the incident RF power. This is accomplished by rotating the magnetic field and measuring the signal strength versus angle. Since only the RF field perpendicular to the dc field causes transitions, the signal in an unsaturated isotropic sample should go as $\cos^2 \theta$; where θ is the angle between H_1 and H_0. From the deviation from this dependence, the saturation parameter can be found. This could also be done by rotating the cavity, but at microwaves is not as easy as rotating the field.

VII. A NOTE ON THE EFFECTIVE BANDWIDTH

There seems to be some confusion as to how narrow one should make an audio amplifier preceding a phase sensitive detector (lock-in) or why the band width of the IF amplifier doesn't enter in a superhet scheme. Those and similar questions have to do with the effective band width of the system $\Delta \nu$ which appears in (26). Since similar questions have been rigorously analyzed by other authors,[13, 14] the present discussion will try to stress some of the physical ideas underlying the different detection schemes.

We consider first the simple scheme illustrated in Fig. 11. It consists of an amplifier with band width $\Delta \nu_1$ centered around ν_1 followed by a phase sensitive detector with a reference voltage at V_1. The output of the phase sensitive detector has an RC filter of band width Δv_2. One can see that in such a system the only noise components centered around

ν_1 (this being also the reference frequency) in a band width $\Delta\nu_2$ will contribute to the output noise. This is because the beat between 2 noise components like ν_n and ν_m (see Fig. 11) is too far removed from ν_1 to produce an output voltage. (This statement implies the condition that $\Delta\nu_1 < \nu_1$ otherwise the beat between $2\nu_1$ and ν_1 could come through.) Thus in this system the band width of the amplifier is immaterial as long as the noise voltages are not so large as to saturate it.

A more serious situation may arise in the absence of a reference voltage. In this case the noise components within the band width $\Delta\nu_1$ can beat with each other and produce a noise output which would increase with the band width. This could become especially detrimental in a superheterodyne scheme in which the IF band width can be a million times larger than the output band width. It can be shown, however, that if the carrier voltage V_c at the output of the IF is large enough the IF bandwidth ΔF_{IF} does not enter into the noise consideration[13] the criterion essentially is that

$$V_c^2 > G^2 2kTZ\Delta F_{IF} \tag{60}$$

where G is the IF amplifier gain, and Z the input impedance. Condition (60) means that we want the noise which beats with the carrier to be greater than the beat between 2 noise terms. Since the former is proportional to the carrier, its predominance can be easily ascertained experimentally by increasing the IF carrier and noting whether the noise output increases proportionally. If it does, (60) is fulfilled.
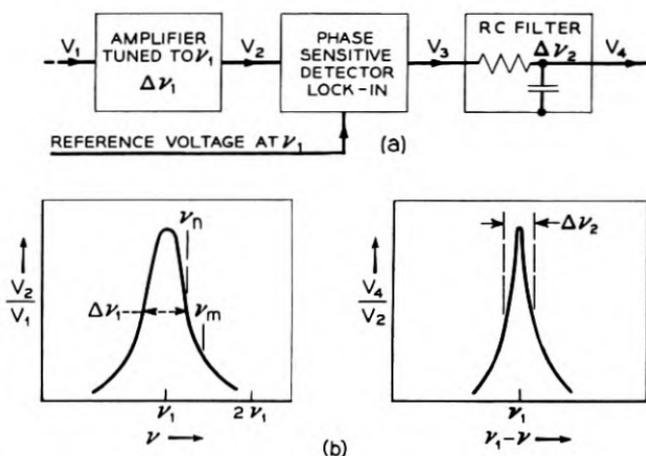
Fig. 11 — Effective band width of a phase sensitive detector $\Delta\nu_{eff} = \Delta\nu_2$. Note that the band width of the amplifier does not enter as long as $\Delta\nu_1 < \nu_1$.

In order to see what maximum gain G (60) imposes on a typical system we assume $\Delta F_{\text{IF}} = 5 \times 10^6$ c.p.sec. $Z = 10^3 \Omega$; $V_c \simeq 1$V. Under those conditions we get from (60) that G has to be smaller than approximately 10^5. If on the other hand G is very small the signal level at the audio amplifier input is so low that the flicker noise of the detector can still come in. A good practical figure for the IF amplifier gain is around 60 db.

VIII. SATURATION EFFECTS

In all the previous considerations RF power saturation effects were neglected, i.e., we have assumed that the power absorbed is proportional to H_1^2, where H_1 is the RF magnetic field. When this assumption is no longer satisfied, the question of sensitivity has to be re-examined for different degrees of saturation. However it is difficult from an experimental point of view to change the conditions of the experiment for each degree of saturation and therefore an elaborate analysis of this case does not seem to be warranted. However it might be of interest to see the effect on the in phase component of the signal at complete or nearly complete saturation

The change in output voltage for a reflection cavity is (15)

$$\Delta V = \sqrt{2}\ V\ \frac{R_0 n^2}{(R_0 n^2 + r)^2}\ \Delta r$$

and from (4)

$$\frac{\Delta r}{r} = \frac{\Delta Q}{Q_0} = 4\pi\eta Q_0 \chi''$$

The RF magnetic field in the cavity is given by

$$H_1^2 = CQ_0(1 - \Gamma^2)P_{in} \tag{71}$$

where C is a constant dependent on the geometry of the cavity the reflection coefficient. Assuming a simple homogeneous saturation behaviour we substitute for χ'' the saturated value of $\chi''_s{}^{(1)}$.

$$\chi''_s = \frac{\chi_u''}{1 + \gamma_1^2 H_1^2 T_1 T_2} = \frac{\chi_u''}{1 + \gamma_1^2 T_1 T_2 C Q_0 (1 - \Gamma^2) P_{in}} \tag{72}$$

where χ_u'' is the unsaturated value of the susceptibility and P_{in} the power from the microwave source.

$$\frac{\Delta r}{r} = 4\pi\eta Q_0 \frac{\chi_u''}{1 + \gamma_1^2 T_1 T_2 Q_0 (1 - \Gamma^2) P_{in}} \tag{73}$$

and the output voltage ΔV.

$$\Delta V = \sqrt{2} \; V_0 \frac{R_0 n^2}{(R_0 n^2 + r)^2} r 4\pi\eta Q_0 \frac{\chi_u''}{1 + \gamma_1^2 T_1 T_2 C Q_0 (1 - \Gamma^2) P_{in}} \quad (74)$$

For a high degree of saturation

$$\gamma_1^2 T_1 T_2 C Q_0 (1 - \Gamma^2) P_{in} \gg 1$$

and substituting for

$$\Gamma = \frac{\dfrac{R_0 n^2}{r} - 1}{\dfrac{R_0 n_2}{r} + 1}$$

we get:

$$\Delta V = \frac{\sqrt{2} \; V_0 \pi\eta \; \chi_u''}{P_{in} \gamma_1^2 T_1 T_2 C} \quad (75)$$

The above relation shows that under saturated conditions the Q of the cavity does not enter and one might as well not use one or use a very much overcoupled cavity. This is one of the reasons why in microwave gas spectroscopy,* where lines are easier saturated a cavity is not used. (The more important reason is that in most cases one sweeps the frequency of the source, so that a cavity is difficult to use.)

Equation (75) also shows that the signal and also signal to noise goes down with increasing RF power. The above argument does not hold for the out-of-phase (dispersion) signal, in particular it breaks down completely for signals observed under fast adiabatic passage conditions.[1] For the latter case one wants as high an RF field as possible.

REFERENCES

1. See for example F. Bloch, Phys. Rev., **70**, p. 460, 1946. N. Bloembergen, E. M. Purcell, R. V. Pound, Phys. Rev., **73**, p. 679, 1948.

---

* In microwave gas spectroscopy the fractional power loss per unit length α is used. Its relation to the susceptibility is $\alpha = 8_\pi \; 2\chi''/\lambda_G$ where λ_G is the guide wavelength.

2. Montgomery, Technique of Microwave Measurements, Rad. Lab. Series, No. 11.
3. C. H. Townes and S. Geschwind, J.A.P., **19,** p. 795, Aug., 1948.
4. Hamilton, Knipp and Kupper, Klystrons and Microwave Triodes. McGraw Hill, 1948, Rad. Lab. Series No. 6, p. 475.
5. Torrey, H. C. and Whitmer, C. A., Crystal Rectifiers, Rad. Lab. Series, Vol. 15, McGraw Hill, 1947.
6. M. W. P. Strandberg, H. R. Johnson, J. R. Eshbach, R.S.I., **25,** pp. 776–792, Aug., 1954.
7. Townes and Schawlow, Microwave Spectroscopy, McGraw Hill, 1955.
8. Miller, P. H., Noise Spectrum of Crystal Rectifiers, Proc. I.R.E., **35,** p. 252, 1947.
9. G. R. Nicoll, Noise in Silicon Microwave Diodes, Proc. I.E.E., **101,** pp. 317–29, Sept., 1954.
10. See for example K. Holbach, Helv. Physica Acta, **27,** p. 259, 1954; A. M. Portis, Phys. Rev., **100,** p. 1219, 1955.
11. Pound, R. V., Microwave Mixers, M.I.T. Radiation Lab. Series 16, McGraw Hill.
12. E. D. Reed, Proceedings of the National Electronics Conference, **7,** p 162, 1951.
13. S. O. Rice, B.S.T.J., **23,** pp. 282–332; B.S.T.J., **24,** pp. 46–156, 1945.
14. A. van der Ziel, Noise, Prentice Hall, Inc., 1954.

The Determination of Pressure Coefficients of Capacitance for Certain Geometries

By D. W. McCALL

Expressions are derived for the pressure coefficients of capacitance of parallel plate capacitors subjected to one-dimensional and hydrostatic pressures and of cylindrical capacitors subjected to radial compression. The derivations apply to systems in which the dielectrics are isotropic, elastic solids.

I. INTRODUCTION

The electrical capacitance between two conductors separated by a dielectric is a quantity which can be calculated with ease only in certain geometrical arrangements of high symmetry. Even the classic example of parallel plates presents major difficulties as one may only perform the calculation exactly for the case of plates of infinite area or vanishing separation. The approximation becomes poor when $(\text{area})^{\frac{1}{2}}/(\text{separation})$ becomes small and the theoretical treatment of edge effects is sufficiently difficult that it has not been solved though the solution would greatly facilitate dielectric constant measurement.

When pressure enters into the situation as a variable the difficulties are enhanced as one must be able to describe the geometry effects as well as the change in dielectric constant.

The engineers responsible for designing submarine cables are confronted with the necessity of knowing the manner in which capacitance depends upon pressure as may be illustrated in the following way. A submarine telephone cable is composed of a central copper conductor surrounded by a sheath of dielectric material. Due to the extreme length repeaters must be placed at intervals, the separation being determined by the attenuation of the cable. The attenuation, α, of a coaxial telephone cable may be written

$$\alpha = (G/2)(L/C)^{\frac{1}{2}} + (R/2)(C/L)^{\frac{1}{2}}$$

where G is the conductance of the dielectric per unit length, C the

485

capacitance, L the inductance, and R the conductor resistance per unit length. The second term contributes about 99 % of the attenuation. Considering only this term we deduce

$$(1/\alpha)(\partial\alpha/\partial P) \cong (1/R)(\partial R/\partial P) + (1/2C)(\partial C/\partial P) - (1/2L)(\partial L/\partial P)$$

Accurate knowledge of the coefficient $(1/C)(\partial C/\partial P)$ is thus essential in designing very long cables which are to be exposed to high pressures.

In evaluating dielectric materials for use in cables it is often desirable to make measurements on sheet specimens rather than cable. It thus becomes necessary to be able to translate sheet data into cable data. It is the purpose of this paper to analyze the problem of calculating pressure coefficients of capacitance for certain simple geometries and to consider the methods of measurement which have been used. It will be shown that results of theory and experiment are in as good agreement as can be expected but more accurate measurements of electric and elastic properties are needed.

The equations which will be derived are also necessary if one wishes to determine the dependence of dielectric constant on pressure using any of the geometries described herein.

The problems treated in this paper are particularly simple and amenable to mathematical treatment but many problems encountered in submarine cable design are at present subject to solution only by empirical means. Fundamental investigations of the effects of pressure on dielectric materials are needed.

II. THEORETICAL TREATMENT

In the following treatment we consider that the dielectric substance is an elastic solid which obeys Hooke's law. We denote the relative permittivity or dielectric constant by ε, the permittivity of free space by ε_0,* the principal stresses and strains by τ_{ii} and e_{ii}, the density by ρ, the compressibility by k, and Poisson's ratio by σ.

A. Calculation of $\dfrac{1}{\varepsilon}\dfrac{\partial\varepsilon}{\partial P}$

One of the quantities which will be needed in the evaluation of

$$\frac{1}{C}\frac{\partial C}{\partial P} \quad \text{is} \quad \frac{1}{\varepsilon}\frac{\partial\varepsilon}{\partial P}$$

As ε is not dependent on the geometric configuration it can be calculated

---

* $\varepsilon_0 = 8.86 \times 10^{-12}$ farads/meter.

in general and the result applied to each of the special cases to follow. A relation between dielectric constant and density is required and usually, when dealing with non-polar dielectrics, one assumes that the Clausius-Mosotti relation gives the proper dependence. That is

$$\frac{\varepsilon - 1}{\varepsilon + 2} = \text{(constant)} \, \rho \tag{1}$$

This formula may be differentiated to give

$$\frac{1}{\varepsilon} \frac{\partial \varepsilon}{\partial P} = \frac{(\varepsilon - 1)(\varepsilon + 2)}{3\varepsilon} \frac{1}{\rho} \frac{\partial \rho}{\partial P} \tag{2}$$

In the theory presented herein, (1) will be used though it is at best an approximation. Corrections to the Clausius-Mosotti formula[1] which have been given do not seem applicable to polymer dielectrics and introduce parameters which must be fitted.

B. *The effect of a One-Dimensional Pressure Acting on a Disc*

Consider a one-dimensional pressure, $-P$, acting along the axis of a circular disc of dielectric material with electrodes affixed to opposite faces. Assume the disc is constrained such that no lateral displacement can occur. Let t be the thickness and A the area of the disc.

The capacitance of such a capacitor is given by the equation

$$C = \varepsilon \varepsilon_0 \frac{A}{t}$$

so the desired pressure coefficient is

$$\frac{1}{C} \frac{\partial C}{\partial P} = \frac{1}{\varepsilon} \frac{\partial \varepsilon}{\partial P} - \frac{1}{t} \frac{\partial t}{\partial P} \tag{3}$$

where use has been made of the condition that the area is constant (i.e., no lateral displacement). Hooke's law states

$$e_{xx} = \frac{k}{3(1 - 2\sigma)} [\tau_{xx} - \sigma(\tau_{yy} + \tau_{zz})] \tag{4}$$

$$e_{yy} = \frac{k}{3(1 - 2\sigma)} [\tau_{yy} - \sigma(\tau_{xx} + \tau_{zz})] \tag{5}$$

$$e_{zz} = \frac{k}{3(1 - 2\sigma)} [\tau_{zz} - \sigma(\tau_{xx} + \tau_{yy})] \tag{6}$$

---

[1] C. J. F. Böttcher, Theory of Electric Polarisation, Elsevier Publishing Co., Amsterdam, 1952, p. 199 et. seq.

We assume the z-axis lies along the disc axis so $\tau_{zz} = -P$ and by symmetry $\tau_{xx} = \tau_{yy}$. The condition of no lateral strain states $e_{xx} = e_{yy} = 0$ which when combined with (4) gives

$$\tau_{xx} = \tau_{yy} = -\frac{\sigma}{1-\sigma}P$$

Using the last result with (6) we obtain

$$e_{zz} = -\frac{kP}{3}\left(\frac{1+\sigma}{1-\sigma}\right)$$

and

$$\frac{e_{zz}}{P} = \frac{1}{t}\frac{\partial t}{\partial P} = -\frac{1}{\rho}\frac{\partial \rho}{\partial P} = -\frac{k}{3}\left(\frac{1+\sigma}{1-\sigma}\right) \tag{7}$$

Combination of (2), (3), and (7) results in

$$\frac{1}{C}\frac{\partial C}{\partial P} = \left[\frac{(\varepsilon-1)(\varepsilon+2)}{3\varepsilon} + 1\right]\frac{k}{3}\left(\frac{1+\sigma}{1-\sigma}\right) \tag{8}$$

C. The Effect of a Hydrostatic Pressure Acting on a Disc

Assume that conditions are similar to those considered in section B except that $e_{xx} = e_{yy} = 0$ is now replaced by

$$\tau_{xx} = \tau_{yy} = \tau_{zz} = -P.$$

The area is no longer independent of pressure so

$$\frac{1}{C}\frac{\partial C}{\partial P} = \frac{1}{\varepsilon}\frac{\partial \varepsilon}{\partial P} - \frac{1}{t}\frac{\partial t}{\partial P} + \frac{1}{A}\frac{\partial A}{\partial P} \tag{9}$$

Hooke's law, (4), (5), (6), now becomes

$$e_{ii} = \frac{-kP}{3}\ (i = x, y, z)$$

Thus

$$\frac{1}{\rho}\frac{\partial \rho}{\partial P} = -\frac{(e_{xx} + e_{yy} + e_{zz})}{P} = k \tag{10}$$

$$\frac{1}{A}\frac{\partial A}{\partial P} = \frac{(e_{xx} + e_{yy})}{P} = -\frac{2k}{3} \tag{11}$$

$$\frac{1}{t}\frac{\partial t}{\partial P} = \frac{e_{zz}}{P} = -\frac{k}{3} \tag{12}$$

Combination of (2), (9), (10), (11), and (12) results in

$$\frac{1}{C}\frac{\partial C}{\partial P} = \left[\frac{(\varepsilon - 1)(\varepsilon + 2)}{3\varepsilon} - \frac{1}{3}\right]k \tag{13}$$

D. The Effect of a Radial Pressure Acting on a Cylindrical Annulus

Consider a radial pressure acting normally to the axis of a cylindrical annulus to which electrodes are affixed to the inner and outer surfaces. Let the inner and outer radii be a and b respectively and assume the cylinder is filled with an incompressible substance so that the inner radius is not pressure dependent. The capacitance per unit length is given by

$$C_t = \frac{2\pi\varepsilon\varepsilon_0}{\ln\frac{b}{a}}$$

so

$$\frac{1}{C}\frac{\partial C}{\partial P} = \frac{1}{\varepsilon}\frac{\partial\varepsilon}{\partial P} - \frac{1}{\ln\frac{b}{a}}\frac{1}{b}\frac{\partial b}{\partial P} \tag{14}$$

We employ cylindrical coordinates (r, θ, z) where the z-axis is taken along the cylinder axis. Hooke's law becomes

$$e_{rr} = \frac{k}{3(1 - 2\sigma)}\left[\tau_{rr} - \sigma(\tau_{\theta\theta} + \tau_{zz})\right] \tag{15}$$

$$e_{\theta\theta} = \frac{k}{3(1 - 2\sigma)}\left[\tau_{\theta\theta} - \sigma(\tau_{rr} + \tau_{zz})\right] \tag{16}$$

$$e_{zz} = \frac{k}{3(1 - 2\sigma)}\left[\tau_{zz} - \sigma(\tau_{rr} + \tau_{\theta\theta})\right] \tag{17}$$

Equilibrium of an arbitrary volume element demands[2]

$$\tau_{rr} = A + \frac{B}{r^2} \tag{18}$$

and

$$\tau_{\theta\theta} = A - \frac{B}{r^2} \tag{19}$$

where A and B are constants with respect to spatial coordinates. (A

[2] J. Prescott, Applied Elasticity, Dover Publications, New York, 1946, p. 330.

should not be confused with the electrode area used in previous sections.) We assume

$$e_{zz} = 0 \text{ for all } (r, \theta, z) \tag{20}$$

$$e_{\theta\theta} = 0 \text{ for } r = a \tag{21}$$

and

$$\tau_{rr} - P \text{ for } r = b \tag{22}$$

Manipulation of (15) through (22) allows the evaluation of the constants A and B as

$$A = -\frac{b^2}{a^2} \frac{P}{\dfrac{b^2}{a^2} + (1 - 2\sigma)}$$

and

$$B = \frac{b^2(1 - 2\sigma)P}{\dfrac{b^2}{a^2} + (1 - 2\sigma)}$$

Thus

$$-\frac{1}{\rho} \frac{\partial \rho}{\partial P} = \frac{e_{rr} + e_{\theta\theta} + e_{zz}}{P} \text{ yields}$$

$$\frac{1}{\rho} \frac{\partial \rho}{\partial P} = \frac{2(1 + \sigma)k}{3} \frac{b^2}{a^2} \frac{1}{\dfrac{b^2}{a^2} + (1 - 2\sigma)} \tag{23}$$

Also

$$\frac{1}{b} \frac{\partial b}{\partial P} = \frac{e_{rr}|_{r=b}}{P} = \frac{k(1 + \sigma)}{3} \left[1 - \frac{b^2}{a^2}\right] \frac{1}{\dfrac{b^2}{a^2} + (1 - 2\sigma)} \tag{24}$$

Combining (2), (14), (23), and (24) we obtain

$$\frac{1}{C} \frac{\partial C}{\partial P} = \frac{2}{3} \left[\frac{(1 + \sigma) \dfrac{b^2}{a^2}}{\dfrac{b^2}{a^2} + (1 - 2\sigma)}\right] \left[\frac{(\varepsilon - 1)(\varepsilon + 2)}{3\varepsilon} + \frac{1 - \dfrac{a^2}{b^2}}{2 \ln \dfrac{b}{a}}\right] k \tag{25}$$

E. The Case $\sigma = \frac{1}{2}$

The equations derived above reduce to the expressions one would obtain if the dielectric were considered to be a compressible fluid when σ is set equal to $\frac{1}{2}$.

Equation (8) for the parallel plate arrangement becomes

$$\frac{1}{C}\frac{\partial C}{\partial P} = \left[\frac{(\varepsilon - 1)(\varepsilon + 2)}{3\varepsilon} + 1\right]k \tag{26}$$

while (13) is unaltered. The difference between the two cases arises from the fact that in (13) the area was allowed to vary while in the former case it was not. The deviation of

$$\frac{1}{C}\frac{\partial C}{\partial P}$$

from (26) when $\sigma \neq 0.5$ is given by the factor

$$\frac{1}{3}\left(\frac{1 + \sigma}{1 - \sigma}\right)$$

The capacitance-pressure coefficient for the cylindrical configuration, (25), becomes

$$\frac{1}{C}\frac{\partial C}{\partial P} = \left[\frac{(\varepsilon - 1)(\varepsilon + 2)}{3\varepsilon} + \frac{1 - \frac{a^2}{b^2}}{2\ln\frac{b}{a}}\right]k \tag{27}$$

The deviation of

$$\frac{1}{C}\frac{\partial C}{\partial P}$$

from the value given in (27) when $\sigma \neq 0.5$ is thus given by the factor

$$\frac{2}{3}\left[\frac{(1 + \sigma)\frac{b^2}{a^2}}{\frac{b^2}{a^2} + (1 - 2\sigma)}\right]$$

III. APPARATUS

The experimental arrangement employed to investigate the validity of (8) is shown in Fig. 1.* Pressure was applied by means of a Baldwin tensile testing machine. The cell makes use of a "sandwich" arrangement wherein two disc samples (2″ in diameter, 0.050″ thick) of dielectric are pressed between three brass electrodes, the outer electrodes being grounded. The capacitance thus formed is well shielded and stray capaci-

---

* This cell was designed by C. A. Bieling.

tances are minimized. Lateral displacements are kept small by an annular ring of steatite ceramic which is in turn surrounded by a ring of Ketos steel. Pressures of 23,000 lb on the two-inch sample discs have been applied without damaging the cell.

Although measurements could be made with ease in this cell it is not without disadvantages. The steatite ring has a rather high dielectric constant which tends to increase fringing effects. These effects are furthermore pressure dependent since the electrode separation varies as pressure is applied. Also loss measurements could not be obtained as leakage along the steatite surface was larger than the leakage through the samples of the polyethylene-butyl rubber compound investigated.

An attempt was made to eliminate fringing effects by making measurements on samples of varying thickness and extrapolating to zero thickness but results were too uncertain to be of quantitative value. The uncertainty resulted from the inability to cast the sample discs with uniform thickness an effect which becomes pronounced with very thin samples. It was possible, however, to estimate the total stray capacitance in this manner and it was found to be about 10 per cent of the sample capacitance and only slightly dependent upon pressure.
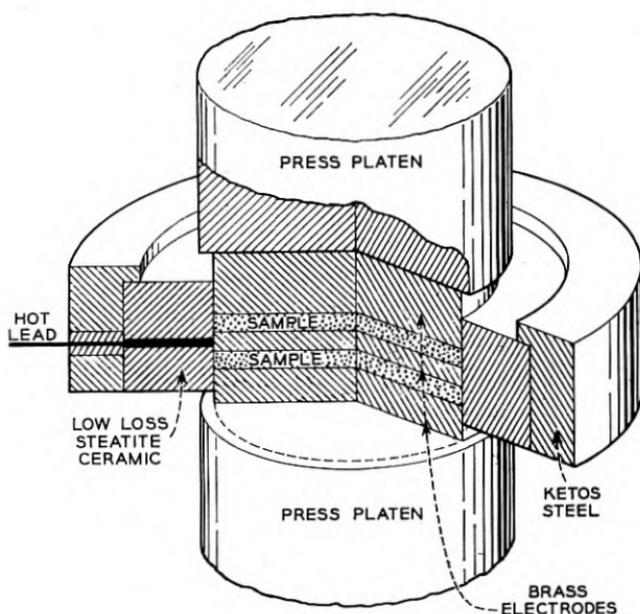
Fig. 1 — Cell employed to measure $(1/C)(\partial C/\partial P)$ with sheet specimens under one dimensional pressure.

Also, due to non-uniformity of the thickness of the specimens, it was found that the capacitance-pressure coefficient was larger at low pressures than at high pressures. This was apparently due to the initial squeezing out of voids between the electrodes and samples and the difficulty was removed by applying silver paint electrodes to the sample discs.

A Western Electric capacitance bridge was used to make capacitance measurements with this cell. The temperature was kept at 25°C and the humidity of the room was maintained at 50 per cent. The frequency used was 10 kc.

It is believed that the fact that the steatite is much more rigid than the specimens makes this experimental arrangement closely approximate the assumptions made in deriving (8) (i.e. lateral strains are negligible). It is important, however, that the specimens be cut to fit the steatite ring very closely.

Experiments which correspond to the cylindrical capacitor under biaxial stress have been performed as follows.* The specimens in this case were lengths of cable which consisted of a copper wire central conductor surrounded by the polyethylene-5 per cent butyl rubber compound. b/a was 3.87 in most of the measurements but some data were obtained for $b/a = 4.68$ (actual dimensions 0.620″/0.160″ and 0.750″/0.160″). Twenty foot lengths of cable were placed in a long tank provided with a seal at one end. The end of the cable inside the tank was closed such that the center conductor was isolated. The tank was then filled with water which served as the outer conductor, tap water having sufficiently high conductivity. Pressure was applied by the water.

A Leeds and Northrup capacitance bridge was used and the measurements reported were made at 10 kc.

IV. RESULTS

It is experimentally observed in all the cases considered that plots of C versus P are nearly linear for polyethylene-5% butyl rubber. This may be shown to be in agreement with the foregoing theories as follows. Equation (8) may be written

$$\int_{C(0)}^{C(P)} d \ln C = \int_0^P \left[\frac{(\varepsilon - 1)(\varepsilon + 2)}{3\varepsilon} + 1 \right] \frac{k}{3} \left[\frac{1 + \sigma}{1 - \sigma} \right] dP \quad (28)$$

* The investigation of radial compression on cylindrical (cable) specimens was carried out by A. W. Lebert and O. D. Grismore of Bell Telephone Laboratories.

The integrand is approximately constant so

$$\ln \frac{C(P)}{C(0)} \cong \left[\frac{(\varepsilon - 1)(\varepsilon + 2)}{3\varepsilon} + 1 \right] \frac{k}{3} \left[\frac{1 + \sigma}{1 - \sigma} \right] P$$

and

$$C(P) = C(0) \exp \left\{ \left[\frac{(\varepsilon - 1)(\varepsilon + 2)}{3\varepsilon} + 1 \right] \frac{k}{3} \left[\frac{1 + \sigma}{1 - \sigma} \right] P \right\}$$

$kP \cong 10^{-2}$ for the highest pressures used in the present experiments and

$$\left[\frac{(\varepsilon - 1)(\varepsilon + 2)}{3\varepsilon} + 1 \right] \frac{1}{3} \left[\frac{1 + \sigma}{1 - \sigma} \right]$$

is of the order of unity so the exponential may be expanded as

$$C(P) \cong C(0) \left\{ 1 + \left[\frac{(\varepsilon - 1)(\varepsilon + 2)}{3\varepsilon} + 1 \right] \frac{k}{3} \left[\frac{1 + \sigma}{1 - \sigma} \right] P \right\}$$

This treatment applies only to dielectrics for which ε, k, and σ are insensitive to pressure. Equations (13) and (25) may be treated similarly.

Values obtained experimentally and theoretically for polyethylene-5% butyl rubber are compared in Table I. The experimental values represent averages of many measurements. Agreement is considered adequate but more careful experiments are needed. The necessary parameters assumed in making these comparisons are:

$$\varepsilon = 2.28$$

$$k = 2.14 \times 10^{-6}/\text{psi}$$

$$\sigma = 0.50$$

TABLE I — EXPERIMENTAL AND THEORETICAL VALUES FOR POLY-
ETHYLENE-5 PER CENT BUTYL RUBBER

Sample	Pressure	$\frac{1}{C} \frac{\partial C}{\partial P}$ (/10^6 psi)	
		Experimental	Theoretical
Sheet..........................	one-dimensional	3.3*	3.74
Cable $\{b/a = 3.87\ldots\ldots\ldots\ldots$	radial	2.4	2.27
$\{b/a = 4.68\ldots\ldots\ldots\ldots$	radial	2.2	2.22

* This value has not been corrected for stray capacitance. Such a correction would tend to make the agreement between experimental and theoretical results better.

V. SUMMARY

Equations relating electrical capacitance and pressure have been derived for plane capacitors under one dimensional and hydrostatic pressures and cylindrical capacitors under radial pressure. The dielectric material has been assumed to be an elastic solid but the relationships also apply to fluid dielectrics when Poisson's ratio is set equal to $\frac{1}{2}$. Experiments corresponding to the assumptions have been described briefly and experimental results are found to be in agreement with the theoretical predictions.

The results are of practical value in making estimates of the dependence of attenuation of submarine cables on pressure. The equations may also be put in forms useful for determining the dependence of the dielectric constant on pressure from capacitance measurements.

ERRATA

The Effects of Surface Treatments on Point Contact Transistor Characteristics by J. H. Forster and L. E. Miller, B.S.T.J., **35,** pp. 767–811, July, 1956. Figs. 3, page 776, and 10, page 787, were inadvertently interchanged.

Cable Design and Manufacture for the Transatlantic Submarine Cable System by A. W. Lebert, H. B. Fisher and M. C. Biskeborn, B.S.T.J., **36,** pp. 189–216. Table I, page 3, the material for type B armor wire should be medium steel instead of mild steel. Page 207, the equation for Z_0 should read

$$Z_0 = \frac{b}{\sqrt{\epsilon}} \log \frac{D}{b} \text{ ohms}$$

ERRATA

The Effects of Surface Treatments on Point Contact Transistor Characteristics by J. H. Forster and L. E. Miller, B.S.T.J., **35,** pp. 767–811, July, 1956. Figs. 3, page 776, and 10, page 787, were inadvertently interchanged.

Cable Design and Manufacture for the Transatlantic Submarine Cable System by A. W. Lebert, H. B. Fisher and M. C. Biskeborn, B.S.T.J., **36,** pp. 189–216. Table I, page 3, the material for type B armor wire should be medium steel instead of mild steel. Page 207, the equation for Z_0 should read

$$Z_0 = \frac{b}{\sqrt{\epsilon}} \log \frac{D}{b} \text{ ohms}$$

Reading Rates and the Information Rate of a Human Channel

By J. R. PIERCE and J. E. KARLIN

The limitation on the rate at which information can be transmitted over an ordinary telephone channel is a human one. In this study people read words as fast as they were able to; from these results some deductions are made about the capacity of a human being as an information channel. The discrepancy between human channel capacity measured thus (40–50 bits/sec) and telephone and television channel capacity (about 50,000 bits/sec and 50,000,000 bits/sec respectively) is provocative.

INTRODUCTION

In communication over an ordinary telephone channel, the limitation on the rate at which information can be transmitted appears to be a human one. For instance, by use of a vocoder, the required channel capacity can be reduced greatly with only a moderate reduction in the quality of the reproduced speech.[1]

It would be of great interest to measure the information rate necessary to provide a satisfactory sensory input to a human being. It is not clear how this could be done. Something which may be related and for which a lower bound can be measured is the capacity of a human being as an information channel.

An evaluation of and understanding of the limitations on the information rate of the human channel might ultimately be of practical importance for two reasons. First, it might help to tell us what sort of task to set a human being when he is necessarily a part of a system involving information transmission. Thus, a man can transmit information faster by reading than by tracking. Secondly, the understanding might somewhat illuminate the problem of the channel capacity necessary to provide a satisfactory sensory input, and so might help to reduce the channel capacity required in electrical communication between human beings.

Previous investigations indicate[2,3] that reading aloud attains the fastest rate at which a human being can be demonstrated to transmit

information, as contrasted with, for example, typing, playing the piano, or tracking.*

The work presented here, while undertaken independently, is in general similar to and in agreement with that reported for reading rate experiments by Licklider, Stevens and Hayes,[2] and by Quastler and Wulff.[3] However, we have considered some factors in more detail than these workers, and also, contrary to the former group, we find that, under optimal conditions, reading with tracking has a lower information rate than reading alone.

The chief problem investigated was:

(1) Taking people as they are, with no additional training, how fast, in bits per second, can they transmit information by reading?

(2) What principal factors control this limiting rate?

The experimental procedure consisted simply of people reading aloud as rapidly as they could typed lists of words. Each list was composed of a single vertical row of 12 groups of 5 words, giving a total of 60 words per page. In each instance, the words were chosen at random from a given vocabulary of words. If n is the number of words in the vocabulary and if the words are chosen with equal probabilities, and if all words are read correctly,† the amount of information which is conveyed or transmitted through the human being measured in bits is[4]

$$\log_2 n \text{ bits/word}$$

When the vocabulary for a particular experiment has much fewer than 60 words, certain words must necessarily be repeated several times within a list. When the vocabulary is much greater than 60 words, repetitions are necessarily few and differences in reading rate among different vocabularies would be expected only if the vocabularies differed in nature, as in syllable length or familiarity of words.

Unless otherwise specified, each result quoted below is the average reading speed for two lists for each of three readers, chosen as representing fast, medium and slow readers for people with at least a high school education. The results on these three readers are substantially similar to those on ten similar readers used in preliminary experiments. The chief experiments performed, and some interpretations of them, follow under numbered headings. Some supplementary experiments are then described briefly and the over-all results are commented on.

---

* Here tracking means successively pointing to a series of marks.

† In preliminary experiments the reader's voice was recorded, and it was found that errors in reading aloud occur very seldom if ever.

PRINCIPAL EXPERIMENTS

Experiment 1: Effect of Vocabulary Size

The larger the vocabulary size the higher the information rate conveyed by a given word reading rate. However, one might think that it would be possible to read randomized lists of, say, 4 words substantially faster than lists of 8, or 16 or more words.* How is the word rate affected as the vocabulary size increases?

To investigate vocabulary size as such, it is necessary as far as possible to avoid the influence of differences in word length or familiarity. To this end, words in each vocabulary were chosen at random from the 500 most common words in the language;[5] a few words were then changed so as to keep an average of 1.5 syllables/word for each vocabulary. Figs. 1(a) and 1(b) show parts of typical lists for vocabulary sizes of 2 and 256 words respectively. The order of reading the different size vocabularies was randomized.

Fig. 2 shows that *reading rate is essentially independent of vocabulary sizes from 4 to 256 words when familiarity and word length are kept fairly constant.* The reading rates for the three readers for the 256-word vocabulary are 3.8, 3.7 and 3.0 words/sec, giving information rates of 30, 30 and 24 bits/sec respectively.

The word rate for a 2-word vocabulary is systematically a little greater than for larger vocabularies. This effect, which is statistically significant, is best seen in Fig. 2 in the average curve (dashed). The writers feel on the basis of subjective impressions that this may result from a tendency to group words in pairs in recognizing and speaking them. Among 2 words there are only 4 ordered pairs. It is apparent from the data that no such effect is noted among the 16 ordered pairs occurring with the 4-word vocabulary.

The last point on the curves in Fig. 2 illustrates the importance of familiarity and word length. When words are taken at random from a 5,000-word dictionary (12.3 bits/word), the reading rates drop to 2.8, 2.7 and 2.1 words/sec, yielding information rates of 34, 33 and 26 bits/sec respectively, which are very close to the rates 30, 30, 24 for the 256-word vocabulary.

However, these dictionary lists involve some unfamiliar words and average 2.2 syllables/word.

---

* When the light is very dim, the reading rate is slowed, and is faster for small vocabularies than for large vocabularies. Reading tests were done at normal light levels, which are very much brighter than those at which a slowing due to inadequate illumination is observed.

Experiment 2: Effect of Word Length and Familiarity

It was not clear from Experiment 1 how much of the drop in word rate for the dictionary list was affected by decreased familiarity and how much by increased word length.

These two variables were then untangled in a separate experiment. Word lists were prepared which kept both length and familiarity relatively constant for a given list. The words were chosen from a list of the 20,000 most frequently encountered words in the language.[6] Reading rates were measured for the thousand most familiar words, for the ninth to tenth thousand most familiar, and for the nineteenth to twentieth thousand most familiar words.

The results are shown in Figs. 3(a), (b), and (c). There is considerable consistency among readers as to the relative effect of length and familiarity. The most familiar trisyllable words, for example, are read about as rapidly as the least familiar monosyllables.

A confirmatory demonstration of the effect of familiarity upon reading rate is shown in Fig. 4. This shows reading rates for randomized lists of eight nonsense words averaging 1.5 syllables/word (e.g., jevhin, tosp) which are necessarily totally unfamiliar when the reader first encounters them. As the reader becomes more familiar with the words on successive readings, his word rate increases until he approaches the rates of familiar words in Fig. 2.

Experiment 3: Preferred Vocabulary for Increasing Transmission Rate

The transmission rate is the product of the reading rate and the logarithm to the base 2 of the vocabulary size. To maximize the rate we

Fig. 1 — Parts of typical lists for vocabulary sizes.

grew	foot
action	tomorrow
grew	count
grew	issue
action	rain
action	month
grew	earth
grew	cook
action	build
action	corner
grew	yard
action	history
grew	forest
action	pleasant
grew	wrong
(a)	(b)
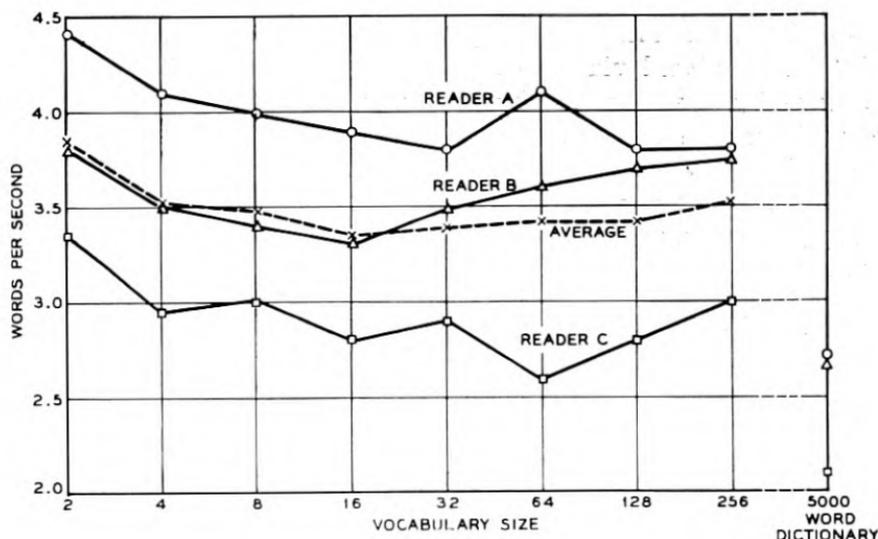
Fig. 2 — Reading rate is essentially independent of vocabulary sizes under certain conditions.

must make each of these factors large. As Fig. 3 indicates, reading speed tends to decrease as vocabulary size increases. From the data in Fig. 3, a rationale (shown in Appendix I) was developed for use in searching for an improved vocabulary which would maximize transmission rate. This indicated that the 2,500 most familiar monosyllables chosen with equal probability should form a very good vocabulary and one which is simple to construct and use. For a 2,500-word list we have 11.3 bits/ word.

Reading speeds for such preferred lists were 3.7, 3.4 and 3.0 words/sec, giving information transmission rates of 42, 39 and 34 bits/sec. Some data on the distribution of this rate found among Bell Telephone Laboratories employees is given in Fig. 5.

Experiment 4: Prose and Scrambled Prose

The experiments above were all with discrete words. Reading rates for non-technical prose* are appreciably higher — 4.8, 4.7 and 3.9 words/sec for the three readers. However, such prose has a good deal of redundancy. Shannon[7] arrives at a figure of around 1 bit/letter for a

---

* Extracts were taken from New York Herald Tribune, the novel "East River" by Sholem Asch, "Vermont Tradition" by Dorothy Canfield Fisher and the *Scientific American*. Such material was chosen as being of the same sort of prose as was used by Dewey[5] in his word counts from which Shannon[7] made his estimate of information content of printed English.

27-word alphabet including the space, or 5.5 bits/word for the average of 4.5 letters/word plus one space following a word. Newman and Gerstman[8] give a figure of 2 bits/letter. It is quite uncertain, however, what the true value may be. Table I compares the information rate for the preferred list with that for prose assuming 5 and 10 bits/word.

When words were taken at random from the same prose sources, the reading rates dropped to 3.7, 3.3 and 2.7 words/sec. These rates are about the same as for the preferred list.

The information content of scrambled prose can be estimated much more accurately than that for prose, since the correlations associated
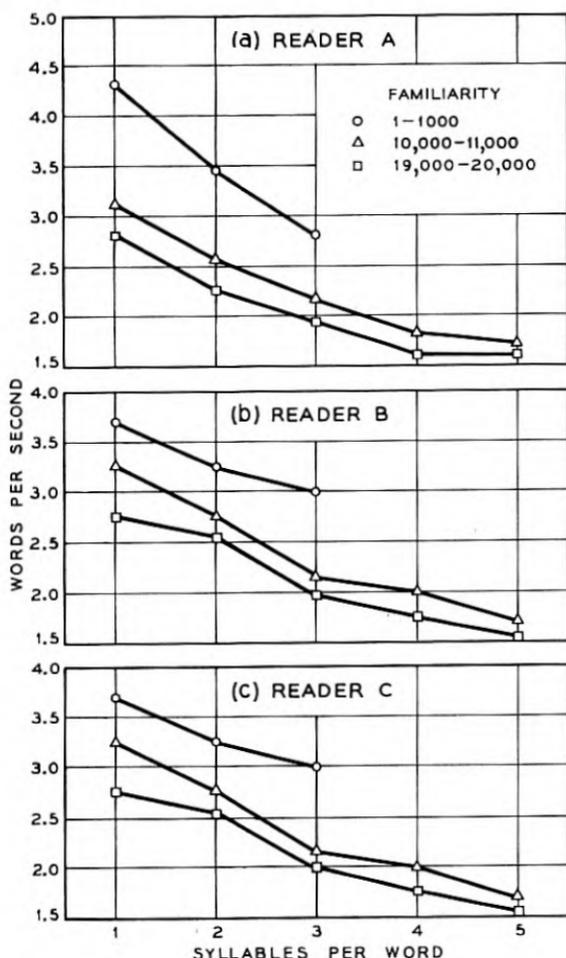
Fig. 3 — Effect of word length and familiarity.
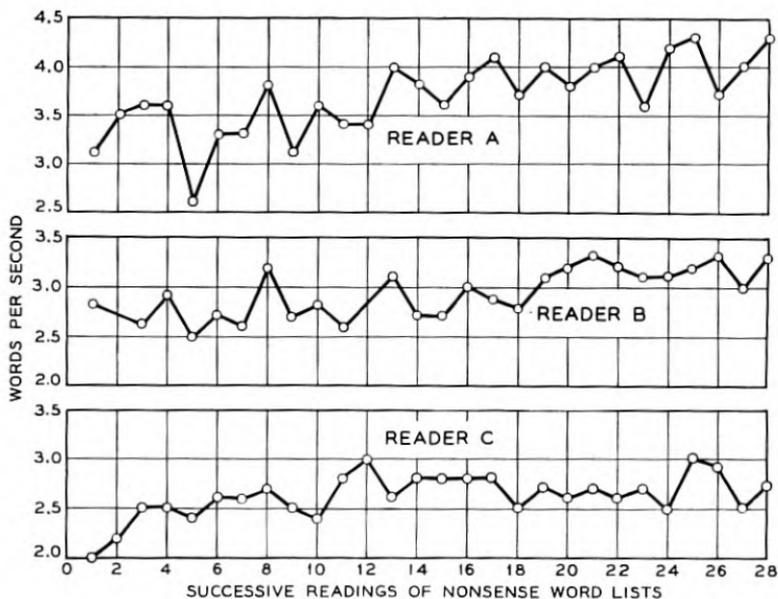
Fig. 4 — Confirmatory demonstration of the effect of familiarity upon reading rate.

with word order have been removed and the bits/word depend only on the frequency of occurrence of words in prose, which is known. Thus, Shannon[7] gives a figure of 11.82 bits/word which applies to scrambled prose, provided the prose has the same word frequencies as that from which the statistics were derived. The information rates for words from a 5,000-word dictionary (Experiment 1) for the preferred lists, and for scrambled prose are given in Table II.

The information rate for scrambled prose is less reliable than the others, because we are not sure that the word frequencies used by Shannon apply to the prose used by us, but we used the type of material cited by the reference he quotes. It is clear that the information rate for scrambled prose is high as compared with most other lists.

Table II shows the gain which may be made by fitting the task to the human being — in this case, by choosing a suitable word list. We may note that the gain appears greater in the case of reader A than in the case of reader B. This need not be experimental error. One would suppose that there are optimal lists for individuals. Indeed, if we compare Figs. 3(a) and 3(b) we see that for reader A the word rate for monosyllables drops by a factor 0.72 in going from the first thousand to the tenth thousand, while for reader B the drop is only a factor 0.88. This
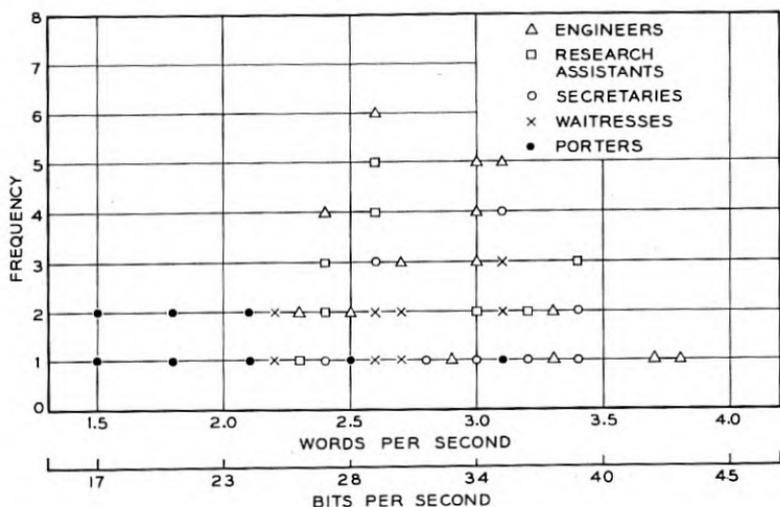
FIG. 5 — Distribution of reading rates for preferred vocabulary.

indicates that the optimal list would be somewhat different for reader A than for reader B. More extensive data would, however, be required to confirm this hypothesis.

Experiments not described here in detail showed that reading rates for digrams (successive pairs of words related as in English text) are intermediate between those for prose and discrete words.

Experiment 5: Effect of Multiple Channels

Licklider[1] has found that when the reader attempts simultaneously to perform a tracking operation while he is reading, his reading rate remains almost unimpaired, and the tracking information is added to that of reading alone. This two-channel transmission gave him his highest rate of transmission. We obtained the reverse finding. Reading the preferred list gave us our highest transmission rate. Simultaneous

TABLE I

Material	Information Rate (bits/sec)		
	A	B	C
Preferred list............................	42	39	34
Prose (5 bits/word)....................	24	23	19
Prose (10 bits/word)....................	48	47	39

TABLE II

Material	Information Rate (bits/sec)		
	A	B	C
5,000-word dictionary	33	33	26
Preferred list	42	39	34
Scrambled prose	43	39	32

reading and tracking gave a lower total transmission rate. However, Licklider and we agree on the magnitude of this maximum — between 40 and 45 bits/sec for facile test subjects.

Measurements on combined reading and tracking rates were made in Experiment 5 using words from the preferred lists. Whereas Licklider's readers made a dot within a box next to the word read, our readers placed a dot as close as possible to a vertical line next to the word read (e.g. dog |·). The computation of transmission rate is shown in Appendix II. The reading-while-tracking rates were 2.4, 2.0 and 1.4 words/ sec. The computed information rates are given in Table III.

It may be seen that the reading rate during tracking dropped so much that the two channels together give a total information rate less than those for reading the preferred list alone. Licklider's reading lists were words chosen randomly from a dictionary and are presumably not chosen optimally for maximum information rate — his information rates for reading alone were 30–35 bits/sec, as compared with the 32–43 bits/sec found here for the scrambled prose and preferred lists. However, if we assume that our reading-while-tracking rate, which is much slower than the reading rate for scrambled prose or for the preferred lists, is limited largely by tracking, we might have obtained a slightly higher information rate in reading-while-tracking by using a larger list of words. This is suggested by the fact that Licklider's and our experiments obtain about the same reading-while-tracking speeds.

TABLE III

	Information Rate (bits/sec)		
	A	B	C
Reading (while tracking)	26.6	22.1	15.4
Tracking (while reading)	10.7	11.0	11.7
Reading and Tracking	37.3	33.1	27.1
(Rates for same word list from Experiment 3 — reading only)	(42)	(39)	(34)

Experiment 6: Effect of Physiological Utterance Limitations

One of our best indications that the maximum reading rate of a subject is determined by mental rather than by physical limitations is that discrete word lists were read no faster silently than aloud. This may appear contrary to very high silent reading rates widely quoted. This can be explained by the fact that in reading much prose we do not and need not recognize every word in order to get the sense. Presumably, if an author made every word say something, his prose could not be read with understanding at such high rates.

We can also show in another way that the mere uttering of the words does not determine the reading speeds observed. A memorized prose phrase ("This is the time for all good men to come to the aid of their country") was repeated several times at rates of 7.5, 9.1 and 8.4 words/ sec for the three readers.

Fig. 6 compares word rates for repeating a phrase with the word rates previously discussed. The radically faster rate for repeating a phrase is not the only feature to be observed in this figure; the three readers are not in the same order of speed as is preserved through the reading experiments. This would suggest that it is word recognition rather than speaking speed which accounts for differences among the reading rates of different people.
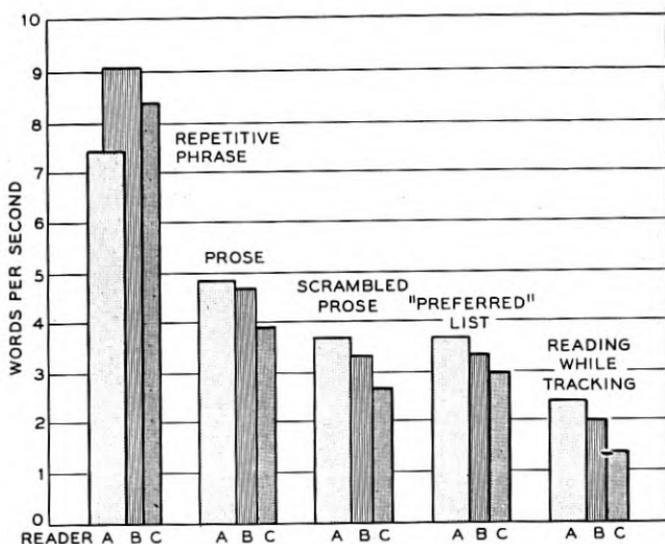
Fig. 6 — Effect of physiological utterance limitations.

DISCUSSION AND SUPPLEMENTARY EXPERIMENTS

Conclusions from Principal Experiments

The conclusions which can be reached with reasonable assurance from these experiments are rather narrow. They might be stated:

1. Information is best transmitted through a human channel by means of well-chosen acts (reading well chosen words in this case) involving many bits per act, that is, much choice per act. Cutting down drastically the bits per act does not substantially increase the speed at which the individual act is accomplished.

2. The lower bound of information transmission through the human channel of rapid readers seems to be about 43 bits/sec. This estimate is a little higher than that found by Licklider,[2] and may be close to a limiting rate.

3. This limiting rate can be achieved by the simple act of reading either randomized lists from suitably selected words or scrambled prose.

4. Both familiarity and length of words are important in determining reading speed. The relative effect of these two variables on reading speed is rather complex.

Beyond these narrow conclusions, there is much understanding yet to be achieved in the general field of the speed of human mental and physical responses and operations. Thus, it seems worth while to mention other experiments which were done in the course of the present investigation and experiments carried out by other workers, and to speculate somewhat concerning the whole of this experimental work.

Multiple Tasks

The reading-while-tracking experiments touch on an important problem. We have all heard of wireless operators who can receive and subsequently type out a message while carrying on a conversation or playing chess. There is nothing in this feat to indicate an information rate greater than that we have found. Actually, the rate of receiving prose by International Morse Code by ear is around 0.58 word/sec;[9] this is slow compared with the rates we have considered.

Our experiments with tracking followed experiments in which words in the lists were randomly printed in red or black, and in which the subject spoke red words in a louder tone of voice than black words, or pressed one key for red words and another for black words. In these cases, the added information, one bit per word, was so small as to make no clearly discernible difference in information rate for the large vo-

cabularies. The speed for reading loud and soft was less than for reading-while-keying. This may imply something about the relative efficiency of human beings performing two tasks by using two sets of muscles as against using one set in two different ways.

It is common experience that we can walk about and carry out other simple tasks while talking or thinking. It is possible though not obvious that some sort of automatic, almost purely reflexive response — as, moving the left hand when the right hand is touched — could with practice be carried out quite independently of a task such as reading. The information rate for such responses would be small, the experimental error would make it difficult to settle the question, and the interpretation of such an experiment would not be entirely clear.

The Patterns Which Govern Reading Time

Early in the experiments the question was raised whether readers may not read letter by letter or syllable by syllable. Several findings bear on this.

Fig. 3 shows clearly that the reading time for a two-syllable word is much less than twice the reading time for a one-syllable word.

One of us knows a negligible amount of German. German syllables are, however, reasonably familiar. It was found that in reading German aloud he had the same reading rate in syllables per second as a man whose native language was German had in words per second. The two readers had substantially the same reading speed in English. Presumably in reading German one man recognized syllables and the other recognized words. This also reinforces the conclusion that reading rate is not limited by the time taken to utter words.

Some experiments were done using lists of common Chinese characters and lists of the corresponding English words. Average word rates over three lists for two readers who could read both languages are given in Table IV. The slightly lower rate for English is plausibly explained by the fact that Chinese was the reader's native language. All words were

TABLE IV

Reader	Words/sec	
	Chinese Words	English Words
E	2.7	2.3
F	3.3	3.2
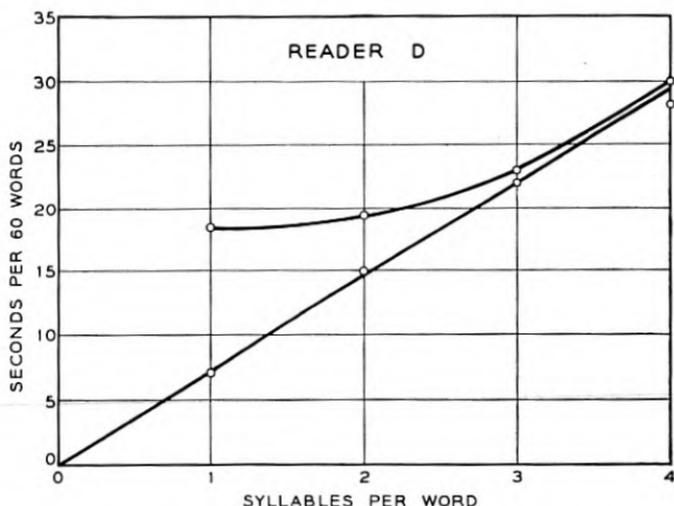
Fig. 7 — Patterns governing reading time.

necessarily monosyllables in Chinese and happened to be monosyllables in English.

In one case a word is made up of a sequence of letters, each standing for a sound, and in the other it is made up of a number of strokes which are meaningless individually, yet in each case a word is taken as a unit or pattern requiring nearly the same time for reading.

We found that the rate for reading arabic numerals is substantially the same as for reading familiar words. Each numeral is an individual pattern to be recognized.

In a first effort to find the effect of syllable length on reading rate, a subject read several lists made up respectively from vocabularies of 16 single-syllable, 16 two-syllable, 16 three-syllable, and 16 four-syllable words. None of the words was very unfamiliar to start with, and all were presumably very familiar after the subject had read several randomized lists composed of the same words.

The outcome of the experiment is shown in Fig. 7. For comparison, the points associated with the lower straight line are *time for 60 words* for repeating, as rapidly as possible, a one-, a two-, a three- and a four-syllable word. The points on the upper curve are reading time for 60 words for the randomized lists of the familiar one-, two-, three- and four-syllable words.

In dealing with such groups of highly and uniformly familiar words, it appears that, roughly, a certain time is required to recognize the word regardless of length, and this time governs the reading rate up to the

TABLE V

Reader	Words/sec		
	Scrambled Prose	Scrambled Paragraph	Prose
A	3.7	4.0	4.8
B	3.3	3.7	4.7
C	2.7	2.9	3.9

point at which the reader is uttering words continuously as fast as he can. This is consistent with a strong subjective feeling that what limits the rate is the difficulty of "recognizing" the word as one looks at it, and that once the word is recognized one can utter it while recognizing the next word.

It would of course be wrong to conclude from this experiment that multisyllable words are in general recognized as quickly as single syllable words, for it would be possible to recognize one among a known group of 16 multisyllable words without looking at the whole word. Indeed, Fig. 3 indicates a substantial difference of reading rate between one- and two-syllable words of like frequency of occurrence. This was not observed in reading the specially familiar lists of one- and two-syllable words.

Why is prose read faster than scrambled prose? It might be that some short phrases are recognized as individual patterns. However, there is another factor at work. A scrambled paragraph of prose is read slower than the same paragraph in its natural word order but faster than scrambled prose from a book or a long stretch of prose, as can be seen from Table V.

It should be noted that reading speed differs for different prose, and that when comparisons among prose, scrambled paragraphs and scrambled prose are made, similar material should be used.

The fact that a scrambled paragraph is read faster than scrambled prose might be explained by saying that we expect, we are more ready to recognize, words which are repetitions of earlier words or words which are closely related in sense to earlier words than we are unrelated words. Thus, the greater reading speed for prose than for scrambled prose seems to be due only in part if at all to the recognition of phrases rather than words as individual patterns.

Rate of Mental Processes

The rate at which information passes through a human channel in reading experiments is indisputable. Quastler[3] has attempted to go

beyond this and estimate information processing rates in the brain from the performance of lightning calculators, by dividing the performance of the calculation into a sequence of tasks equivalent to consulting memorized multiplication tables and performing additions. It is hard to interpret such a study clearly, for it is quite possible that there are many sorts of mental acts which take different times to perform, just as multiplication and addition take different times in an electronic computer. A tentative experiment we performed indicated something of the sort.

Randomized lists were made up from vocabularies (a) of names of common animals and vegetables in equal numbers, and (b) of common men's and women's names in equal numbers. In reading these, a subject was asked, not to read the word aloud, but merely to press one key with his right and another key with his left hand; in (a) left-animal, right-vegetable; in (b) left-man, right-woman. The same subject later read the lists aloud. Pressing keys took 40 per cent longer than reading aloud. (The additional time is not related to the keying operation itself; for a 2 word list, for example, keying speed is much faster than reading speed.) Presumably an additional mental operation was involved, but it was not one for which the time was equal to that for reading. This experiment was not pursued further, partly because no clear conclusion could be drawn from it. Had it been pursued and randomized lists of the same words used repeatedly, the rate might have gone up. Conceivably, cow and horse could become for a subject merely different ways of spelling left, and lettuce and carrot variant spellings of right. In this case we would end with a two-word reading experiment.

Reading Rate as a Psychometric Datum

It is interesting to speculate on the possible relationship of reading rate to general intelligence or some other aptitude. Certainly, Fig. 5 indicates some such relationship. We might also ask in connection with Fig. 3, does a rate which falls less rapidly with frequency of occurrence indicate a larger vocabulary, and can we measure vocabulary by reading speed tests? Certainly, measuring the speed of reading aloud is very simple, and such tests might have some psychometric utility.

The Channel Capacity Required for Satisfactory Communication

In conclusion, we cannot help but wonder that the highest information rate noted — 43 bits/second — is so much lower than the channel capacity* of a telephone or a television circuit (around 50 thousand

---

* This is the limiting channel capacity given by (2.1) of Appendix II. The practical rate at which binary digits can be sent over a telephone circuit with simple equipment is less than 1000 bits/second.

bits/second for telephone and 50 million bits/second for TV). This would not be surprising if the limitation we observe had been one of the speeds at which words can be uttered, but it appears rather to be a mental one, one of recognizing what is before the eyes. To the authors, it seems reasonable that this mental limitation may apply to a human being's ability to absorb information, that is, to the information rate needed to present a satisfactory sensory input to a human being. If it does, then why do we need so much channel capacity to convey to him an acceptable sound or picture?

This can be explained in part by the inefficiency of our present communication methods. Despite its present imperfections, the vocoder makes it clear that clearly understandable speech can be transmitted using far less channel capacity than that required in ordinary telephony.[1]

However, it is quite likely that even with the most efficient of encoding means we will have to use far more than 43 bits/second for a picture transmission channel. While only a portion of the image of the transmitted picture falls on the fovea at any instant, we can cast our eyes on any portion of the received picture. If the pick-up camera device and the received picture followed eye movements, a much less detailed picture would serve. Even with our eyes fixed, we can concentrate our attention on a particular part of our field of vision, and this is something that the pick-up camera cannot track. There may be similar effects in our apprehension of sounds.

In the light of present knowledge it is impossible to estimate the minimum channel capacity required to transmit sound and pictures in a satisfactory manner. It will take work far beyond the measurement of reading rates to enable us to make such an estimate.

APPENDIX I

ON OBTAINING GOOD VOCABULARIES

The experiments in the body of the paper indicate that the choice of a good vocabulary is important in attaining a high information rate in reading lists of words.

In these experiments the randomized lists may be regarded as an information source consisting of a sequence of code elements or symbols (words) in which there is no correlation between successive symbols. If in making up the lists the sth word of the vocabulary is used with a normalized probability p_s, the entropy in H in bits per word, and hence the amount of information per word, is

$$H = -\sum_s p_s \log_2 p_s \text{ bits} \tag{1.1}$$

If all words appear with an equal probability $1/m$ where m is the number of words in the vocabulary, as in the case of experiments 1–3, p_s is $1/m$ for each of the m words and in this special case

$$H = \log_2 m \tag{1.2}$$

In the case of scrambled prose, for instance, the probabilities are different for different words. This will be true also if in making up word lists we choose words randomly from a box containing different numbers of different words.

Let t_s be the time taken to read the sth word of the vocabulary. *Let us assume that t_s is the same for the sth word no matter what context that word appears in in the randomized list.* If this is so, the average reading time per word, t, will be

$$\bar{t} = \sum_s p_s t_s \tag{1.3}$$

the word rate will be $1/\bar{t}$, and the information rate R will be

$$R = \frac{H}{\bar{t}} = \frac{\sum_s p_s \log_2 p_s}{\sum_s p_s t_s} \tag{1.4}$$

Suppose we have available a vocabulary of words and know the reading time t_s for each word. The problem is to choose p_s in terms of t_s as to maximize R. This is easily done; however the result can also be obtained as a special case of the problem treated in Appendix 4 of "The Mathematical Theory of Communication."[4] In Shannon's $\ell_{ij}^{(s)}$, the subscripts i, j refer to passing from state i to state j. In our case there is only one state, and $\ell_{ij}^{(s)}$ should be identified with t_s for all i and j. Similarly, we identify $p_{ij}^{(s)}$ with p_s. C is the maximum rate, so $\log_2 W = C$. Shannon's equation

$$p_{ij}^{(s)} = \frac{B_j}{B_i} W^{-\ell_{ij}^{(s)}}$$

becomes

$$p_s = 2^{-Rt_s} \tag{1.5}$$

since there is only one B.

Shannon's determinantal equation

$$\left| \sum_s W^{-t_{ij}(s)} - S_{ij} \right| = 0$$

becomes

$$\sum 2^{-Rt_s} = 1 \tag{1.6}$$

In (1.5) and (1.6) we have a means of evaluating p_s in order to attain the maximum information rate R.

The data we actually have concerning words is that for some class s of words, say, the monosyllables in the 8,000–9,000 words in order of familiarity, the reading time has some value t_s, presumed to be the same for all words in the class, and that there are N_s words in this class. In this case we must assign to each word in the sth class the same probability p_s given by

$$p_s = 2^{-Rt_s} \tag{1.7}$$

and we must have

$$\sum_s N_s p_s = \sum_s N_s 2^{-Rt_s} = 1 \tag{1.8}$$

Using the same amount of data given in Fig. 3, for the 20,000 most common words, but for a different reader, estimates were made of N_s and t_s for all the classes consisting of words of each number of syllables in each range of occurrence of 1,000 words. Then the optimum values of p_s for words in each class and the maximum rate R were computed.

Using (1.4), rates were also computed for choosing words with equal probability from among the first m thousand words and from among the first m thousand monosyllables, as functions of m. These rates had

TABLE VI

Nature	Computed Rate, bits/sec
Maximum Rate...	33.5
Maximum for equi-probability monosyllables (from first 8,000 words)..	32.4
Maximum for equi-probability among words of all lengths (first 5,000 words)...	30.2

maxima for vocabularies of optimal sizes. Table VI compares the various rates computed.

As it is much easier to make up lists from the 2,500 monosyllables among the first 8,000 words with equal probabilities than it is to make up lists from among all words with a different probability for each class, and as the information rates computed were close together, the former alternative was chosen.

The use of scrambled prose provided an easy way to make up good lists.

Appendix II

TRACKING EXPERIMENT

A well-known formula for channel capacity R in bits/sec is[4]

$$R = B \log_2 \left(1 + \frac{P_s}{P_n} \right) \tag{2.1}$$

This gives the limiting rate at which information can be transmitted over a channel with a bandwidth B by a signal of power P_s, in the presence of a gaussian noise of power P_n, with an error rate smaller than any assignable number.

In most cases, the actual rate is much smaller than this limiting rate. In general, the rate is the entropy of the received signal minus the entropy of the noise. In the particular case of a gaussian signal source as well as a gaussian noise, each represented by 2B samples a second, the calculation based on entropies gives exactly (2.1). Let us then apply (2.1) to the tracking experiment.

Suppose that a large number N of samples do have a gaussian distribution of mean square amplitude $\overline{x^2}$. Suppose that we make an error d_n in reproducing the nth sample, that these errors are gaussian, and that the mean square error is $\overline{d^2}$

$$\overline{d^2} = \frac{1}{N} \sum_n \overline{d_n^2}$$

We see from (2.1) that ideally we can use these reproduced samples to transmit M bits of information where

$$M = \frac{N}{2} \log_2 \left(1 + \frac{\overline{x^2}}{\overline{d^2}} \right) \tag{2.2}$$

In the reading and tracking experiments, randomized words from the 2,500 commonest monosyllables were arranged with equal vertical

spacings but with various horizontal positions. To the right of each word was a short vertical line. The distances x_n of these lines from the vertical centerline of the paper were obtained from a list of random numbers with a gaussian distribution such that for the list $\overline{x^2} = 1$ inch. Of course, $\overline{x^2}$ for each list would depart from this value. As the words were read, the reader used a pencil to make a dot as near as possible to the corresponding vertical line. For each sheet, the departures d_n from the vertical lines in inches were measured and $\overline{d^2}$ was computed. The number of bits M for pointing for that sheet were then taken as

$$ M = \frac{N}{2} \log_2 \left(1 + \frac{1}{\overline{d^2}} \right) \tag{2.3} $$

REFERENCES

1. E. E. David, Naturalness and Distortion in Speech Processing Devices, Jour. Acoustical Soc. Am., July, 1956.
2. J. C. R. Licklider, K. N. Stevens, J. R. M. Hayes, Studies in Speech, Hearing and Communication, Technical Report, Acoustics Laboratory, MIT, Sept. 30, 1954.
3. H. Quastler et al, Human Performance in Information Transmission, Report No. R-62, Control Systems Laboratory, University of Illinois, March, 1955.
4. C. E. Shannon and W. Weaver, The Mathematical Theory of Communication, University of Illinois Press, 1949.
5. G. Dewey, Relative Frequency of English Speech Sounds, Harvard University Press, 1923.
6. E. L. Thorndike, A Teacher's Word Book of the Twenty Thousand Words Found Most Frequently, Teachers College, Columbia University, 1932.
7. C. E. Shannon, Prediction and Entropy of Printed English, B.S.T.J., 30, pp. 50–64, Jan., 1951.
8. E. B. Newman and C. J. Gerstman, A New Method for Analyzing Printed English, J. Exp. Psychol., 44, pp. 114–125, 1952.
9. Keith Henney, Radio Engineers Handbook, 3rd Ed., p. 568, McGraw-Hill, 1941.

Binary Block Coding

By S. P. LLOYD

From the work of Shannon one knows that it is possible to signal over an error-making binary channel with arbitrarily small probability of error in the delivered information. The effects of errors produced in the channel are to be eliminated, according to Shannon, by using an error correcting code. Shannon's proof that such codes exist does not provide a practical scheme for constructing them, however, and the explicit construction and study of such codes is of considerable interest.

Particularly simple codes in concept are the ones called here close packed *strictly e-error-correcting (the terminology is explained later). It is shown that for such a code to exist, not only must a condition due to Hamming be satisfied, but also another condition. The main result may be put as follows: a close-packed strictly e-error-correcting code on n, n > e, places cannot exist unless e of the coefficient vanish in* $(1 + x)^e(1 - x)^{n-1-e}$ *when this is expanded as a polynomial in x.*

I. INTRODUCTION

In this paper we investigate a certain problem in combinatorial analysis which arises in the theory of error correcting coding. A development of coding theory is to be found in the papers of Hamming[1] and Shannon[2]; this section is intended primarily as a presentation of the terminology used in subsequent sections.

We take (0, 1) as the range of binary variables. By an *n-word* we mean a sequence of n symbols, each of which is 0 or 1. We call the individual symbols of an *n*-word the *letters* of the *n*-word. We denote by B_n the set consisting of all the 2^n possible distinct *n*-words. The set B_n may be mapped onto the vertices of an *n*-dimensional cube, in the usual way, by regarding an *n*-word as an *n*-dimensional Cartesian coordinate expression. The *distance* $d(u, v)$ between *n*-words u and v is defined to be the number of places in which the letters of u and v differ; on the *n*-cube, this is seen to be the smallest number of edges in paths along edges between the vertices corresponding to u and v. The *weight* of an *n*-word u

is the number of 1's in the sequence u; it is the distance between u and the n-word $00\cdots0$, all of whose letters are 0.*

A *binary block code of size K on n places* is a class of K nonempty disjoint subsets of B_n where in each of the K sets a single n-word is chosen as the *code word* of the set.† Each such set is the *detection region* of the code word it contains, and we shall say that any n-word which falls in a detection region *belongs to* the code word of the detection region. The set consisting of those n-words which do not lie in any detection region we call *limbo*.‡ A *close packed* code is one for which limbo is an empty set; i.e., a code in which the detection regions constitute a partition (disjoint covering) of B_n.

A *sphere* of radius r centered at n-word u is the set $[v:d(u, v) \leqq r]$ of n-words v which differ from u in r or fewer places. A binary block code is *e-error-correcting* if each detection region includes the sphere of radius e centered at the code word of the detection region. We say that a binary block code is *strictly e-error-correcting* if each detection region is exactly the sphere of radius e centered at the code word of the detection region.

This paper is devoted to the consideration of close packed strictly e-error-correcting binary block codes. We shall refer to such a code as an *e-code*, for brevity. Hamming[1] observes that a necessary condition for the existence of an e-code on n places is that

$$1 + n + \frac{1}{2}n(n-1) + \cdots + \binom{n}{e} \tag{1}$$

be a divisor of 2^n. In this paper we derive an additional necessary condition. Our condition includes as a special case a condition of Golay[4] for the existence of e-codes of group type, and applies to all e-codes, whether or not they are equivalent to group codes.§

---

* If B_n is regarded as a subset of the real linear vector space consisting of all sequences $\alpha = (\alpha_1, \alpha_2, \cdots, \alpha_n)$ of n real numbers, then the "weight" of an n-word is simply the ℓ_1 norm (defined as $\| \alpha \|_1 = \sum_1^n |\alpha_n|$), and our "distance" is the metric derived from this norm.

† The term "block code", due to P. Elias, serves to distinguish the codes of fixed length considered here from the codes of unbounded delay introduced by Elias, Reference 3.

‡ In a communications system[2] using such a code, the transmitter sends only code words. If, due to errors in handling binary symbols, the receiver delivers itself of an n-word other than a code word then: (a) if the n-word lies in a detection region, one assumes that the code word of the detection region was intended; (b) if the n-word lies in limbo, one makes a note to the effect that errors have occurred in handling the word but that one is not attempting to guess what they were.

§ The terms "group alphabet" (Slepian[5]), "systematic code" (Hamming[1]), "symbol code" (Golay[4]), "check symbol code" (Elias[3]), "parity check code", are roughly synonymous. More precisely, a group code is a parity check code in which all of the parity check forms are homogeneous ("even"), so that $00\cdots0$ is one of the code words; see Reference 5.

II. DISTRIBUTION OF CODE WORDS

Suppose an e-code on n places is given. Let us inquire as to the distribution of weights of code words. We denote by ν_s the number of code words of weight s, $0 \leqq s \leqq n$, and by

$$G(x) = \sum_{s=0}^{n} \nu_s x^s \tag{2}$$

the generating function for these numbers, with x a complex but otherwise free variable. We show in this section that $G(x)$ satisfies a certain inhomogeneous linear differential equation of order e.

If there exists an e-code on n places then this differential equation will have $G(x)$ as a *polynomial* solution; the necessary condition for the existence of an e-code on n places given in Section 4 is essentially a restatement of this fact.* First, however, we must derive the differential equation and obtain its solutions.

If w_α is a code word of the given e-code $(1 \leqq \alpha \leqq K)$, define the set of j-*neighbors of* w_α as the set of n-words which lie at distance exactly j from w_α; designate this set by $S_j(w_\alpha)$. $(S_0(w_\alpha)$ is the set whose only element is w_α itself.) Our derivation is based on the observation that, in an e-code on n places,

$$\bigcup_{\alpha=1}^{K} \bigcup_{j=0}^{e} S_j(w_\alpha) = B_n \; \dagger \tag{3}$$

is a partition of B_n. For, the detection regions:

$$\bigcup_{j=0}^{e} S_j(w_\alpha), \qquad 1 \leqq \alpha \leqq K$$

are disjoint, and in each such sum representing a detection region the summands are disjoint (the distance function being single valued). Furthermore, each n-word of B_n lies in some detection region (close packed property) and hence appears in one of the sets $S_j(w_\alpha)$ for some α and for some j satisfying $0 \leqq j \leqq e$.

The set

$$\bigcup_{\alpha=1}^{K} S_j(w_\alpha)$$

---

* The author is not yet able to demonstrate the converse. That is, suppose one obtains a polynomial solution $G(x)$ of (11), below, satisfying appropriate boundary conditions, and from it some coefficients ν_s, $0 \leqq s \leqq n$. It does not follow from the methods of this article that there is actually some e-code on n places for which these ν_s represent the number of code words of weight s.

$\dagger \; \bigcup = $ set union.

consists of the n-words which are j-neighbors of some (not specified) code word; let us refer to these n-words simply as j-*neighbors*. Denote by $\nu_{j,s}$ the number of j-neighbors which are of weight s (with $\nu_{0,s} = \nu_s$, as above). Applying (3) to the n-words of weight s, we see that

$$\nu_s + \nu_{1,s} + \cdots + \nu_{e,s} = \binom{n}{s}, \qquad 0 \leqq s \leqq n \qquad (4)$$

is the total number of n-words of weight s. If we multiply (4) by x^s and sum on s, we have

$$G(x) + G_1(x) + \cdots + G_e(x) = (1 + x)^n \qquad (5)$$

where

$$G_j(x) = \sum_{s=0}^{n} \nu_{j,s} x^s \qquad (6)$$

is the generating function (with respect to s) for the numbers $\nu_{j,s}$.

We now express $G_j(x)$, $0 \leqq j \leqq e$, in terms of $G(x)$. Suppose code word w is of weight s; that is, w consists of s ones and $n - s$ zeros in some order. A j-neighbor of w is obtained by choosing j places out of n and changing the letters of w in these places, 0's to 1's and 1's to 0's. If, in this procedure, q of the 1's of w are changed to 0's, so that $j - q$ of the 0's are changed to 1's, then the resulting j-neighbor of w is of weight $s - q + (j - q)$. Now, there are $\binom{s}{q}$ ways of choosing q places among the s where the letters of w are 1, and there are independently $\binom{n - s}{j - q}$ ways of choosing $j - q$ places among the $n - s$ where the letters of w are 0. Thus, of the $\binom{n}{j}$ different j-neighbors of w, the number $\binom{s}{q}\binom{n - s}{j - q}$ are of weight $s + j - 2q$. We may regard each of these as contributing $1 \cdot x^{s+j-2q}$ to the generating function $G_j(x)$ of (6) (provided $0 \leqq j \leqq e$, so that there is no overlap); hence, summing over all j-neighbors of a code word and then over all code words,

$$G_j(x) = \sum_{s=0}^{n} \nu_s \sum_{q=0}^{\infty} \binom{s}{q}\binom{n - s}{j - q} x^{s+j-2q} \qquad 0 \leqq j \leqq e * \qquad (7)$$

From the easily verified polynomial identity

$$(x + y)^s (1 + xy)^{n-s} = \sum_{j=0}^{\infty} y^j \sum_{q=0}^{\infty} \binom{s}{q}\binom{n - s}{j - q} x^{s+j-2q}$$

---

* The limits $(0, \infty)$ on the q summation are merely for convenience; the binomial coefficients vanish outside the proper range, under the usual convention.

$(n, s$ integers, $0 \leqq s \leqq n)$ it follows that

$$\sum_{q=0}^{\infty} \binom{s}{q}\binom{n-s}{j-q} x^{s+j-2q} = \frac{1}{2\pi i} \int_C \frac{(x+y)^s (1+xy)^{n-s}}{y^{j+1}} \, dy$$

where contour C is, say, a small circle around the origin, taken positively. Thus

$$\begin{aligned} G_j(x) &= \sum_{s=0}^{n} \frac{\nu_s}{2\pi i} \int_C \frac{(x+y)^s (1+xy)^{n-s}}{y^{j+1}} \, dy \\ &= \frac{1}{2\pi i} \int_C \frac{(1+xy)^n}{y^{j+1}} G\left(\frac{x+y}{1+xy}\right) dy \\ &\equiv L_j G(x) \end{aligned} \qquad (8)$$

where the operator L_j is thus defined. Change of integration variable gives

$$\begin{aligned} L_j G(x) &= \frac{(1-x^2)^{n+1}}{2\pi i} \int_{C_x} \frac{G(z) \, dz}{(1-xz)^{n-j+1}(z-x)^{j+1}} \\ &= \frac{(1-x^2)^{n+1}}{j!} \frac{\partial^j}{\partial z^j} \frac{G(z)}{(1-xz)^{n-j+1}} \bigg|_{z=x} \\ &= \sum_{p=0}^{j} \binom{n-p}{j-p} \frac{x^{j-p}(1-x^2)^p}{p!} \frac{d^p G(x)}{dx^p} \end{aligned} \qquad (9)$$

(with C_x a small circle enclosing x but not x^{-1}, $x^2 \neq 1$). Thus L_j may be regarded as a linear differential operator of order j, $(L_0 \equiv 1)$.

Using this result, (5) may be given the form

$$\begin{aligned} (1+x)^n &= [L_0 + L_1 + \cdots + L_e]G(x) \\ &= \frac{1}{2\pi i} \int_C \frac{y^{-e-1} - 1}{1-y} (1+xy)^n G\left(\frac{x+y}{1+xy}\right) dy \\ &\equiv M G(x) \end{aligned} \qquad (10)$$

this last expression as a definition of operator M. Written as a differential equation, (10) is

$$\sum_{p=0}^{e} \frac{(1-x^2)^p}{p!} \sum_{r=0}^{e-p} \binom{n-p}{r} x^r \frac{d^p G(x)}{dx^p} = (1+x)^n \qquad (11)$$

It is straightforward that the only singularities of this equation are regular singularities[6] at $x = \pm 1$, ∞.

III. THE DIFFERENTIAL EQUATION

In this section we discuss (11) without reference to the fact that $G(x)$ is supposed to be a generating function. That is to say, with n and e

fixed but arbitrary non-negative integers, we denote by

$$G(x) = \sum_{s=0}^{\infty} \nu_s x^s \tag{12}$$

any solution of (11) regular in the unit circle.

It proves convenient to introduce certain functions $f_{n,\xi}(x)$ defined by

$$f_{n,\xi}(x) \equiv (1 + x)^{\xi}(1 - x)^{n-\xi}$$
$$= \sum_{s=0}^{\infty} \varphi_s(n, \xi)x^s \tag{13}$$

where the coefficients $\varphi_s(n, \xi)$ are given by

$$\varphi_s(n, \xi) = \sum_{r=0}^{s} (-1)^r \binom{n - \xi}{r}\binom{\xi}{s - r} \tag{14}$$

Here, ξ is to be regarded as a free complex variable. By $(1 + x)^{\xi}(1 - x)^{n-\xi}$ we mean exp $(\xi \log (1 + x) + (n - \xi) \log (1 - x))$, each logarithm vanishing at $x = 0$. As a function of x this function is single valued in, say, the x-plane cut on $(-\infty, -1]$ and $[1, \infty)$, and the series (13) converges to it in: $|x| < 1$.

Binomial coefficients are defined by

$$\binom{\zeta}{s} \equiv \frac{\Gamma(\zeta + 1)}{s!\Gamma(\zeta + 1 - s)}$$
$$= \frac{\zeta(\zeta - 1) \cdots (\zeta - s + 1)}{s!} \qquad s > 0$$

when ζ is not an integer, and $\varphi_s(n, \xi)$ is seen to be a polynomial in ξ of degree s:

$$\varphi_s(n, \xi) = \frac{2^s}{s!} \xi^s + \cdots + (-1)^s \binom{n}{s} \tag{15}$$

The recurrence relation

$$\varphi_0(n, \xi) + \varphi_1(n, \xi) + \cdots + \varphi_s(n, \xi) = \varphi_s(n - 1, \xi) \tag{16}$$

obtained by expanding the various factors [ ] in the identity

$$[(1 + x)^{\xi}(1 - x)^{n-\xi}][(1 - x)^{-1}] = [(1 + x)^{\xi}(1 - x)^{n-1-\xi}]$$

is an important one. We note also for reference that

$$\varphi_0(n, \xi) = 1$$
$$\varphi_s(n, n - \xi) = (-1)^s \varphi_s(n, \xi)$$
$$\varphi_s(n, n) = \binom{n}{s} \tag{17}$$
$$\varphi_s(n - 1, n) = 1 + \binom{n}{1} + \cdots + \binom{n}{s}$$

valid for all n, ξ and non-negative integers s. We see, by the way, that $\varphi_e(n - 1, n)$ is simply the Hamming expression (1).

The function $f_{n,\xi}(x)$ has the property that

$$f_{n,\xi}\left(\frac{x + y}{1 + xy}\right) = \frac{f_{n,\xi}(x)f_{n,\xi}(y)}{(1 + xy)^n} \tag{18}$$

at least if, say, given x, $|y|$ is small enough. From this and (8) for the operator L_j it is apparent that

$$L_j f_{n,\xi}(x) = \varphi_j(n, \xi)f_{n,\xi}(x) \tag{19}$$

Similarly, using (19) and (16), or directly from (10) for the operator M,

$$Mf_{n,\xi}(x) = [L_0 + L_1 + \cdots + L_e]f_{n,\xi}(x)$$
$$= \varphi_e(n - 1, \xi)f_{n,\xi}(x) \tag{20}$$

If ξ_β is one of the roots of the polynomial $\varphi_e(n - 1, \xi)$ then (20) becomes

$$M(1 + x)^{\xi_\beta}(1 - x)^{n-\xi_\beta} = 0$$

If we assume for the moment for simplicity that $\varphi_e(n - 1, \xi)$ has e *distinct* roots ξ_β, $1 \leqq \beta \leqq e$, then (11) has as complementary function

$$\sum_{\beta=1}^{e} A_\beta(1 + x)^{\xi_\beta}(1 - x)^{n-\xi_\beta}$$

where the A_β are e arbitrary constants.

Fortunately, the function $(1 + x)^n = f_{n,n}(x)$ is also a member of the family (13); hence

$$M(1 + x)^n = \varphi_e(n - 1, n)(1 + x)^n$$

and the function

$$\frac{(1 + x)^n}{\varphi_e(n - 1, n)}$$

is a particular integral of (11). [We see from (17) that $\varphi_e(n - 1, n)$ does not vanish in cases of interest.] Finally, when the roots of $\varphi_e(n - 1, \xi)$ are distinct, the general solution of (11) must be of the form

$$G(x) = \frac{(1 + x)^n}{\varphi_e(n - 1, n)} + \sum_{\beta=1}^{e} A_\beta(1 + x)^{\xi_\beta}(1 - x)^{n-\xi_\beta} \tag{21}$$

If $\varphi_e(n - 1, \xi)$ has multiple roots then the general solution will contain additional terms

$$(\text{const.}) (1 + x)^{\xi_\beta}(1 - x)^{n-\xi_\beta}\left[\log \frac{1 + x}{1 - x}\right]^\mu \tag{22}$$

i.e., the μth derivative of $f_{n,\xi}(x)$ with respect to ξ, with μ any positive integer less than the multiplicity of root ξ_β.

Before applying these results to e-codes in detail, let us derive a certain modification of (21). First, we see from (17) that if n is a positive integer, then n is not one of the roots of $\varphi_e(n - 1, \xi)$. If the roots ξ_β of $\varphi_e(n - 1, \xi)$ are distinct and if A_β, $1 \leqq \beta \leqq e$, are any e numbers then a polynomial $\theta(\xi)$ of formal degree e is uniquely determined by the $e + 1$ conditions:

$$\theta(\xi_\beta) = (\xi_\beta - n)\varphi_e'(n - 1, \xi_\beta)A_\beta, \qquad\qquad 1 \leqq \beta \leqq e,^* \tag{23}$$
$$\theta(n) = 1$$

using, e.g., the Lagrange interpolation formula. It is obvious that $G(x)$, (21), may be expressed in terms of this polynomial as

$$G(x) = \frac{1}{2\pi i} \int_\Gamma \frac{(1 + x)^\xi(1 - x)^{n-\xi}\theta(\xi)}{(\xi - n)\varphi_e(n - 1, \xi)}\, d\xi \tag{24}$$

where Γ is any simple closed contour surrounding the roots: n, ξ_1, ξ_2, $\cdots$, ξ_e of the denominator of the integrand; (the numerator is an entire function of ξ provided $x^2 \neq 1$).

Analysis a little more detailed shows that even if $\varphi_e(n - 1, \xi)$ has multiple roots the general solution of (11) can be represented in the form (24), again with $\theta(\xi)$ any polynomial of formal degree e such that $\theta(n) = 1$. The e constants of integration appear as the $e + 1$ parameters of $\theta(\xi)$ restricted by $\theta(n) = 1$.[†]

Expansion of the integrand in (24) according to (13) yields the form

$$\nu_s = \frac{1}{2\pi i} \int_\Gamma \frac{\varphi_s(n, \xi)\theta(\xi)}{(\xi - n)\varphi_e(n - 1, \xi)}\, d\xi \qquad s = 0, 1, 2, \cdots \tag{25}$$

for the coefficients of $G(x)$, (12).

If we denote by

$$L_j G(x) \equiv G_j(x) = \sum_{s=0}^{\infty} \nu_{j,s} x^s \tag{26}$$

the result of applying the operator L_j to any solution (24) of (11), then it is straightforward that

$$G_j(x) = \frac{1}{2\pi i} \int_\Gamma \frac{(1 + x)^\xi(1 - x)^{n-\xi}\varphi_j(n, \xi)\theta(\xi)}{(\xi - n)\varphi_e(n - 1, \xi)}\, d\xi, \tag{27}$$

---

* The prime denotes differentiation with respect to ξ.

† If $G(x)$ of (24) is to satisfy (11) it is sufficient that $\theta(\xi)$ be any function regular within (and on) Γ and that $\theta(n) = 1$, as may be easily verified. Since $G(x)$ depends on $\theta(\xi)$ only by way of the values of $\theta(\xi)$ at the zeros of the denominator in (24), the condition that $\theta(\xi)$ be a polynomial of formal degree e serves merely to determine $\theta(\xi)$ uniquely for a given solution $G(x)$.

and that

$$\nu_{j,s} = \frac{1}{2\pi i} \int_\Gamma \frac{\varphi_s(n, \xi)\varphi_j(n, \xi)\theta(\xi)}{(\xi - n)\varphi_e(n - 1, \xi)} \, d\xi, \qquad s = 0, 1, \cdots \qquad (28)$$

(An interesting reciprocity $\nu_{j,s} = \nu_{s,j}$ is apparent from (28). In an e-code one has (number of j-neighbors of weight s) = (number of s-neighbors of weight j) only for $0 \leq s, j \leq e$, since $L_j G(x)$ is the generating function for j-neighbors only if $0 \leq j \leq e$.)

IV. BOUNDARY CONDITIONS

The coefficients ν_s, (25), of any solution of (11) satisfy the relation:

$$\nu_0 + \nu_1 + \cdots + \nu_e = \frac{1}{2\pi i} \int_\Gamma \frac{\theta(\xi)}{\xi - n} \, d\xi = 1 \qquad (29)$$

by virtue of (16) and the normalizing condition $\theta(n) = 1$.

With γ an integer such that $0 \leq \gamma \leq e$, denote by

$$G^{(\gamma)}(x) = \sum_{s=0}^{\infty} \nu_s^{(\gamma)} x^s \qquad (30)$$

a solution of (11) which satisfies the e boundary conditions

$$\begin{aligned} \nu_0^{(\gamma)} &= \nu_1^{(\gamma)} = \cdots = \nu_{\gamma-1}^{(\gamma)} = 0 \\ \nu_{\gamma+1}^{(\gamma)} &= \nu_{\gamma+2}^{(\gamma)} = \cdots = \nu_e^{(\gamma)} = 0 \end{aligned} \qquad (31)$$

We must have $\nu_\gamma^{(\gamma)} = 1$ in such a solution, from (29). Thus the conditions (31) are equivalent to specifying the values of $G^{(\gamma)}(x)$ and its first $e - 1$ derivatives at the ordinary point $x = 0$ of (11), so that such a solution $G^{(\gamma)}(x)$ exists and is uniquely determined.[6]

Given an e-code on n places, each n-word of B_n lies at distance e or less from exactly one code word; namely, the code word to which it belongs. In particular, the n-word $00\cdots0$ must lie at distance e or less from a single code word. That is to say, there is exactly one code word in the sphere of radius e centered at $00\cdots0$. If this code word is of weight γ, then the generating function for the given e-code can be none other than the solution $G^{(\gamma)}(x)$ of (11) defined in the preceding paragraph.

If there exists an e-code on n places in which the code word of least weight is of weight γ, then there can be derived from it an e-code on n places in which the code word of least weight is of weight γ', where γ' is any integer satisfying $0 \leq \gamma' \leq e$. The transformation is that of choosing certain places among n and then changing the letters of each n-word of B_n in these places, 0's to 1's and 1's to 0's. (Such a transformation

corresponds to one of the operations of the orthogonal group which leaves invariant the n-cube representing B_n .) Metric properties in B_n are invariant under such a transformation, clearly, and an e-code is transformed into an e-code. Thus if there exists any e-code on n places then (11) must have $e + 1$ distinct polynomial solutions $G^{(\gamma)}(x)$, satisfying boundary conditions (31) for each case $\gamma = 0, 1, \cdots, e$.

In (25) for the coefficients ν_s , move contour Γ out to a circle sufficiently large that the expansion

$$\frac{1}{(\xi - n)\varphi_e(n - 1, \xi)} = \frac{e!}{2^e\xi^{e+1}} + \frac{(\text{const.})}{\xi^{e+2}} + \cdots$$

converges on Γ. Suppose that the polynomial $\theta(\xi)$, of formal degree e, is of actual degree f: $\theta(\xi) = c\xi^f + 0(\xi^{f-1})$, $c \neq 0$, where $0 \leq f \leq e$. Then the numerator of the integrand in (25) is of the form: $(2^s c\xi^{s+f}/s!) + 0(\xi^{s+f-1})$, and it is clear that

$$\nu_s = 0 \qquad 0 \leq s \leq e - f - 1$$

$$\nu_{e-f} = \frac{e!c}{2^f(e - f)!} \neq 0$$

Hence, if $\theta^{(\gamma)}(\xi)$ denotes the polynomial which gives $G^{(\gamma)}(x)$ in the representation (24), then $\theta^{(\gamma)}(\xi)$ must be of actual degree $e - \gamma$.

A particularly simple case is the one $\gamma = e$; the polynomial $\theta^{(e)}(\xi)$ must be of degree zero, and is determined by the normalization as $\theta^{(e)}(\xi) \equiv 1$. Thus

$$G^{(e)}(x) = \frac{1}{2\pi i} \int_\Gamma \frac{(1 + x)^\xi(1 - x)^{n-\xi}}{(\xi - n)\varphi_e(n - 1, \xi)} d\xi \qquad (32)$$

From this we have immediately the following

Theorem: If there exists an e-code on n places then the equation $\varphi_e(n - 1, \xi) = 0$ in ξ has e distinct integer roots.

Proof: If there exists an e-code on n places, then there exists an e-code on n places in which the code word of least weight is of weight e. The solution (32) of (11) must be the generating function for this e-code; hence (32) must reduce to a polynomial of formal degree n. If $\varphi_e(n - 1, \xi)$ had multiple roots then noncancelling logarithmic terms (22) would appear in the $G^{(e)}(x)$ of (32). Thus $\varphi_e(n - 1, \xi)$ must have e distinct roots ξ_β, $1 \leq \beta \leq e$. Each solution $(1 + x)^{\xi_\beta}(1 - x)^{n-\xi_\beta}$ of the homogeneous equation appears in $G^{(e)}(x)$ with nonvanishing coefficient:

$$A_\beta = \frac{1}{(\xi_\beta - n)\varphi_e'(n - 1, \xi_\beta)}$$

Since $G^{(e)}(x)$ must be a polynomial in x, it must be expressible as a polynomial in $1 + x$; hence each root ξ_β must be an integer.* (It is not necessary to require further that $0 \leqq \xi_\beta \leqq n$, since it follows easily from (14) that any real root of $\varphi_e(n - 1, \xi)$ satisfies $0 \leqq \xi_\beta \leqq n - 1$ provided n and e are integers such that $0 \leqq e \leqq n$.)

As a corollary we have that if e is odd then n must be odd. This follows from the theorem and the fact that $\frac{1}{2}(n - 1)$ is a root of $\varphi_e(n - 1, \xi)$ when e is odd, from (17).

We consider next the case $\gamma = 0$. If $00\cdots0$ is a code word, then its e-neighbors are the n-words of weight e. Furthermore, the n-words of weight less than e belong to the code word $00\cdots0$, and can be e-neighbors neither of $00\cdots0$ nor of any other code word. Hence it must be true that

$$G_e^{(0)}(x) = \binom{n}{e} x^e + 0(x^{e+1}) \tag{33}$$

With $G_e^{(0)}(x)$ represented in the form (27), divide the factor $\varphi_e(n, \xi)\theta^{(0)}(\xi)$ in the numerator by the denominator; the result will be

$$\varphi_e(n, \xi)\theta^{(0)}(\xi) = [(\xi - n)\varphi_e(n - 1, \xi)]q(\xi) + r(\xi) \tag{34}$$

with quotient $q(\xi)$ a polynomial of degree $e - 1$ and remainder $r(\xi)$ a polynomial of formal degree e. The term involving $q(\xi)$ obviously contributes nothing to $G_e^{(0)}(x)$ in (27), so that from (33) and arguments similar to those giving $G^{(e)}(x)$, above, $r(\xi)$ must be the constant

$$r(\xi) = \binom{n}{e} = \varphi_e(n, n)$$

From (34) we then obtain the values of $\theta^{(0)}(\xi)$ at the poles of the integrand in (24), and thus

$$G^{(0)}(x) = \frac{(1 + x)^n}{\varphi_e(n - 1, n)} + \sum_{\beta=1}^{e} \frac{\varphi_e(n, n)(1 + x)^{\xi_\beta}(1 - x)^{n-\xi_\beta}}{\varphi_e(n, \xi_\beta)(\xi_\beta - n)\varphi_e{}'(n - 1, \xi_\beta)} \tag{35}$$

Before obtaining $G^{(\gamma)}(x)$ explicitly for intermediate values of γ, we must first discuss a certain set of recursion relations holding between the coefficients ν_s of any solution of (11). These relations are

$$\sum_{s=e-\rho+1}^{e+\rho} (-1)^{e+s} k_{\rho,s}\nu_s = 0, \quad \rho = 1, 2, \cdots, \tag{36}$$

---

* The condition of Golay for the existence of group codes, obtained by different means, is essentially that $\varphi_e(n - 1, \xi)$ have at least one root an integer. Cf.: (4) of Reference 4, in view of (16), above.

where we define $\nu_s = 0$ for $s < 0$ and where the coefficients $k_{\rho,s}$ are

$$k_{\rho,s} = \sum_{\sigma=0}^{\rho} \binom{s}{\sigma}\binom{n-s}{\rho-\sigma}\binom{\rho-1}{e-s+\sigma} \tag{37}$$

(The derivation of (36) is given in Appendix A.) Equations (36), written out, are of the form

$$k_{1,\,e}\nu_e - k_{1,\,e+1}\nu_{e+1} = 0$$

$$k_{2,\,e-1}\nu_{e-1} - k_{2,\,e}\,\nu_e + k_{2,\,e+1}\nu_{e+1} - k_{2,\,e+2}\nu_{e+2} = 0$$

$$\vdots$$

from which we see that (36) may be used to determine

$$\nu_{e+1},\ \nu_{e+2},\ \cdots$$

recursively in terms of

$$\nu_e,\ \nu_{e-1},\ \cdots,\ \nu_0$$

We see also that if

$$\nu_e = \nu_{e-1} = \cdots = \nu_{\gamma+1} = 0$$

(with γ such that $0 \leq \gamma \leq e - 1$) then

$$\nu_{e+1} = \nu_{e+2} = \cdots = \nu_{2e-\gamma} = 0.$$

This has the following interpretation in terms of e-codes. It is well known (and obvious) that two different code words in an e-code must be separated by distance at least $2e + 1$. Hence if the code word of least weight in an e-code is of weight γ then all other code words are of weight not less than $2e + 1 - \gamma$. In the generating function for such a code it must be the case that not only

$$G^{(\gamma)}(x) = x^{\gamma} + 0(x^{e+1})$$

but in fact

$$G^{(\gamma)}(x) = x^{\gamma} + 0(x^{2e+1-\gamma}) \tag{38}$$

Equations (36) insure that this condition is satisfied automatically.*

As a particular case of (38), we have

$$G^{(0)}(x) = 1 + 0(x^{2e+1}).$$

We see that if we apply the operator L_γ to $G^{(0)}(x)$ there will result

$$L_\gamma G^{(0)}(x) = \varphi_\gamma(n, n)x^{\gamma} + 0(x^{2e+1-\gamma}) \tag{39}$$

---

* It is also necessary for the existence of an e-code that (36) determine ν_{e+1}, ν_{e+2}, $\cdots$ as non-negative integers when ν_e, ν_{e-1}, $\cdots$, ν_0 are those of (31). This condition is discussed a little further in Appendix A.

using the differential operator form for L_γ, (9). On the other hand, the function

$$\frac{L_\gamma G^{(0)}(x)}{\varphi_\gamma(n, n)} = \frac{1}{2\pi i} \int_\Gamma \frac{(1 + x)^\xi (1 - x)^{n-\xi}}{(\xi - n)\varphi_e(n - 1, \xi)} \left[\frac{\theta^{(0)}(\xi)\varphi_\gamma(n, \xi)}{\varphi_\gamma(n, n)} \right] d\xi \quad (40)$$

is a solution of differential equation (11), in view of the discussion following (24). From (39) we see that this function can be none other than $G^{(\gamma)}(x)$. Finally, applying L_γ to $G^{(0)}(x)$ in the form (35), we have explicitly

$$G^{(\gamma)}(x) = \frac{(1 + x)^n}{\varphi_e(n - 1, n)} + \frac{\varphi_e(n, n)}{\varphi_\gamma(n, n)} \sum_{\beta=1}^{e}$$
$$\frac{\varphi_\gamma(n, \xi_\beta)(1 + x)^{\xi_\beta}(1 - x)^{n-\xi_\beta}}{\varphi_e(n, \xi_\beta)(\xi_\beta - n)\varphi_e'(n - 1, \xi_\beta)} \quad 0 \le \gamma \le e. \quad (41)$$

V. EXAMPLES

The known cases where the condition of Hamming is satisfied are the following:

Case I: $e = 0, n \ge 1$

The Hamming expression (1) reduces to unity. In fact,

$$\varphi_0(n - 1, \xi) \equiv 1,$$

and the condition that all roots be integers is vacuous. The generating function for code words is (uniquely):

$$G^{(0)}(x) = \frac{(1 + x)^n}{\varphi_0(n - 1, n)} = (1 + x)^n$$

Each n-word of B_n is a detection region and thus a code word. There is no error correction.

Case II: $e \ge 1, n = e$

The Hamming expression becomes the sum of all the terms in the binomial expansion of $(1 + 1)^n$. The "codes" in this class consist of a single code word surrounded by its detection region consisting of the sphere B_n of radius n. No signalling is possible, of course, but our methods still apply.

From the representation

$$\varphi_s(n, \xi) = \frac{1}{2\pi i} \int_c \frac{(1 + x)^\xi (1 - x)^{n-\xi}}{x^{s+1}} dx$$
$$= \frac{1}{2\pi i} \int_c \frac{(1 + 2v)^\xi}{v^{s+1}(1 + v)^{n-s+1}} dv \quad (42)$$

(valid for all n, ξ) we have immediately

$$\varphi_n(n - 1, \xi) = 2^n \binom{\xi}{n} = \frac{2^n}{n!} \xi(\xi - 1) \cdots (\xi - n + 1)$$

and the roots are $0, 1, \cdots, n - 1$. The generating function $G^{(e)}(x)$ of (32) becomes*

$$G^{(n)}(x) = \frac{n!}{2^n} \cdot \frac{1}{2\pi i} \int_\Gamma \frac{(1 + x)^\xi (1 - x)^{n-\xi}}{(\xi)_{n+1}} \, d\xi$$

$$= \frac{n!}{2^n} \sum_{\xi=0}^n \frac{(-1)^{n-\xi}}{\xi!(n - \xi)!} (1 + x)^\xi (1 - x)^{n-\xi}$$

$$= \frac{1}{2^n} [(1 + x) - (1 - x)]^n = x^n$$

as one might expect. The explicit form for $\varphi_n(n, \xi)$ is somewhat complicated, but for ξ an integer it follows immediately from definition (13) that

$$\varphi_n(n, \xi) = (-1)^{n-\xi} \qquad \xi = 0, 1, \cdots, n$$

From (35), then,

$$G^{(0)}(x) = \frac{1}{2^n} \sum_{\xi=0}^n \binom{n}{\xi} (1 + x)^\xi (1 - x)^{n-\xi}$$

$$= \frac{1}{2^n} [(1 + x) + (1 - x)]^n = 1$$

which, again, is not surprising. The details for other values of γ seem to be more tedious, although one expects (41) to yield $G^{(\gamma)}(x) = x^\gamma$.

Case III: $e \geq 1, n = 2e + 1$

The Hamming expression in this case:

$$1 + \binom{2e + 1}{1} + \cdots + \binom{2e + 1}{e} = 2^{2e}$$

consists of the first half of the terms in the binomial expansion of $(1 + 1)^{2e+1}$. The code words in a code of this class are any two n-words separated by distance n (i.e., two vertices at opposite corners of the n-cube). The group codes in this class are the "majority rule" codes.† From (42) we have (using the substitution $y = 4v + 4v^2$)

---

* $(\zeta)_s \equiv s! \binom{\zeta}{s}$ denotes the descending factorial.

† The two code words in such a code are $00 \cdots 0$ and $11 \cdots 1$. An n-word belongs to $00 \cdots 0$ if it contains more 0's than 1's, and to $11 \cdots 1$ if it contains more 1's than 0's.

$$\varphi_s(n, \xi) = \frac{2^n}{2\pi i} \int_c \frac{(1 + y)^{\frac{1}{2}(\xi-1)} \, dy}{[(1 + y)^{\frac{1}{2}} - 1]^{s+1}[(1 + y)^{\frac{1}{2}} + 1]^{n-s+1}}, \qquad (43)$$

and, without difficulty,

$$\varphi_e(2e, \xi) = 2^{2e} \binom{\frac{1}{2}(\xi - 1)}{e} = \frac{2^e}{e!} (\xi - 1)(\xi - 3) \cdots (\xi - 2e + 1)$$

The roots are $1, 3, \cdots, 2e - 1$, and from (32):

$$G^{(e)}(x) = \frac{e!}{2^e} \cdot \frac{1}{2\pi i} \int_\Gamma \frac{(1 + x)^\xi (1 - x)^{2e+1-\xi} \, d\xi}{(\xi - 2e - 1)(\xi - 1)(\xi - 3) \cdots (\xi - 2e + 1)}$$

$$= 2^{-2e}(1 + x)(1 + x)^2 - (1 - x)^2]^e = x^e + x^{e+1}$$

In the case $\gamma = 0$ we need the result

$$\varphi_e(2e + 1, \xi) = 2^{2e+1} \left[\binom{\frac{1}{2}\xi}{e + 1} - \binom{\frac{1}{2}(\xi - 1)}{e + 1} \right]$$

from (43). It is then tedious but straightforward to obtain from (35)

$$G^{(0)}(x) = \frac{1}{2^{2e}} \sum_{r=0}^e \binom{2e + 1}{2r + 1} (1 + x)^{2r+1} (1 - x)^{2e-2r}$$

$$= 2^{-2e-1}\{[(1 - x) + (1 + x)]^{2e+1} - [(1 - x) - (1 + x)]^{2e+1}\}$$

$$= 1 + x^{2e+1}$$

One expects to get

$$G^{(\gamma)}(x) = x^\gamma + x^{2e+1-\gamma}$$

from (41), but verification appears to be complicated.

Case IV: $e = 1$, $n = 2^t - 1$ ($t = 3, 4, \cdots$)

The single error correcting codes of Hamming[1] are included here. (The examples for $t = 1$, resp. $t = 2$, appear under Case II, resp. Case III, above.) Since n is always odd the condition that $\varphi_1(n - 1, \xi) = 2\xi - n + 1$ have an integer root is automatically satisfied. For $\gamma = 1$ the generating function is

$$G^{(1)}(x) = \frac{1}{2\pi i} \int_\Gamma \frac{(1 - x)^\xi (1 - x)^{n-\xi}}{(\xi - n)(2\xi - n + 1)} \, d\xi$$

$$= \frac{(1 + x)^n - (1 + x)^{\frac{1}{2}(n-1)}(1 - x)^{\frac{1}{2}(n+1)}}{1 + n}$$

from which we have

$$\nu_s^{(1)} = \frac{1}{1 + n} \left\{ \binom{n}{s} - (-1)^{\frac{1}{2}s} \binom{\frac{1}{2}(n - 1)}{\frac{1}{2}s} \right\} \qquad s \text{ even}$$

$$\nu_s^{(1)} = \frac{1}{1+n}\left\{\binom{n}{s} - (-1)^{\frac{1}{2}(s+1)}\binom{\frac{1}{2}(n-1)}{\frac{1}{2}(s-1)}\right\} \quad s \text{ odd}$$

For $\gamma = 0$, Eq. (35) works out as

$$G^{(0)}(x) = \frac{(1+x)^n + n(1+x)^{\frac{1}{2}(n-1)}(1-x)^{\frac{1}{2}(n+1)}}{1+n}$$

so that

$$\nu_s^{(0)} = \frac{1}{1+n}\left\{\binom{n}{s} + n(-1)^{\frac{1}{2}s}\binom{\frac{1}{2}(n-1)}{\frac{1}{2}s}\right\} \quad s \text{ even}$$

$$\nu_s^{(0)} = \frac{1}{1+n}\left\{\binom{n}{s} + n(-1)^{\frac{1}{2}(s+1)}\binom{\frac{1}{2}(n-1)}{\frac{1}{2}(s-1)}\right\} \quad s \text{ odd}$$

Case V: $e = 2, n = 90$

The double error correcting codes for $n = 2, 5$ are covered by Cases II, III, respectively. The discovery that

$$1 + 90 + \tfrac{1}{2}(90)(89) = 2^{12}$$

is due to Golay.[7] We have

$$2\varphi_2(n-1, \xi) = (2\xi - n + 1)^2 - (n-1)$$

with roots

$$\tfrac{1}{2}[n - 1 \pm (n-1)^{\frac{1}{2}}]$$

Since these roots are not integers when $n = 90$, there can be no 2-code for $n = 90$.* H. S. Shapiro has shown (in unpublished work) that the Hamming condition for $e = 2$ is satisfied only in the cases $n = 2, 5, 90$, so that the only nontrivial 2-codes are those equivalent to the majority rule code on 5 places.

Case VI: $e = 3, n = 23$

Golay[7] finds:

$$1 + 23 + \tfrac{1}{2}(23)(22) + (23)(22)(21)/6 = 2^{11}$$

and gives explicitly a 3-code on 23 places of group type. We have

$$6\varphi_3(n-1, \xi) = (2\xi - n + 1)[(2\xi - n + 1)^2 - (3n - 5)]$$

and when $n = 23$ we verify that the roots are the integers 7, 11, 15. Computations by the author show that for $n < 10^{10}$ the Hamming condition for $e = 3$ holds only when $n = 3, 7, 23$.

---

* This settles a question raised by Golay, who shows that there is no code of group type in this case, but not that there is no code at all.

For $e = 4$ we have

$$24\varphi_4(n - 1, \xi) = [(2\xi - n + 1)^2 - (3n - 7)]^2 - (6n^2 - 30n + 40)$$

For $n = 4, 9$ this reduces to the forms given under Cases II, III. Preliminary calculations by the author shows that any other solutions of the Hamming condition for $e = 4$ must be such that $n > 10^{10}$, so that the question of the existence of 4-codes (other than the majority rule code) is somewhat academic.

Computations of Mrs. G. Rowe of the Mathematical Research Department show that Cases I–VI cover all cases of the Hamming condition being satisfied in the range

$$0 \leqq e \leqq n, \qquad 1 \leqq n \leqq 150$$

APPENDIX A

From (13) we have

$$\left(\frac{1 - x}{1 + x}\right)^{n - \xi} = \frac{1}{(1 + x)^n} \sum_{s=0}^{\infty} \varphi_s(n, \xi) x^s \tag{A1}$$

Applying the operator $D = -(1 + x)^2 d/dx$ to both sides of (A1) ρ times, there results

$$2^\rho (n - \xi)_\rho \left(\frac{1 - x}{1 + x}\right)^{n - \xi - \rho} = \sum_{s=0}^{\infty} \varphi_s(n, \xi) D^\rho [x^s (1 + x)^{-n}] \tag{A2}$$

The substitution $v = (1 + x)^{-1}$ reduces D to d/dv, so that

$$D^\rho x^s (1 + x)^{-n} = \frac{d^\rho}{dv^\rho} (1 - v)^s v^{n-s}$$

$$= \sum_{\sigma=0}^{\rho} \binom{\rho}{\sigma} (-1)^\sigma (s)_\sigma (1 - v)^{s-\sigma} (n - s)_{\rho-\sigma} v^{n-s-\rho+\sigma}$$

$$= \rho! \sum_{\sigma=0}^{\rho} (-1)^\sigma \binom{s}{\sigma} \binom{n - s}{\rho - \sigma} x^{s-\sigma} (1 + x)^{\rho-n}$$

using Leibnitz's rule. We substitute this into Eq. (A2), multiply both sides of the result by

$$(1 + x)^{n-\rho} (1 - x)^{\rho-\tau} / \rho!$$

(with τ arbitrary), and then equate coefficients of x^t on both sides; there obtains

$$2^\rho \binom{n - \xi}{\rho} \varphi_t(n - \tau, \xi) = \sum_{s=0}^{t+\rho} (-1)^{t+s} \kappa_{\rho,s}(n, \tau; t) \varphi_s(n, \xi) \tag{A3}$$

valid for all n, ξ, τ and all non-negative integers ρ, t, where

$$\kappa_{\rho,s}(n, \tau; t) = \sum_{\sigma=0}^{\rho} \binom{s}{\sigma}\binom{n-s}{\rho-\sigma}\binom{\rho-\tau}{t-s+\sigma} \tag{A4}$$

The coefficients $\kappa_{\rho,s}(n, \tau; t)$ vanish unless $s \leq t + \rho$; if n and $\rho - \tau$ are non-negative integers then the coefficients $\kappa_{\rho,s}(n, \tau; t)$ are positive integers provided $t - \rho + \tau \leq s$ and vanish otherwise. In particular, (setting $\tau = 1$, $t = e$),

$$2^{\rho}\binom{n-\xi}{\rho}\varphi_e(n-1, \xi) = \sum_{s=e-\rho+1}^{e+\rho} (-1)^{e+s}k_{\rho,s}\varphi_s(n, \xi), \rho = 1, 2, \cdots, \tag{A5}$$

where we define $\varphi_s(n, \xi) \equiv 0$ for $s < 0$; the $k_{\rho,s} = \kappa_{\rho,s}(n, 1; e)$ are those of (37) of the text. If we multiply ν_s of (25) by $(-1)^{e+s}k_{\rho,s}$ and sum on s there results (36), since the left hand member of (A5) is a polynomial multiple of the denominator of the integrand in (25).

If the code word of least weight in an e-code is of weight γ, then the first nontrivial one of the (37) is the one for $\rho = e + 1 - \gamma$, and it gives (since $\nu_\gamma^{(\gamma)} = 1$)

$$\nu_{2e+1-\gamma}^{(\gamma)} = \frac{k_{e+1-\gamma,\gamma}}{k_{e+1-\gamma,2e+1-\gamma}}$$

$$= \frac{(n-\gamma)(n-\gamma-1)\cdots(n-e)}{(2e+1-\gamma)(2e-\gamma)\cdots(e+1)}$$

A necessary condition for the existence of an e-code on n places is that this expression be a non-negative integer in each case $\gamma = 0, 1, \cdots, e$. It is not clear, however, that this condition is independent of the one set forth in the theorem of Section IV.

Appendix B

We give here a relation due to K. M. Case[8] which shows that the statement of our main result as it appears in the Abstract heading this article agrees with the theorem proved in Section IV.

In the defining relation

$$(1 + x)^r(1 - x)^{n-r} = \sum_{s=0}^{\infty} x^s\varphi_s(n, r) \tag{B1}$$

for the coefficients $\varphi_s(n, r)$ assume that n and r are integers, multiply both sides by $(-1)^r \binom{n}{r} y^r$, and sum on r, $0 \leq r \leq n$. The result is

$$[(1 - x) - y(1 + x)]^n = \sum_{r=0}^{n}\sum_{s=0}^{n} (-1)^r \binom{n}{r} y^r x^s\varphi_s(n, r) \tag{B2}$$

Rearrange the left hand member and re-expand it, to get

$$[(1 - x) - y(1 + x)]^n = [(1 - y) - x(1 + y)]^n$$

$$= \sum_{s=0}^{n} (-1)^s \binom{n}{s} x^s (1 + y)^s (1 - y)^{n-s} \quad \text{(B3)}$$

$$= \sum_{s=0}^{n} \sum_{r=0}^{n} (-1)^s \binom{n}{s} x^s y^r \varphi_r(n, s)$$

Comparing coefficients of $x^s y^r$ in (B2) and (B3), we have, finally,

$$(-1)^r \binom{n}{r} \varphi_s(n, r) = (-1)^s \binom{n}{s} \varphi_r(n, s) \quad (n, r, s \text{ integers}), \quad \text{(B4)}$$

or, changing notation slightly,

$$\varphi_\xi(n - 1, e) = (-1)^{\xi-e} \frac{\binom{n - 1}{\xi}}{\binom{n - 1}{e}} \varphi_e(n - 1, \xi) \quad \text{(B5)}$$

(with n, e, ξ integers and $0 \leqq e, \xi \leqq n - 1$). Thus if $\varphi_e(n - 1, \xi)$ vanishes for e different integers ξ then so must $\varphi_\xi(n - 1, e)$, at least when $e < n$. But $\varphi_\xi(n - 1, e)$ is the coefficient of x^ξ in $(1 + x)^e (1 - x)^{n-1-e}$ when this is written out as a polynomial in x, by definition.

REFERENCES

1. R. W. Hamming, B.S.T.J., **29**, p. 147, 1950.
2. C. E. Shannon, B.S.T.J., **27**, p. 379, 1948.
3. P. Elias, Trans. I.R.E., **PGIT-4**, p. 29, 1954.
4. M. J. E. Golay, Trans. I.R.E., **PGIT-4**, p. 23, 1954.
5. D. Slepian, B.S.T.J., **35**, p. 203, 1956.
6. E. L. Ince, *Ordinary Differential Equations* (Dover), Ch. V, XV.
7. M. J. E. Golay, Proc. I.R.E., **37**, p. 637, 1949.
8. K. M. Case, Phys. Rev., **97**, p. 810, 1955.

Selecting the Best One of Several Binomial Populations

By MILTON SOBEL and MARILYN J. HUYETT

(Manuscript received July 17, 1956)

Tables have been prepared for use in any experiment designed to selec that particular one of k binomial processes or populations with the highest (long time) yield or the highest probability of success. Before experimentation the experimenter chooses two constants d* and P* (0 < d* ≦ 1; 0 ≦ P* < 1) and specifies that he would like to guarantee a probability of at least P* of a correct selection whenever the true difference between the long-time yields associated with the best and the second best processes is at least d*. The tables show the smallest number of units required per process to be put on test to satisfy this specification. Separate tables are given for k = 2, 3, 4 and 10. Each table gives the result for d* = 0.05 (0.05) 0.50 and for P* = 0.50, 0.60, 0.70, 0.75, 0.80, 0.85, 0.90, 0.95, and 0.99. For values of d* and P* not considered in the tables, graphs are given on which interpolation can be carried out. Graphs have also been constructed to make possible an interpolation or extrapolation for other values of k. An alternative specification is given for use when the experimenter has some a priori knowledge of the processes and their probabilities of success. This specification is then compared with the original specification. Applications of these tables to different types of problems are considered.

INTRODUCTION AND SUMMARY

A frequently encountered problem is that of selecting the "best" one of k (k ≧ 2) processes or populations on the basis of the same number n of observations from each process. We shall assume that the given processes are all binomial or "go — no go" processes and that the best process is the one with the highest probability of obtaining a "success" on a single observation. We shall consider a single sample or nonsequential procedure which means that the common number n of observations from each process is to be determined before experimentation starts. The corresponding sequential problem is being investigated.[1]

Briefly, the technique employed here is to let the experimenter decide how "close" the best and second best processes can be before he is willing to relax his control on the probability of a correct selection. The selection of a best process will, of course, be made on the basis of the largest observed frequency of "success"; the only remaining problem is to determine the value of n. Tables and graphs which cover almost all practical problems in this framework are given for determining the required value of n. In particular, tables and graphs are given for $k = 2$, 3, 4 and 10. Graphs are also given to approximate the result for any value of k up to 100.

This problem arises in many widely different fields of endeavor; we shall briefly consider two industrial applications. One application of the binomial problem is to comparative yield studies. Here success corresponds to the making of a good unit, and the goal is to select the process with the highest (long-time) yield. Another application of the binomial problem is to comparative life testing studies. In this case the experimenter selects a fixed time T and defines the best process as the one for which the probability of any one unit surviving this time T is highest. Then, of course, a successful unit is one which survives the time T. In treating this as a binomial we are discarding the information contained in the exact times of failure. In many cases the times of failure are either unknown or very inexact; in other cases it is not known how to utilize the knowledge of the exact times of failure. Hence, it would be valuable to know the results for the more basic binomial problem. The time T is considered fixed throughout; its value is determined by non-statistical considerations. The specification and the final decision of the experimenter all refer to this predetermined time T. It should be noted that the experimenter cannot use information obtained from the continuation of the test beyond time T since the best process for T is not necessarily the best process for a longer time, say $10T$. This binomial type of analysis has the advantage that it does not assume any particular form of the life distribution. In particular, the assumption of exponential life is avoided.

The presence of à priori information changes the number of observations required. An alternative specification is given which is justified by certain à priori information based on past experimentation. The amount of saving is briefly examined. This area of utilizing à priori information to reduce the number of observations required should be investigated further.

The treatment of the problem in this paper is based on the assumption that, after experimentation is carried out, the experimenter must

choose one of the k processes and assert that it is best. If he allows himself the possibility of hedging and asserting that he needs further experimentation, then the problem changes and the tables of this paper are not appropriate.

The following additional assumptions will be made:

1. Observations from the same or different processes are independent.

2. Observations from the same process have a common fixed probability of "success".

3. There is no chance of error in determining whether a success or a failure has occurred.

The assumption of a common probability fixed once and for all for each process is one that should be checked carefully in any practical application of the results in this paper. Roughly speaking, this assumption states that each of the processes is in a state of statistical control as far as the probability of success is concerned.

We shall consider only the case in which the same number n of observations are taken from each process. This is certainly reasonable for a single sample procedure if no à priori information is assumed.

STATISTICAL FORMULATION OF THE PROBLEM

Each of k given binomial populations Π_i is associated with a fixed probability of success p_i where $0 \leqq p_i \leqq 1$ $(i = 1, 2, \cdots, k)$. For example, in the yield problem p_i is the long-time yield for process Π_i or the probability that any one unit from Π_i is a good one. Let the ordered values of the p_i be denoted by

$$p_{[1]} \geqq p_{[2]} \geqq \cdots \geqq p_{[k]} \tag{1}$$

No à priori information is assumed about the values of the p_i or about the correspondence between the ordered $p_{[i]}$ and the k identifiable populations Π_i. In particular, we have no idea before experimentation starts whether $p_{[1]}$ is associated with Π_1, Π_2, $\cdots$, or Π_k.

The problem is to select the population associated with $p_{[1]}$ on the basis of n observations from each population. If there are t ties for first place, say

$$p_{[1]} = p_{[2]} = \cdots = p_{[t]} > p_{[t+1]} \qquad (t < k) \tag{2}$$

then we shall certainly be content with the selection of any one of the associated t populations as the best one.

As an index of the true difference (or distance) between the best and second best populations we introduce the symbol

$$d = p_{[1]} - p_{[2]} \tag{3}$$

It is assumed that if the difference d between the best and second best populations is small enough, then the error involved in wrongly selecting the second best process as the best one is an error of little or no consequence. The experimenter is therefore asked to specify two quantities which will determine the number n of observations he is required to take from each process.

> Specification: He specifies the smallest value d^*
> ($0 < d^* \leqq 1$) of d for which it would be economically
> desirable to make the correct selection. He also specifies   (4)
> a probability P^* ($0 \leqq P^* < 1$) of making a correct
> selection that he would like to guarantee whenever the
> true difference $d \geqq d^*$.

Letting $P_{cs} = P_{cs}(p_{[1]}, \cdots, p_{[k]})$ denote the probability of a correct selection we can now rewrite the specification that the experimenter wants to satisfy in the simple form

$$P_{cs} \geqq P^* \quad \text{for} \quad d \geqq d^* \tag{5}$$

[The word "specification" will be used below to denote the specified pair of constants (d^*, P^*) as well as the condition (5); it will be clear from the text which is meant.] Since the final selection is to be made on the basis of the observed frequency of success, the essential problem is to find the number n of observations required per process to satisfy the specification (5).

The possibility that d may be less than d^* is not being overlooked. The region $d < d^*$ is being regarded as a zone of indifference in the sense that if $d < d^*$, then we do not care which process is selected as best so long as its p-value is within d^* of the highest p-value $p_{[1]}$. For values of $P^* \leqq 1/k$ no tables are needed since a probability of $1/k$ can be attained by chance alone.

Some comments on the above approach and on a possible modification have been placed in Appendix I in order to preserve the continuity of the paper.

CONFIDENCE STATEMENT

After the experiment is completed and the selection of a best process is made, the experimenter can make a confidence statement with confidence level P^*. Let p_s denote the true p-value of the selected population and let p_u denote the maximum true p-value over all unselected popula-

tions. Then the confidence statement, consisting of two sets of inequalities

$$\begin{cases} p_{[1]} - d^* \leq p_s \leq p_{[1]} \\ p_{[2]} \leq p_u \leq p_{[2]} + d^* \end{cases} \quad or \quad \begin{cases} 0 \leq p_{[1]} - p_s \leq d^* \\ 0 \leq p_u - p_{[2]} \leq d^* \end{cases}$$

has confidence level P^*. It should be noted that the above confidence statement is not a statement about the value of any p but is a statement about the correctness of the selection made.

LEAST FAVORABLE CONFIGURATION

The main idea used in the construction of the tables was that of a least favorable configuration. Before defining this concept we shall define the set of configurations

$$p_{[1]} - d = p_{[2]} = p_{[3]} = \cdots = p_{[k]} \tag{6}$$

obtained by letting d in (6) vary over the closed interval $(d^*, 1)$ as the *Less-Favorable* set of configurations. It is intuitively clear and will be rigorously shown in Appendix II that if our procedure satisfies the specification for any true configuration (6) with $d = d^0$ and $p_{[1]} = p_{[1]}^0$, then it will also satisfy the specification when

$$p_{[1]}^0 - d^0 \geq p_{[2]} \geq p_{[2]} \geq \cdots \geq p_{[k]} \tag{7}$$

Of course, we shall be interested particularly in the case in which d equals the specified value d^*. If $d = d^*$ is fixed in (6), then (6) specifies the differences between the p-values, but the "location" of the set is still not specified. We shall use $p_{[1]}$ to locate the set of p-values. The probability P_{cs} of a correct selection for configurations like (6) with $d = d^*$ depends not only on d^*, n and k but also on the location $p_{[1]}$ of the largest p-value (except for the special case $k = 2$ and $n = 1$). [In the corresponding problem for selecting the largest population mean of k independent *Normal* distributions with unit variance,[2] this probability P_{cs} depends *only on the differences* and, hence, only on d in the configuration corresponding to (6)].

When (6) holds with any *fixed* value of d, the probability P_{cs} (for any fixed n) may be regarded as a function of $p_{[1]}$ where $d \leq p_{[1]} \leq 1$). This function is continuous and bounded over a closed interval and therefore assumes its minimum value at some point $p_{[1]}(d) = p_{[1]}(d;n)$ in the closed interval $(d,1)$. Fig. 1(b) gives the value of $p_{[1]}(d)$ as a function of d for $k = 3$ and for $n = 1, 2, 4, 10$ and ∞. For any particular value

of n and for $d = d^*$ we shall be particularly interested in the value $p_{[1]}^L = p_{[1]}(d^*;n)$ since this (as shown in Appendix II) gives the smallest probability P_{cs}^L of a correct selection *for all the configurations included in the statement of the experimenter's specification*. This particular configuration (6) with $d = d^*$ and $p_{[1]} = p_{[1]}^L$ (which depends on n) is called the *Least-Favorable Configuration*.

Although the least favorable configuration depends on n, it has been empirically found that for $n \geqq 10$ (and in some cases for $n \geqq 4$) the least favorable configuration is approximately given by $p_{[1]}^L = \frac{1}{2}(1 + d^*)$ in which the two values, $p_{[1]}^L$ and $p_{[2]}^L = p_{[1]}^L - d^*$ are symmetric about $\frac{1}{2}$. This symmetric configuration clearly does not depend on n. Fig. 1(b) shows that as $n \to \infty$ the least favorable configuration approaches this symmetric configuration (i.e., the straight line marked $n = \infty$) *quite rapidly* for any value of d. In Appendix III it is proved that the symmetric configuration is least favorable as $n \to \infty$. Fig. 1(a) shows for $k = 3$, $n = 10$, and any value of d the error in P_{cs} which arises as a result of using the symmetric configuration instead of the true least favorable configuration.
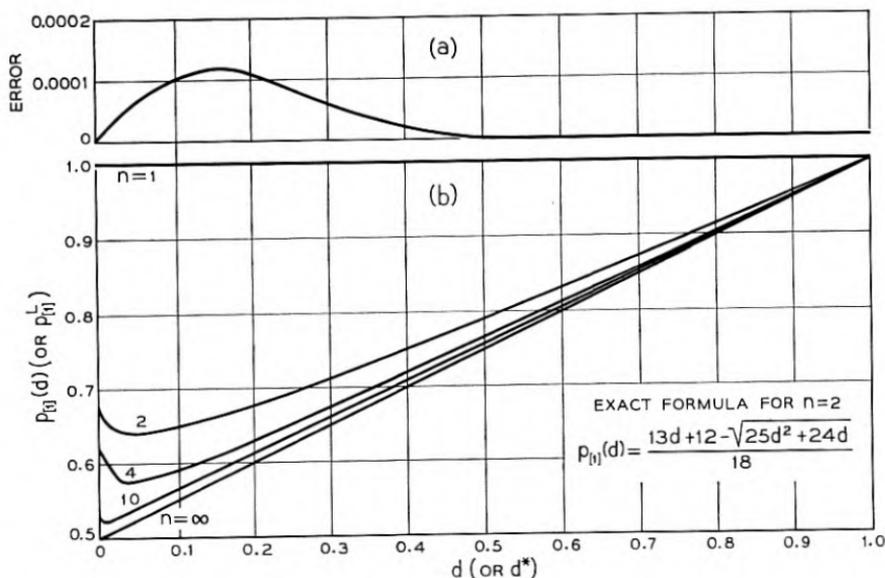
Fig. 1 — (a) Error in P_{CS} as a result of using the symmetric configuration instead of the least favorable configuration for $k = 3$, $n = 10$, and any common true difference d. (b) Least favorable value $p_{[1]}(d)$ of $p_{[1]}$ as a function of the common true difference $d = p_{[1]} - p_{[2]}$, $i \geqq 2$, for $k = 3$ and selected values of n. (for $d = d^*$, $p_{[1]}(d) = p_{[1]}^L$)

CONSTRUCTION OF THE TABLES

Consider any fixed value of d^*. For each of a set of increasing values of n the minimum probability P_{cs}^L of a correct selection for $d \geq d^*$ (i.e., the probability for the least favorable configuration) was computed. These calculations were then inverted to find the smallest n for which the P_{cs}^L is greater than or equal to the specified value P^*. Tables I through IV give the smallest value of n for $k = 2, 3, 4$, and 10, for $d^* = 0.05$ (0.05) 0.50, and for selected values of P^*. Graphs corresponding to these tables are given in Figs. 2 through 5.

For small values of n (say, $n < 10$) it was necessary to approximate $p_{[1]}^L$ by calculating the P_{cs} *exactly* for several values of $p_{[1]}$ and proceeding in the direction of the minimum probability P_{cs}^L. For the special case $n = 2$ and $k = 3$ an explicit formula for $p_{[1]}^L$ is given on Fig. 1.

For large values of n (say, $n > 10$) the P_{cs}^L was calculated by assuming the symmetric configuration. Here it was necessary to make use of the normal approximation to the binomial. Fortunately the appropriate table needed in this normal approximation is already published.[2] The proof that this table is appropriate is given in Appendix III. The resulting value of n is given by

$$n = \frac{B}{d^{*2}} (1 - d^{*2}) \cong \frac{B}{d^{*2}} \tag{8}$$

where the constant B, depending on P^* and k, is equal to $\frac{1}{4} C^2$ and C is the entry in the appropriate column of Table I of R. E. Bechhofer's paper.[2] A short table of B values, Table V (see page 550), is included in this paper to make it self-contained.

The middle expression in (8) will be referred to as the normal approximation and the right hand expression in (8) will be referred to as the "straight line" approximation. In many cases it has been *empirically* found that these two expressions give close lower and upper bounds to the true value. Thus by noting the curves drawn in Figs. 4 and 6 for $k = 4$, $P^* \geq 0.75$ it appears that for all values of d^* the true P_{cs}^L is between the normal approximation and the straight line approximation. Assuming this to be so, it follows that for $k = 4$, $P^* \geq 0.75$ the required value of n satisfies the inequalities

$$\left[\frac{B}{d^{*2}} (1 - d^{*2}) \right] \leq n \leq \left[\frac{B}{d^{*2}} \right] \tag{9}$$

where $[x]$ denotes the smallest integer greater than or equal to the enclosed quantity x. This result (9) is empirical and not based on any mathematically proven inequalities. It is used here only to estimate the

TABLE I — NUMBER OF UNITS REQUIRED PER PROCESS TO GUARANTEE A PROBABILITY OF P^* OF SELECTING THE BEST OF k BINOMIAL PROCESSES WHEN THE TRUE DIFFERENCE $p_{[1]} - p_{[2]}$ IS AT LEAST d^*. $(k = 2)$

The three values in each group are: (1) Normal approximation, (2) Straight line approximation, and (3) Smallest integer required.

d^*					P^*				
	0.50	0.60	0.75	0.80	0.85	0.90	0.95	0.99
0.05	0	12.81	90.77	141.30	214.29	327.66	539.77	1079.70
	0	12.84	90.99	141.66	214.83	328.48	541.12	1082.41
	0	14	92	142	215	329	541	1082
0.10	0	3.18	22.52	35.06	53.17	81.30	133.93	267.90
	0	3.21	22.75−	35.41	53.71	82.12	135.28	270.60
	0	4	23	36	54	83	135	270
0.15	0	1.39	9.88	15.39	23.33	35.68	58.78	117.57
	0	1.43	10.11	15.74	23.87	36.50−	60.12	120.27
	0	2	11	16	24	37	60	120
0.20	0	0.77	5.46	8.50−	12.89	19.71	32.47	64.94
	0	0.80	5.69	8.85+	13.43	20.53	33.82	67.65+
	0	1	6	9	14	21	34	67
0.25	0	0.48	3.41	5.31	8.06	12.32	20.29	40.59
	0	0.51	3.64	5.67	8.59	13.14	21.64	43.30
	0	1	4	6	9	14	22	42
0.30	0	0.32	2.30	3.58	5.43	8.30	13.68	27.36
	0	0.36	2.53	3.93	5.97	9.12	15.03	30.07
	0	1	3	4	6	9	15	29
0.35	0	0.23	1.63	2.54	3.85−	5.88	9.69	19.38
	0	0.26	1.86	2.89	4.38	6.70	11.04	22.09
	0	1	2	3	5	7	11	21
0.40	0	0.17	1.19	1.86	2.82	4.31	7.10	14.21
	0	0.20	1.42	2.21	3.36	5.13	8.46	16.91
	0	1	2	3	4	5	9	16
0.45	0	0.13	0.90	1.39	2.11	3.23	5.33	10.65+
	0	0.16	1.12	1.75−	2.65+	4.06	6.68	13.36
	0	1	2	2	3	4	7	13
0.50	0	0.10	0.68	1.06	1.61	2.46	4.06	8.12
	0	0.13	0.91	1.42	2.15−	3.28	5.41	10.82
	0	1	1	2	3	4	5	10

TABLE II — NUMBER OF UNITS REQUIRED PER PROCESS TO GUARAN-
TEE A PROBABILITY OF P^* OF SELECTING THE BEST OF k BINOMIAL
PROCESSES WHEN THE TRUE DIFFERENCE $p_{[1]} - p_{[2]}$ IS AT LEAST
d^*. ($k = 3$)

The three values in each group are: (1) Normal approximation, (2)
Straight line approximation, and (3) Smallest integer required.

d^*	P^*							
	0.50	0.60	0.75	0.80	0.85	0.90	0.95	0.99
0.05	30.89	78.16	205.06	272.36	363.06	496.14	732.63	1305.21
	30.97	78.36	205.58	273.04	363.97	497.38	734.46	1308.49
	31	79	206	273	364	498	735	1308
0.10	7.66	19.39	50.88	67.58	90.08	123.10	181.78	323.85+
	7.74	19.59	51.39	68.26	90.99	124.34	183.62	327.12
	8	20	52	69	91	125	184	327
0.15	3.36	8.51	22.33	29.66	39.53	54.02	79.77	142.12
	3.44	8.71	22.84	30.34	40.44	55.26	81.61	145.39
	4	9	23	31	41	55	82	145
0.20	1.86	4.70	12.33	16.38	21.84	29.84	44.07	78.51
	1.94	4.90	12.85−	17.07	22.75−	31.09	45.90	81.78
	3	5	13	17	23	31	46	81
0.25	1.16	2.94	7.71	10.24	13.65−	18.65+	27.54	49.07
	1.24	3.13	8.22	10.92	14.56	19.90	29.38	52.34
	2	4	9	11	15	20	29	52
0.30	0.78	1.98	5.20	6.90	9.20	12.57	18.57	33.08
	0.86	2.18	5.71	7.58	10.11	13.82	20.40	36.35−
	2	3	6	8	10	14	20	35
0.35	0.55+	1.40	3.68	4.89	6.52	8.91	13.15+	23.43
	0.63	1.60	4.20	5.57	7.43	10.15	14.99	26.70
	2	2	5	6	8	10	15	26
0.40	0.41	1.03	2.70	3.58	4.78	6.53	9.64	17.17
	0.48	1.22	3.21	4.27	5.69	7.77	11.48	20.45−
	1	2	4	5	6	8	11	20
0.45	0.30	0.77	2.02	2.69	3.58	4.90	7.23	12.88
	0.38	0.97	2.54	3.37	4.49	6.14	9.07	16.15+
	1	2	3	4	5	6	9	15
0.50	0.23	0.59	1.54	2.05−	2.73	3.73	5.51	9.81
	0.31	0.78	2.06	2.73	3.64	4.97	7.34	13.08
	1	2	3	3	4	5	7	12

TABLE III — NUMBER OF UNITS REQUIRED PER PROCESS TO GUARANTEE A PROBABILITY OF P^* OF SELECTING THE BEST OF k BINOMIAL PROCESSES WHEN THE TRUE DIFFERENCE $p_{[1]} - p_{[2]}$ IS AT LEAST d^*. ($k = 4$)

The three values in each group are : (1) Normal approximation, (2) Straight line approximation, and (3) Smallest integer required.

d^*	P^*							
	0.50	0.60	0.75	0.80	0.85	0.90	0.95	0.99
0.05	69.85− 70.02 71	132.65+ 132.99 134	282.27 282.98 283	357.52 358.42 359	456.82 457.96 458	599.53 601.03 601	848.30 850.42 850	1438.12 1441.72 1442
0.10	17.33 17.51 18	32.91 33.25− 34	70.04 70.74 71	88.71 89.61 90	113.35− 114.49 114	148.76 150.26 150	210.48 212.61 212	356.83 360.43 360
0.15	7.61 7.78 8	14.44 14.78 15	30.74 31.44 32	38.93 39.82 40	49.74 50.88 51	65.29 66.78 67	92.37 94.49 94	156.61 160.19 160
0.20	4.20 4.38 5	7.98 8.31 9	16.98 17.69 18	21.51 22.40 23	27.48 28.62 29	36.06 37.56 38	51.03 53.15+ 53	86.50+ 90.12 89
0.25	2.63 2.80 3	4.99 5.32 6	10.61 11.32 12	13.44 14.34 14	17.17 18.32 18	22.54 24.04 24	31.89 34.02 34	54.06 57.67 57
0.30	1.77 1.95− 3	3.36 3.69 4	7.15+ 7.86 8	9.06 9.96 10	11.58 12.72 13	15.19 16.70 17	21.50− 23.62 23	36.44 40.05− 39
0.35	1.25+ 1.43 2	2.38 2.71 3	5.07 5.77 6	6.42 7.31 7	8.20 9.35− 9	10.76 12.27 12	15.23 17.36 17	25.82 29.42 28
0.40	0.92 1.09 2	1.75− 2.08 3	3.71 4.42 5	4.70 5.60 6	6.01 7.16 7	7.89 9.39 9	11.16 13.29 13	18.92 22.53 21
0.45	0.69 0.86 2	1.31 1.64 2	2.79 3.49 4	3.53 4.42 5	4.51 5.65+ 6	5.92 7.42 7	8.37 10.51 10	14.19 17.80 17
0.50	0.53 0.70 2	1.00 1.33 2	2.12 2.83 3	2.69 3.58 4	3.43 4.58 5	4.51 6.01 6	6.38 8.50+ 8	10.81 14.42 13

TABLE IV — NUMBER OF UNITS REQUIRED PER PROCESS TO GUARANTEE A PROBABILITY OF P^* OF SELECTING THE BEST OF k BINOMIAL PROCESSES WHEN THE TRUE DIFFERENCE $p_{[1]} - p_{[2]}$ IS AT LEAST d^*. ($k = 10$)

The three values in each group are: (1) Normal approximation, (2) Straight line approximation, and (3) Smallest integer required.

| d^*	P^*							
	0.50	0.60	0.75	0.80	0.85	0.90	0.95	0.99
0.05	216.96	312.51	511.15+	604.04	722.50−	887.54	1165.49	1798.01
	217.50+	313.29	512.43	605.55+	724.31	889.77	1168.41	1802.51
	218	314	513	606	725	890	1169	1803
0.10	53.83	77.54	126.83	149.87	179.27	220.22	289.18	446.12
	54.38	78.32	128.11	151.39	181.08	222.44	292.10	450.63
	55	79	128	151	181	222	291	449
0.15	23.62	34.03	55.66	65.77	78.67	96.64	126.90	195.77
	24.17	34.81	56.94	67.28	80.48	98.86	129.82	200.28
	25	35	57	67	80	98	129	198
0.20	13.05+	18.80	30.75−	36.33	43.46	53.39	70.10	108.15
	13.59	19.58	32.03	37.85−	45.27	55.61	73.03	112.66
	14	20	32	38	45	55	72	111
0.25	8.16	11.75−	19.22	22.71	27.16	33.37	43.82	67.59
	8.70	12.53	20.50−	24.22	28.97	35.59	46.74	72.10
	9	13	20	24	29	35	46	70
0.30	5.50−	7.92	12.95+	15.31	18.31	22.49	29.53	45.56
	6.04	8.70	14.23	16.82	20.12	24.72	32.46	50.07
	7	9	14	17	20	24	32	48
0.35	3.90	5.61	9.18	10.84	12.97	15.93	20.92	32.28
	4.44	6.39	10.46	12.36	14.78	18.16	23.85−	36.79
	5	7	11	13	15	18	23	35
0.40	2.85+	4.11	6.73	7.95−	9.51	11.68	15.34	23.66
	3.40	4.90	8.01	9.46	11.32	13.90	18.26	28.16
	4	5	8	10	11	13	17	26
0.45	2.14	3.08	5.05−	5.96	7.13	8.76	11.50+	17.75−
	2.69	3.87	6.33	7.48	8.94	10.98	14.42	22.25+
	3	4	6	8	9	11	14	20
0.50	1.63	2.35−	3.84	4.54	5.43	6.67	8.76	13.52
	2.18	3.13	5.12	6.06	7.24	8.90	11.68	18.03
	3	4	5	6	7	9	11	16
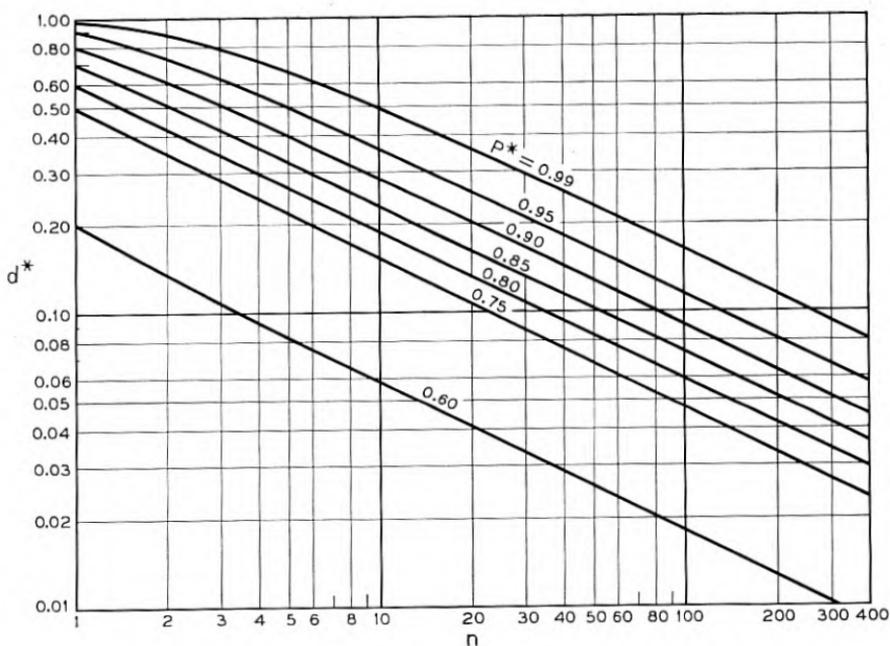
Fig. 2. — Number of units n required per process to guarantee a probability of P^* of selecting the better of two binomial processes when the true difference d is at least d^*.
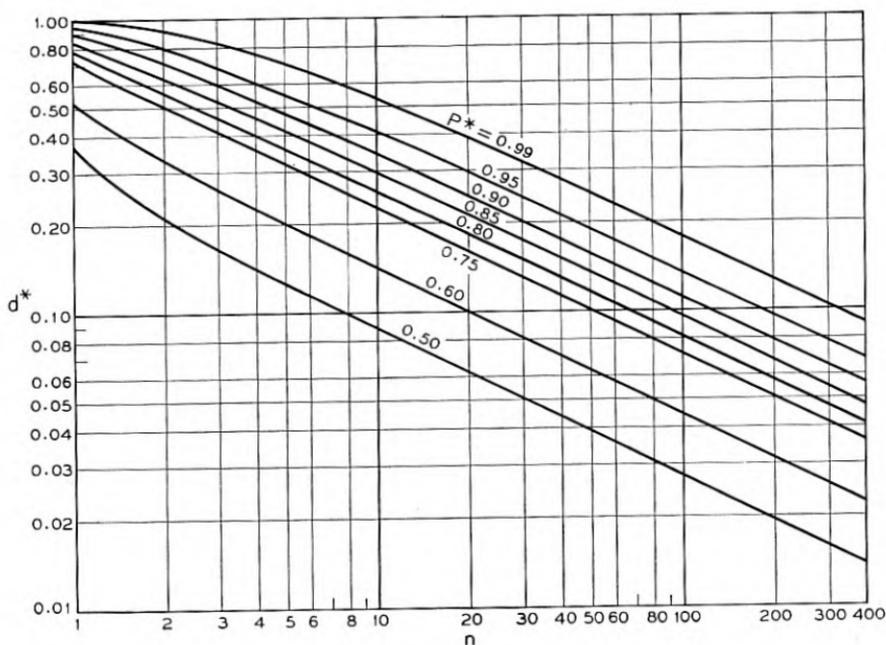

Fig. 3. — Number of units n required per process to guarantee a probability of P^* of selecting the best of three binomial processes when the true difference d is at least d^*.
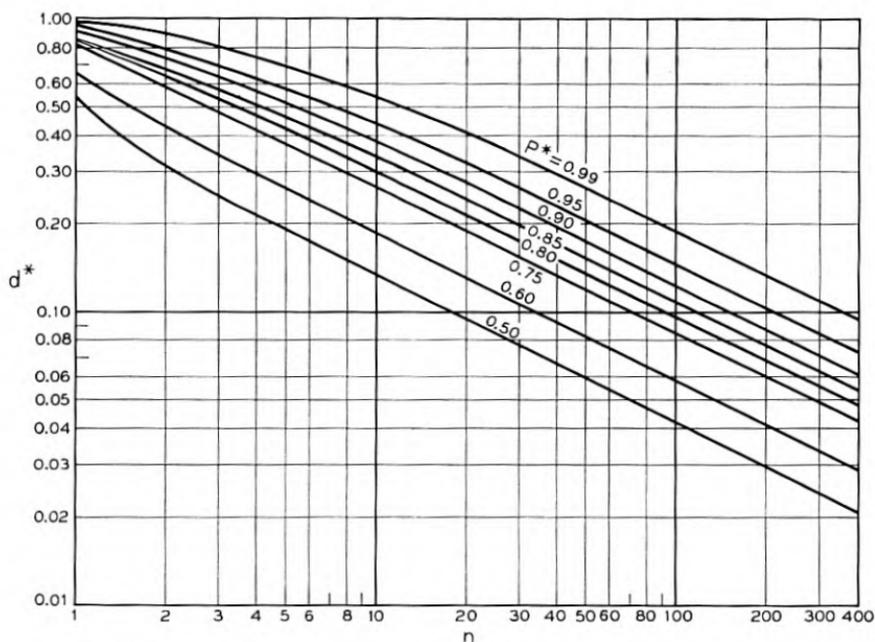
Fig. 4 — Number of units n required per process to guarantee a probability of $P*$ of selecting the best of four bionimal processes when the true difference d is at least $d*$.
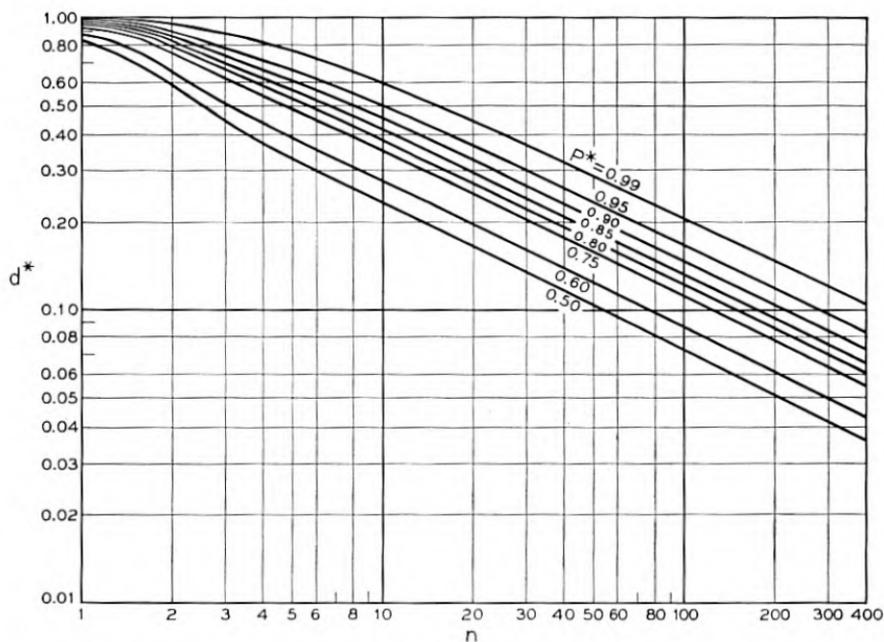

Fig. 5 — Number of units n required per process to guarantee a probability of $P*$ of selecting the best of ten binomial processes when the true difference d is at least $d*$.
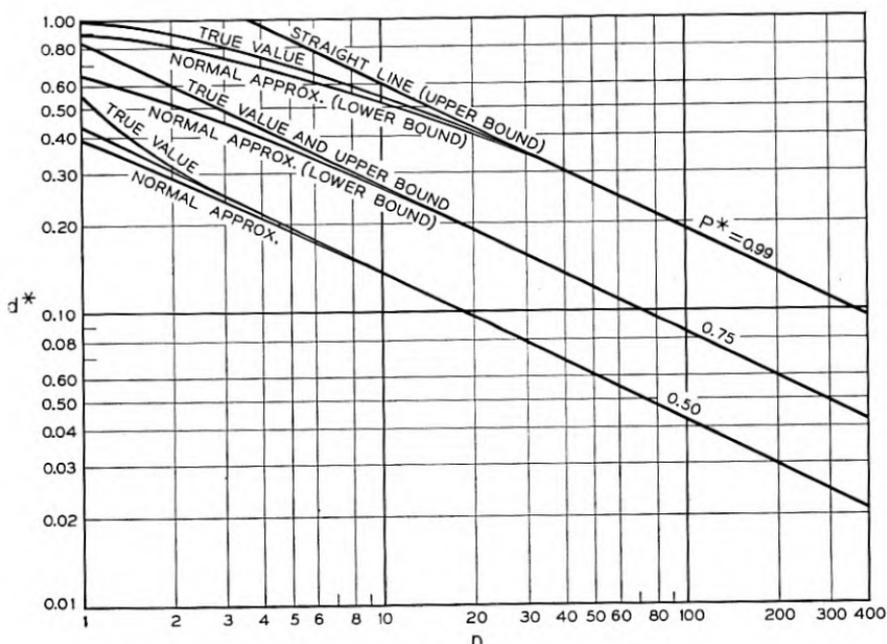
Fig. 6 — Bounds for the number of units n required per process to guarantee a probability of P^* of selecting the best of four binomial processes when the true difference d is at least d^*.

TABLE V — VALUES OF $B = \frac{1}{4}C^2$ TO BE USED WITH THE NORMAL APPROXIMATION (8) WHERE C IS OBTAINED FROM TABLE I OF R. E. BECHHOFER'S PAPER[1]

Prob. of Correct Selection	$k = 2$	$k = 3$	$k = 4$	$k = 10$
0.99	2.7060	3.2712	3.6043	4.5063
0.95	1.3528	1.8362	2.1261	2.9210
0.90	0.8212	1.2434	1.5026	2.2244
0.85	0.5371	0.9099	1.1449	1.7965+
0.80	0.3541	0.6826	0.8961	1.5139
0.75	0.2275−	0.5139	0.7074	1.2811
0.70	0.1375−	0.3832	0.5575−	1.0892
0.65	0.0742	0.2792	0.4347	0.9256
0.60	0.0321	0.1959	0.3325−	0.7832
0.55	0.0079	0.1294	0.2468	0.6569
0.50	0.0000	0.0774	0.1751	0.5438

order of magnitude of the error in our large sample calculations. For example, if $k = 4$, $d^* = 0.05$ and $P^* = 0.90$, then from Table V we find that $B = 1.5026$ and the two expressions in (8) yield 599.54 and 601.04. Hence, it would follow from (9) that n is 600 or 601 or 602. Based on an investigation of the behavior of these two approximations in the case of smaller P^* or larger d^* values, it is estimated that the true value of n is 601. Even if the correct value is 600 or 602 the error would be less than $\frac{1}{6}$ of 1 per cent. Fig. 6 illustrates these bounds on the P_{CS} for $k = 4$, $P^* = 0.50, 0.75$ and 0.99. For $P^* \leq 0.60$ the straight line approximation is a closer lower bound than the normal approximation.

It is estimated that all integer entries in Tables I through IV have an error of at most 1 per cent and, in particular, that all entries under 100 are exact.

OTHER VALUES OF k

In addition to the tables and graphs for $k = 2, 3, 4$ and 10 there are also graphs (Figs. 7 through 14) on which interpolation can be carried out for $k = 5$ through 9 and on which extrapolation can be carried out for $k = 11$ through 100. By plotting n versus log k (or n versus k on semi-log paper) and drawing a straight (dashed) line through the values of n for $k = 4$ and $k = 10$ we obtain results which are remarkably good approximations for $k > 10$. The solid curve in these figures connects the true values obtained for $k = 2, 3, 4$ and 10.

For large values of k the theoretical justification for a straight line approximation is given in Appendix V. In order to check the accuracy of our procedure of drawing the straight line through the values of n computed for $k = 4$ and $k = 10$, we have chosen two points at $k = 101$ for an independent computation of the probability of a correct selection. For $P^* = 0.90$, $d^* = 0.10$ and $k = 101$ the dashed line in Fig. 12 gives n as approximately 400. To check this we computed the normal approximation to the probability P_{CS}^L of a correct selection for the least favorable configuration in the form

$$P_{CS}^L \cong \int_{-\infty}^{\infty} F^{100}(x + h)f(x) \, dx = \frac{1}{\sqrt{n}} \int_{-\infty}^{\infty} F^{100}(x\sqrt{2} + h)e^{-x^2} \, dx \qquad (10)$$

where

$$h = \frac{2d^*\sqrt{n}}{\sqrt{1 - d^{*2}}} \quad (= 4.02015 \text{ in this example}) \qquad (11)$$

$f(x)$ is the normal density and $F(x)$ is its c.d.f. This was computed by a method suggested by Salzer, Zucker and Capuano[3] and the result was
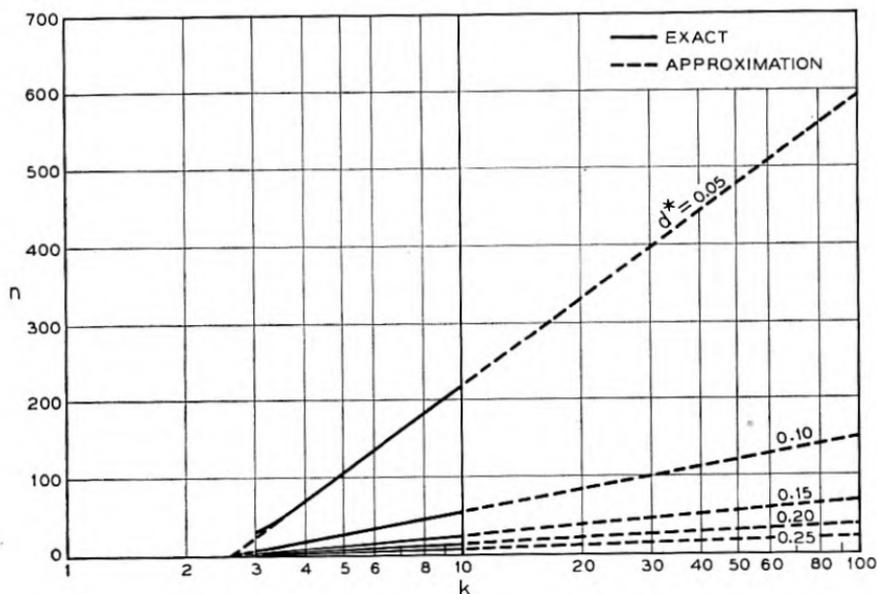
Fig. 7 — Number of units n required per process to guarantee a probability of $P^* = 0.50$ of selecting the best of k binomial processes when the true difference $p_{[1]} - p_{[2]}$ is at least d^*.
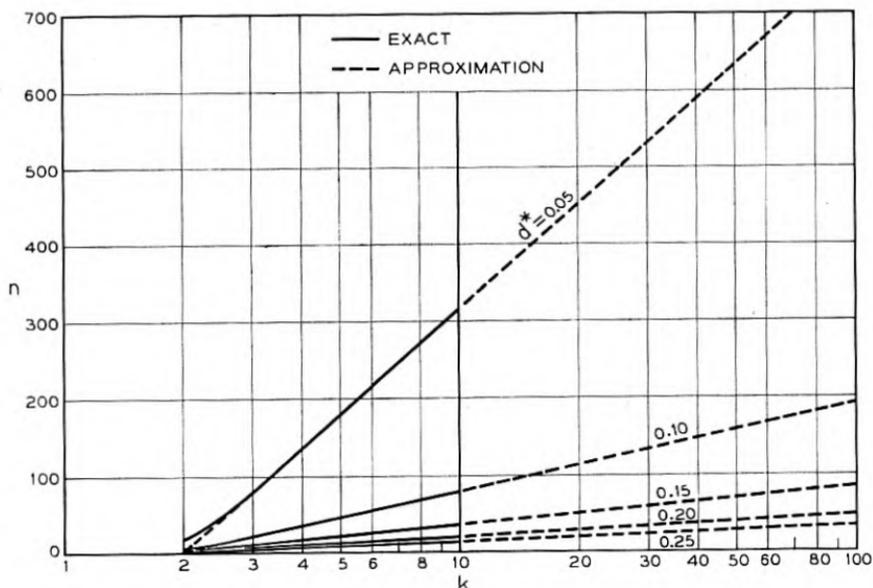
Fig. 8 — Number of units n required per process to guarantee a probability of $P^* = 0.60$ of selecting the best of k binomial processes when the true difference $p_{[1]} - p_{[2]}$ is at least d^*.
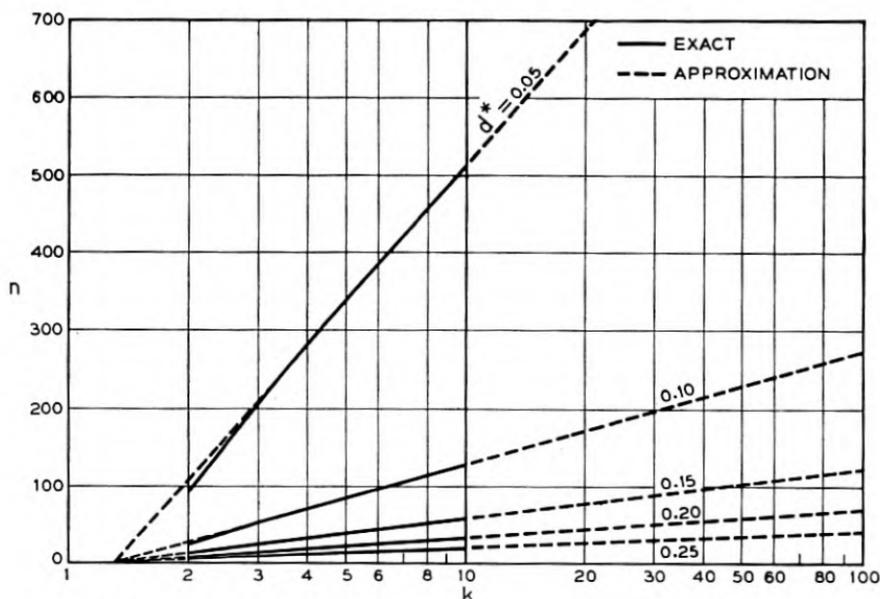
Fig. 9 — Number of units n required per process to guarantee a probability of $P^* = 0.75$ of selecting the best of k binomial processes when the true difference $p_{[1]} - p_{[2]}$ is at least d^*.
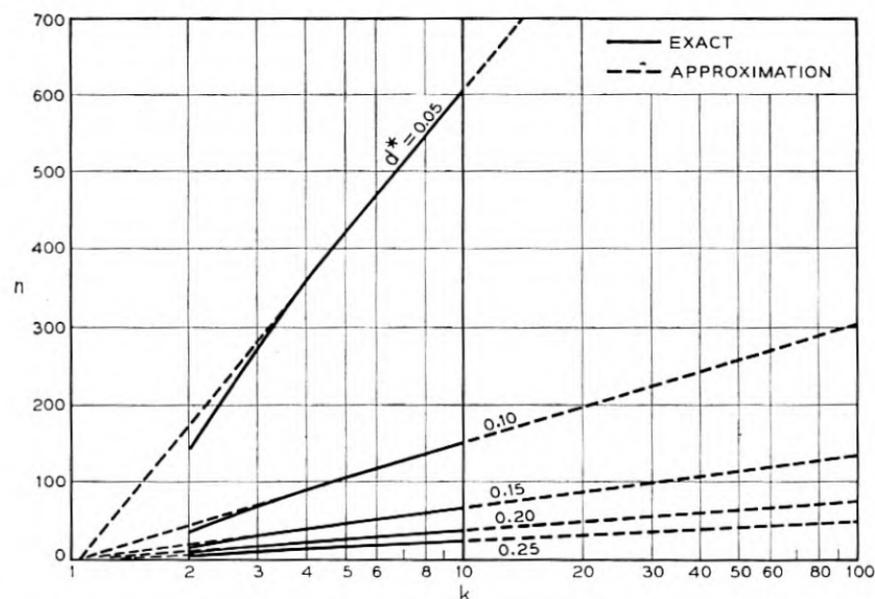

Fig. 10 — Number of units n required per process to guarantee a probability of $P^* = 0.80$ of selecting the best of k binomial processes when the true difference $p_{[1]} - p_{[2]}$ is at least d^*.
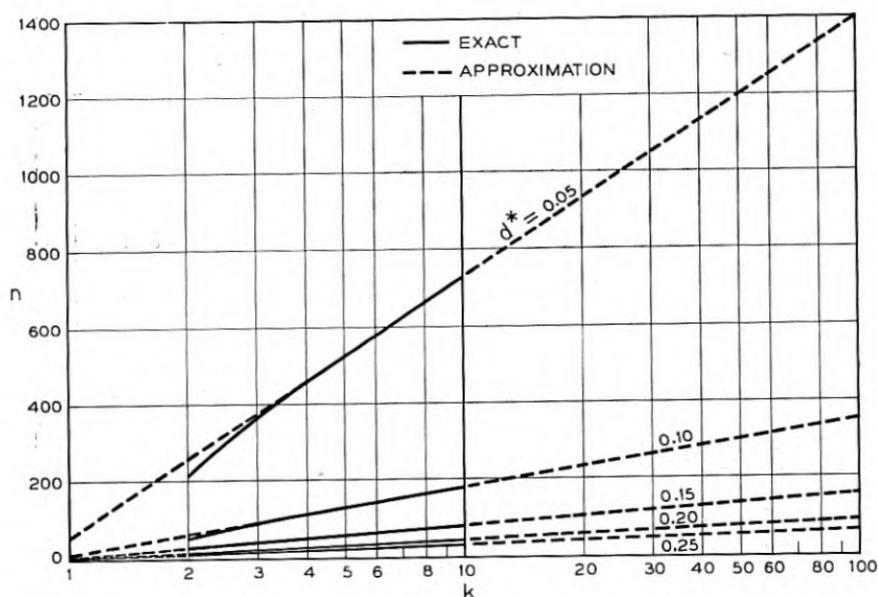
FIG. 11. — Number of units n required per process to guarantee a probability of $P^* = 0.85$ of selecting the best of k binomial processes when the true difference $p_{[1]} - p_{[2]}$ is at least d^*.
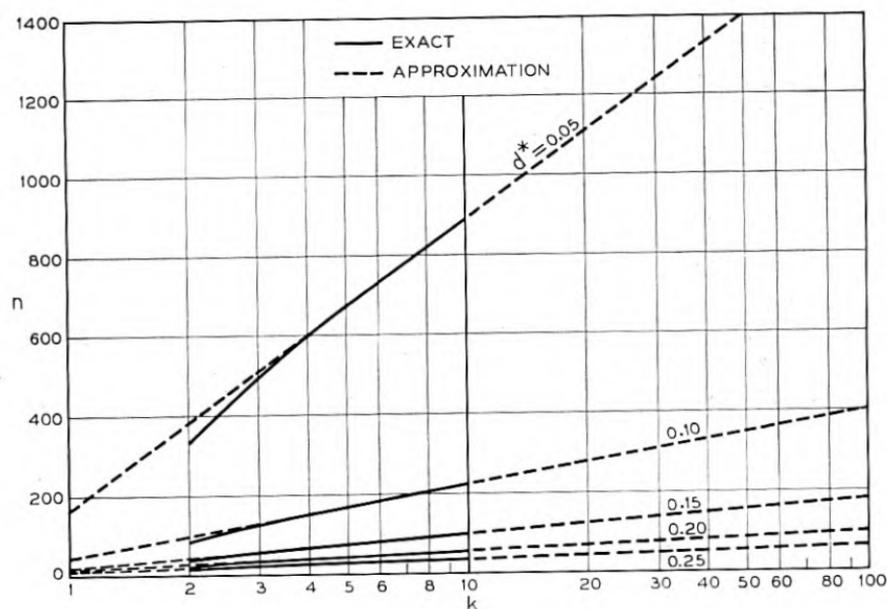

Fig. 12 — Number of units n required per process to guarantee a probability of $P^* = 0.90$ of selecting the best of k binomial processes when the true difference $p_{[1]} - p_{[2]}$ is at least d^*.
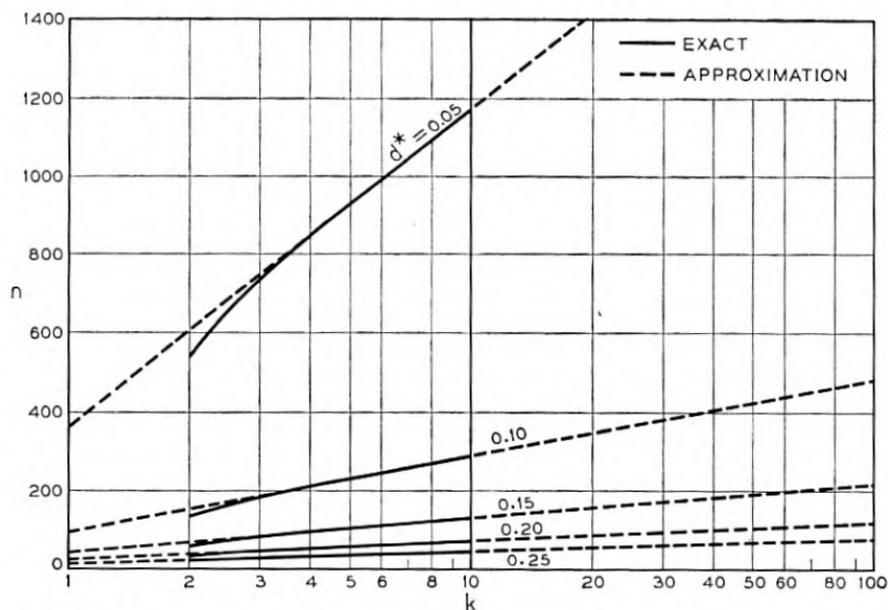
Fig. 13 — Number of units n required per process to guarantee a probability of $P^* = 0.95$ of selecting the best of k binomial processes when the true difference $p_{[1]} - p_{[2]}$ is at least d^*.
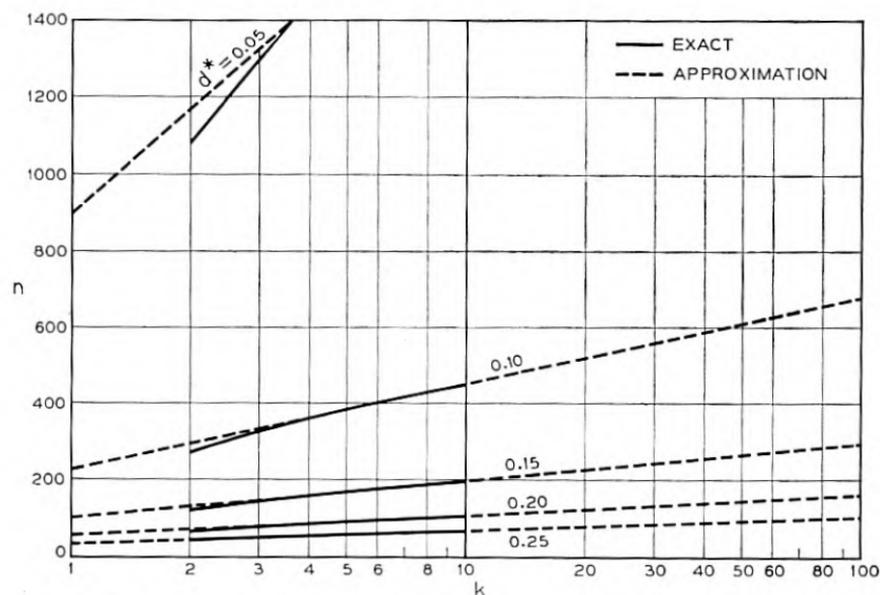

Fig. 14 — Number of units n required per process to guarantee a probability of $P^* = 0.99$ of selecting the best of k binomial processes when the true difference $p_{[1]} - p_{[2]}$ is at least d^*.

$P_{cs}^L \cong 0.9168$ as compared to the value 0.90 in Fig. 12. The expression (10) is derived in Appendix III. Another check was made at $P^* = 0.99$, $d^* = 0.20$ and $k = 101$. The value of n from Fig. 14 is 162. The value of the P_{cs}^L computed from (10) using Salzer, Zucker and Capuano[3] is $0.9925+$.

Further calculation using (10) yielded the more accurate results 378 and 154 instead of 400 and 162, respectively, in the above illustrations. The error in both cases is less than 6 per cent; for smaller values of k the percentage error will, of course, be much less.

For interpolation the results are estimated to be within 1 per cent of the correct value. For example we estimate from Fig. 11 that the required value of n for $k = 5$, $P^* = 0.85$ and $d^* = 0.05$ is 523. This value was computed by the normal approximation and found to be 522.

TIED POPULATIONS

In computing the tables and graphs it was assumed that if two or more populations are tied for first place then one *of these* is selected by a chance device which assigns equal probability to each of them. The experimenter may want to select one of these contenders for first place by economic or other considerations. In most practical problems we may assume that such a selection is at random as far as the probability of a correct selection is concerned. Hence, it appears reasonable to use the tables in this paper without any corrections even when the rule for tied populations is altered in the manner described above.

It is interesting to note that in the yield problem the experimenter may settle the question of ties for first place by taking more observations until the tie is broken. However, in the life-testing problem he may not settle ties by letting the test run beyond time T since the best process for time T is not necessarily the best for a time greater than T.

In some applications when there are two or more populations tied for first place, the experimenter may prefer to recommend all these contenders for first place rather than select one of them by a chance device. In this case we shall agree to call the selection a correct one if the recommended set contains the best population (or, when $p_{[1]} = p_{[2]}$, if the recommended set contains at least one of the best populations). Exact tables for the procedure so altered have not been computed. However, if the value of n is large and this rule for tied populations is used, then the experimenter may reduce the tabled values by an amount equal to the largest integer contained in $1/d^*$. For example, using the above rule for tied populations for the case $k = 2$, $P^* = 0.99$, $d^* = 0.30$, the tabled value 29 can be reduced by 3 giving the result 26.

ALTERNATIVE SPECIFICATION

If the experimenter has some à priori knowledge about the processes, then he will prefer to specify the following *three* quantities in order to determine the number n of observations he is required to take from each process.

> Specification: He specifies $p^*_{[1]}$ and $p^*_{[2]}$ $(0 \leq p^*_{[2]} \leq p^*_{[1]} \leq 1)$ in the neighborhood of his estimate of the probabilities associated with his processes. He also speci-   (12) fies a probability P^* $(0 \leq P^* < 1)$ that he would like to guarantee of making a correct selection whenever the true $p_{[1]} \geq p^*_{[1]}$ and the true $p_{[2]} \leq p^*_{[2]}$.

TABLE VI — NUMBER OF UNITS REQUIRED PER PROCESS TO GUARANTEE A PROBABILITY OF P^* OF SELECTING THE BETTER OF TWO BINOMIAL PROCESSES WHEN THE TRUE $p_{[1]} \geq p^*_{[1]}$ AND THE TRUE $p_{[2]} \leq p^*_{[2]}$. (ALTERNATIVE SPECIFICATION, $k = 2$)

P^*	$p^*_{[1]} = 0.75$ $p^*_{[2]} = 0.60$	$p^*_{[1]} = 0.95$ $p^*_{[2]} = 0.80$	$p^*_{[1]} = 0.90$ $p^*_{[2]} = 0.80$	$p^*_{[1]} = 0.85$ $p^*_{[2]} = 0.80$	$p^*_{[1]} = 0.95$ $p^*_{[2]} = 0.90$
0.50	1	1	1	1	1
0.60	2	2	3	9	6
0.75	10	6	13	53	27
0.80	14	8	19	83	40
0.85	21	11	28	124	60
0.90	32	16	42	189	91
0.95	53	25	68	312	149
0.99	106	49	135	623	298

TABLE VII — NUMBER OF UNITS REQUIRED PER PROCESS TO GUARANTEE A PROBABILITY OF P^* OF SELECTING THE BEST OF FOUR BINOMIAL PROCESSES WHEN THE TRUE $p_{[1]} \geq p^*_{[1]}$ AND THE TRUE $p_{[2]} \leq p^*_{[2]}$. (ALTERNATIVE SPECIFICATION, $k = 4$)

P^*	$p^*_{[1]} = 0.75$ $p^*_{[2]} = 0.60$	$p^*_{[1]} = 0.95$ $p^*_{[2]} = 0.80$	$p^*_{[1]} = 0.90$ $p^*_{[2]} = 0.80$	$p^*_{[1]} = 0.85$ $p^*_{[2]} = 0.80$	$p^*_{[1]} = 0.95$ $p^*_{[2]} = 0.90$
0.50	7	4	10	42	21
0.60	14	8	18	79	39
0.75	28	14	37	168	80
0.80	35	18	46	211	101
0.85	45	22	59	268	128
0.90	59	28	77	350	171
0.95	83	39	107	493	239
0.99	139	65	182	831	399

Again we can rewrite the specification that the experimenter wants to satisfy in the simple form

$$P_{cs} \geqq P^* \quad \text{for} \quad p_{[1]} \geqq p_{[1]}^* \quad \text{and} \quad p_{[2]} \leqq p_{[2]}^* \tag{13}$$

Tables VI and VII give the number of observations required per process for several selected triplets of specified constants $(p_{[1]}^*, p_{[2]}^*, P^*)$ when $k = 2$ and $k = 4$. These results are also given in graphical form in Figs. 15 and 16.
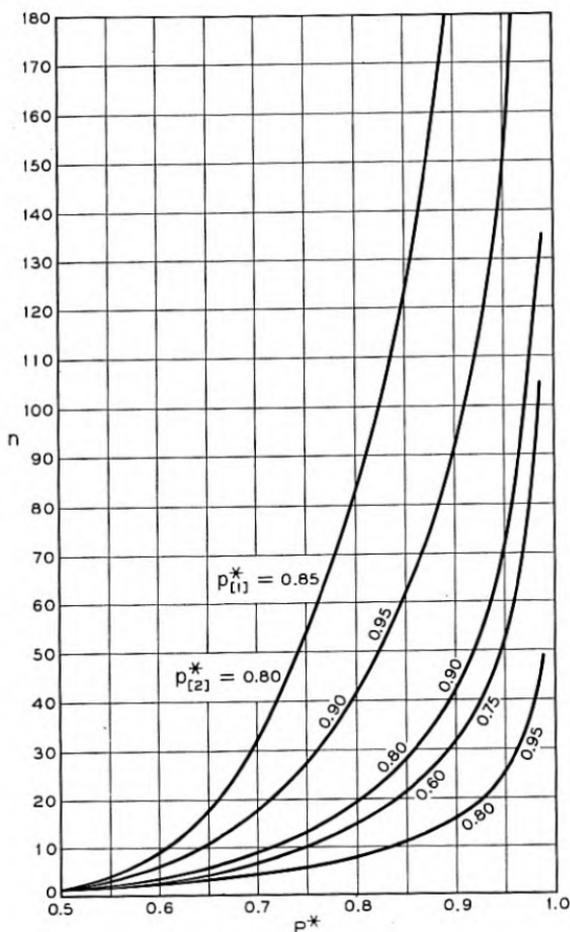

Fig. 15 — Number of units required per process to guarantee a probability of P^* of selecting the better of two binomial processes when the true $p_{[1]} \geqq p_{[1]}^*$ and the true $p_{[2]} \leqq p_{[2]}^*$.

For example, on the basis of past experience the experimenter may estimate that the probabilities associated with his $k = 4$ processes are all in the neighborhood of 0.60. This constitutes his à priori knowledge. He may then decide that he would like to make a correct selection with probability $P^* = 0.85$ when the best process has a yield of at least 75 per cent and all the others have a yield of at most 60 per cent. Entering column 1 of Table VII we find that $n = 45$ observations per process are required.

It is much more difficult to furnish tables for the alternative specifica-
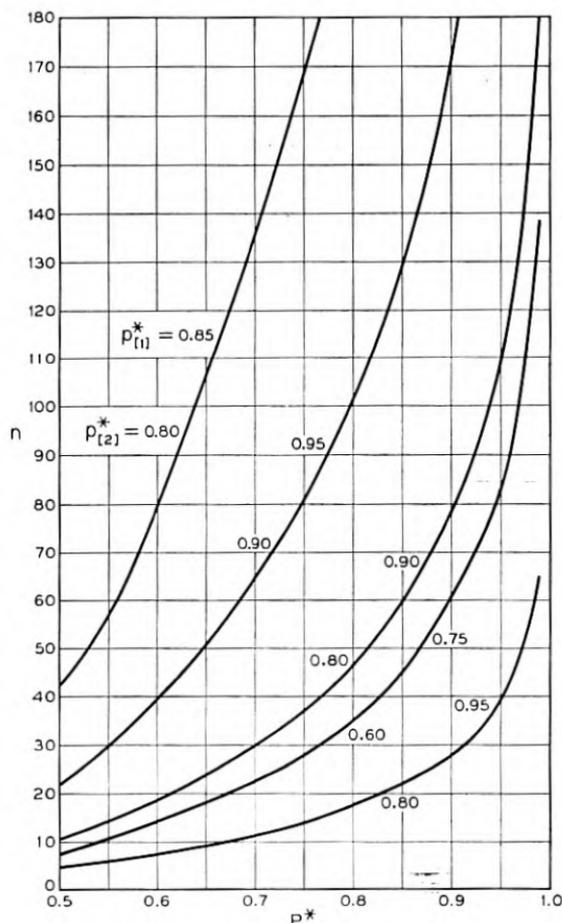

Fig. 16 — Number of units required per process to guarantee a probability of P^* of selecting the best of four binomial processes when the true $p_{[1]} \geq p^*_{[1]}$ and the true $p_{[2]} \leq p^*_{[2]}$.

tion since there is an extra parameter to vary and the appropriate tables for the normal approximation are not available.

In the computation of these probabilities the least favorable configuration

$$p_{[1]} = p_{[1]}^* \quad \text{and} \quad p_{[2]}^* = p_{[2]} = p_{[3]} = \cdots = p_{[k]} \tag{14}$$

was used. It follows from Appendix II that if the probability of a correct selection is at least P^* when (14) holds, then it will also be at least P^* when

$$p_{[1]} \geqq p_{[1]}^* \quad \text{and} \quad p_{[2]}^* \geqq p_{[2]} \geqq p_{[3]} \geqq \cdots \geqq p_{[k]} \tag{15}$$

For small values of n, exact calculations were carried out. A typical exact calculation is shown in Appendix IV. The approximations used for large n are given in Appendix III.
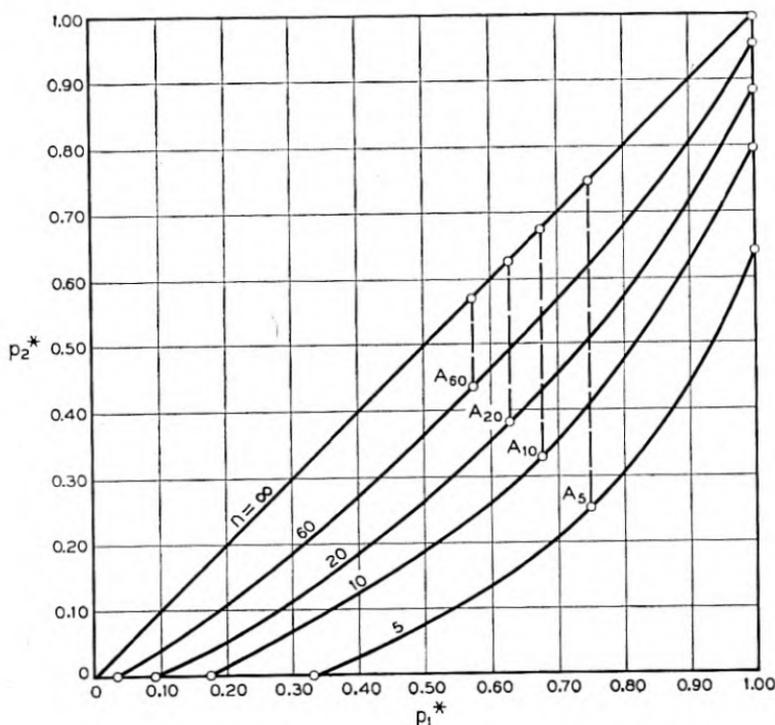

Fig. 17 — Illustration of the varying zones of indifference and the least favorable configuration for $k = 4$ and $P^* = 0.85$. (For $n \geqq 5$ the longest vertical segment occurs at the point A_n where the abcissa and the ordinate are symmetrical about 0.5)

COMPARISON OF THE TWO SPECIFICATIONS

It should be pointed out that for a given k the same value of n would satisfy the specification for different specified triplets

$$P^*, \; p_{[1]}^*, \; p_{[2]}^*$$

For example with $k = 4$, $P^* = 0.85$ and n fixed we could vary $p_{[1]}^*$ in the alternative specification and compute for each $p_{[1]}^*$ the corresponding largest value of $p_{[2]}^*$ such that the specification $(P^*, p_{[1]}^*, p_{[2]}^*)$ is satisfied. This is shown in Fig. 17 for $n = 5, 10, 20$ and 60. The vertical distance in Fig. 17 between the appropriate curve and the 45° line $(n = \infty)$ is the length of the indifference zone $(p_{[1]}^*, p_{[2]}^*)$. The indifference zone widens in the center and narrows at both ends. In fact we find just as in the original specification that for n greater than (say) 4 the indifference zone is widest when $p_{[1]}^*$ and $p_{[2]}^*$ are symmetrical about 0.5. It is clear that the two specifications would coincide if we took d^* in the original specification and set $p_{[1]}^* = \frac{1}{2}(1 + d^*)$, $p_{[2]}^* = \frac{1}{2}(1 - d^*)$
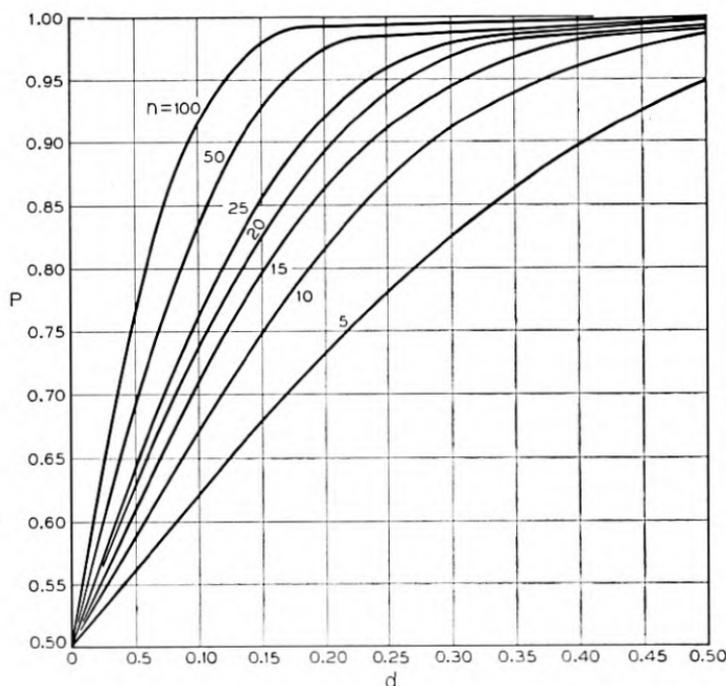
Fig. 18 — Probability of a correct selection as a function of the true difference $d = p_{[1]} - p_{[2]}$ under the least favorable configuration for $k = 2$ and selected values of n.

in the alternative specification. We shall be interested in comparing the alternative specification $(P^*, p^*_{[1]}, p^*_{[2]})$ with the original specification with the same P^* and with d^* set equal to $p^*_{[1]} - p^*_{[2]}$. It is clear that the value of n required for the original specification will always be larger.

The original specification is simpler and is preferable to the alternative specification when little or nothing is known about the processes on test, but the price that has to be paid for ignorance is an increase in the
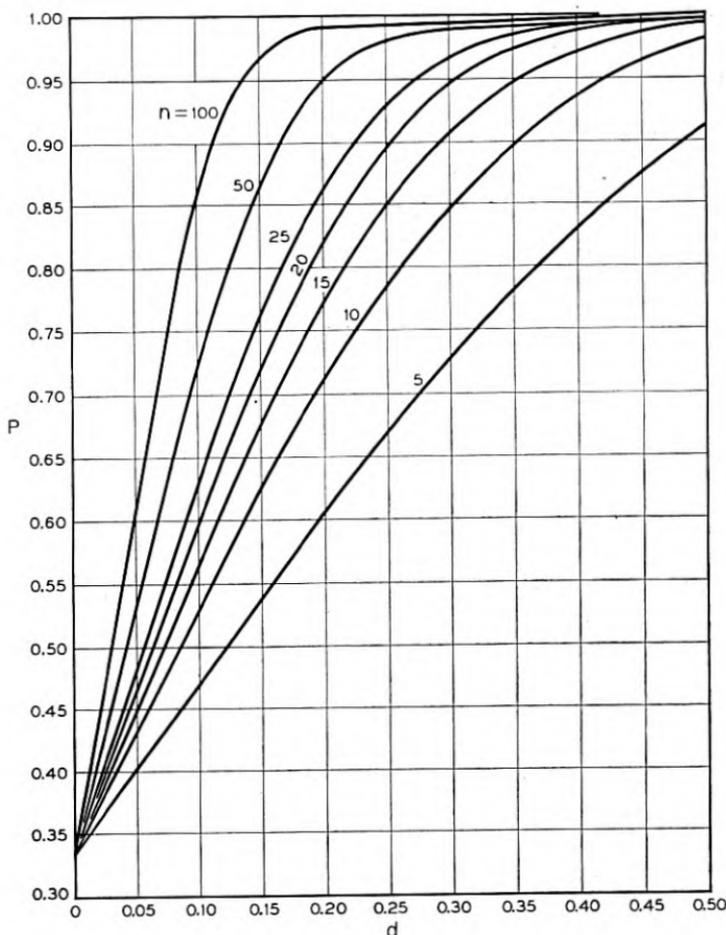
Fig. 19 — Probability of a correct selection as a function of the true difference $d = p_{[1]} - p_{[2]}$ under the least favorable configuration for $k = 3$ and selected values of n.

required number of observations. In the example of the preceding section the value of n required for the alternative specification is 45 as compared to 51 observations per process required to satisfy the original specification with the same P^* and with $d^* = p^*_{[1]} - p^*_{[2]}$. Here the saving is only moderate. The saving will be much larger if $p^*_{[1]}$ and
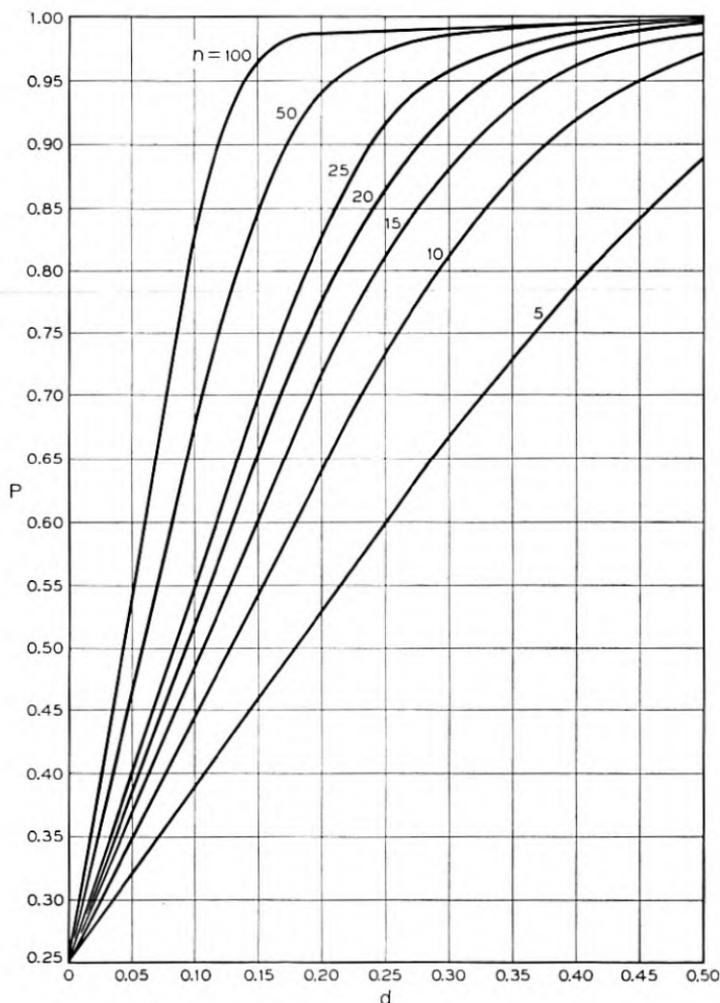

Fig. 20 — Probability of a correct selection as a function of the true difference $d = p_{[1]} - p_{[2]}$ under the least favorable configuration for $k = 4$ and selected values of n.

$p_{[2]}^*$ are further from 0.5 and d^* is small. For example, for $k = 4$, $P^* = 0.95$, $p_{[1]}^* = 0.95$ and $p_{[2]}^* = 0.90$ the value of n required for the alternative specification is 239 as compared to 850 observations per process required to satisfy the original specification with the same P^* and with $d^* = 0.05$. The alternative specification is justified on the basis of à priori or previous information about the approximate values of the p's.

REVERSING THE TABLES

The experimenter may wish to use the tables of this paper in reverse. For example, if n is fixed and d^* is specified by the experimenter, then by using the appropriate table he can find the probability of a correct selection that is guaranteed for $d \geqq d^*$; i.e., a greatest lower bound to the probability of a correct selection for $d \geqq d^*$. This process of reversing the given values and the values to be computed can most easily be carried out on graphs. For example, the above problem of finding the guaranteed probability of a correct selection given d^* and n is most easily carried out on Figs. 18, 19, and 20.

APPENDIX I

MODIFICATION OF THE ORIGINAL SPECIFICATION

The same value of n will, of course, satisfy the specification for different pairs of specified values (d^*, P^*). From a purely mathematical point of view it is not necessary that d^* should be the *smallest* difference for which the experimenter desires to make a correct selection. For example, if $k = 3$ the experimenter could specify any one of the four pairs (0.10, 0.60), (0.25, 0.90), (0.30, 0.95) or (0.40, 0.99) and obtain the same result, namely $n = 20$. The experimenter may prefer to specify the *curve* or set of points corresponding to a fixed n. Several such curves are given in Figs. 18, 19, and 20 for $k = 2$, 3, and 4, respectively. The experimenter would decide in advance on some property of the curve that he considers desirable and from the appropriate figure he could find the curve with the smallest n-value that satisfies the desired property.

The main point of the above paragraph is to point out that the original specification in the body of the paper is one particular way, but not the only way, of stating a specification that will determine a value of n. The only criterion for a good way to state the specification is that the experimenter should be able to bring his best judgment (or best guesses) to bear on the quantities that have to be specified in advance.

APPENDIX II

MONOTONICITY PROPERTIES

We shall prove that for any fixed d $(0 \leq d \leq 1)$ the probability P_{cs} of a correct selection is smaller for the configuration:

$$p_{[1]} - d = p_{[2]} = p_{[3]} = \cdots = p_{[k]} \qquad \text{(A1)}$$

than for any configuration given by

$$p_{[1]} - d \geq p_{[2]} \geq p_{[3]} \geq \cdots \geq p_{[k]} \qquad \text{(A2)}$$

where $p_{[1]}$ is considered fixed and the $p_{[i]}$ $(i \geq 2)$ are variables. In other words, for fixed $p_{[1]}$ the probability P_{cs} is a strictly increasing function of each of the differences

$$p_{[1]} - p_{[i]} \qquad (i \geq 2)$$

We shall need the following lemma.

Lemma 1: For any pair of integers x, n $(0 \leq x \leq n)$ and any θ $(0 \leq \theta \leq 1)$, not depending on p, the function

$$H(x; p, \theta) = \sum_{j=0}^{x-1} C_j{}^n p^j (1 - p)^{n-j} + \theta C_x{}^n p^x (1 - p)^{n-x} \qquad \text{(A3)}$$

is a decreasing function of p over the unit interval $(0 \leq p \leq 1)$. Moreover, it is strictly decreasing unless $(x = 0$ and $\theta = 0)$ or $(x = n$ and $\theta = 1)$.

Proof: Differentiating (A3) with respect to p gives after telescoping terms

$$(\theta - 1)x C_x{}^n p^{x-1}(1 - p)^{n-x} - \theta(n - x)C_x{}^n p^x (1 - p)^{n-x-1} \qquad \text{(A4)}$$

which is negative for $0 < p < 1$ unless $(x = 0$ and $\theta = 0)$ or $(x = n$ and $\theta = 1)$. Since H is continuous in p at $p = 0$ and $p = 1$ the lemma follows.

Let $X_{(i)}$ denote the chance number of successes that arises from the binomial process associated with

$$p_{[i]} \qquad (i = 1, 2, \cdots, n)$$

the value of the integer n is assumed to be fixed throughout this discussion and it will usually not be listed as an argument. The probability P_{cs} of a correct selection for any configuration with $p_{[1]} > p_{[2]}$ is given by the expression on the top of the next page.

$$P_{cs} = P\{X_{(i)} < X_{(1)} \quad \text{for} \quad i \geq 2\} + \tfrac{1}{2} \sum_{\alpha=2}^{k} P\{X_{(\alpha)} = X_{(1)} \quad \text{and}$$

$$X_{(i)} < X_{(1)} \quad \text{for } i \geq 2, i \neq \alpha\} + \cdots \tag{A5}$$

$$+ \frac{1}{k} P\{X_{(1)} = X_{(2)} = \cdots = X_{(k)}\}$$

It will be necessary to write the P_{cs} for any configuration with $p_{[1]} > p_{[2]}$ in another form which is more useful for the purpose at hand. Corresponding to any binomial chance variable X (which takes on integer values from 0 to n) we define a "Continuous Binomial" chance variable Y by letting Y be *uniformly* distributed in the interval $(j - \tfrac{1}{2}, j + \tfrac{1}{2})$ with the same total probability in this interval as the ordinary binomial assigns to the integer j, namely

$$C_j{}^n p^j (1 - p)^{n-j} \qquad (j = 0, 1, \cdots, n)$$

We will now show that the probability P_{cs} of a correct selection is unaltered if we replace each of the k discrete binomials by its corresponding continuous binomial. Let $Y_{(i)}$ denote the continuous binomial (CB) chance variable associated with $p_{[i]}$ and let $y_{(i)}$ denote any value it can take on. Let $X_{(i)}$ denote the nearest integer to $Y_{(i)}$ and let $x_{(i)}$ denote the nearest integer to $y_{(i)}$ $(i = 1, 2, \cdots, k)$. Then $X_{(i)}$ is a discrete binomial (DB) with the same parameters $(p_{[i]}, n)$. Let

$$g(x, p) = C_x{}^n p^x (1 - p)^{n-x} \qquad (x = 0, 1, \cdots, n)$$

Then the *density* $g(y, p)$ of the continuous binomial (disregarding the half-integers) is given by $g(y, p) = g(x, p)$ where x is the nearest integer to y.

For two continuous binomials (i.e., $k = 2$) the probability P_{cs} of a correct selection for any configuration with $p_{[1]} > p_{[2]}$ is given by

$$P_{cs}(CB) = \int_{-1/2}^{n+1/2} P\{Y_{(2)} < y_{(1)}\} g(y_{(1)}; p_{[1]}) \, dy_{(1)} \tag{A6}$$

$$= \sum_{x_{(1)}=0}^{n} \int_{x_{(1)}-1/2}^{x_{(1)}+1/2} P\{Y_{(2)} < y_{(1)}\} g(y_{(1)}; p_{[1]}) \, dy_{(1)} \tag{A7}$$

Within any interval $(x_{(1)} - \tfrac{1}{2}, x_{(1)} + \tfrac{1}{2})$ we have

$$P\{Y_{(2)} < y_{(1)}\} = P\{X_{(2)} < x_{(1)}\}$$

$$+ P\{X_{(2)} = x_{(1)}\} P\{Y_{(1)} < y_{(1)} \mid X_{(2)} = x_{(1)}\} \tag{A8}$$

$$= P\{X_{(2)} < x_{(1)}\} + \tfrac{1}{2} P\{X_{(2)} = x_{(1)}\} \tag{A9}$$

which depends only on $x_{(1)}$. Hence from (A7)

$P_{CS}(CB)$

$$= \sum_{x_{(1)}=0}^{n} [P\{X_{(2)} < x_{(1)}\} + \tfrac{1}{2}P\{X_{(2)} = x_{(1)}\}]P\{X_{(1)} = x_{(1)}\} \quad \text{(A10)}$$

$$= P\{X_{(2)} < X_{(1)}\} + \tfrac{1}{2}P\{X_{(2)} = X_{(1)}\} \quad \text{(A11)}$$

$$= P_{CS}(DB) \quad \text{(A12)}$$

The above is easily generalized to hold for any $k > 2$. The details of this generalization are omitted. For general k this equality holds not only for the important special case $p_{[1]} > p_{[2]}$ but also for the more general case (2) for any $t < k$. Since the latter result is not needed here, the proof is omitted.

If we let $G(y;p)$ denote the c.d.f. of the continuous binomial then lemma 1 can be restated in the following form.

Lemma 2: For any integer n and any y, the function $G(y;p)$ is a non-increasing function of p. In particular, for $-\tfrac{1}{2} < y < n + \tfrac{1}{2}$ it is a strictly decreasing function of p.

Proof: For any y, set $x = x(y)$ and $\theta = \theta(y)$ equal to the integer part and the fractional part of $(y + \tfrac{1}{2})$, respectively. Then for any y we have the identity in p

$$G(y;p) \equiv H(x;p, \theta) \qquad (0 \leq p \leq 1) \quad \text{(A13)}$$

For any y_0 such that $-\tfrac{1}{2} < y_0 < n + \tfrac{1}{2}$ we have $0 \leq x(y_0) \leq n$ and $0 \leq \theta(y_0) \leq 1$. The inverse function $y(x,\theta) = x + \theta - \tfrac{1}{2}$ is a *single-valued* function of the pair (x,θ); the two particular pairs $(0,0)$ and $(n,1)$ correspond to the *unique* values $y = -\tfrac{1}{2}$ and $y = n + \tfrac{1}{2}$, respectively. Hence the pair $[x(y_0), \theta(y_0)]$ must be different from these two particular pairs above since it corresponds *only* to y_0 which is in the *interior* of the interval $(-\tfrac{1}{2}, n + \tfrac{1}{2})$. Lemma 2 then follows from lemma 1 and the fact that $G(y;p)$ is identically zero in p for $y \leq -\tfrac{1}{2}$ and identically one in p for $y \geq n + \tfrac{1}{2}$.

The probability P_{CS} of a correct selection for k discrete or k continuous binomials for any configuration with $p_{[1]} > p_{[2]}$ can now be written as

$$P_{CS} = \int_{-1/2}^{n+1/2} \left[\prod_{i=2}^{k} P\{Y_{(i)} < y_{(1)}\} \right] g(y_{(1)} ; p_{[1]}) \, dy_{(1)} \quad \text{(A14)}$$

$$= \int_{-1/2}^{n+1/2} \left[\prod_{i=2}^{k} G(y;p_{[i]}) \right] g(y;p_{[1]}) \, dy. \quad \text{(A15)}$$

Clearly if any one or more of the $p_{[i]}$ $(i \geq 2)$ decreases, holding $p_{[1]}$ fixed, then it follows from lemma 2 that the right member of (A15) is

strictly increasing, i.e., for fixed $p_{[1]}$ the P_{cs} is a strictly increasing function of each of the differences $p_{[1]} - p_{[i]}$ ($i \geqq 2$) as was to be shown.

It follows from the above result that in searching for a least favorable configuration among all those in which the experimenter wants his specification satisfied we may restrict our attention to those of the form (A1). Moreover, we may set d in (A1) equal to d^* since, for $d > d^*$ and fixed $p_{[1]}$, the difference $d - d^*$ may be added to each $p_{[i]}$ ($i \geqq 2$) and the probability of a correct selection is increased. Then (A15) reduces to

$$P_{cs} = \int_{-1/2}^{n+1/2} G^{k-1}(y;p_{[1]} - d^*)g(y;p_{[1]}) \, dy \tag{A16}$$

It was shown in the section on the least favorable configuration that there is a value $p_{[1]}^{L}$ of $p_{[1]}$ which when substituted in (A16) gives the minimum value P_{cs}^{L} of P_{cs}.

We can now prove the following result in which $p_{[1]}$ is not fixed. For any specified pair $p_{[2]}^* \leqq p_{[1]}^*$ the probability P_{cs} of a correct selection is smaller for the configuration

$$p_{[1]} = p_{[1]}^* ; \qquad p_{[2]}^* = p_{[2]} = p_{[3]} = \cdots = p_{[k]} \tag{A17}$$

than for any configuration given by

$$p_{[1]} \geqq p_{[1]}^* ; \qquad p_{[2]}^* \geqq p_{[2]} \geqq p_{[3]} \geqq \cdots \geqq p_{[k]} \tag{A18}$$

This is shown by considering two separate steps.

The first step is to increase $p_{[1]}$ holding all the other p's fixed at $p_{[2]}^*$. For any arbitrary set of values of $p_{[i]}$ with $p_{[1]} > p_{[2]}$ the probability of a correct selection can be written as

$$P_{cs} = \sum_{j=2}^{k} \int_{-1/2}^{n+1/2} \left[\prod_{i=2, \ i\neq j}^{k} G(y,p_{[i]}) \right] [1 - G(y,p_{[1]})]g(y,p_{[j]}) \, dy \tag{A19}$$

by adding the probabilities that

$$Y_{(1)} > Y_{(j)} > \min \{ Y_{(2)} , \cdots , Y_{(j-1)} , Y_{(j+1)} , \cdots , Y_{(k)} \}$$

for

$$j = 2, 3, \cdots , k$$

For

$$p_{[1]} > p_{[2]} = p_{[3]} = \cdots = p_{[k]} = p_{[2]}^*$$

this reduces to

$$P_{cs} = (k - 1) \int_{-1/2}^{n+1/2} [1 - G(y;p_{[1]})]G^{k-2}(y;p_{[2]}^*)g(y,p_{[2]}^*) \, dy \tag{A20}$$

This result can also be obtained by starting with (A16) with

$$p_{[2]} = \cdots = p_{[k]} = p_{[1]} - d^* = p_{[2]}^*$$

and integrating by parts. It is clear from (A20) that for fixed $p_{[i]}$ ($i \geq 2$) the P_{cs} is an increasing function of $p_{[1]}$ and is indeed strictly increasing for $p_{[1]}$ in the unit interval.

The second step is to hold $p_{[1]}$ fixed and to decrease the values of $p_{[i]}$ ($i \geq 2$). This increases the probability of a correct selection by our previous result above. This proves the monotonicity property for the alternative specification.

APPENDIX III

LARGE SAMPLE THEORY — ORIGINAL SPECIFICATION

For $p_{[1]} > p_{[2]}$ the probability of a correct selection satisfies the inequalities

$$P\{X_{(1)} > X_{(i)} \ (i = 2, 3, \cdots, k)\} < P_{cs}$$
$$< P\{X_{(1)} \geq X_{(i)} \ (i = 2, 3, \cdots, k)\} \qquad \text{(A21)}$$

unless $p_{[1]} = 1$ *and* $p_{[2]} = 0$ in which case equality signs hold since the three quantities above are all unity. Letting $q_{[1]} = 1 - p_{[1]}$, we can write the left member of (A21) as

$$P\left\{Z_i > \frac{- d^* \sqrt{n}}{\sqrt{p_{[1]}q_{[1]} + (p_{[1]} - d^*)(q_{[1]} + d^*)}} \ (i = 1, 2, \cdots, k - 1)\right\}$$
$$\text{(A22)}$$

where

$$Z_i = \frac{X_{(1)} - X_{(i+1)} - nd^*}{\sqrt{n[p_{[1]}q_{[1]} + (p_{[1]} - d^*)(q_{[1]} + d^*)]}} \ (i = 1, 2, \cdots, k - 1)$$
$$\text{(A23)}$$

For the configuration (A1) with $d = d^*$ the chance variables Z_i tend to normal chance variables $N(0,1)$ with zero mean and unit variance as $n \to \infty$. We have purposely omitted any continuity correction in (A22) in order to get a better approximation for the smaller values of n.

To derive the least favorable configuration for large n we can restrict our attention to those configurations given by (A1) with $d = d^*$. The quantity $p_{[1]}^L$, which minimizes (A22), is obtained by maximizing the expression in (A22)

$$Q(p) = p(1 - p) + (p - d^*)(1 - p + d^*) \qquad \text{(A24)}$$
$$= -2p^2 + 2(1 + d^*)p - d^*(1 + d^*) \qquad \text{(A25)}$$

The derivative of $Q(p)$ vanishes at

$$p_{[1]}^L = \tfrac{1}{2}(1 + d^*); \qquad q_{[1]}^L = \tfrac{1}{2}(1 - d^*) \tag{A26}$$

which gives the symmetric configuration. Clearly this value of p gives to $Q(p)$ its maximum value, $\tfrac{1}{2}(1 - d^{*2})$. This proves that the symmetrical configuration is least favorable in the limit as $n \to \infty$.

Under the configuration (A1) with $d = d^*$ and $n \to \infty$ the distribution of the chance variables Z_i $(i = 1, 2, \cdots, k - 1)$ approaches a joint multivariate normal distribution with zero means, unit variances and correlations given by

$$\rho(Z_i Z_j) = \frac{p_{[1]} q_{[1]}}{p_{[1]} q_{[1]} + (p_{[1]} - d^*)(q_{[1]} + d^*)} \qquad (i \neq j) \tag{A27}$$

which do not depend on n. For the symmetric configuration this reduces to the simple form

$$\rho(Z_i Z_j) = \tfrac{1}{2} \qquad (i \neq j). \tag{A28}$$

This is precisely the case which arises in [1] and consequently the tables in [1] can be used for our problem when (the answer) n is large. The constants $C = C(P^*, k)$ tabulated in [1] solve the equation

$$P\left\{ Z_i > -\frac{C}{\sqrt{2}} (i = 1, 2, \cdots, k - 1) \right\} = P^* \tag{A29}$$

for standard normal chance variables Z_i satisfying (A28). If we equate $C/\sqrt{2}$ and the corresponding member of (A22), then we obtain for the symmetric configuration

$$\frac{C}{\sqrt{2}} \cong \frac{d^* \sqrt{n}}{\sqrt{\dfrac{1}{2}(1 - d^{*2})}} \tag{A30}$$

or solving for n and letting $B = \tfrac{1}{4}C^2$ this yields the large sample normal approximation

$$n \cong \frac{B}{d^{*2}}(1 - d^{*2}) \tag{A31}$$

Since d^* is usually small when n is large and since the solution in (A31) is usually somewhat smaller than the true value, then it is of interest to examine the simpler approximation

$$n \cong \frac{B}{d^{*2}} \tag{A32}$$

which is greater than the result in (A31). This is called the straight line approximation since it plots as a straight line on log-log paper as shown

in Figs. 2 through 5. As $d^* \to 0$ both the normal approximation and the true value are asymptotically equivalent to the straight line approximation.

The normal approximation to the probability of a correct selection can also be written in another form similar to (A16) which is actually more useful for numerical calculations. The left member of (A21) can be written as

$$\sum_{w_1} \left[\prod_{i=2}^{k-1} P \left\{ W_i \right. \right.$$
$$\left. \left. < \frac{W_1 \sqrt{p_{[1]}q_{[1]}} + (p_{[1]} - p_{[i]}) \sqrt{n}}{\sqrt{p_{[i]}q_{[i]}}} \right\} \right] P \{W_1 = w_1\} \qquad \text{(A33)}$$

where

$$W_i = \frac{X_{(i)} - np_{[i]}}{\sqrt{np_{[i]}q_{[i]}}} \qquad (i = 1, 2, \cdots, k) \quad \text{(A34)}$$

and w_1 is the same function of $x_{(1)}$ as W_1 is of $X_{(1)}$. The outside summation in (A33) is over the values taken on by w_1 as $x_{(1)}$ runs from 0 to n. As $n \to \infty$ the expression in (A33) approaches

$$P_{cs} \cong \int_{-\infty}^{\infty} \left[\prod_{i=2}^{k-1} F \left(\frac{w \sqrt{p_{[1]}q_{[1]}} + (p_{[1]} - p_{[i]}) \sqrt{n}}{\sqrt{p_{[i]}q_{[i]}}} \right) \right] f(w) \, dw \quad \text{(A35)}$$

where $f(t)$ is the standard normal density and $F(t)$ is the standard normal c.d.f. For the symmetric configuration, which is least favorable for large n, (A35) reduces to

$$P_{cs}^L \cong \int_{-\infty}^{\infty} F^{k-1} \left(w + \frac{2d^* \sqrt{n}}{\sqrt{1 - d^{*2}}} \right) f(w) \, dw \qquad \text{(A36)}$$

A straightforward integration by parts gives the alternative form

$$P_{cs}^L \cong (k - 1) \int_{-\infty}^{\infty} \left[1 - F \left(w - \frac{2d^* \sqrt{n}}{\sqrt{1 - d^{*2}}} \right) \right] F^{k-2}(w) f(w) \, dw \quad \text{(A37)}$$

which corresponds to (A20).

A simple method for computing such integrals based on Hermite polynomials is described by Salzer, Zucker, and Capuano.[3]

LARGE SAMPLE THEORY — ALTERNATIVE SPECIFICATION

The expression corresponding to (A22) for the alternative specification is

$$P \left\{ Z_i > \frac{- (p_{[1]}^* - p_{[2]}^*) \sqrt{n}}{\sqrt{p_{[1]}^* q_{[1]}^* + p_{[2]}^* q_{[2]}^*}} \qquad (i = 1, 2, \cdots, k - 1) \right\} \quad \text{(A38)}$$

which is already written for the least favorable configuration. The tables[2] are not immediately applicable since the correlations

$$\rho(Z_i Z_j) = \frac{p_{[1]}^* q_{[1]}^*}{p_{[1]}^* q_{[1]}^* + p_{[2]}^* q_{[2]}^*} \qquad (i \neq j) \quad \text{(A39)}$$

are not, in general, equal to $\frac{1}{2}$. In the cases treated in Tables VI and VII, $p_{[2]}^* \geqq 0.5$ and hence $p_{[1]}^* q_{[1]}^* < p_{[2]}^* q_{[2]}^*$ so that the correlations (A39) are all less than $\frac{1}{2}$. It was found that linear interpolation on the required value of n between the results for $\rho = 0$ and $\rho = \frac{1}{2}$ gives moderately good results when n is large. The result for $\rho = \frac{1}{2}$ is given by

$$n \cong \lambda \frac{(p_{[1]}^* q_{[1]}^* + p_{[2]}^* q_{[2]}^*)}{(p_{[1]}^* - p_{[2]}^*)^2} \qquad \text{(A40)}$$

with $\lambda = 2B$ where B is given in Table V. The result for $\rho = 0$ is given by (A40) with $\lambda = \lambda_0^2$ where λ_0 is the solution of the equation

$$P\{Z > -\lambda_0\} = P^{*1/(k-1)} \qquad \text{(A41)}$$

which can easily be found from univariate normal probability tables. An explicit expression for the result of this linear interpolation is

$$P_{cs}^L \cong \frac{p_{[1]}^* q_{[1]}^* (4B - \lambda_0^2) + p_{[2]}^* q_{[2]}^* \lambda_0^2}{(p_{[1]}^* - p_{[2]}^*)^2} \quad \text{(for } p_{[2]}^* \geqq 0.5) \qquad \text{(A42)}$$

The expressions for the probability of a correct selection for the alternative specification corresponding to (A36) and (A37) are

$$P_{cs}^L \cong \int_{-\infty}^{\infty} F^{k-1} (aw + b) f(w) \, dw \qquad \text{(A43)}$$

$$= a(k - 1) \int_{-\infty}^{\infty} \left[1 - F\left(\frac{w - b}{a}\right) \right] F^{k-2}(w) f(w) \, dw \quad \text{(A44)}$$

where

$$a = \sqrt{\frac{p_{[1]}^* q_{[1]}^*}{p_{[2]}^* q_{[2]}^*}} > 0 \quad \text{and} \quad b = \frac{(p_{[1]}^* - p_{[2]}^*)\sqrt{n}}{\sqrt{p_{[2]}^* q_{[2]}^*}} \geqq 0 \quad \text{(A45)}$$

These expressions can also be evaluated by the method described by Salzer, Zucker and Capuano.[3]

Appendix IV

TYPICAL EXACT CALCULATION

A. Original Specification

The exact expression (A5) for the probability of a correct selection for any configuration simplifies if the configuration is least favorable. For any pair of integers (j,n) we define

$$b_{1j} = P\{X_{(1)} = j\} = C_j^{n}(p_{[1]}^{L})^{j}(q_{[1]}^{L})^{n-j} \qquad (0 \leqq j \leqq n) \quad \text{(A46)}$$

$$b_{2j} = P\{X_{(2)} = j\} = C_j^{n}(p_{[1]}^{L} - d^*)^{j}(q_{[1]}^{L} + d^*)^{n-j} \quad (0 \leqq j \leqq n) \quad \text{(A47)}$$

$$B_{2j} = P\{X_{(2)} \leqq j\} \qquad \text{(A48)}$$

Then the exact probability P_{CS}^{L} of a correct selection for the least favorable configuration can be written as

$$P_{CS}^{L} = \sum_{j=0}^{n} b_{1j} \sum_{i=0}^{k-1} \frac{C_i^{k-1}}{1+i} b_{2j}^{i} B_{2,j-1}^{k-1-i} \qquad \text{(A49)}$$

where $B_{2,-1}$ is defined to be zero. Here, for each value of $X_{(1)}$, the letter i denotes the number of processes that tie with $X_{(1)}$ for first place and for any given value of i the conditional probability of a correct selection is $1/(1 + i)$. Taking $k = 4$ as a typical case, we can write (A49) more explicitly as

$$P_{CS}^{L} = \sum_{j=1}^{n} b_{1j} B_{2,j-1}^{3} + \frac{3}{2} \sum_{j=1}^{n} b_{1j} b_{2j} B_{2,j-1}^{2} + \sum_{j=1}^{n} b_{1j} b_{2j}^{2} B_{2,j-1}$$
$$+ \frac{1}{4} \sum_{j=0}^{n} b_{1j} b_{2j}^{3} \qquad \text{(A50)}$$

If $n \geqq 10$ then we may use the symmetric configuration, i.e., we may set $p_{[1]}^{L} = \frac{1}{2}(1 + d^*)$, in computing from (A49) or (A50).

B. Alternative Specification

The probability P_{LS}^{C} of a correct selection for the alternative specification is the same as in (A49) and (A50) except that we now define

$$b_{ij} = P\{X_{(i)} = j\} = C_j^{n}(p_{[i]}^{*})^{j}(q_{[i]}^{*})^{n-j} (i = 1, 2) \qquad \text{(A51)}$$

$$B_{2j} = P\{X_{(2)} \leqq j\} \qquad \text{(A52)}$$

A typical exact calculation for $k = 4$, using (A50), (A51) and (A52) with

$$p_{[1]} = p_{[1]}^{*} = 0.75$$

and

$$p_{[2]} = p_{[3]} = p_{[4]} = p_{[2]}^*$$

is given in Table AI. Exact values for the individual and cumulative binomial probabilities were obtained from References 4, 5 and 6.

TABLE AI — CALCULATION OF THE P_{cs}^L

$p_{[1]} = p_{[1]}^* = 0.75;$ $p_{[2]} = p_{[3]} = p_{[4]} = p_{[2]}^* = 0.60;$ $k = 4$

j	$b_{1,j}$	$b_{2,j}$	$B_{2,j-1}$	$b_{2,j}^2$	$b_{2,j}^3$	$B_{2,j-1}^2$	$B_{2,j-1}^3$
0	0.00000	0.00010	—	0.00000	0.00000	—	—
1	0.00003	0.00157	0.00010	0.00000	0.00000	0.00000	0.00000
2	0.00039	0.01062	0.00168	0.00011	0.00000	0.00000	0.00000
3	0.00309	0.04247	0.01229	0.00180	0.00008	0.00015	0.00000
4	0.01622	0.11148	0.05476	0.01243	0.00139	0.00300	0.00016
5	0.05840	0.20066	0.16624	0.04026	0.00808	0.02764	0.00459
6	0.14600	0.25082	0.36690	0.06291	0.01578	0.13462	0.04939
7	0.25028	0.21499	0.61772	0.04622	0.00994	0.38158	0.23571
8	0.28157	0.12093	0.83271	0.01462	0.00177	0.69341	0.57741
9	0.18771	0.04031	0.95364	0.00162	0.00007	0.90943	0.86727
10	0.05631	0.00605	0.99395	0.00004	0.00000	0.98794	0.98196
Check totals....	1.00000	1.00000					

$$\sum_{j=1}^{10} b_{1,j} B_{2,j-1}^3 = 0.44715$$

$$\frac{3}{2} \sum_{j=1}^{10} b_{1,j} b_{2,j} B_{2,j-1}^2 = 0.08493$$

$$\sum_{j=1}^{10} b_{1,j} b_{2,j}^2 B_{2,j-1} = 0.01464$$

$$\frac{1}{4} \sum_{j=0}^{10} b_{1,j} b_{2,j}^3 = 0.00145$$

$$\text{Total} = \overline{0.54817} = P_{cs}^L$$

APPENDIX V

In this appendix it will be shown that for large values of k the value of n required to meet any fixed specification (d^*, P^*) is approximately equal to some constant multiple of $(\ln k)$.

Let $n = n(k)$ denote the unique positive decimal solution of the equation

$$\int_{-\infty}^{\infty} F^{k-1}(w + b\sqrt{n}) f(w)\, dw = P^* \tag{A53}$$

where $f(w)$ and $F(w)$ are defined above, P^* and b are known constants with $1/k < P^* < 1$ and $b > 0$ and the argument k is a positive integer. Let ε be a (small) *fixed* number such that $0 < \varepsilon < \text{Min } (P^*, 1 - P^*)$. Then $\varepsilon < P^* - 1/k$ for sufficiently large k. Let $A = A(\varepsilon)$ be defined by

$$\int_{-A}^{A} f(w) \, dw = 1 - \varepsilon \qquad (A54)$$

so that

$$0 < \int_{|w| > A} F^{k-1}(w + b \sqrt{n}) f(w) \, dw \leqq \varepsilon \qquad (A55)$$

for any integer $k \geqq 1$, any $n > 0$ and any $b > 0$. Let n' and n'' be the unique positive decimal solutions, respectively, of the equations

$$\int_{-A}^{A} F^{k-1}(w + b \sqrt{n'}) f(w) \, dw = P^* - \varepsilon \qquad (A56)$$

$$\int_{-A}^{A} F^{k-1}(w + b \sqrt{n''}) f(w) \, dw = P^* \qquad (A57)$$

where P^*, b and k are the same as in (A53). It follows from (A55), (A56) and (A57) that for any integer $k \geqq 1$

$$n' \leqq n \leqq n'' \qquad (A58)$$

From (A54) and (A57) we have

$$\int_{-A}^{A} F^{k-1}(w + b\sqrt{n''}) f_A(w) \, dw = \frac{P^*}{1 - \varepsilon} \qquad (A59)$$

where $f_A(w)$ is the density of the normal distribution, truncated at A and $-A$. The right hand member of (A59) is positive and less than unity since $\varepsilon < 1 - P^*$. Hence there exists a w_A with $|w_A| \leqq A$ such that

$$\int_{-A}^{A} F^{k-1}(w + b\sqrt{n''}) f_A(w) \, dw = F^{k-1}(w_A + b\sqrt{n''}) \qquad (A60)$$

Since w_A is bounded and n'' is large for large k we can use the well-known approximation

$$F^{k-1}(w_A + b\sqrt{n''}) \cong \left[1 - \frac{\exp\left[-(w_A + b\sqrt{n''})^2/2\right]}{\sqrt{2\pi}(w_A + b\sqrt{n''})} \right]^{k-1}$$

$$\cong \exp\left\{ - \frac{(k - 1) \exp\left[-(w_A + b\sqrt{n''})^2/2\right]}{\sqrt{2\pi}(w_A + b\sqrt{n''})} \right\} \qquad (A61)$$

where only the leading term is considered. Hence from (A59), (A60)

and (A61)

$$- \ln \ln \left(\frac{1-\varepsilon}{P^*}\right)^{\sqrt{2\pi}} + \ln (k-1) \tag{A62}$$

$$\cong \tfrac{1}{2}(w_A + b\sqrt{n''})^2 + \ln (w_A + b\sqrt{n''})$$

Since w_A is bounded and $ln \sqrt{n''} = o(n'')$ it follows that for large k

$$n'' \cong (2/b^2) \ln (k-1) \cong C \ln k \tag{A63}$$

where C is a proportionality factor. Starting with (A54) and (A56) the same argument gives the same result as (A63) for n'. Hence, by (A58), the same result must hold for n.

ACKNOWLEDGMENT

REFERENCES

1. Bechhofer, R. E., and Sobel, M., On a Class of Sequential Multiple Decision Procedures for Ranking Parameters of Koopman-Darmois Populations with Special Reference to Means of Normal Populations, in preparation.
2. Bechhofer, R. E., A Single-Sample Multiple Decision Procedure for Ranking Means of Normal Populations with Known Variances, Ann. Math. Stat., **25**, pp. 16–39, 1954.
3. H. E. Salzer, R. Zucker, and R. Capuano, Table of the Zeros and Weight Factors of the First Twenty Hermite Polynomials, Journal of Research of the N. B. S., **48**, pp. 111–116, 1952.
4. National Bureau of Standards, Tables of the Binomial Probability Distribution, App. Math. Series 6, 1950.
5. Ordnance Corps, Tables of the Cumulative Binomial Probabilities, ORDP 20-1, 1952.
6. Harvard Computation Laboratory, Tables of the Cumulative Binomial Probability Distribution, Harvard University Press, Cambridge, 1955.

Bell System Technical Papers Not Published in This Journal

ALLISON, H. W., see Moore, G. E.

ANDERSON, P. W., and TALMAN, J. D.[1]

Pressure Broadening of Spectral Lines at General Pressures, Conf. Proc. Breadth of Spectral Lines, pp. 29–61, Oct., 1956.

ARNOLD, S. M.[1]

The Growth and Properties of Metal Whiskers, Tech. Proc. Am. Electroplaters Soc., pp. 26–31, 1956.

BALA, V. B., see Geller, S.

BASHKOW, T. R.[1]

Effect of Nonlinear Collector Capacitance on Collector Current Rise Time, Trans. I.R.E. PGED, **ED-3,** pp. 167–172, Oct., 1956.

BEACH, A. L., see Thurmond, C. D.

BIRDSALL, H. A.,[1] and GILKENSEN, P. B.[3]

The Application of Electrical Instruments for Measuring Moisture Contents of Textiles, Am. Dyestuff Reporter, Proc. Am. Assoc. Tex. Chem. and Colorists, **45,** pp. 935–945, Dec. 17, 1956. Committee report of which Messrs. Birdsall and Gilkensen were members.

BRIDGERS, H. E.,[1] and KOLB, E. D.[1]

The Distribution Coefficient of Boron in Germanium, J. Chem. Phys., **25,** pp. 648–650, Oct., 1956.

[1] Bell Telephone Laboratories, Inc.
[3] Western Electric Company.

BUCK, T. M.,[1] and McKIM, F. S.[1]

Depth of Surface Damage Due to Abrasion on Germanium, J. Electrochem. Soc., **103,** pp. 593–597, Nov., 1956.

COMPTON, K. G.[1]

Potential Criteria for the Cathodic Protection of Lead Cable Sheath, Corrosion, **12,** pp. 37–44, Nov., 1956.

DAVID, E. E., JR.,[1] and McDONALD, H. S.[1]

Note on Pitch-Synchronous Processing of Speech, J. Acous. Soc. Am., **28,** pp. 1261–1266, Nov., 1956.

DICKINSON, D. J.,[4] POLLAK, H. O.,[1] and WANNIER, G. H.[1]

On a Class of Polynomials Orthogonal Over a Denumerable Set, Pacific J. Math., **6,** pp. 239–247, 1956.

FELKER, J. H.[1]

Complexity With Reliability, I.R.E. Student Quarterly, **3,** pp. 7–11, Dec., 1956.

GELLER, S.[1]

A Set of Effective Coordination Number (12) Radii for the β-Wolfram Structure Elements, Acta Crys., **9,** pp. 885–899, Nov. 10, 1956.

GELLER, S.,[1] and BALA, V. B.[1]

Crystallographic Studies of Perovskite-like Compounds. II — Rare Earth Aluminates, Acta Crys., **9,** pp. 1019–1025, Dec. 10, 1956.

GULDNER, W. G.[1]

The Application of Vacuum Techniques to Analytical Chemistry, Vakuum-Technik, pp. 159–166, Oct., 1956.

GULDNER, W. G.[1]

Tentative Method for Analysis of Carbon in Nickel, A.S.T.M., Chem. Anal. Electronic Nickel (E107–56T), pp. 20–25, Sept. 1956.

[1] Bell Telephone Laboratories, Inc.
[4] Pennsylvania State University, University Park.

GULDNER, W. G.[1]

Tentative Method of Test for Oxygen, Hydrogen and Nitrogen in Nickel, A.S.T.M., Chem. Anal. Electronic Nickel (E107–56T), pp. 26–33, Sept., 1956.

GULDNER, W. G., see Thurmond, C. D.

HAGSTRUM, H. D.[1]

Auger Ejection of Electrons from Molybdenum by Noble Gas Ions, Phys. Rev., **104,** pp. 672–683, Nov. 1, 1956.
Auger Ejection of Electrons from Tungsten by Noble Gas Ions, Phys. Rev., **104,** pp. 317–318, Oct. 15, 1956.
Metastable Ions of the Noble Gases, Phys. Rev., **104,** pp. 309–316, Oct. 15, 1956.

HARING, H. E., see Taylor, R. L.

KLEMM, G. H.[1]
Automatic Projection Switching for TD-2 Radio System, Commun. and Electronics, **27,** pp. 520–527, Nov., 1956.

KOLB, E. D., see Bridgers, H. E.

KOMPFNER, R.[1]

Some Recollections of the Early History of the Traveling Wave Tube, 1956 Yearbook Phys. Soc. London, pp. 30–33, 1956.

KRUSEMEYER, H. J.,[1] and PURSLEY, M. V.[1]

Donor Concentration Changes in Oxide Coated Cathodes Due to Changes in Electric Field. J. Appl. Phys., **27,** pp. 1537–1545, Dec., 1956.

LEWIS, H. W.[1]

Surface Energies in Superconductors, Phys. Rev., **104,** pp. 942–947, Nov. 15, 1956.

LOVELL, L. CLARICE, see Vogel, F. L., Jr.

[1] Bell Telephone Laboratories, Inc.

MALLINA, R. F.[1]

Solderless Wrapped Connections, Trans. I.R.E., **PGT-1,** pp. 12–22, Sept., 1956.

MATTHIAS, B. T.,[1] MILLER, C. E.,[1] and REMEIKA, J. P.[1]

Ferroelectricity of Glycine Sulfate, Phys. Rev., **104,** pp. 849–850, Nov. 1, 1956.

MASON, W. P.[1]

Internal Friction and Fatigue in Metals at Large Strain Amplitudes, J. Acous. Soc. Am., **28,** pp. 1207–1218, Nov., 1956.
Physical Acoustics and the Properties of Solids, J. Acous. Soc. Am., **28,** pp. 1197–1206, Nov., 1956.

MATREYEK, W., see Winslow, F. H.

McDONALD, H. S., see David, E. E., Jr.

McKIM, F. S., see Buck, T. M.

McSKIMIN, H. J.[1]

Wave Propagation and the Measurement of the Elastic Properties of Liquids and Solids, J. Acous. Soc. Am., **28,** pp. 1228–1232, Nov., 1956.

MILLER, C. E., see Matthias, B. T.

MILLER, R. C.,[1] and SAVAGE, A.[1]

Diffusion of Aluminum in Single Crystal Silicon, J. Appl. Phys., **27,** pp. 1430–1432, Dec., 1956.

MONFORTE, F. R., see Van Uitert, L. G.

MOORE, G. E.,[1] and ALLISON, H. W.[1]

Emission of Oxide Cathodes Supported on a Ceramic, J. Appl. Phys., **27,** pp. 1316–1321, Nov., 1956.

OSWALD, A. A.[1]

Early History of Single Sideband Transmission, Proc. I.R.E., **44,** pp. 1676–1679, Dec., 1956.

---

[1] Bell Telephone Laboratories, Inc.

PIERCE, J. R.,[1] and WALKER, L. R.[1]

Growing Electric Space-Charge Waves, Phys. Rev., **104,** pp. 306–307, Oct. 15, 1956.

POLLAK, H. O., see Dickinson, D. J.

PURSLEY, M. V., see Krusemeyer, H. J.

REMEIKA, J. P., see Matthias, B. T.

RICE, J. W.[3]

Manufacture of Wire Spring Relays for Communication Switching Systems, Commun. and Electronics, **27,** pp. 513–518, Nov., 1956.

ROSE, D. J.[1]

The Townsend Ionization Coefficient for Hydrogen and Deuterium, Phys. Rev., **104,** pp. 273–277, Oct. 15, 1956.

SAVAGE, A., see Miller, R. C.

STRUTHERS, J. D.[1]

Solubility and Diffusity of Gold, Iron, and Copper in Silicon, J. Appl. Phys., Letter to the Editor, **27,** p. 1560, Dec., 1956.

SUHL, H., see Walker, L. R.

SWANEKAMP, F. W., see Van Uitert, L. G.

TAYLOR, R. L.,[1] and HARING, H. E.[1]

Metal-Semiconductor Capacitor, J. Electrochem. Soc., **103,** pp. 611–613, Nov., 1956.

TALMAN, J. D., see Anderson, P. W.

THURMOND, C. D.,[1] GULDNER, W. G.,[1] and BEACH, A. L.[1]

THURMOND, C. D.,[1] GULDNER, W. G.,[1] and BEACH, A. L.[1]

Hydrogen and Oxygen in Single-Crystal Germanium as Determined by Vacuum Fusion Gas Analysis, J. Electrochem. Soc., **103,** pp. 603–605, Nov., 1956.

---

[1] Bell Telephone Laboratories, Inc.

TORREY, MARY N.[1]

Quality Control in Electronics, Proc. I.R.E., **44,** pp. 1521–1530, Nov., 1956.

TRUMBORE, F. A.[1]

Solid Solubilities and Electrical Properties of Tin in Germanium Single Crystals, J. Electrochem. Soc., **103,** pp. 597–600, Nov., 1956.

VAN UITERT, L. G.,[1] SWANEKAMP, F. W.,[1] and MONFORTE, F. R.[1]

Method for Forming Large Ferrite Parts for Microwave Applications, J. Appl. Phys., Letter to the Editor, **27,** pp. 1385–1386, Nov., 1956.

VOGEL, F. L., JR.,[1] and LOVELL, L. CLARICE[1]

Dislocation Etch Pits in Silicon Crystals, J. Appl. Phys., **27,** pp. 1413–1415, Dec., 1956.

WALKER, L. R., see Pierce, J. R.

WALKER, L. R.,[1] and SUHL, H.[1]

Propagation in Circular Waveguides Filled With Gyromagnetic Material, Trans. I.R.E., **AP-4,** pp. 492–494, July, 1956.

WANNIER, G. H., see Dickinson, D. J.

WEINREICH, G.[1]

Acoustodynamic Effects in Semiconductors, Phys. Rev., **104,** pp. 321–324, Oct. 15, 1956.

WERTHEIM, G. K.[1]

Carrier Lifetime in Indium Antimonide, Phys. Rev., **104,** pp. 662–664, Nov. 1, 1956.

WINSLOW, F. H.,[1] and MATREYEK, W.[1]

Pyrolysis of Cross-Linked Styrene Polymers, J. Poly. Sci., **22,** pp. 315–324, Nov., 1956.

---

[1] Bell Telephone Laboratories, Inc.

Recent Monographs of Bell System Technical Papers Not Published in This Journal*

ANDERSON, O. L.

Effect of Pressure on Glass Structure, Monograph 2666.

BEMSKI, G.

Quenched-In Recombination Centers in Silicon, Monograph 2681.

BRIDGERS, H. E.

p-n Junctions in Semiconductors by Variation of Crystal Growth Parameters, Monograph 2668.

BROWN, W. L., see Montgomery, H. C.

CAMPBELL, MARY E., see Luke, C. L.

CARLITZ, L., and RIORDAN, J.

The Number of Labeled Two-Terminal Series-Parallel Networks, Monograph 2667.

CHASE, F. H.

Power Regulation by Semiconductors, Monograph 2685.

DAVID, E. E., JR.

Naturalness and Distortion in Speech-Processing Devices, Monograph 2687.

DODGE, H. F., and TORREY, Miss M. N.

A Check Inspection and Demerit Rating Plan, Monograph 2669.

EDER, M. J., see Veloric, H. S.

FISHER, J. R., and POTTER, J. F.

Apparent Density for Evaluating the Physical Structure of Steatite, Monograph 2688.

FULLER, C. S., see Reiss, H.

GELLER, S., and GILLEO, M. A.

Gadolinium Orthoferrite: Crystal Structure and Magnetic Properties, Monograph 2670.

GILLEO, M. A., see Geller, S.

GOHN, G. R.

Hardness Conversion Table for Copper-Beryllium Alloy Strip, Monograph 2665.

HARROWER, G. A.

Dependence of Electron Reflection on Contamination of Reflecting Surface, Monograph 2689.

HARROWER, G. A.

Energy Spectra of Secondary Electrons from Mo and W for Low Primary Energies, Monograph 2690.

HOVGAARD, O. M.

Capability of Sealed Contact Relays, Monograph 2697.

KNAPP, H. M.

Design Features of Bell System Wire Spring Relays, Monograph 2693.

LEWIS, H. W.

Two-Fluid Model of an "Energy-Gap" Superconductor, Monograph 2671.

LUKE, C. L., and CAMPBELL, MARY E.

Photometric Determination of Germanium and Tin With Phenyl-fluorone, Monograph 2608.

MANLEY, J. M., and ROWE, H. E.

Some General Properties of Nonlinear Elements. I — General Energy Relations, Monograph 2672.

MCLEAN, D. A., and POWER, F. S.

Tantalum Solid Electrolytic Capacitors, Monograph 2673.

MCMAHON, W.

Dielectrics by Solidifying Certain Organic Compounds in Electric or Magnetic Fields, Monograph 2694.

MONTGOMERY, H. C., and BROWN, W. L.

Field-Induced Conductivity Changes in Germanium, Monograph 2695.

MOORE, E. F., and SHANNON, C. E.

Reliable Circuits Using Less Reliable Relays, Monograph 2696.

PIETRUSZKIEWICZ, A. J., see Reiss, H.

POTTER, J. F., see Fisher, J. R.

POWER, F. S., see McLean, D. A.

PRINCE, M. B., see Veloric, H. S.

REISS, H.

Refined Theory of Ion Pairing, Monograph 2698.

REISS, H., FULLER, C. S., and PIETRUSZKIEWICZ, A. J.

Solubility of Lithium in Doped and Undoped Silicon, Monograph 2702.

RIESS, H.

Theory of Ionization of Hydrogen and Lithium in Silicon and Germanium, Monograph 2700.

REMEIKA, J. P.

Growth of Single Crystal Rare-Earth Orthoferrites and Related Compounds, Monograph 2699.

RICHARDS, A. P., see Snoke, L. R.

RIORDAN, J., see Carlitz, L.

ROWE, H. E., see Manley, J. M.

SHANNON, C. E., see Moore, E. F.

SHULMAN, R. G., and WYLUDA, B. J.

Trapping Center Properties of Germanium, Monograph 2674.

SNOKE, L. R., and RICHARDS, A. P.

Marine Borer Attack on Lead Cable Sheath, Monograph 2675.

TORREY, Miss M. N., see Dodge, H. F.

UHLIR, A., JR.

Two-Terminal p-n Junction Devices for Frequency Conversion and Computation, Monograph 2704.

VAN UITERT, L. G.

Nickel Copper Ferrites for Microwave Applications, Monograph 2676.

VELORIC, H. S., PRINCE, M. B., and EDER, M. J.

Avalanche Breakdown Voltage in Silicon Diffused p-n Junctions, Monograph 2705.

WEINREICH,

Transit Tim. 'ransistor, Monograph 2706.

WERNICK, J. H.

Diffusivities in Liquid Metal by Temperature-Gradient Zone Melting, Monograph. 2677.

WOLFF, P. A.

Theory of Plasma Resonance, Monograph 2707.

WYLUDA, B. J., see Shulman, R. G.

Contributors to This Issue

RICHARD C. BOYD, B.S., Northwestern University, 1946; B.S.E.E., University of Michigan, 1947; M.S.E.E., University of Michigan, 1948; Bell Telephone Laboratories, 1948–. After completion of the Laboratories Communication Development Training program in 1950, Mr. Boyd was concerned with transmission engineering and systems studies. He was a supervisor during the exploratory trial of experimental P1 carrier in 1953 and 1954. He is now responsible for transmission engineering of P1 carrier for rural subscriber use, and for adaptation of P and N1 carrier to exchange trunk use. He is a member of Tau Beta Pi and Phi Kappa Phi.

ROBERT W. DAWSON, Newark College of Engineering; Rutgers University; Bell Telephone Laboratories, 1941–. All of Mr. Dawson's work has been with the Radio Research Department. Together with A. C. Beck, he was concerned with conductivity measurements at microwave frequencies, and they were co-authors of an article on this subject. Mr. Dawson, a member of the Institute of Radio Engineers, worked on the Manhattan Project at Los Alamos while serving in the Army from 1942 to 1946.

GEORGE FEHER, B.S. in Engineering Physics, University of California, 1950; M.S.E.E., University of California, 1952; Ph.D. in Physics, University of California, 1954; Bell Telephone Laboratories, 1954–. Dr. Feher has been a member of the Semiconductor Research Department since joining the Laboratories. He has been engaged particularly in studies of electron spin resonance absorption, and is the author of several articles on this subject. He is a member of the American Physical Society, the Institute of Radio Engineers, and Sigma Xi.

JOHN D. HOWARD, B.E.E., University of Louisville, 1947; Southern Bell Telephone Company, 1947–. After a year and a half in the Plant Department at Southern Bell, Mr. Howard joined the Engineering Department and remained there until late 1952. At that time he was called to the O. & E. Department of the A. T. & T. Co. where he was concerned with exchange transmission. After completing this assignment he

returned to Southern Bell where he is now Exchange Transmission Engineer. Mr. Howard is a member of the A.I.E.E.

MARILYN J. HUYETT, A.B., Susquehanna University, 1954; Bell Telephone Laboratories, 1954–. Since joining the Laboratories, Miss Huyett has been concerned with statistical research for the reliability group at Allentown, where she has had a great deal of experience with IBM computing machines. She is a member of the American Statistical Association. While in college, she received the Stine Mathematical Prize, an award for proficiency in mathematics.

JOHN E. KARLIN, B.A., University of Cape Town, 1938; M.A., University of Cape Town, 1939; Ph.D., University of Chicago, 1942; Bell Telephone Laboratories, 1945–. Dr. Karlin was engaged in psychoacoustic research from 1945 to 1947. From 1947 until the present he has been concerned with user preference research, and since 1952 he has been in charge of the group doing this research. During the war years, 1942–1945, Dr. Karlin was at Harvard University, engaged in communications research on military projects. He is a member of the I.R.E., the Acoustical Society of America, the American Psychological Association and Sigma Xi.

STUART P. LLOYD, S.B., 1943, University of Chicago; M.S., 1949 and Ph.D., 1951, University of Illinois. Bell Telephone Laboratories, 1952–. Engaged in work relating to probability theory and information theory. Member, Institute for Advanced Study, Princeton, 1951–52. Member of American Mathematical Society, Institute of Mathematical Statistics, American Physical Society, A.A.A.S., Phi Kappa Phi, Sigma Xi and Phi Beta Kappa.

D. W. McCALL, B.S., University of Wichita, 1950; M.S., 1951 and Ph.D., 1953, University of Illinois; Bell Telephone Laboratories, 1953–. Dr. McCall is engaged in fundamental studies of the properties of dielectrics. He is a member of the American Chemical Society, the American Physical Society, Sigma Xi, and Phi Lambda Upsilon.

LUDWIG PEDERSEN, Christiania Technical School (Norway), 1919; Western Electric International Co. (Oslo), 1919–20; Western Electric Co., 1920–25; Western Electric Co., Field Engineering Force, 1944–45; Bell Telephone Laboratories, 1925–. He has been concerned with circuit design for machine switching systems, development of telegraph equip-

ment, design of transmission equipment for the armed forces, and toll transmission systems. He served as a technical observer with the U. S. Army in the European theater. He is now Systems Development Engineer at the Merrimack Valley Laboratory with responsibility for voice frequency, broadband carrier, short haul carrier and rural carrier systems. Member of the A.I.E.E.

JOHN R. PIERCE, B.S., 1933, M.S., 1934 and Ph.D., 1936, California Institute of Technology; Bell Telephone Laboratories, 1936–. Director of Research in Electrical Communications at Bell Telephone Laboratories. He has specialized in the development of electron tubes, microwave research, electronic devices for military applications, and communications circuits. Dr. Pierce has been granted 55 patents and is the author of three books. For his research leading to the development of the beam traveling wave tube, he was awarded the 1947 Morris Liebmann Memorial Prize of the I. R. E. He was voted the "Outstanding Young Electrical Engineer of 1942" by Eta Kappa Nu. Member of National Academy of Sciences, British Interplanetary Society, A.I.E.E., Sigma Xi, Tau Beta Pi and Eta Kappa Nu. Fellow of American Physical Society and I.R.E.

JOHN H. ROWEN, B.E.E., 1948 and M.Sc., 1951, Ohio State University. Mr. Rowen worked at the Antenna Laboratory of the Ohio State University Research Foundation in Columbus, O. from 1948 to 1951. He joined Bell Telephone Laboratories in 1951, shortly after being awarded his master's degree. Since then Mr. Rowen has specialized in the applied physics of solids, and the development of microwave ferrite devices. He is a member of the Solid State Device Development Department at the Murray Hill Laboratory. Mr. Rowen is a member of the Institute of Radio Engineers and of Eta Kappa Nu.

HAROLD SEIDEL, B.E.E., 1943, College of the City of New York; M.E.E., 1947 and D.E.E., 1954, Polytechnic Institute of Brooklyn; Microwave Research Institute of Polytechnic Institute of Brooklyn, 1947; Arma Corp., 1947–48; Federal Telecommunications Laboratories, 1948–53; Bell Telephone Laboratories, 1953–. He has been concerned with general electromagnetic problems, especially regarding wave-guide applications, and with analysis of microwave ferrite devices. Member of Sigma Xi and I.R.E.

MILTON SOBEL, B. S., 1940, College of the City of New York; M.A., 1946 and Ph.D., 1951, Columbia University; U. S. Census Bureau, stat-

istician, 1940–41; U. S. Army War College, statistician, 1942–44; Columbia University, department of mathematics, 1946–50; Wayne University, assistant professor of mathematics, 1950–52; Columbia University, visiting lecturer, 1952; Cornell University, fundamental research in mathematical statistics, 1952–54; Bell Telephone Laboratories, 1954–. He has been engaged in fundamental research on life testing and reliability problems with special application to transistors. Consultant on many Bell Laboratories projects. Member of Institute of Mathematical Statistics, American Statistical Association and Sigma Xi.

WILHELM VON AULOCK, Dipl. Ing., Technische Hochschule, Berlin, 1937; Dr. Ing., Technische Hochschule Stuttgart, 1953; Dr. von Aulock worked in Berlin from 1938 to 1942 for the A.E.G., Kabelwerk; in Gotenhafen (Gdynia) for the Torpedoversuchsanstalt from 1942 to 1945; and for the United States Navy Bureau of Ships in Washington from 1947 to 1953, where he was involved in work on torpedo countermeasures and studies of electromagnetic induction fields in sea water. He joined Bell Telephone Laboratories in 1954. Since then he has been principally engaged in analytical and experimental studies of phase shift and loss characteristics of ferrite-loaded waveguides, and the application of these properties. He is an associate member of the Institute of Radio Engineers.